University of Nottingham
UK | CHINA | MALAYSIA

Dissection of flagellar pocket function in *Trypanosoma brucei*

Sarah Whipple

MRes, BSc (Hons)

Thesis submitted to the University of Nottingham towards the degree of Doctor of Philosophy

September 2017

Abstract

To survive in the host bloodstream, the extracellular protozoan parasite *Trypanosoma brucei* must perform the critical cellular processes of nutrient uptake and secretion, whilst evading the host immune system. Central to this is the compartmentalisation of the parasite surface membrane into biochemically and functionally distinct domains. One of these domains, the flagellar pocket (FP), is the only region of the parasite surface competent for endo- and exocytosis and, as such, forms the primary site of exchange and communication between the parasite and its host. The overall importance of the FP for parasite virulence, and the essentiality of the few FP receptors characterised to date, make proteins that reside at this interface potentially attractive therapeutic targets. The identification of novel FP proteins, as part of a recent surface proteomics study, has provided a large set of putative receptors and transporters to explore and, as part of this thesis, I present work towards their functional characterisation. To this end, I carried out individual knockdown of 13 FP components by RNA interference. This revealed that ablation of these proteins was not detrimental to parasite survival *in vitro*, implying they could instead have critical functions in host-parasite interactions *in vivo*.

Potential determinants of protein sorting to the FP were also investigated. FP localisation was seemingly independent of protein topology, or identifiable amino acid sequence motifs. Thus I examined the potential role of N-glycosylation in this process. Enzymatic treatment revealed that most FP proteins studied here were glycosylated, yet the type of N-glycan modification alone could not be used to predict surface domain localisation. On the other hand, knockdown of a key component of the flagellar pocket collar, which forms a putative barrier between the FP and cell body membranes, caused the mis-localisation of some resident FP proteins. This suggests a role for the collar in FP protein retention. Furthermore, movement of macromolecules in and out of the protected environment of the FP has been suggested to require motor proteins. In agreement with this, I hereby show that overexpression of a non-functional variant of Kinesin-17, which localises to the FP region, is detrimental to parasite survival. Overall the work presented in this thesis provides new

insights into the mechanisms of FP membrane specialisation in *T. brucei*, highlights potential protein redundancy at this region, and begins to characterise the function of a novel FP-localised kinesin.

Declaration

This thesis is the result of my own work, except where included data is explicitly mentioned, which has been undertaken during my period of registration for this degree at The University of Nottingham.

Acknowledgments

First and foremost, I would like to thank my supervisor Dr Catarina Gadelha, for her guidance, support and encouragement during this PhD. The experience was made all the more enjoyable and rewarding by the opportunities to travel to Brazil and the USA to present my work - so thank you! I'd also like to thank Dr Bill Wickstead – the man with all the answers! His input into my project has been incredibly useful throughout, and particularly with regard to the final chapter of this thesis.

I am also really grateful to all the members of the Gadelha, Wickstead, Huett, Friel, Allers, and Nieduszynski labs for making the past 4 years that bit more enjoyable. Special thanks goes to James, Simon, and Jennifer, for keeping me sane, always being available when I wanted to discuss or whine about science, and for dragging me to the pub when all else failed!

I would also like to thank Jamie, for his constant support, the use of his computer, and providing me with regular cups of tea for the duration of this process (especially critical during the last few months!). Finally, I am incredibly grateful to my parents who have supported me throughout my life, and the past four years have been no exception!

The work presented in this thesis was funded by the School of Life Sciences (University of Nottingham) and the Royal Society.

Abbreviations

ATP	adenosine triphosphate
BES	bloodstream expression site
BLAST	Basic Local Alignment Tool
bp	base pairs
BSD	blasticidin S resistance marker
BSF	bloodstream form
CDS	coding DNA sequence
CLH	clathrin heavy chain
CME	clathrin-mediated endocytosis
CMM	Creek's Minimal Medium
DAPI	4,6-diamidino-2-phenylindole
DNA	deoxyribonucleic acid
dsRNA	double stranded RNA
DYNC1H1	cytoplasmic dynein 1
EDTA	ethylenediaminetetraacetic acid
Endo-H	endoglycosidase-H
ER	endoplasmic reticulum
ESAG	expression site associated gene
ESB	expression site body
ESP	enriched in surface proteome
FAZ	flagellum attachment zone
FCS	foetal calf serum
FP	flagellar pocket
FPC	flagellar pocket collar
GFP	green fluorescent protein
GPI	glycosylphophatidylinositol
HpHbR	haptoglobin-haemoglobin receptor
HYG	hygromycin resistance marker
IC	intermediate chromosome
IFT	intraflagellar transport
ISG	invariant surface glycoprotein
Kb	kilobases

kDa	kilodaltons
KIN17	kinesin-17
KO	knockout
MC	minichromosome
MBC	megabase chromosome
mRNA	messenger RNA
mSt	mStrawberry
MT	microtubule
NEO	neomycin resistance marker
nm	nanometres
OE	overexpression
ORF	open reading frame
PAD	protein associated with differentiation
PAGE	polyacrylamide gel electrophoresis
PBS	phosphate buffered saline
PNGase-F	peptide-N-glycosidase F,
PCF	procyclic form
PCR	polymerase chain reaction
RNA	ribonucleic acid
RNAi	RNA interference
SDS	sodium dodecyl sulphate
sfGFP	superfolder GFP
SIF	stumpy induction factor
TM	transmembrane
TfR	transferrin receptor
UTR	untranslated region
VSG	variant surface glycoprotein

Contents

Chapter 1. Introduction 1

1.1. Membrane compartmentalisation 1

1.2. Maintenance of a specialised membrane 4

1.2.1. Physical barriers 4

1.2.2. Membrane properties 6

1.2.3. Active protein targeting 8

1.3. Transport between membrane compartments 9

1.3.1. Vesicle formation 9

1.3.2. Vesicle trafficking and fate 12

1.4. Surface membrane specialisation in *Trypanosoma brucei* 13

1.4.1. The trypanosome surface 14

1.4.2. Flagellar membrane 19

1.4.3. Flagellar pocket 20

1.4.4. Mechanisms of maintaining specialised surface architecture of *Trypanosoma brucei* 39

1.5. Conclusions 43

1.6. Aims 44

Chapter 2. Materials and methods 45

2.1. Cell lines 45

2.1.1. Culture of *Trypanosoma brucei* 45

2.1.2. Transfection of *Trypanosoma brucei* 45

2.2. Plasmid production 46

2.2.1. For the inducible knockdown of flagellar pocket (FP) proteins 46

2.2.2. For the endogenous-locus tagging of FP ESP proteins 46

2.2.3. For the endogenous-locus tagging of KIN17 and DYNC1H1 47

2.2.4. For the generation of KIN17 knockout fragments 48
2.2.5. For the inducible overexpression of KIN17 and kin17-rigor 49
2.3. Plasmid integration analysis 50
2.3.1. Integration of endogenous locus tagging constructs 50
2.3.2. Integration of KIN17 knockout fragments 51
2.4. Growth analysis 51
2.4.1. Manual cell counts 51
2.4.2. ATP-based luciferase assay 52
2.5. Protein biochemistry 52
2.5.1. Sample preparation, SDS-PAGE and Western blotting 52
2.5.2. Deglycosylation with Endo-H and PNGase-F 53
2.5.3. Cytoskeleton preparation 54
2.6. Microscopy 54
2.6.1. Native fluorescence 54
2.6.2. Imaging 55
2.7. Flow cytometry 55
Chapter 3. Investigating the role of flagellar pocket proteins in *Trypanosoma brucei* 62
3.1. Introduction 62
3.1.1. Flagellar pocket proteins of *Trypanosoma brucei* 62
3.1.2. RNA interference as a tool to interrogate protein function in *T. brucei* 67
3.2. Results 69
3.2.1. Testing validated FP components for essentiality *in vitro* 69
3.2.2. Localisation of putatively essential components to the FP 74
3.3. Discussion 89
3.4. Supplemental Figures 92

Chapter 4. Investigating mechanisms of surface specialisation in *Trypanosoma brucei* 93

4.1. Introduction 93

4.2. Results 96

4.2.1. Most ESPs are predicted to be N-glycosylated 96

4.2.2. Most ESPs are glycosylated *in vivo* 99

4.2.3. Glycosylation pattern alone is not sufficient to dictate surface subdomain localisation 103

4.2.4. A component of the FPC has a role in flagellar pocket protein retention 105

4.3. Discussion 113

Chapter 5. Investigating mechanisms of macromolecule transport in and out of the flagellar pocket 117

5.1. Introduction 117

5.2. Results 123

5.2.1. KIN17 localises to the neck region in BSFs 123

5.2.2. KIN17 is not essential for parasite growth *in vitro* 129

5.2.3. Impairment of KIN17 function causes a severe growth defect. 132

5.3. Discussion 146

Chapter 6. Discussion 151

6.1. Flagellar pocket proteins: essential or redundant? 151

6.2. The collar as a flagellar pocket barrier 153

6.3. Glycosylation as a potential flagellar pocket protein sorting factor 156

6.4. Overexpression of a kinesin rigor mutant is detrimental to parasite survival 158

References 161

Appendix 183

Chapter 1. Introduction

1.1. Membrane compartmentalisation

Plasma membranes of eukaryotic cells are highly compartmentalised. This segregation allows the polarisation of cellular functions to distinct regions of the membrane via the differential accumulation of necessary protein and lipid components, and the exclusion of others. A striking example of this is the division of an epithelial cell into apical and basolateral domains, demarcated by tight junctions (Figure 1.1A/B). This organisation is necessary for the epithelia to perform absorptive and secretory functions at either side of a tissue layer, whilst providing a barrier to the free movement of molecules between compartments of the body (Martin-Belmonte and Mostov 2008; Roignot et al. 2013; Peterson and Artis 2014).

Epithelial cells can have an additional level of specialisation on the apical surface in the form of an immotile membrane projection, the primary cilium (Figure 1.1C). This sensory organelle is built via the trafficking of the assembly material along the axoneme towards the distal tip of the growing cilium, a process termed intraflagellar transport (Kim and Dynlacht 2013). Disruption of primary cilium function can lead to ciliopathies (Reiter and Leroux 2017), highlighting the importance of maintaining this specialised region of plasma membrane.

Membrane specialisation is also required for neuronal communication, which forms the basis of motor control, sensory perception and memory in animal cells. Central to a neuron’s ability to process, propagate and receive stimulatory signals, is the segregation of the membrane into the somatodentritic compartment, axon, and dendritic spines (Figure 1.2) (Caudron and Barral 2009). Outside of animal cells, compartmentalisation of the cell cortex is also necessary for yeast as they undergo asymmetric cell division to produce a daughter bud (Takizawa et al. 2000; Trimble and Grinstein 2015).

A highly specialised surface architecture can also be found on the unicellular protozoan parasite, *T. brucei*. Here, the parasite plasma membrane

is segregated into at least four morphologically distinct domains: the cell body, flagellum, flagellar pocket, and neck membranes (Figure 1.3). Each of these domains contribute significantly towards the ability of this extracellular parasite to survive and proliferate in the bloodstream of the mammalian host, enabling them to inflict sleeping sickness on humans (*T. b. gambiense* and *T. b. rhodesiense*) and a wasting disease (Nagana) on livestock (*T. b. brucei*). The function of each of these membrane domains and their relative contribution to parasitism will be discussed in more detail in section 1.4.

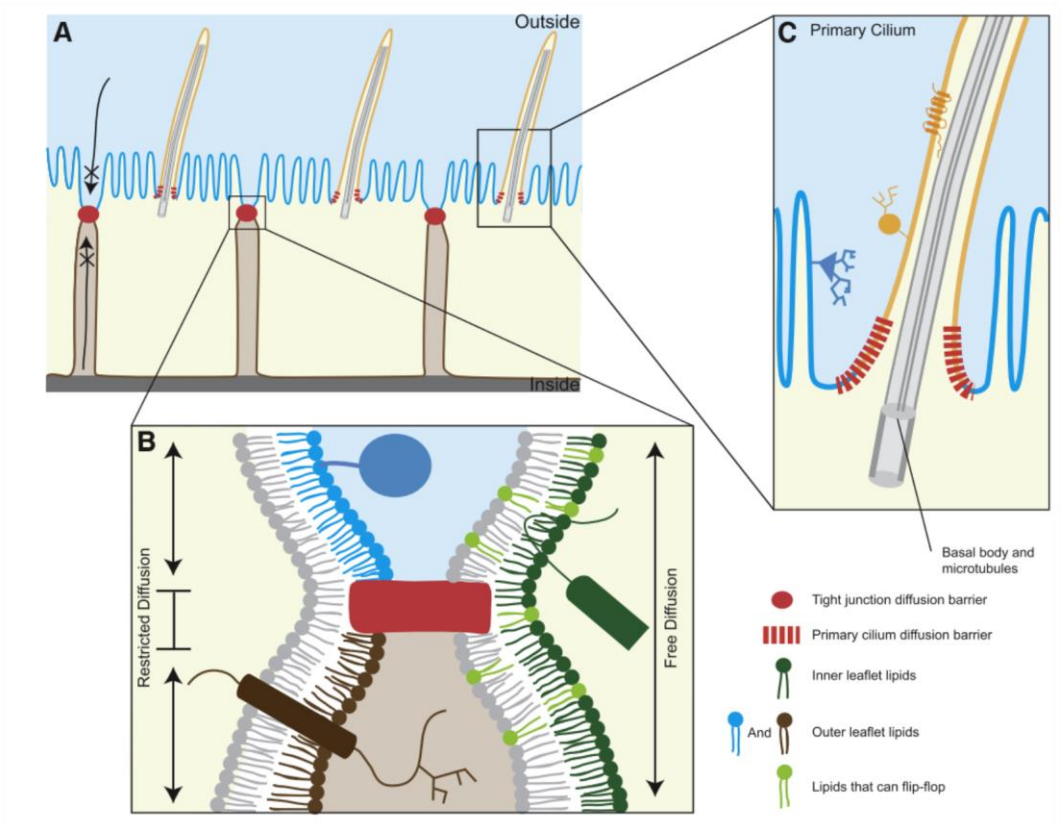


Figure 1.1. Surface domain specialisation in epithelial cells.
A) Architecture of an epithelial cell membrane, depicting the apical (blue) and basolateral (brown) membranes, separated by a tight junction. The presence of the tight junction also prevents free diffusion across the epithelial layer. **B)** Magnification of the tight junction diffusion barrier. The diffusion barrier (red) limits the diffusion of proteins and lipids on the outer leaflet of the plasma membrane (shown in brown and blue on the left), but does not affect movement of those on the inner leaflet (green). **C)** Magnification of the mammalian primary cilium, an additional region of specialised membrane on the apical membrane. The ciliary membrane (yellow) has a distinct protein composition from the neighbouring plasma membrane (blue), which is maintained by a diffusion barrier (red) (from Caudron & Barral, 2009).

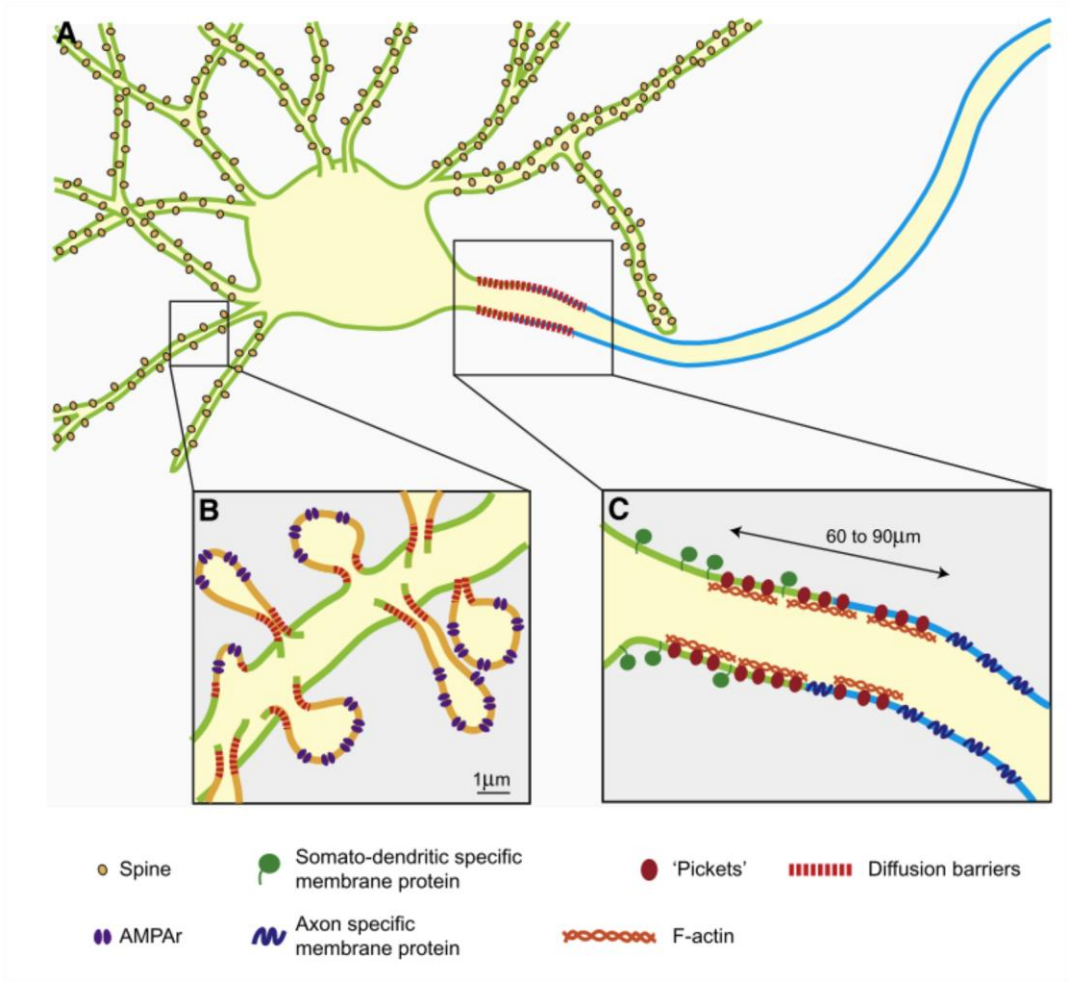


Figure 1.2 Compartmentalisation of neurons.
A) Schematic demonstrating the segregation of the plasma membrane of neurons into the somatodentritic compartment (green), the axon (blue) and the dendritic spines (orange circles). At the axon initial segment is a diffusion barrier (red dashed line) that facilitates the differentiation of the axon. **B)** Magnification of the dendritic spines showing the diffusion barrier at the neck (red) that separates the post-synaptic membrane from the rest of the somatodentritic membrane, restricting the diffusion of receptors (such as the AMPA receptor, purple). **C)** Magnification of the initial segment of the axon, highlighting the diffusion barrier maintained by association of the actin cytoskeleton with membrane proteins, forming a picket fence (from Caudron & Barral, 2009).

1.2. Maintenance of a specialised membrane

To be able to preserve specialised regions of plasma membrane, the cell must first be able to direct the required proteins and lipids to these sub-domains. Once they reach their target membrane, there must also be “barriers” in place to prevent the lateral diffusion of these molecules across the plasma membrane. For *T. brucei*, the precise strategies used to maintain its distinctive surface architecture are predominately unknown; yet in other eukaryotes, a range of mechanisms are employed.

1.2.1. Physical barriers

One way in which a cell can divide the plasma membrane into distinct domains is by creating physical barriers between them. An example of this is the aforementioned segregation of apical and basolateral membranes in epithelial cells, the boundary of which is defined by a tight junction. This type of junction is a multiprotein complex composed predominately of tetra-spanning transmembrane proteins, claudins and occludins (Furuse et al. 1998, 1993). Claudins in particular form the protein strands that cross the lateral junction between adjacent epithelial cells, which prevent the passage of lipids between the outer leaflets of the apical and basolateral membranes (Furuse 2010). In addition, their ion-transporting properties facilitate the passage of molecules in-between cells in the epithelial layer (Tang and Goodenough 2003; Hartsock and Nelson 2008). The function of the tight junction as a diffusion barrier was exemplified using fluorescently-labelled lipids which, when inserted into the apical membrane, could not diffuse past the tight junction and onto the basolateral membrane (Dragsten et al. 1981). In addition to distinct lipid compositions, the proteomes either side of this barrier also differ (Stoops and Caplan 2014). It has been speculated that the movement of transmembrane and lipid-anchored proteins could also be restricted by the tight junction, although at present experimental evidence to support this hypothesis is lacking.

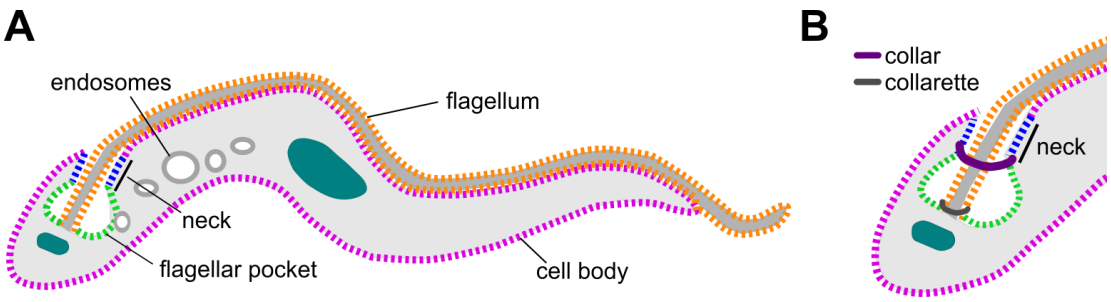


Figure 1.3. Surface architecture of *Trypanosoma brucei.*
A) Schematic representation depicting the distinct domains of the surface membrane of *T. brucei:* the cell body (magenta), flagellum (orange), flagellar pocket (green) and the neck (blue). In teal is the mitochondrial and nuclear DNA. **B)** Higher magnification of FP region showing the two cytoskeletal structures located at the boundaries between the FP and neck membranes (collar) and the FP and flagellum membranes (collarette).

Other examples of protein-based diffusion barriers involve a family of GTP-binding proteins known as septins. In yeast, the organism in which they were first described, septins form a ring-shaped structure at the site of bud emergence during cytokinesis (Longtine and Bi 2003). Here, they are involved in recruitment of proteins to the site of bud formation (Gladfelter et al. 2001), as well as preventing the free diffusion of membrane proteins between mother and bud (Takizawa et al. 2000). Often associated with regions of membrane curvature (Bridges et al. 2016), septins are also found at the base of the primary cilium in mammalian cells, where they are required for maintaining the distinct protein compositions of the ciliary and plasma membranes (Hu et al. 2010). Additionally, at the annulus of sperm cells, septins create a division between the posterior and anterior regions of the tail membrane (Ihara et al. 2005). Sequestration and redistribution of proteins between these regions (and indeed the head region) is critical for the functionality of spermatozoa up to the point of egg fertilisation (Flesch and Gadella 2000; Caudron and Barral 2009)

Cytoskeletal structures can also play a role in the specialisation of cell surface membranes. Situated just beneath the plasma membrane, the cortical cytoskeleton forms an actin-based mesh, which plays a role in protein distribution within the bilayer via interactions with the cytoplasmic tails of transmembrane proteins (Fujiwara et al. 2002; Kusumi et al. 2010). The anchorage of these transmembrane proteins to the actin cytoskeleton can form structures resembling a picket-fence (Fujiwara et al. 2002). This then poses an

obstacle to both lipid-anchored and peripheral membrane proteins, creating nanodomains within the lipid bilayer that molecules can “hop” between (Fujiwara et al. 2002). As the actin cytoskeleton is a highly dynamic structure (reviewed in Letort et al. 2015), it is likely that these nanodomains are being constantly remodelled. Consequently, the actin cytoskeleton is unlikely to form permanent membrane barriers, like the aforementioned tight junction of epithelial cells. Yet, the presence of these picket-fence-like structures could instead contribute to membrane specialisation as it affects the mobility of proteins and lipids within membrane regions (Fujiwara et al. 2002; Trimble and Grinstein 2015).

The actin cytoskeleton also functions in the generation of a more permanent protein diffusion barrier, the one that occurs between the axonal and somatodendritic domains of neurons. Here, a region of highly condensed transmembrane proteins are formed via their anchorage to F-actin in the underlying cytoskeleton. These transmembrane proteins form “pickets” that prevents the free diffusion of molecules between the two regions (Nakada et al. 2003). Supporting this, the depolymerisation of F-actin decreased the number of immobile molecules at this membrane boundary (Winckler et al. 1999; Nakada et al. 2003). A second diffusion barrier has also been suggested in the same region, involved in the retention of Tau protein in neurons. This barrier resembles a valve as it facilities transport of Tau into axon but prevents retrograde transport back into the somatodentritic compartment (Li et al. 2011). Furthermore, failure of this diffusion barrier has been linked to the onset of neurodegenerative diseases (Li et al. 2011), thus reiterating the importance of correct membrane organisation.

1.2.2. Membrane properties

The intrinsic properties of the lipid bilayer itself can also contribute to surface membrane organisation by introducing local membrane asymmetry, which can impair the mobility of membrane proteins and lipids. One way this can occur is when lipids with altered head or tail groups are inserted into a section of membrane creating defects in lipid packing, which can produce membrane curvature. Indeed, as mentioned above, regions of membrane

curvature can promote the association of proteins (such as septins) with known functions as diffusion barriers (Bridges et al. 2016; Hu et al. 2010; Takizawa et al. 2000). Membrane curvature can also be generated upon force provided by cytoskeletal components. The cytoskeleton can push on membranes to force a protrusion, constrict the neck of a membrane invagination, or modify tubular/circular membrane compartments with assistance from motor proteins (Jarsch et al. 2016).

Membrane electrostatic properties can also influence protein location within the lipid-bilayer. This is largely dictated by the presence of the negatively charged lipid phosphatidylserine, which is typically enriched on the plasma membrane compared to the endoplasmic reticulum (ER) (Bigay and Antonny 2012). The influence of electrostatics on protein localisation within the membrane has been exemplified by G proteins, whereby their locations on either the plasma membrane or endosomes are dependent on the number of basic residues in their C-terminal regions (Ahearn et al. 2011; Magalhaes and Glogauer 2010).

In addition, the height of membrane lipids, dictated by the length of the acyl chains, can influence protein localisation. This is evident along the secretory pathway, as a systematic analysis of bitopic transmembrane domains in vertebrates and fungi revealed a bias for shorter transmembrane domains in the ER and Golgi, and longer transmembrane domains in the endosomes and plasma membrane, correlating with differences in bilayer thickness (Sharpe et al. 2010).

Lipid bilayer composition can also be used to generate dynamic lateral nanodomains on a submicron scale within a continuous membrane. The formation of these lipid rafts, via the aggregation of sterols and sphingolipids, promotes the localisation of GPI (glycosylphosphatidylinositol)-anchored and acylated proteins to these nanodomains. In addition, protein localisation within a membrane can be influenced by its ability to associate with certain lipids, or indeed with other proteins, via specific domains. Examples of this include proteins with pleckstrin homology (PH) domains that can associate with phosphoinositides, or proteins with Src Homology 2 (SH2) domains that can

recognise phosphotyrosine residues on other proteins (Lemmon 2008; Pawson 2004; Trimble and Grinstein 2015).

1.2.3. Active protein targeting

Besides controlling the organisation of proteins and lipids within a given membrane using the mechanisms described above, the cell can be selective towards the proteins it delivers to these membranes in the first instance. One way in which this can be achieved is via the polarised trafficking of proteins to different subdomains of the plasma membrane. This mechanism is used, for example, to deliver specific proteins to the apical or basolateral domains of epithelia, and the growing bud of yeast (Trimble and Grinstein 2015). Alternatively, a cell can perform endocytosis and exocytosis in close proximity of one another, forming a focal zone of uptake and secretion (Wahl et al. 2013). Here, the constant regeneration of proteins within this zone could possibly alleviate the need for a diffusion barrier to maintain a distinct membrane composition.

Sorting signals contained within a protein can also influence which membrane, or region of membrane, they are distributed to. This is indeed the case for the direction of proteins to either the apical or basolateral membranes of epithelia. For example, the delivery of integral or secreted proteins to the basolateral membrane is often linked to the presence of tyrosine or leucine-containing motifs within the proteins cytosolic region (Stoops and Caplan 2014). Although less is known with regards to the targeting of transmembrane proteins, some transporters can dimerise with their associated single-pass subunits, which convey the relevant sorting information (Castorino et al. 2011). Alternatively, it has been shown that the N-terminal cytosolic region of multipass transporters, possibly in combination with their cytosolic C-terminus, can affect protein basolateral targeting (Kuo et al. 2013).

Direction of proteins to the apical domain is seemingly more complex; sorting signals can reside within any protein domain, and can include protein, lipid and sugar moieties (Stoops and Caplan 2014). For GPI-anchored proteins, oligomerisation is necessary for sorting to the apical domain, which in turn is thought to be dictated by the GPI-attachment signal, and thus the GPI

anchor itself (Paladino et al. 2008). In addition, transmembrane domains themselves have been implicated in the apical sorting of both single and multipass transmembrane proteins (Dunbar et al. 2000; Brock et al. 2005). The attachment of sugars to a protein, via N- or O-linked glycosylation can also influence a proteins apical fate. This has so far been determined using glycosylation-deficient cells or site-directed mutagenesis approaches, where in some instances the originally apical protein then localised to the basolateral membrane (Stoops and Caplan 2014). It is also possible that, given the established role of glycosylation in protein folding and stability (Xu and Ng 2015), by removing these residues, proteins are mis-targeted due to a change in conformation that masks the genuine targeting signal, rather than the glycans themselves.

1.3. Transport between membrane compartments

The transfer of material between membrane compartments within a cell is mediated by vesicles that bud from one membrane and fuse with another. This can occur via two major routes: the inward endocytic and the outward secretory pathways. Endocytosis encompasses the internalisation of macromolecules and receptors at the plasma membrane into endosomes, which either mature into late endosomes destined for degradation by the lysosome, or are recycled back to the surface membrane. Whilse the exocytic pathway traffics proteins and lipids from the ER/Golgi to the plasma membrane for secretion.

1.3.1. Vesicle formation

Prior to its transport, material is typically packaged into vesicles, the process of which comprises five main stages: initiation, cargo selection, coat assembly, scission and uncoating (Figure 1.5). At the plasma membrane the most-well characterised vesicles are those coated in clathrin, which facilitate clathrin-mediated endocytosis (CME) (Figure 1.4). CME occurs in all eukaryotic cells and is utilised for a wide range of functions, including the regulation of surface protein expression, nutrient uptake and environmental sensing (McMahon and Boucrot 2011; Elkin et al. 2016).

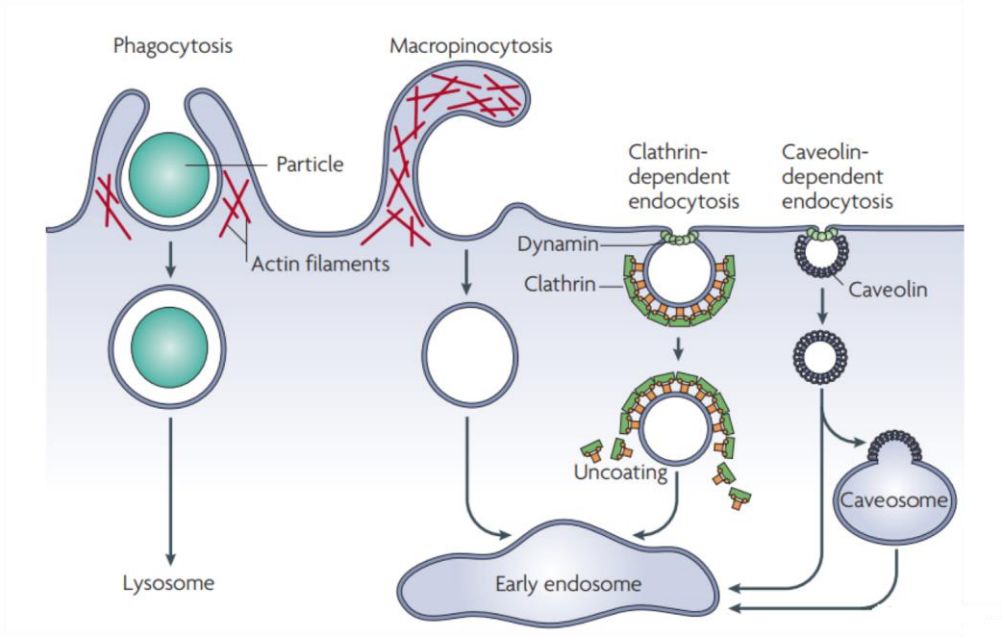


Figure 1.4. Pathways of entry into cells.
Diagram summarising the major routes of entry to a cell via clathrin-dependent or clathrin-independent (phagocytosis, micropinocytosis, caveolin-dependent) mechanisms (adapted from Mayor & Pagano 2007).

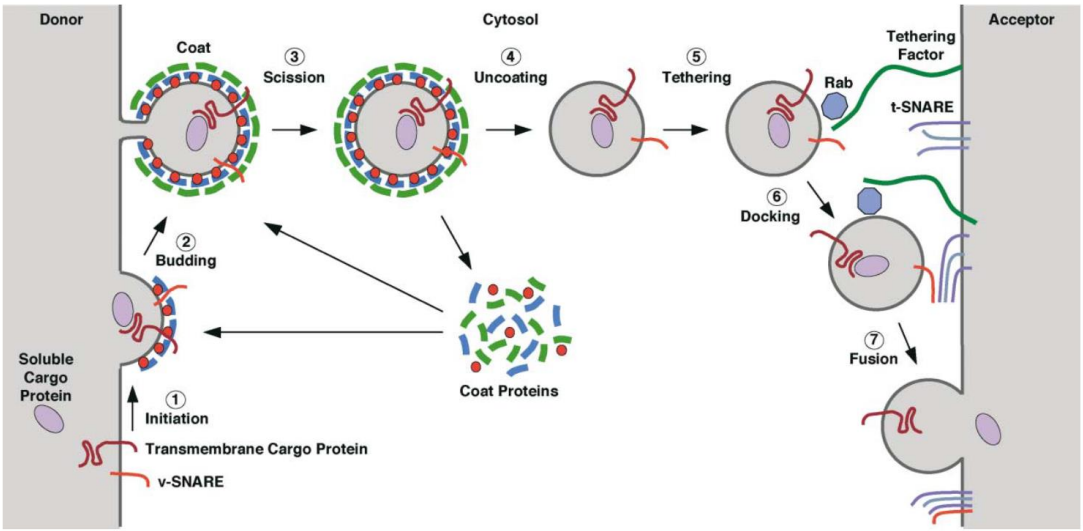


Figure 1.5. Steps of vesicle assembly, budding and fusion.
Diagram highlighting the key steps required for the budding of a vesicle from one membrane to another (from Bonifacino & Glick, 2004)

Vesicle formation is initiated by the recruitment of adaptor protein (AP) 2 to the plasma membrane. This can occur via the binding of AP2 to endocytic motifs present on the cytoplasmic tails of receptors, or to the phosphatidylinositol lipids $PI(4,5)P_2$ enriched at the plasma membrane (Höning et al. 2005; Cocucci et al. 2012). The range of different functions of CME are in part due to the versatility in the cargo it can transport. Clathrin itself does not bind to receptors, so cargo selection is regulated by AP2 in combination with associated adaptor proteins (Edeling et al. 2006). Some cargo adaptors such as epsin N-terminal homology (ENTH) and AP180 amino-terminal homology (ANTH) proteins have proposed roles not only in cargo selection, but in generating membrane curvature and vesicle formation (Ford et al. 2002; Ford 2001; McMahon and Boucrot 2011).

The concentration of adaptors on the membrane provides the nucleation site of clathrin assembly. At this site, clathrin triskelia polymerise to form the classic lattice structure (made up of pentagons and hexagons), building a cage around the vesicle (Cheng et al. 2007). Vesicle budding is dependent on the recruitment of dynamin, which in turn is recruited by BAR domain-containing proteins (Ferguson et al. 2009). The intrinsic concave shape of BAR domain proteins promotes their association with the high curvature at the neck of the bud. Once recruited, dynamin polymerises around the neck region and vesicle scission is thought to be induced upon a GTP hydrolysis-dependent conformational change (Hinshaw and Schmid 1995; Sweitzer and Hinshaw 1998; Bashkirov et al. 2008). After membrane detachment, the vesicle is uncoated via ATPase heat shock cognate 70 (HSC70) and additional cofactors (Schlossman et al. 1984), enabling it to fuse with its target endosome. Clathrin components are released back into the cytoplasm ready for use in subsequent vesicle formation (Figure 1.5).

It should be noted that, although CME is the most prominent form of uptake, clathrin-independent endocytosis (CIE) can also occur (Figure 1.4), but the mechanisms and cargo specificity are less well understood (Hansen and Nichols 2009; Mayor et al. 2017). Uptake via caveolae, or “little caves”, bears some resemblance to CME in that it involves the formation of pits (flask-shaped membrane invaginations), recruitment of dynamin for budding and the

involvement of adapter proteins (cavins) that assist in membrane curvature (Busija et al. 2017). Caveolae are established when caveolins, the major component of these invaginations, fuse with the cell surface membrane in association with lipid rafts (Parton and Collins 2016). Other modes of internalisation also include micropinocytosis: the internalisation of extracellular fluid via ruffled regions of plasma membrane, and phagocytosis, whereby opsonised material is taken up through the formation of membrane protrusions around the target cargo (Mayor and Pagano 2007; Hansen and Nichols 2009; Mayor et al. 2017).

1.3.2. Vesicle trafficking and fate

Following budding, vesicles are translocated across the cytoplasm. For long range transport, this involves a mixture of free diffusion motion coupled with short bursts of active transport along a cytoskeletal track of actin or microtubules (Zajac et al. 2013). The latter requires the action of motor proteins, and in mammalian cells, vesicle trafficking typically begins on the actin cytoskeleton directly beneath the plasma membrane, at the site of vesicle budding. Here, myosins, a family of ATP-dependent motor proteins with actin-based motility, associate with the budding vesicle, often aiding in the budding process (Cheng et al. 2012; Granger et al. 2014). In order to move away from the cell cortex, the vesicles are transferred to a microtubule-based motor (i.e. kinesin or dynein). The structure and function of these two motor proteins are discussed in greater depth in Chapter 6. In a typical mammalian cell, the inward movement of endosomes is predominately performed by dynein, due to its minus-end directed motility (Granger et al. 2014). Indeed, the role of dynein in endosomal transport has been demonstrated via dynein inhibition experiments, and the consequential disruption of endosome motility both *in vitro* and *in vivo* (Bananis 2004; Zajac et al. 2013). Conversely, the outward motility of vesicles, back towards the cell cortex, is generally facilitated by plus-end directed kinesins, namely Kinesin-3, but Kinesin-1 and -2 also can also move endosomes, at least *in vitro* (Granger et al. 2014).

Targeting of vesicles to specific membranes occurs via interactions with tethering and fusion machinery, present on both the vesicle itself and the

acceptor membrane (Figure 1.5). A further level of regulation is provided by members of the Rab GTPase family, which often mediate these tethering and fusion events (Numrich and Ungermann 2014). When in their active GTP-bound states, Rabs can associate with effector molecules, such as the membrane tethering complexes HOPs and CORVET, or indeed the motor proteins required for the initial vesicle trafficking steps (Numrich and Ungermann 2014). The latter has been exemplified by co-immunoprecipitation of dynein with Rab5 (Satoh et al. 2008). Each Rab protein has a characteristic vesicular localisation within the endocytic and secretory pathways, and thus can be used as a marker for vesicle type. For example, early endosomes are usually enriched in Rab5, while late endosomes in Rab7, and recycling endosomes in Rab11 (Harris and Littleton 2011). Once vesicles reach their target membrane, tethering complexes form an initial vesicle-membrane attachment, to dock the vesicle (Figure 1.5). As part of the docking process, SNAREs (soluble N-ethylmaleimide sensitive factor attachment protein receptor) on the vesicle and target membranes (V-SNAREs and t-SNAREs, respectively) combine to form a helical bundle, which initiates fusion of the lipid membranes (Chia and Gleeson 2014).

1.4. Surface membrane specialisation in *Trypanosoma brucei*

For unicellular organisms, the plasma membrane must be highly specialised in order to perform all the key surface functions necessary for its survival and proliferation as a single entity. For example, as a parasite of the mammalian bloodstream, *T. brucei* must perform basic cell functions, such as nutrient uptake and secretion, whilst modulating infection dynamics and avoiding elimination by the host immune system (Gadelha et al. 2011). This is made possible by the specialisation of its surface landscape into at least four morphologically distinct membrane regions already mentioned earlier: the cell body, the flagellum, the flagellar pocket and the neck membranes. The first three of these domains are considered to be biochemically distinct, with different intramembrane particle (IMP) densities found in each, in combination with evidence of discrete surface protein localisation to one or more of these subdomains (Gadelha et al. 2009, 2015). While the IMP density in the neck domain is similar to that of the cell body membrane, indicating these

membranes may be similar in protein composition (Gadelha et al. 2009). The relative contribution each of these domains makes towards the success of this parasite, as well as the mechanisms in place to maintain surface compartmentalisation, will be discussed below.

1.4.1. The trypanosome surface

1.4.1.1. Major surface coats

As an exclusively extracellular parasite, remodelling of the surface coat facilitates the adaption of the cell to the contrasting environments of the insect vector and mammalian host (Figure 1.6). Within the tsetse fly midgut, procyclic form (PCF) parasites are coated in procyclin; generating a protease-resistance layer against the digestive enzymes of the tsetse midgut (Roditi et al. 1989). There are two main variants of procyclin: EP(1-3) and GPEET containing distinct C-terminal repeat regions Glu-Pro and Gly-Pro-Glu-Glu-Thr, respectively (Vassella et al. 2000; Mowatt et al. 1989). Initially, both variants are expressed, then after 7-9 days of infection (which coincides with parasite entry to a different portion of the midgut) GPEET is repressed, indicative of its role in establishing the initial fly infection (Acosta-Serrano et al. 2001). Upon colonisation of salivary glands of the fly, differentiation to epimastigotes is coupled with an upregulation of an alanine-rich protein (BARP) in place of procyclin (Urwyler et al. 2007). While, in preparation for entry into the mammalian bloodstream, the surface of metacyclic trypanosomes is altered once more, to one composed of metacyclic variant surface glycoprotein (mVSG) (Graham and Barry 1995; Ramey-Butler et al. 2015).

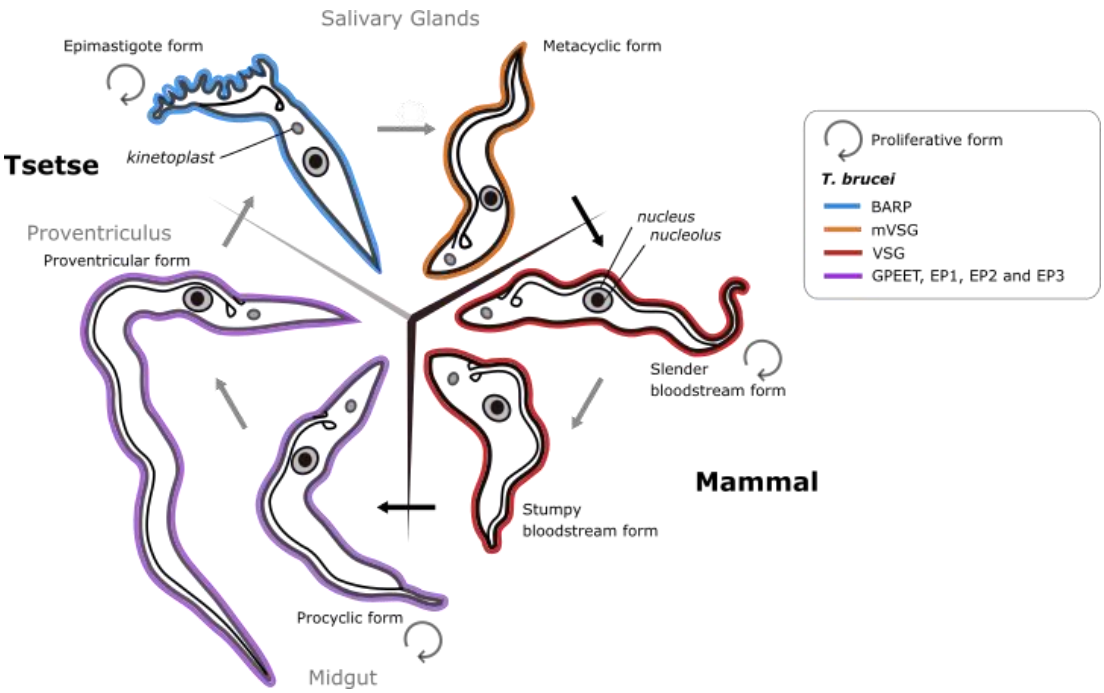


Figure 1.6. Major surface protein coats expressed during the *T. brucei* life cycle. Diagram highlighting the key stages of the *T. brucei* life cycle. Different coloured outlines of the cell correspond to a different surface coat type (see legend). Bold arrows indicate a switch between host and vector stages. Courtesy of Jennifer McDonald, University of Nottingham.

During the mammalian host stages, approximately 5 million GPI-anchored VSG dimers form the major cell surface constituent of the parasite (Cross 1975). The attachment of the protein to the membrane via a C-terminal GPI anchor is a commonality between the different life cycle-specific proteins coats, including procyclins, BARP and mVSGs. By coating the cell with a dense VSG monolayer, this is thought to provide a physical barrier protecting the parasite from elimination by complement-mediated lysis (Schwede et al. 2015). In support of this, it has been shown that immunoglobulins can only bind the membrane-distal N-terminal region of VSG on live cells, whilst the membrane-proximal C-terminal region is seemingly shielded (Schwede et al. 2011). Another attribute of the VSG coat is that it is highly immunogenic, and as a consequence the host eventually builds up sufficient antibodies against it to eliminate the parasites from the bloodstream. To overcome this, *T. brucei* has evolved an intuitive mechanism of antigenic variation, in combination with a rapid endocytic system capable of turning over the cell-surface pool of VSG within 12 minutes (Engstler et al. 2004; Mugnier et al. 2015).

Antigenic variation relies on the monoallelic expression of a single VSG variant on the cell surface at any one time. *T. brucei* then periodically switches to the expression of an immunologically distinct variant, preventing population elimination (Horn 2014). This results in consecutive waves of parasitaemia that reflect the parasite clearance by the host humoral response, and subsequent outgrowth of those that have switched their VSG coat (Ross and Thomson 1910; Mugnier et al. 2015).

The unusual genome architecture of the parasite contributes in part to its ability to perform antigenic variation. *T. brucei* is a diploid organism and its genome is organised into 11 homologous pairs of megabase chromosomes (MBCs, 1-6 Mb), ~5 intermediate chromosomes (ICs, 200-900 kb) and ~100 minichromosomes (MCs, 50-150 kb) (Daniels et al. 2010). The transcription of *VSG* occurs from one of ~15 BSF expression sites (BESs) located subtelomerically on the MBCs and ICs chromosomes (Hertz-Fowler et al. 2008). It has been shown that transcription is initiated from multiple BESs, but only stabilised in a single BES, and monoallelic expression of the active *VSG* occurs within a discrete site within the nucleus, referred to as the expression site body (ESB) (Kassem et al. 2014; Navarro and Gull 2001).

A vast library of over 2500 *VSG* genes (~80% of which are considered pseudogenes) are maintained across the MBCs, ICs and MCs (Cross et al. 2014). *VSG* genes from these libraries can be introduced into the active BES by homologous recombination between subtelomeres, or via duplicative gene conversion events which replace and delete the existing *VSG* gene (McCulloch et al. 1997; Hovel-Miner et al. 2016). Alternatively, expression of the active BES can be silenced, and transcription from one of the other ~15 activated instead, referred to as an *in situ* switch (Michels et al. 1984). VSG switching is thought to occur at rate of ~1 in every 100 generations in the host, compared ~1 in every 10,000 generations in culture (Turner 1997; Aitcheson et al. 2005), with the reduced rate seen in culture is presumably due to the lack of immune pressure from the host.

1.4.1.2. Other surface-localised proteins

Although it is certainly the most abundant, VSG is not the only protein localised to the surface membrane of BSFs. Various members of the invariant surface glycoprotein (ISGs) family also reside here, of which ISG65 and ISG75 have been best characterised (Ziegelbauer and Overath 1992, 1993). The nomenclature of these type I transmembrane proteins reflects their apparent molecular weights of 65 and 75 kDa, and they are present on the surface at approximately 70,000 and 50,000 copies per cell, respectively (Ziegelbauer and Overath 1993). This equates to roughly one ISG molecule for every 50 VSGs, reinforcing the dominance of VSG at the cell surface. Despite their identification over 20 years ago, the function of ISGs at the surface is still unknown. Recently, ISG75 has been implicated in the uptake of the trypanocidal drug suramin, suggesting it could function as a receptor for host ligands (Alsford et al. 2012). Other surface localised proteins include Proteins Associated with Differentiation (PADs) and a family of pyruvate transporters (TbPT1-5). Due to its life-cycle-stage dependent expression and surface localisation, PAD1 is commonly used as a surface membrane marker for identifying differentiated, quiescent BSF parasites; while PAD2 only localises to the cell body membrane when the parasite enters the fly, promoting differentiation of BSFs to PCFs (see section 1.4.3.4) (Dean et al. 2009). On the other hand, the *TbPT* family are involved in pyruvate export. In BSFs, pyruvate is the major end product of glycolysis and, if not secreted, is toxic to cells (Sanchez 2013).

Knowledge of the parasite surface protein landscape has increased dramatically in recent years, following the publication of two surface membrane proteomes (Shimogawa et al. 2015; Gadelha et al. 2015). Shimogawa and colleagues isolated novel surface proteins in both BSFs and PCFs by chemically modifying the cell surface with biotin, coupled with the affinity purification of biotin-associated material and mass spectrometry. The differences in protein enrichment noted between the BSF and PCF proteomes reinforces the drastic surface re-modelling these parasites undergo in order to adapt to the different environments of the vector and host (Shimogawa et al. 2015).

Gadelha and colleagues took a slightly different approach towards the identification of novel surface components. They chose to focus specifically on BSF cells, with the aim of identifying novel proteins involved in host-parasite interactions, and labelled the cell surface with fluorescein instead of biotin, and included unlabelled and dead cell fractions as controls. An alternative surface labelling procedure was chosen because trypanosomatids have been shown to incorporate biotin in their endogenous proteins *in vivo,* and indeed when testing the biotin-avidin based system, a high background was observed in unlabelled cells (Gadelha et al. 2015). Validation of 23/175 BSF surface proteome (or “surfeome”) components by cellular localisation, revealed a set of 18 novel surface proteins, termed ESPs for Enriched in Surface Proteome. The majority of these were found to localise to the FP; given that they were identified using a technique that labels the whole plasma membrane, this enrichment at the FP conforms to the idea that the majority of invariant receptors are sequestered within this membrane domain. Another key observation from the surfeome dataset was that most proteins identified were specific to kinetoplastids, with the majority of GPI-anchored proteins confined to African trypanosomes (Gadelha et al. 2015). This distribution suggests that GPI-anchored proteins, which predominate on the surface of *T. brucei* and related parasites, have evolved to suit their different parasitic lifestyles.

This certainly appears to be the case for *Trypanosoma cruzi* and *Leishmania* species, which cause Chagas disease and Leishmaniasis respectively. Like *T. brucei*, these parasites cycle between mammalian hosts and insect vectors, although, within the host they both adopt primarily intracellular lifestyles (de Morais et al. 2015). Consequently, their surface protein repertoire has adapted accordingly. For *T. cruzi*, the major surface constituents during mammalian host stages are transialidases, mucins and mucin-associated proteins (MASPs), all encoded by large heterogeneous gene families. Notably, mucins and MASPs are exclusive to *T. cruzi,* while a reduced cohort of transialidases are present in *T. brucei,* and completely absent from *Leishmania* spp*.* (De Pablos and Osuna 2012)*.* Conversely, the success of *Leishmania* can be attributed to a surface of lipophosphoglycans (LPGs), glycosylinositol phospholipids and gp63 molecules (de Morais et al.

2015). Collectively, the surface molecules of *T. cruzi* and *Leishmania* predominately function in host-cell invasion and intracellular survival once they gain entry to host cells (Bartholomeu et al. 2014), while the surface of *T. brucei* is clearly adapted for immune evasion.

1.4.2. Flagellar membrane

T. brucei possesses a single flagellum which emerges from the FP at the posterior end of the cell and is attached along the cell body for most of its length by a flagellum attachment zone (FAZ). As well as the organelle as a whole functioning in cell motility and division (Langousis and Hill 2014), proteins within the flagellar membrane have also been implicated in parasite virulence, thus reinforcing the importance of maintaining a distinct flagellar proteome. These include glycosylphosphatidylinositol–phospholipase C (GPI-PLC), calflagins and ESAG4.

GPI-PLC is BSF-specific and, along with calflagins (calcium-binding proteins), is required for parasite virulence in mice (Webb et al. 1997; Emmer et al. 2010; Sunter et al. 2013). In addition, GPI-PLC promotes the release of VSG from the surface membrane, and thus is critical for VSG shedding during differentiation to PCFs (Grandgenett et al. 2007). On the other hand, (GR)ESAG4, a family of adenylate cyclases that catalyse the conversion of ATP to cAMP (Paindavoine et al. 1992), have been shown to function in modulating the host innate immune response by inhibiting tumour necrosis factor alpha production (Salmon et al. 2012b). Importantly, the flagellar membrane can also release dynamic nanotubules that go on to form extracellular vesicles containing *T. brucei* virulence factors (including (GR)ESAG4 and GPI-PLC), facilitating protein exchange between cells (Szempruch et al. 2016).

Other flagellar membrane-localised proteins have been identified from proteomics studies on isolated flagella (Oberholzer et al. 2011; Subota et al. 2014). The first of these identified a handful of novel flagellar membrane proteins, resembling putative receptors and transporters that were upregulated in BSFs (Oberholzer et al 2011). The second proteomics study then went on to identify a further 9 flagellum-associated proteins. Strikingly the majority of

these proteins localised to distinct regions along the flagellar membrane, demonstrating the presence of additional protein subdomains within the flagellum (Subota et al. 2014).

1.4.3. Flagellar pocket

1.4.3.1. Architecture

The flagellar pocket (FP), an invagination surrounding the base of the flagellum, is a conserved element of trypanosomatid biology. It has morphological and functional similarities to the ciliary pocket found at the primary and motile cilia in mammalian cells (Molla-Herman et al. 2010). The FP of *T. brucei* and its surrounding cellular architecture have been defined in great detail by a combination of electron microscopy and tomography techniques (Figure 1.7C-E) (Lacomble et al. 2009; Gadelha et al. 2009; Lacomble et al. 2010). Polarised towards the posterior end of the cell, the FP is in close proximity with the membranes of the Golgi and ER and distal to the kinetoplast. The kinetoplast is a defining feature of kinetoplastids and contains the parasite mitochondrial DNA (Simpson 1986). Situated between the kinetoplast and the FP are the probasal and basal bodies, which are physically connected to the kinetoplast via the Tripartite Attachment Complex (Ogbadoyi et al 2003). From the basal body originates the flagellum, which intersects the FP lumen and emerges through the flagellar pocket neck (Lacomble et al. 2010).

The flagellar pocket membrane is continuous with that of the cell body and flagellum membranes; the junctions of which are abutted by two electron dense structures: the collar and collarette, respectively (Figure 1.3, Figure 1.7) (Gadelha et al. 2009). Coinciding with the collarette, yet embedded within the protoplasmic face of the membrane (i.e. the leaflet of the lipid bilayer associated with the cytoplasm), an additional arrangement resembling a ciliary necklace has been observed. This was identified by freeze-fracture electron microscopy which showed clusters of intramembrane particles (IMPs) situated at this membrane junction (Gadelha et al. 2009). Notably, rows of IMPs spanning both the exoplasmic and protoplasmic leaflets of the plasma

membrane have also been observed at the bilayer region bordered by the flagellar pocket collar (FPC) (Gadelha et al. 2009).

A fourth morphological subdomain of the surface membrane also exists, the flagellar pocket neck (Henley et al. 1978; Lacomble et al. 2009), which surrounds the flagellum at the post-collar point of the FP, thus connecting the FP and cell body membranes (Figure 1.7, Figure 1.8). The neck membrane is held in close proximity to that of the flagellum, presumably by the FPC, and a small luminal space between these membranes forms a channel that connects the FP lumen to the extracellular milieu (Gadelha et al. 2009).

The neck channel, which runs along the length of the neck membrane, ranges from 25-150 nm in diameter and provides the only route of macromolecule transport in and out of the flagellar pocket lumen. It is possible that the channel functions as a size-selective barrier to control the movement of molecules, as 20 nm gold particles can enter, while entry is restricted when gold particle size is increased to 40 nm (Gadelha et al. 2009). Given that the 4MTs are closely associated with the neck channel, it is possible that these microtubules provide an active escalator on which motor proteins can transport receptor-bound material between the pocket lumen and extracellular space, facilitating movement of macromolecules across this membrane. It could also be hypothesised that the neck membrane is involved in plasma membrane specialisation. Here, the rows of intramembrane particles present at the neck-flagellar pocket junction (Gadelha et al. 2009) could provide a physical barrier to control the movement of membrane proteins between the flagellar pocket and cell body membranes. Overall, the function of this specialised region of membrane remains to be elucidated.

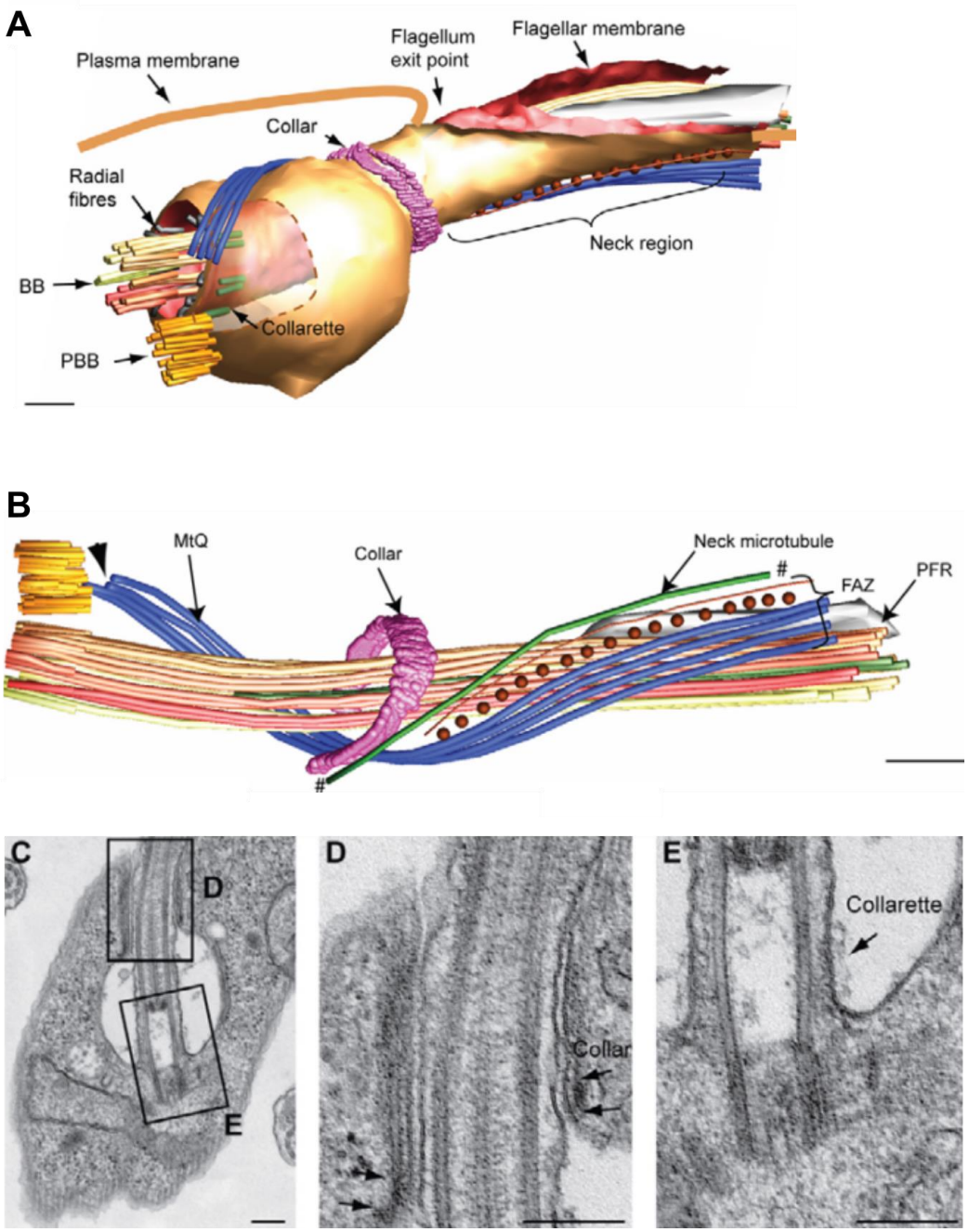


Figure 1.7. Flagellar pocket architecture.
A) Reconstruction of the FP membrane and cytoskeletal architecture by 3D electron tomography. The collar defines the FP and neck membrane barriers, whilst the collarette defines the flagellum boundary. Abbreviations: BB, basal body, PBB, probasal body. **B)** FP cytoskeletal elements with the membranes excluded. Abbreviations: MtQ, four microtubules (or 4MTs); FAZ, flagellum attachment zone; PFR, paraflagellar rod. **C)** Thin section micrographs illustrating the FP boundaries. Rectangles represent the collar and collarette membrane boundaries, with higher magnifications depicted in **D** and **E**. Scale bars: 200nm. From Gadelha et al. 2009)

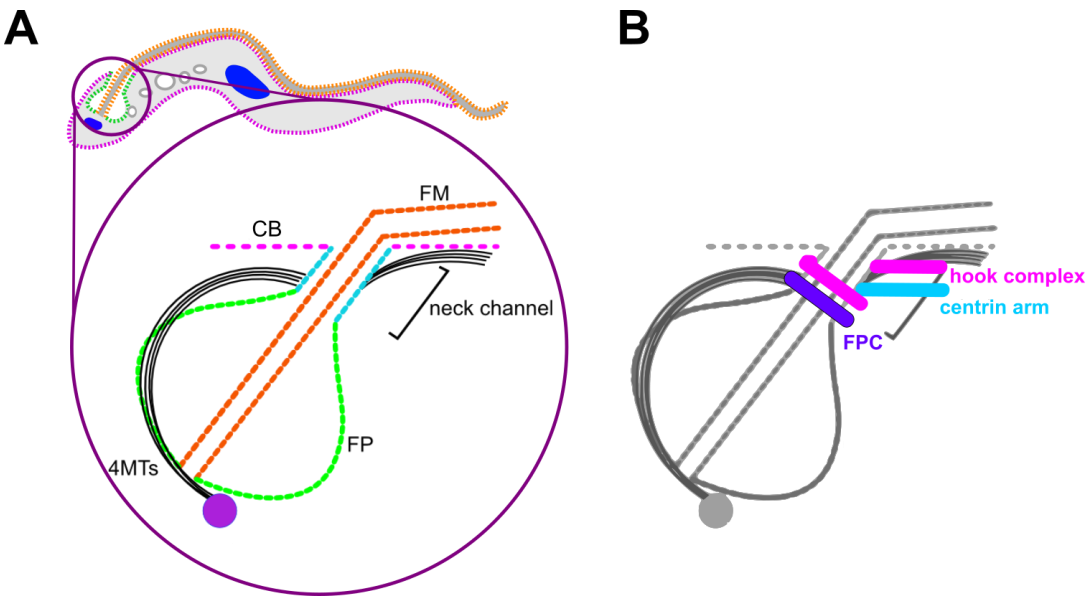


Figure 1.8. Cytoskeletal architecture of the flagellar pocket.
A) Diagrammatic representation of the distinct surface subdomains: the flagellar pocket (FP) membrane, flagellar membrane (FM) and the plasma membrane (PM). Between the FP and PM membrane is the neck membrane (light blue). Connecting the FP lumen to the extracellular space is the neck channel, which is demarcated by a set of 4 specialised MTs, originating between the basal and probasal bodies (magenta circle), and wrapping around the FP in a left-handed helix. **B)** Summary of the major cytoskeletal structures associated with flagellar pocket. These include the flagellar pocket collar (FPC), the hook complex and the centrin arm.

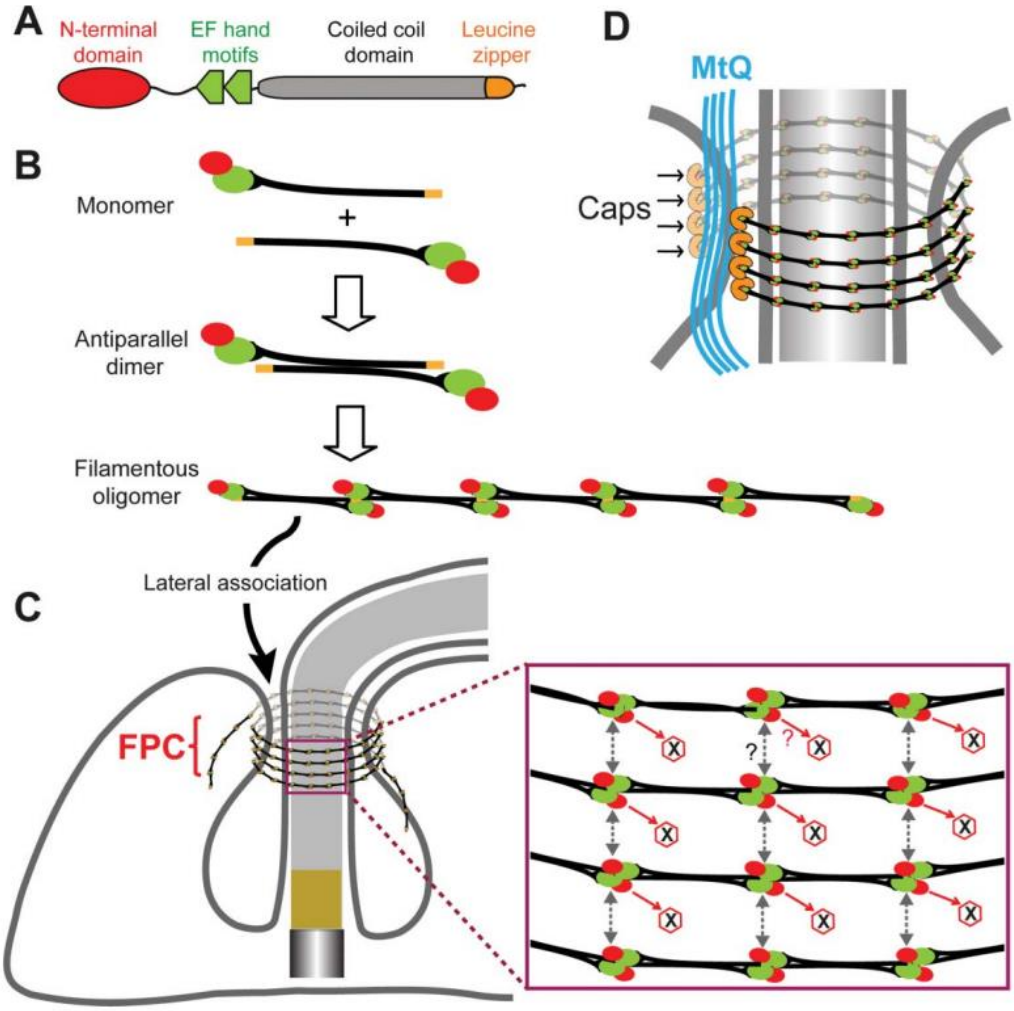


Figure 1.9. Structural domains and putative assembly mechanism of BILBO1.
A) Schematic representation of the 4 main structural domains of BILBO1. **B)** Hypothetical model of BILBO1 filament formation. **C)** Hypothetical model showing formation of a solenoid-like BILBO1-containing structure that encircles the flagellar pocket. Enlarged boxed view highlights possible lateral interactions between BILBO1 filaments (grey arrows). Here the N-terminal domain may interact with an unknown FPC component/regulatory protein (shown as hexagons). **D)** An alternative model whereby BILBO1 filaments are arranged into a horseshoe-like structure, capped by a putative capping protein at the tip of the filaments. These filaments are then intersected by the set of four microtubules (MtQ). From Vidilaseris et al. 2015.

1.4.3.2. Associated cytoskeleton

The shape and form of a trypanosome cell is defined by an array of subpellicular microtubules, lying just beneath the plasma membrane (Angelopoulos 1970; Robinson et al. 1991). The FP is the only region of plasma membrane devoid of these microtubules. Yet, other cytoskeletal structures exist in the vicinity of the FP that are likely to contribute to its specialisation. These are the flagellar pocket collar (FPC), the hook complex, the centrin arm and a set of four rootlet microtubules (4MTs) (Figure 1.8).

At present, the only published component of the horseshoe-shaped FPC is the cytoskeletal protein BILBO1, of which orthologues are encoded in all sequenced kinetoplastid genomes to date (Bonhivers et al. 2008; Perdomo et al. 2016). BILBO1 is composed of at least four structural domains (Figure 1.9A): an ubiquitin-like N-terminal domain, two EF-hand calcium binding domains, a coiled-coil domain and a putative leucine zipper (Vidilaseris et al. 2014; Perdomo et al. 2016). Collectively, these domains have been shown to facilitate the formation of anti-parallel BILBO1 homodimers via interactions between the coiled-coil domains (Figure 1.9B), with the EF-hand domains controlling the resultant polymer shape (Florimond et al. 2015). The assembly of BILBO1 into its ring-shaped conformation is proposed to act as a scaffold on which the rest of the FPC can be constructed (Florimond et al. 2015; Vidilaseris et al. 2015).

Identification of BILBO1 in *T. brucei* facilitated the investigation into FPC biogenesis and function. Bonhivers and colleagues observed that during cell division, the existing FPC elongates along its principle axis when the kinetoplast is in early S-phase, and then constricts to form two discrete collar structures. The segregation step occurs at the same time as that of the new flagellum, and most likely the new FP too (Bonhivers et al. 2008; Lacomble et al. 2010).

Knockdown of *BILBO1* by RNA interference (RNAi) leads to distinct phenotypes in BSFs and PCFs, both of which prove lethal to the parasite (Bonhivers et al. 2008). In insect forms, cells exhibit elongated morphologies with a detached daughter flagellum (Figure 1.10). Strikingly, thin section

micrographs revealed that at the site of aberrant flagellum growth, the FP (and indeed the FPC) were completely absent, which suggests a role for BILBO1 in FP duplication (Bonhivers et al. 2008). Other implications of *BILBO1* knockdown include the inhibition of flagellum attachment zone (FAZ) formation and cytokinesis defects. These two phenotypes are undoubtedly linked, as the new FAZ forms the site of cleavage furrow initiation during cytokinesis (Robinson et al. 1995). In BSF cells, depletion of BILBO1 was still lethal, but the resultant phenotype was somewhat different. Here, after 12 hours of RNAi induction, spherical rather than elongated cells were produced (Bonhivers et al. 2008). Though, the effect of *BILBO1* knockdown on FP biogenesis in these cells is not yet fully understood.

Located distally to the FPC are at least two other multiprotein cytoskeletal components (Figure 1.8B): the “centrin arm” with a rod-shaped morphology, and the “hook complex”; aptly named due to its hook-like shape that wraps around the FP neck region (Esson et al. 2012; Morriswood et al. 2013). Like BILBO1, orthologues of the major protein component of the hook complex, TbMORN1, can be found in other trypanosomatids, perhaps suggestive of a FP-related function. In support of this, knockdown of *TbMORN1* in BSFs resulted in an enlarged FP (Morriswood and Schmidt 2015), which is generally associated with disruption of FP function (i.e. a defect in endocytosis) (Allen et al. 2003).

Another FP-associated cytoskeletal structure is the set of 4MTs, sometimes referred to as the microtubule quartet (Figure 1.8). These microtubules have the opposite polarity to the subpellicular microtubules (Robinson et al. 1995), and in doing so nucleate between the probasal and basal bodies, then proceed to wrap around the FP in a left handed helix, intersecting the FPC as they pass across the FP neck region (Lacomble et al. 2009). Here they join up with the subpellicular MT array and follow the line of the FAZ along the cell body (Lacomble et al. 2009). The 4MTs are also thought to interact with the arms of TbCentrin4 (a component of the centrin arm) and TbMORN1, providing a link between all the aforementioned cytoskeletal structures (Esson et al. 2012). In addition to the 4MTs, a single microtubule spans the neck region between the collar and the subpellicular array

(Lacomble et al. 2009), yet the polarity and function of this microtubule remain to be elucidated.

The functions of the 4MTs are also not yet fully understood. However, when endocytosis is blocked by cold temperatures, endocytic markers accumulate along the neck channel, specifically at the membrane region bordered by the 4MTs (Gadelha et al. 2009). It is not yet clear why these markers selectively cluster here, or indeed how they migrate away from this zone to be internalised by the FP membrane. Though, it has been suggested that the neck channel may operate as an active escalator for bound marker entry into the FP lumen (Gadelha et al. 2009). The 4MTs could then provide a platform on which molecular motors transport this membrane-associated material into the FP lumen. Alternatively, the accumulation of endocytic markers could be explained by the 4MTs acting as a cytoskeletal barrier to the lateral movement of receptors along this region (Gadelha et al. 2009).

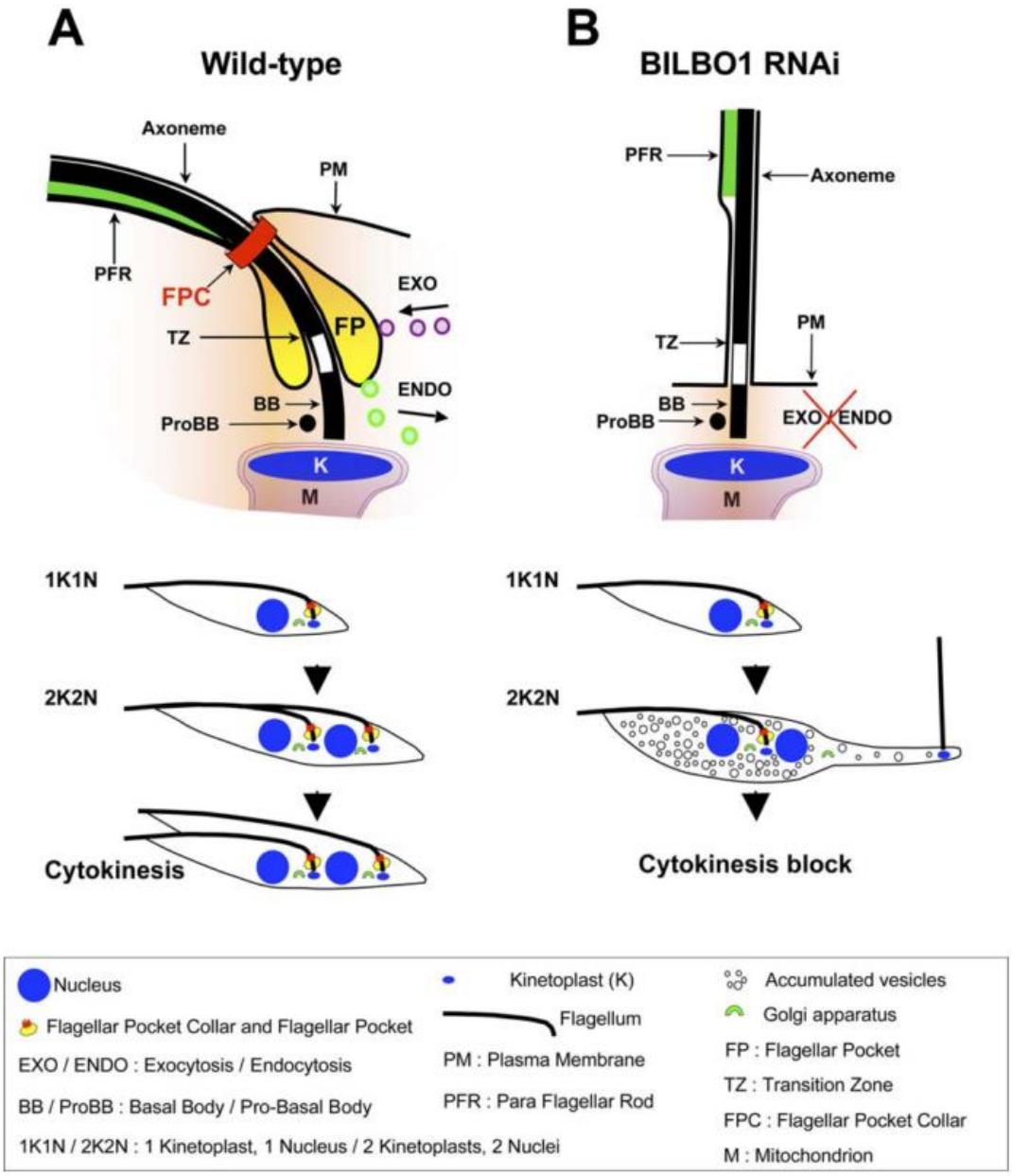


Figure 1.10. Consequences of BILBO1 RNAi knockdown in procyclic cells.
A) Schematic diagram illustrating the cell architecture surrounding the flagellar pocket in wildtype cells, with the stages of normal cell division shown below. Here the four microtubules would originate between the pro-basal and basal bodies, and wrap around the flagellar pocket in a left-handed helix and intersect the FPC (as shown in Figure 1.8 and Figure 1.9). **B)** Abnormal cell architecture and cell cycle progression as a consequence of BILBO1 RNAi knockdown. This shows the key phenotypes observed in the absence of BILBO1, which include flagellum detachment, inhibition of FP biogenesis, inhibition of endo- and exocytosis and block in cytokinesis (from Bonhivers et al., 2008).

Thus far, a single protein has been localised to these rootlet microtubules via immunoprecipitation experiments with TbLRRP1 (another component of the hook complex) (Gheiratmand et al. 2013; Esson et al. 2012). This protein, TbSpef1 (also known as TbCMF18), forms a curved structure that traces the path of the 4MTs from the probasal body, passing through the FPC/hook-complex (Gheiratmand et al. 2013). RNAi depletion of TbSpef1 in both PCFs and BSFs was lethal, producing cells with detached flagella, along with motility and cytokinesis defects (Baron et al. 2007). When Gheiratmand and colleagues focused specifically on post-mitotic TbSpef1 RNAi cells in PCFs, they noted that these cells had not assembled a new set of 4MTs, nor had they been able to duplicate the FPC, hook complex and FAZ (Gheiratmand et al. 2013). This suggests that the 4MTs may be critical for duplication of the FP-associated cytoskeleton. Indeed, the *de novo* formation of a new set of 4MTs is the first visible marker of trypanosome cell division (Lacomble et al. 2010).

1.4.3.3. FP architecture in other trypanosomatids

The flagellar pocket is a key component of trypanosomatid biology, yet there are some differences in FP architecture seen across the pathogenic *T. brucei*, *T. cruzi* and *Leishmania* species, perhaps reflective of their different cell morphologies and parasitic lifestyles. Comparisons between *T. brucei* and *Leishmania* have been aided by the recent 3D reconstruction of *Leishmania* FP architecture, using electron tomography (Wheeler et al. 2016).

Wheeler and colleagues determined that, like *T. brucei*, the *Leishmania* FP is positioned asymmetrically within the cell, with a bulbous shape intersected by the flagellum. There was also evidence of a FPC, followed by a cylindrical neck region connecting the FP to the pellicular membrane. Here, the orthologue of BILBO1 also localises within the vicinity of the FP, yet other aspects of the FP-associated cytoskeleton differ slightly from *T. brucei*. *Leishmania* also possess a set of 4MTs, which wrap around the FP in a left-handed helix passing through a gap in the collar; but there they abruptly terminate at the neck region (as does the FAZ). Given that the *Leishmania* flagellum is not attached to the cell body, this is perhaps expected, and reinforces a strong link between the FAZ and the 4MTs. Another key difference

observed between the FP architecture of *T. brucei* and *Leishmania* is that the FPC appears as a double ring of electron dense material, the relevance of which is not yet understood (Wheeler et al. 2016). Collectively, this suggests a slight alteration in the arrangement of the cytoskeletal architecture associated with the FP in *Leishmania*, but otherwise the overall FP structures are conserved.

Although in-depth characterisation of the FP ultrastructure in *T. brucei* and *Leishmania* have been performed, much less is known about the FP structure of the third member of the pathogenic trypanosome trio, *T. cruzi*. This is perhaps in part because, unlike *T. brucei* and *Leishmania*, the FP is not the principle site of endocytosis in proliferative forms and, consequently, has received less attention. Instead, much of nutrient uptake in *T. cruzi* occurs via a second endocytosis-competent invagination of the surface membrane, the cytostome-cytopharynx complex (Porto-Carreiro et al. 2000). The 'cytopharynx' forms the tubular element of the invagination, whilst the 'cytostome' refers to the region that opens out onto the cell surface membrane (Milder and Deane 1969; Vatarunakamura et al. 2005). Separating the cytostome from the pocket is a specialised domain known as the preoral ridge (De Souza et al. 1978). Recent ultrastructural analysis of the cytostome-cytopharynx complex has provided the first 3D view of this organelle (Alcantara et al. 2014). Although not the primary focus of this work, the close proximity of the FP to the cytostome also meant that the results also shed some light on the ultrastructure of FP, in particular the surrounding cytoskeleton. Like the related trypanosomatids, the FP of *T. cruzi* contains a set of 4MTs that wrap around the flagellar pocket in a helical pattern. However, the presence of a second set of 4MTs was also observed, which originate at the FP and connect to the cytostome-cytopharynx. Further to this, a third set of microtubules was identified, this time in triplet formation, which originated at the cytostome and followed a helical route down the membrane of the cytopharynx (Alcantara et al. 2014). Collectively, this suggests that the two endocytic organelles in *T. cruzi* may have their own set of specialised microtubules, as well as a set that forms a connection between the two. Whether this connection provides an anchorage and/or transport-based function remains to be elucidated. In

addition, the presence of a channel, as seen for *T. brucei,* has yet to be determined. An interesting attribute of the cytostome-cytopharynx complex is that, the only point in the *T. cruzi* life cycle in which is it absent is the extracellular human-infective stage (Vidal et al. 2016), perhaps because it is of detriment to survival in the bloodstream. It could therefore be speculated that this why the cytostome is still present in the closest free-living relative, *Bodo saltans*, yet absent from *T. brucei,* which resides extracellularly in the bloodstream throughout its mammalian host stage (Webster and Russell 1993).

1.4.3.4. Function

The flagellar pocket (FP) of *T. brucei* is the sole site of endo- and exocytosis in the cell, forming the primary interface between parasite and host. It is possible that the ancestral function of the FP primarily concerned the uptake of nutrients, given its conservation across trypanosomatids, including non-pathogenic species. Indeed, due to the organisation of the subpellicular array, it is the only region of the cell where molecules can gain access to the cytoplasm. However, for *T. brucei* at least, the FP has become far more than just a point of entry to the cell, and its current, seemingly central role in parasitism has even prompted the description of the FP as an evolutionary trap, as it has rendered itself indispensable (Field and Carrington 2009). The various functions of the FP in *T. brucei* are highlighted below.

Nutrient uptake

As the principle site of uptake and secretion, the FP is thought to contain the majority of surface-localised receptors and transporters. Indeed, for receptors involved in scavenging nutrients, their restriction to the FP would be advantageous for rapid uptake. This was found to be the case for the two FP-localised receptors that have been extensively characterised to date: the transferrin receptor (TfR) and the haptoglobin-haemoglobin receptor (HpHbR), which scavenge iron and haem, respectively (Salmon et al. 1994; Vanhollebeke et al. 2008).

Like most organisms, *T. brucei* requires iron for growth (Schell et al. 1991). Iron is acquired from the host in complex with transferrin, via the TfR

(Steverding et al. 1995). TfR in *T. brucei* is structurally dissimilar to the human receptor equivalent, as it is heterodimeric and both subunits of the dimer are required for transferrin uptake (Salmon et al. 1994; Steverding 2000; Steverding et al. 2012). The two subunits making up this dimer are encoded by *ESAG6* and *ESAG7* genes (Steverding et al. 1994), which are transcribed in a polycistronic manner alongside *VSG*, from one of the ~15 aforementioned BESs. Homology between the two subunits is found at the N-terminal region, which has also been likened in structure to the N-terminus of VSG (Salmon et al. 1997). However, the C-termini differ, as only ESAG6 has a GPI anchor insertion site, which facilitates receptor attachment to the FP membrane (Steverding et al. 1995; Salmon et al. 1997). Molecular modelling of TfR within the VSG coat predicts that the receptor sits lower than VSG within the pocket membrane, and suggests that access of transferrin to the ligand binding region is facilitated by N-glycosylation of this receptor (Mehlert et al. 2012).

Another ligand that the parasite must acquire from the host is haem. This occurs via the HpHbR, which internalises high density lipoproteins (HDLs). HDLs contain apolipoprotein L1 (ApoL1) and haptoglobin-related protein (Hpr) complexed to haemoglobin (Hb) (Vanhollebeke et al. 2008). HpHbR is also associated to the FP membrane by a GPI anchor, but otherwise bears little structural similarity to either VSG or TfR (Higgins et al. 2013).

A secondary consequence of haem uptake via HpHbR is that the ApoL1 portion of the HDL is actually a trypanosome lytic factor (TLF1), and protects humans from infection by *T. b. brucei* (Vanhamme et al. 2003). Following uptake, ApoL1 is transported to the lysosome, where it forms pores in the surrounding membrane. This facilities the influx of chlorine ions, which causes osmotic swelling and ultimately cell lysis (Pérez-Morga et al. 2005). The two sub-species capable of causing sleeping sickness, *T. b. gambiense* and *T. b. rhodesiense,* are immune to this effect. *T. b. rhodesiense* avoids lysis by expressing serum resistance-associated (SRA) protein, which localises to the lysosome and binds ApoL1, inactivating its pore-forming ability (Oli et al. 2006; Bart et al. 2015). The presence of an *SRA* gene is in fact the only genetic distinction between *T. b. rhodesiense* and *T. b brucei* subspecies (Xong et al. 1998). The mechanism of TLF resistance in *T. b. gambiense,* on the other

hand, is less straightforward. This sub-species does not encode *SRA*; instead, it has been proposed that a combination of sequence polymorphisms and fewer HpHbRs leads to the reduced uptake of TLF1, thus conveying immunity (Kieft et al. 2010; Uzureau et al. 2013).

Furthermore, aquaglyceroporins (AQP1-3), one of which localises to the FP (AQP2), have been implicated in the bi-directional transport of water, small solutes and glycerol across the plasma membrane; the latter of which can be used as a carbon source (Uzcategui et al. 2004; Bassarak et al. 2011; Jeacock et al. 2017). For energy production, BSF parasites rely exclusively on glycolysis using host-derived glucose or, in some instances, glycerol (Bakker et al. 1997; Haanstra et al. 2008). Under anaerobic conditions, glucose can also be metabolised to glycerol in addition to pyruvate, both of which must then be secreted from the cell (Eisenthal and Panes 1985). The function of AQPs was exemplified more recently by the generation of null mutants lacking all *AQPs,* which were defective in uptake, utilisation and export of glycerol and consequently had a mild growth defect (Jeacock et al. 2017). Interestingly, the major contributor to this phenotype was AQP2, perhaps due to its FP-specific localisation, compared to AQP1 and AQP3, which localise to the flagellar and cell body membranes, respectively (Bassarak et al. 2011; Baker et al. 2012). Notably, AQP2 has also been linked to the uptake of anti-trypanosomal drugs, melarsoprol and pentamadine, with mutations to AQP2 leading to melarsoprol resistance (Baker et al. 2012).

Immune evasion

In addition to antigenic variation, another way in which the parasite can persist in the host bloodstream is via the rapid clearance of VSG-antibody complexes. The polarised location of the FP at the posterior end of the cell, in combination with the motility generated by the flagellum, are critical to this process. Here, VSG-antibody complexes act as a ‘sail’ and are selectively swept towards the flagellar pocket by hydrodynamic flow created by the forward movement of the cell (Engstler et al. 2007). Once internalised, VSG is then recycled back to the membrane, whilst the antibody is sent to the lysosome for degradation (Overath & Engstler 2004). This clearance

mechanism presumably extends the time it takes for the antibody titre against VSG to build up above the threshold required for parasite elimination.

Another proposed function of the FP is that it houses the majority of invariant receptors, keeping the surface free of proteins that might otherwise elicit a humoral immune response. In support of this, modelling of HpHbR predicts that this receptor would protrude above the VSG layer (Higgins et al. 2013). Therefore, its FP localisation may be advantageous for reasons other than haem acquisition. Equally, many cell body-localised transporters have small extracellular domains, and so are likely shielded by the VSG coat (Schwede et al. 2015). The situation becomes more complex when considering other cell-body localised invariant proteins with large extracellular domains proposed to extend above the VSG layer, such as the ISGs (Schwede et al. 2015). Reports of ISG-antibody recognition in live cells suggests that ISG epitopes are at least partially accessibly to immunoglobulins (Ziegelbauer and Overath 1993; Schwede et al. 2011). Yet, prior immunisation of mice with ISGs does not provide protection against subsequent infection with trypanosomes (Ziegelbauer and Overath 1993). Moreover, antibodies against ISGs have also been detected in the circulation of infected humans and animals, which do not confer protection either (Sullivan et al. 2013). Altogether, this could suggest that, although immunoglobulins can recognise invariant proteins, the low binding frequency at which they do could prevent these antibodies from triggering a response. Antibody binding is also possibly limited by the low copy number of invariant proteins relative to VSG, perhaps in combination with the steric hindrance imposed by the VSG coat itself. Therefore, it could be speculated that it would still be advantageous for the parasite to restrict high copy number proteins with large extracellular domains in the protected site of the pocket.

Parasite transmission and host adaptation

The FP also has a potential a role in controlling infection dynamics, both to limit the level of parasitaemia, and to promote parasite transmission (MacGregor and Szöőr 2012; Silvester et al. 2017). To ensure that parasite numbers do not overwhelm the host, proliferative “slender” BSFs differentiate

into quiescent “stumpy” forms in a density-dependent manner, likened to quorum sensing in bacteria (Waters and Bassler 2005; Mony et al. 2014). This occurs in response to the accumulation of a parasite-secreted stumpy induction factor (SIF), the identity of which remains unknown (Vassella et al. 1997). Stumpy forms are transmission-competent, thus SIF-dependent differentiation increases the likelihood of parasite transmission upon the bite of a tsetse fly. Given that the FP is the exclusive site of endo- and exocytosis, a role in SIF secretion and density sensing seems likely.

T. brucei also encodes a set of carboxylate transporters, known as Proteins Associated with Differentiation (PAD), with roles in perceiving differentiation signals once the parasite has been ingested by the fly (Dean et al. 2009). Localised to the FP in stumpy cells, PAD2 is upregulated in response to a reduction in temperature in the insect, and is redistributed from the FP onto the cell body membrane (Dean et al. 2009). This is thought to enable the cold-stimulated perception of cis-aconitate and citrate signals that drive the differentiation of bloodstream to procyclic forms (Engstler and Boshart 2004; Dean et al. 2009).

Receptors in the FP have also been implicated in parasite adaptation within the host, as well as to different host environments. At present, this is best exemplified by the iron-scavenging transferrin receptor. At least in culture, during periods of iron starvation, TfR is upregulated and redistributed from the FP onto the cell body, presumably to increase likelihood of transferrin capture in this instance (Mussmann et al. 2003, 2004). Equally, when cells usually cultured in bovine serum are challenged with canine serum, these cells switch expression to a different BES, encoding a different TfR variant with greater affinity for canine transferrin (Gerrits et al. 2002; van Luenen et al. 2005). Given the requirement of iron for parasite survival, it follows that the cell has adopted multiple strategies to ensure its uptake.

There are undoubtedly other receptors and transporters within the FP that also function in the multitude of roles described above. Indeed, it is possible that the novel FP proteins identified in the recent surfeome could fulfil such roles (Gadelha et al. 2015). Hence, their functional characterisation will form a significant part of this thesis.

1.4.3.3 Trafficking at the FP

All of the aforementioned functions are founded on the FP's ability to perform endocytosis and/or secretion. Not only that, but all surface proteins must traffic via the FP before reaching their final destination, that being the cell body, flagellar membranes, or secretion. Endocytosis in *T. brucei* is exclusively clathrin-mediated, both in PCF and BSFs (Allen et al. 2003; Hung et al. 2004). In support of this, knockdown of clathrin in BSFs blocks endocytosis and causes a "BigEye" phenotype, which refers to the enlargement of the FP lumen due to an imbalance in membrane trafficking (Allen et al. 2003). Knockdown of actin (García-Salcedo et al. 2004), ARF1 (Price et al. 2007), and a modulator of $PI(4,5)P_2$ (Demmel et al. 2014), which are critical components of CME in higher eukaryotes, produces a similar morphological phenotype. Notably, when CME is inhibited in the mammalian ciliary pocket, pocket morphology is unaffected (Molla-Herman et al. 2010). This is presumably because, in this instance, additional clathrin-independent pathways are active so endocytosis is not completely abolished.

On the surface, the *T. brucei* endocytic system is canonical to that of higher eukaryotes (see section 1.3, Figure 1.11), albeit highly polarised and dominated by GPI-anchored proteins. Here, all endocytic and secretory organelles are concentrated at the posterior end of the cell, between the FP and nucleus, except for part of the ER membrane, which extends across the entire cytoplasm (Figure 1.11). The restriction of uptake and secretion to a focal point in *T. brucei* has been likened to that observed at an immunological synapse, in primary cilia, and trichocyst secretion from *Paramecium tetraurelia* (a ciliated unicellular protozoan) (Griffiths et al. 2010).

In *T. brucei*, typical components of eukaryotic transport systems have been identified, including Arfs, Rabs and SNAREs, which collectively regulate formation, targeting, and fusion of vesicles (Ackers et al. 2005; Berriman et al. 2005; Murungi et al. 2014). On the other hand, a major difference between *T. brucei* and other eukaryotes is the loss of AP2 complex (Berriman et al. 2005; Field et al. 2007; Manna et al. 2013), responsible for the recruitment of clathrin and cargo selection (see section 1.3.1). There has also been some debate as to whether CME in *T. brucei* is dynamin-independent, with two

research groups obtaining contrasting results (Morgan et al. 2004; Chanez et al. 2006). Dynamin is encoded by a single gene in *T. brucei* (Berriman et al. 2005), yet recent evidence would suggest that sequence polymorphisms between the two alleles means that only one of two copies can function in endocytosis (Benz et al. 2017). Therefore CME likely requires dynamin in *T. brucei*. The loss of AP2 is restricted to African trypanosomes and correlates with the emergence of the VSG coat, leading to the suggested co-evolution of these two traits (Manna et al. 2013). It has been postulated that the dense packing of VSG on the surface could negate the need for a cargo concentration step, or that the exceptionally high rates of endocytosis in *T. brucei* are in part due to the lack of regulation imposed by AP2 (Field and Carrington 2009). Regardless of the reasoning, the lack of AP2 suggests that the mechanisms of clathrin-mediated endocytosis may be different in trypanosomes compared with other eukaryotes.

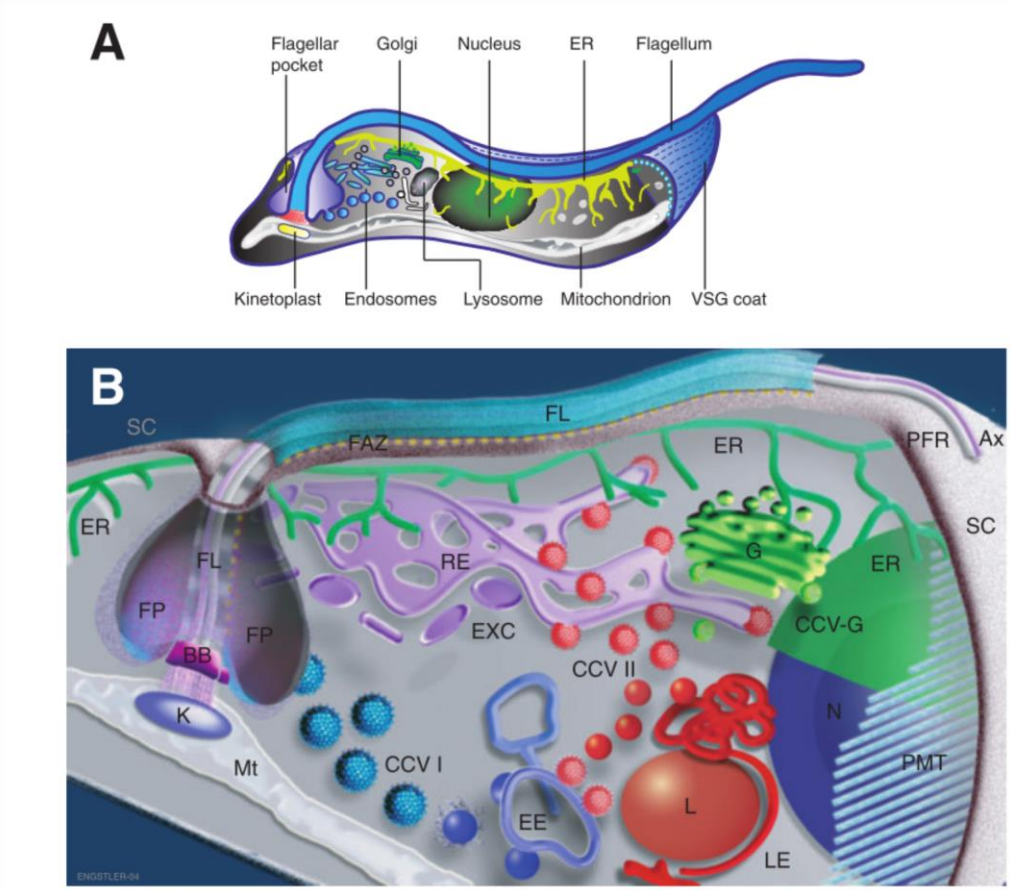


Figure 1.11. The endomembrane system of *T. brucei*
A) Schematic representation of the ultrastructure of *T. brucei* highlighting key organelles. B) Magnified view of the posterior end of the cell, showing the key structures involved in vesicular trafficking. Abbreviations relevant to this thesis: BB, basal body; CCV I and CCV II, clathrin-coated vesicles; EE, early endosome; ER, endoplasmic reticulum; EXC, exocytic carrier (recycling vesicles); FAZ, flagellar attachment zone; FL, flagellum; FP, flagellar pocket; G, Golgi apparatus; K, kinetoplast; L, lysosome; LE, late endosome; Mt, mitochondrion; N, nucleus (from Overath & Engstler, 2004).

The latter suggestion was investigated further when putative clathrin-associated proteins (CAPs) were isolated via co-immunoprecipitation with antibodies against clathrin heavy chain (CLH), combined with mass spectrometry (Adung'a et al. 2013). Several of the TbCAPs identified using this method, found to localise the endomembrane system, were essential for cell viability (with enlarged FPs), and involved in surface protein trafficking (Adung'a et al. 2013). This included TbHsc70, which in higher eukaryotes functions in the uncoating of clathrin vesicles after budding (see section 1.3.1). Interestingly, the majority of the TbCAPs were specific to trypanosomatids (Adung'a et al. 2013). When searching for encoded adaptor accessory proteins in the *T. brucei* genome, the cohort was limited to a single ENTH (EpsinR) domain and single ANTH (TbCALM) domain-containing protein (Gabernet-Castello et al. 2009; Manna et al. 2015), both of which participate in CME, and are thus essential for parasite survival. Collectively, this findings suggest a minimalist approach towards CME, divergent from that of higher eukaryotes and with resultant selective pressure driving the development of a more efficient endocytosis (Field et al. 2007; Manna et al. 2015), which undoubtedly contributes to the success of this parasite.

1.4.4. Mechanisms of maintaining specialised surface architecture of *T. brucei*

Each specialised domain on the surface membrane of *T. brucei* performs distinct cellular functions promote cell survival. The observation that surface proteins can access one or more of these domains suggests that movement between them is regulated. Like other eukaryotes, this may involve a combination of intrinsic sorting mechanisms to direct proteins to the desired domain in the first instance, and a barrier to limit protein diffusion between domains. The remainder of this section will discuss the potential ways the parasite may achieve this.

1.4.4.1. Putative diffusion barriers

To date, no definitive membrane diffusion barriers have been characterised in *T. brucei*. Yet, the rows and clusters of intramembrane particles (IMPs) observed at the membrane junctions between the FP and neck region, as well as at the FP-flagellum junction (Gadelha et al. 2009), form obvious candidates.

The proteins that make up these putative membrane fences are currently unknown. Based on diffusion barriers found in other eukaryotes, it would be reasonable to assume that these barriers could be septin-based, particularly given the high degree of membrane curvature at the base of the flagellum (see section 1.2). However, as the *T. brucei* genome does not encode any septin homologues, this does not appear to be the case here (Berriman et al. 2005).

The FPC, located at the FP-neck junction, has also been implicated in protein domain segregation, as a reduction in BILBO1 as a consequence of *IFT140* knockdown leads to the redistribution of an FP-localised transmembrane protein (CRAM) onto the flagellum in PCFs (Absalon et al. 2008). It is possible that this redistribution is also linked to the initial knockdown of the flagellum transport machinery, and so, the role of the FPC as a barrier to protein movement requires further investigation.

1.4.4.2. Membrane properties

As mentioned above, the highly curved nature of the plasma membrane at the junction of the flagellum and the FP resembles that at the ciliary and plasma membranes of the primary cilium. Here, lipid composition, which is influenced by membrane curvature, has been shown to affect the distribution of membrane probes and GPI-anchored YFP between the cillium and plasma membranes (Vieira et al. 2006). A similar scenario could be envisaged for proteins at the flagellum and FP boundary. Additionally, the flagellar membrane is enriched in sterols and sphingolipids, which promote the formation of lipid rafts and likely contribute to the further sub-localisation of flagellar membrane proteins within the flagellar membrane itself (Tyler et al. 2009; Subota et al. 2014; Serricchio et al. 2015; Emmer et al. 2010; Sharma et al. 2017). The lipid compositions also differ between the flagellum, FP and cell body membranes, which may influence which surface proteins can reside in each lipid bilayer (Serricchio et al. 2015).

1.4.4.3. Protein targeting

Protein targeting to distinct surface domains is independent of protein topology or identifiable sequence motifs, at least for a set of surface-localised ESPs (Gadelha et al. 2015). There have been two models put forward to

explain how the parasite differentially localises proteins to the flagellar pocket and cell body membranes, both of which are based on just a handful of proteins. One is that surface localisation is dictated in part by protein abundance, which is has been shown for a type I transmembrane (TM) protein (*Tb*MBAP1) and a GPI-anchored protein (TfR). The other is applicable to GPI-anchored proteins only, whereby the number of GPI-anchors on a given protein dictates surface localisation (Schwartz et al. 2005).

Evidence to suggest that protein abundance can affect surface localisation comes from experiments involving the manipulation of protein expression levels. At endogenous levels, *Tb*MBAP1 localises exclusively to the endosomes. Conversely, when overexpressed 3-4 fold, under the control of a tetracycline inducible promotor, the endosomal phosphatase can also be found in the FP. When cells were induced over a longer time period, protein level increased 10-20 fold relative to endogenous, which caused *Tb*MBAP1 to then be redistributed onto the flagellar and cell body membranes in addition to the FP and endosomes (Engstler et al. 2005). Equally, when the FP-localised TfR and PAD2 proteins are upregulated, in response to iron starvation or a temperature change, respectively, they become detectable on the cell body membrane, further supporting a possible saturable mechanism for FP protein retention (Mussmann et al. 2003, 2004; Dean et al. 2009).

The second GPI-centred model suggests that the number of GPI anchors attached to a protein dictates surface localisation; this has been termed the valence hypothesis (Schwartz et al. 2005). VSG is a homodimer with two GPI anchors and localises across the entire surface membrane; heterodimeric TfR (composed of ESAG6 and ESAG7 subunits) has one GPI anchor on the ESAG6 portion and localises to the FP and endosomes, whilst ESAG7 homodimers or truncated VSGs lacking GPI-anchors entirely are degraded in the lysosome (Schwartz et al. 2005). The valence hypothesis was initially challenged by the aforementioned release of TfR onto the surface under iron starvation. However, further evidence would suggest that the surface-localised TfR is actually a non-functional ESAG6 homodimer with two GPI anchors (Schwartz et al. 2005). In addition, a recent study showed that when an ESAG6/ESAG7 dimer modified to have two GPI anchors was expressed at

endogenous levels, it too localised to the entire surface (Tiengwe et al. 2017). This result conforms to the valence hypothesis and suggests protein sorting to cell body and flagellar membranes (for this specific GPI-anchored protein at least) is not entirely a consequence of FP saturation. This model bears some similarity with other eukaryotes, whereby oligomerisation of GPI-anchored proteins affects their apical or basolateral fate (Paladino et al. 2008 and section 1.2.3).

The covalent attachment of fatty acids to proteins (e.g. myristate and palmitate) has also been shown to influence protein localisation in *T. brucei* (Goldston et al. 2014). While N-myristoylation involves the irreversible attachment of myristate to the N-terminal glycine residue, palmitoylation is potentially reversible process in which palmitate is transferred to a cysteine sulfydryl. Recent work has shown that correct protein targeting to the flagellar membrane is dependent upon protein acylation. Calflagin is both myristoylated and palmitoylated and has a flagellum localisation. However, when palmitoylation is inhibited, myristoylated Calflagin localises to the pellicular membrane (Emmer et al. 2010). Though, dual acylation alone cannot be the sole determinant of flagellum localisation, as CAP5.5 is another example of a protein with both these fatty acid modifications, yet CAP5.5 localises to the pellicular membrane (Hertz-Fowler et al. 2001).

Further evidence for a role of fatty acylation in protein targeting is provided via knockdown of *T. brucei* N-myristoyltransferase (NMT). Depletion of the enzyme responsible for the addition of the myristate leads to endocytosis defects and enlargement of the flagellar pocket, which suggests that myristoylation has a role in protein trafficking. African trypanosomes are also unusual in that the GPI-anchors present on surface proteins (such as VSG) are often di-myristoylated (Morita et al. 2000). Although the function of GPI-anchor myristoylation remains unknown, it is possible that a mono-myristoylated GPI anchor may be targeted differently to a di-myristoylated anchor, which could also influence the GPI-valence hypothesis.

Another way in which cells can modulate protein sorting to specific membranes, is via post-translational modifications such as glycosylation, like the sorting of proteins to the apical membrane in epithelial cells (Vagin et al. 2009). It is possible that glycosylation may also have a role in protein sorting at the host-parasite interface. In support of this, it was shown that N-linked glycans containing poly-*N*-acetyllactosamine residues were confined to proteins localised within the FP and endosomal system of *T. brucei* (Nolan et al. 1999). This was highlighted by the selective binding of tomato lectin (TL, which has marked specificity for tri-*N*-acetyllactosamine) to the FP/endosomal region of the cell (Nolan et al. 1999; Atrih et al. 2005). When isolated and analysed by mass spectrometry, TL-bound fractions encompassed FP-localised TfR subunits and excluded whole surface-localised VSG and ISGs (Nolan et al. 1999). It was then proposed that these long linear glycan chains on FP proteins could act as sorting signals within the endosomal pathway. However, more recent and finer mapping of the sugar moieties of TfR did not identify any *N*-acetyllactosamine-containing glycans (Mehlert et al. 2012). Instead, they found that TfR is able to bind other glycoproteins, which in turn may bind TL (Mehlert et al. 2012). Therefore the link between N-glycosylation and FP localisation appears more complex than first anticipated.

1.5. Conclusions

The success of the parasite weighs heavily on its capacity to evade the host immune system, whilst ensuring the uptake of essential nutrients and controlling levels parasitaemia. At the heart of it all is the flagellar pocket. Yet, only a handful of the components of this specialised surface domain are known, and even fewer have been characterised in detail. The essential nature of receptors such as TfR and HpHbR highlights the FP as an area of vulnerability that could be exploited in a therapeutic context. The same is also true for the barriers that maintain the critical surface architecture of the parasite.

1.6. Aims

This thesis aims to characterise the functions of novel flagellar pocket proteins identified as part a recent surface proteomics study, in an attempt to elucidate their roles at the host-parasite interface. In addition to the functional characterisation of these proteins, I will examine the contributions post-translational modifications (glycosylation) and cytoskeletal structures (the flagellar pocket collar) make towards the direction and restriction of these proteins to the flagellar pocket membrane. The final part of this thesis aims to elucidate the role of a kinesin that has been localised along the neck channel in procyclic form cells. As the neck channel connects the FP lumen to the extracellular milieu it is possible that this motor protein functions in the transport of membrane-associated material across the channel.

Chapter 2. Methods

2.1. Cell lines

2.1.1. Culture of *Trypanosoma brucei*

Bloodstream-form (BSF) *T. b. brucei* S16 cell lines (Wirtz et al. 1999) were used for all experiments, except for those described in Chapter 5 which utilised BSF *T. b. brucei* SmOxB427 cells (Poon et al. 2012). All cell lines were routinely cultured in HMI-9 supplemented with 15% foetal calf serum (Hirumi and Hirumi 1989) at 37°C with 5% CO_2. Cells were maintained in logarithmic phase of growth (<$2x10^6$ cells/ml). For experiments performed in minimal medium, cells were cultured in Creeks minimal medium (Creek et al. 2013), supplemented with 10% foetal calf serum Gold (PAA laboratories), the composition of which is defined. This simplified growth medium was developed by comparing the metabolite content of fresh and spent standard culture medium to determine which nutrients were significantly consumed by bloodstream form trypanosomes. Creek and colleagues determined that the minimal nutrient combination required for continuous *in vitro* culture was glucose, cysteine and glutamine (all of which were lowered to concentrations more representative of those found in human blood), in addition to 10% FCS plus basal medium (salts, buffers and antioxidants). Therefore, this medium provides a more biologically relevant alternative to standard culture conditions. In all instances, tetracycline-inducible RNA interference (RNAi) or overexpression was induced by adding 1 µg/ml tetracycline to the culture medium.

2.1.2. Transfection of *T. brucei*

For the stable transfection of BSF cells, 10 µg of plasmid was linearised with NotI, purified by anion exchange chromatography and ethanol precipitation, then resuspended in 30 µl Tb-BSF buffer (90 mM $NaHPO_4$, 5 mM KCl, 0.15 mM $CaCl_2$, 50 mM HEPES pH 7.3, Schumann Burkard et al. 2011). DNA was transfected into $2.5x10^7$ cells (resuspended in 120 µl Tb-BSF buffer) using Amaxa™ Nuclefector™ (Lonza), program Z-001. Cells were recovered for ~6-8 hours and then plated to limiting dilution under the appropriate drug

pressure to select for positive transformants. The probability that each positive well was an independent clone was estimated based on the Poisson distribution. For transfection of KIN17 knockout (KO) fragments, 10 µg of purified PCR product was used in place of a linearised plasmid.

2.2. Plasmid production

For the generation of all plasmids described below, *T. b. brucei* genomic DNA (TREU427 strain) was used as PCR template, unless stated otherwise. A typical PCR reaction included 25 ng of genomic template DNA, 0.2 mM dNTPs (NEB), 0.4 µM of each primer and 1.25 units of Phusion High-Fidelity DNA polymerase (NEB). DNA ligation and bacterial transformation steps were identical for all, except that two-way ligations were carried out at room temperature for 1 hour, and 3-way ligations were performed at 16°C for 2 hours. Generally, all ligations were carried out with T4 DNA ligase, using a 1:3 molar ratio of plasmid to insert. Constructs were cloned into XL1-Blue *Escherichia coli* by heat shock and grown at 37°C. Resultant constructs were Sanger-sequenced across the ligation site prior to transfection into *T. b brucei* cells to ensure the correct plasmid had been produced. For a summary of all plasmids produced, see Appendix. For a summary of all cell lines produced see Table 2.3.

2.2.1. For the inducible knockdown of flagellar pocket (FP) proteins

Oligonucleotides were designed and generated to amplify a ~500bp central region of each FP ESP (Enriched in Surface Proteome) coding sequence (CDS), with BamHI and HindIII restriction endonuclease sites incorporated on the forward and reverse primers, respectively. For a list of primers used and the gene IDs of each ESP, see Table 2.1. To generate RNA interference (RNAi) constructs, RNAi fragments were amplified from genomic DNA, digested with BamHI and HindIII and ligated into p2T7-177 vector (Wickstead et al. 2002a), cut with the same restriction enzymes.

2.2.2. For the endogenous-locus tagging of FP ESP proteins

For a list of ESP gene IDs and the primers used to generate CDS and UTR targeting fragments for both N-terminal and C-terminal tagging, see Table 2.2.

To tag the N-terminus of ESP26 with superfolder GFP (sfGFP), ~250 bp PCR fragments containing the 5' untranslated region (UTR) and the N-terminal 5' end of the coding sequence (minus the predicted signal peptide, as determined by SignalP 3.0) were amplified from genomic DNA. Resultant PCR products were digested with XbaI and NotI (CDS fragment) or NotI and BamHI (UTR fragment) and ligated into pSiS-HhsfG (Gadelha et al. 2015), cut with XbaI and BamHI.

For C-terminal tagging of ESP27-31 with sfGFP, ~250 bp PCR fragments containing the 3'-UTR and the C-terminal 3' end of the coding sequence (minus the stop codon) were amplified from genomic DNA. PCR products were digested with HindIII and NotI (UTR fragment) or NotI and XbaI (CDS fragment) and ligated into pSiS-HhsfG (Gadelha et al. 2015), cut with HindIII and AvrII.

2.2.3. For the endogenous-locus tagging of KIN17 and DYNC1H1

To tag KIN17 (Tb927.3.2040) at the N-terminus with sfGFP, targeting fragments (~250 bp) corresponding to the 5'-end of *KIN17* CDS (primer sequences CATCTAGAATGAACACTTCCGCGTGT, TAGCGGCCGCTTTGGAGTGAATGGAGTTGC) and 5'-UTR (TAGCGGCCGCGGCACTTATTCCCCCATC and CTAGGATCCTTGTTACCTACAGTCCCACT) were amplified from genomic DNA. Primer sequences contained the appropriate restriction sites (underlined) for the digestion of the CDS fragment with NotI and XbaI and the UTR fragment with BamHI and NotI. Fragments were ligated into pEnNsfG0 plasmid (kindly provided by Jennifer McDonald, University of Nottingham), cut with BamHI and XbaI. pEnNsfG0 was derived from the pEnNY0 vector series (D'Archivio and Wickstead 2017) by substituting the *YFP* open reading frame for *sfGFP*. To be able to tag the C-terminus of KIN17, a second construct (pEnG05) was obtained from Bill Wickstead (University of Nottingham), which is a modified version of the pEnG0 series of plasmids (Wickstead et al. 2010) This plasmid contains the endogenous 3'-UTR of *KIN17* downstream of *GFP* which should produce KIN17::GFP levels of expression similar to wildtype.

Generation of a DYNC1H1 (Tb927.7.3160) N-terminal tagging construct was performed essentially as described for *KIN17.* Primers CATCTAGAATGATGCGGCAGGAAAAG and TAGCGGCCGCCCATCAGACGAAAGAAAACAGT were used to amplify the *DYNC1H1 CDS* targeting fragment, and primers TAGCGGCCGCTCACCTTTTCCTGTCGTTG and TAGGATCCCTGCAAAACAAACTAGGCG were used to amplify the UTR. Underlined regions of sequence represent restriction sites. CDS and UTR fragments were ligated into pEnNsfG0 (see above).

To tag the second allele of KIN17, the *HYG* (hygromycin) resistance gene was excised from pEnNsfG-KIN17 using BamHI and StuI restriction endonucleases and replaced with a *BLAST* (blasticidin) resistance gene (with an actin 5'-UTR included upstream), generating pEnNsfG-KIN17-B.

2.2.4. For the generation of KIN17 knockout fragments

Fragments containing either *NEO* (neomycin) or *BLAST* resistance genes flanked by *KIN17* 5'- and 3'-UTRs were generated by fusion PCR. To generate KIN17-BLAST KO fragment, 5'-UTR fragment was amplified from genomic DNA using primers CATTTTGCCACTTCCAGTTG and ATTCTTCTTGAGACAAAGGCATTTGTTACCTACAGTCCCAC. The 3'-UTR fragment was produced using primers TATGTGTGGGAGGGCTAACGAAAGCAATTCGCTATGGA and ACAAAAAGAGCATCGATTGCA. The underlined regions of primer sequence correspond to *BLAST*-specific overhangs that form for the primers for the amplification of *BLAST* during the subsequent fusion PCR step. Formation of the full-length KO fragment was achieved by combining equimolar amounts of 5'-UTR and 3'-UTR fragments, and template plasmid containing a *BLAST* ORF. Fusion PCR reaction was performed using the forward primer used in the amplification of the 5'-UTR with the reverse primer used to generate the 3'-UTR amplicon.

Production of the KIN17-NEO KO fragment was performed as described for KIN17-BLAST, except the reverse primer to amplify the 5'-UTR was GCAATCCATCTTGTTCAATCATTTGTTACCTACAGTCCCAC and the

sequence of the forward primer to generate the 3'-UTR fragment was TTCTTGACGAGTTCTTCTGACGAAAGCAATTCGCTATGGA.

2.2.5. For the inducible overexpression of KIN17 and kin17-rigor

2.2.5.1. From a 177-bp repeat locus

To introduce a tetracycline-inducible ectopic copy of KIN17 or kin17-rigor, tagged with either sfGFP or mStrawberry (mSt) at the N-terminus, overexpression plasmids were produced from derivatives of the pDex577-series of vectors (Kelly et al. 2007). pDex577-YFP was first modified to contain *sfGFP* or *mSt* coding sequences in place of *YFP*, by digestion of the plasmid with HindIII and XbaI. Amplicons of *sfGFP* and *mSt,* containing HindIII and XbaI restriction sites were then ligated into cut pDex577 to produce pDex577-sfG and pDex577-mSt.

Full length *KIN17* was amplified from genomic DNA using primer sequences GATCTAGAATGAACACTTCCGCGTG and TCAGGATCC TCATGACTGCATCGCCT, which add XbaI and BamHI restriction sites respectively (underlined in primer sequence). Resultant amplicon was ligated into pDex577-sfG and pDex577-mSt cut with XbaI and BamHI to produce pDex577-sfG-KIN17 and pDex577-mSt-KIN17. To ensure no mutations had been introduced by PCR, these plasmids were Sanger-sequenced across the *KIN17* ORF.

To produce kin17-rigor variants of these plasmids for the ectopic expression of KIN17 rigor mutants, full length *KIN17* was mutated using a fusion PCR strategy. The N-terminal portion of *KIN17* (upstream of mutation) was amplified using primers GATCTAGAATGAACACTTCCGCGTG and TTTTCCCGCACCCGTCT and pDex577-sfG-KIN17 as the template DNA. The C-terminal portion (downstream of mutation) was amplified with forward primer AGACGGGTGCGGGAAAAaacTACACAATGGAGGGGTTTGC, and reverse primer TCAGGATCCTCATGACTGCATCGCCT. Here, the forward primer included a region of complementary sequence to the 3' end of the N-terminal fragment (underlined) to prime the subsequent fusion PCR reaction, as well as the rigor mutation (shown in lowercase) which encodes a T210N amino acid

substitution. Reactions were digested with DpnI, resolved in and excised from agarose gels (followed by gel extraction and silica-adsorption-based DNA purification) to be sure to remove template plasmid DNA. Fusion PCR was performed by combining equimolar amounts of the N-terminal and C-terminal *KIN17* amplicons in the presence of primers GATCTAGAATGAACACTTCCGCGTG and TCAGGATCCTCATGACTGCATCGCCT, which anneal to the 5' end of the N-terminal and 3' end of the C-terminal regions, respectively. Resultant kin17-rigor coding sequence was digested with XbaI and BamHI and ligated into pDex577-sfG and pDex577-mSt, producing pDex577-sfG-kin17-rigor and pDex577-mSt-kin17-rigor. To ensure the mutagenesis was successful, and that no other mutations had been introduced by PCR, the kin17-rigor ORF was sequence Sanger-sequenced.

2.2.5.2. From a VSG-G4 locus

For the inducible expression of chimeric mSt-KIN17 and mSt-kin17-rigor from the VSG-G4 (V4) locus, a plasmid based on the pDex series was produced by Bill Wickstead and Lorenzo Brusini (University of Nottingham), pV4Δ-Dex-mSt. This plasmid was modified to contain the KIN17 and kin17-rigor sequences produced above by digestion with XbaI and BamHI. pDex577-sfG-KIN17 and pDex577-sfG-kin17-rigor (produced above) were cut alongside with the same restriction endonucleases, and the excised *KIN17* and *kin17-rigor* sequences were ligated into pV4Δ-Dex-mSt. This generated pV4Δ-Dex-mSt-KIN17 and pV4Δ-Dex-mSt-kin17-rigor plasmids.

2.3. Plasmid integration analysis

For diagnostic PCRs, genomic DNA was isolated from *T. brucei* cell lines by alkaline lysis: ~$2x10^5$ cells were harvested, resuspended in 120 µl of 50 mM NaOH, 2 mM EDTA pH 8.0. Samples were heated at 98°C for 10' and neutralised with 24 µl of 450 mM Tris-HCl pH 6.8.

2.3.1. Integration of endogenous locus tagging constructs

Confirmation that pSiS-HhsfG-ESP26-Nt, pSiS-HhsfG-ESP27-Ct and pSiS-HhsfG-ESP30-Ct endogenous-locus tagging constructs had integrated

correctly was provided by diagnostic PCR. For the N-terminal tagging construct pSiS-HhsfG-ESP26-Nt, a universal reverse primer was designed to anneal within the *ESP26* open reading frame (GGTTCAATGTATAGGATAGCATCA), downstream of the target sequence, in combination with a forward primer specific to *sfGFP* (ACGCATGGTATGGATGAA) to confirm plasmid integration, and a forward primer annealing within the 5'-UTR of *ESP26* (TTTACCACGTAGTGTCTACC) to amplify the untagged copy.

For the two C-terminal tagging constructs, diagnostic PCRs were designed so that a universal forward primer annealed within either the *ESP27* or *ESP30* ORF, upstream of the target sequence (TTGAAATGTTGCAGGCG or TGCCTTTGAATCTCTATTGGT), multiplexed with a reverse primer specific to *sfGFP* (TCTTCGCCTTTACGCA) to confirm plasmid integration, and forward primer annealing within the 5'-UTR of *ESP27* or *ESP30* (TCAGACACGAAACATTCATTGT or TGAACGATTCACCCCTTT) to amplify the untagged copy. See Chapter 3 (Figure 3.5) for a schematic representation of all diagnostic PCRs and expected product sizes.

2.3.2. Integration of KIN17 knockout fragments

Diagnostic PCRs were performed to confirm the correct genomic integration of *KIN17-NEO* and *KIN17-BLAST* knockout fragments. A universal reverse primer (CGAGAAGCCTTCACACC) that annealed within the 3'-*UTR* of *KIN17* was multiplexed with forward primers specific to the *KIN17 ORF*, *BLAST* resistance gene or *NEO* resistance gene (sequences: GCGTAGTGCTCACTCG, ATGCCTTTGTCTCAAGAAGAATC, and CGCATCGCCTTCTATCG respectively). See Chapter 5 (Figure 5.6) for a schematic representation diagnostic PCR and expected product sizes.

2.4. Cell growth analysis

2.4.1. Manual cell counts

Assessment of parasite growth to determine the effects of either protein ablation or protein overexpression was determined by cell counts of induced and non-induced populations every 24 hours, using an Improved Neubauer

haemocytometer, unless specified otherwise. Growth curves were initiated at densities of $1x10^4$ cells/ml, with cells diluted every 48 hours to maintain them in log-phase growth. Cells were grown in either HMI-9 or Creek's minimal medium (as specified).

2.4.2. ATP-based luciferase assay

To monitor cell growth over the course of a 6-day RNAi induction for the FP ESPs, RNAi cell lines (and their corresponding parental cell lines) were plated into black 96-well plates at cell densities of either $1x10^3$ or $1x10^4$ cells/ml and grown in the presence or absence of 1 µg/ml tetracycline. At time zero (t=0) and at 24-hour intervals, 50 µl of CellTiter-Glo 2.0 reagent (Promega) was added to 100 µl of cells, incubated for 10 minutes, and luminescence was detected using a GloMax® 96 microplate luminometer. Here, luminescence is proportional to the amount of ATP available, which is provided by the cells. For each luminescence reading, a set of 6 ATP standards were included, ranging from 100 nM to 316 pM in a √10 dilution series, to normalise reads between time points. Arbitrary luminescence values were converted to cell density by calculating the average amount of ATP per cell (using a √10 cell dilution series, ranging from $1×10^6$ to $1×10^3$ cells/ml). Within this range, there was a linear relationship between luminescence signal and cell density, setting the limits of detection. Cumulative growth curves were plotted for all cell lines and all starting cell densities were normalised to $1x10^3$ cells/ml using the t=0 reading.

2.5. Protein biochemistry

2.5.1. Sample preparation, SDS-PAGE and Western blotting

To confirm either RNAi knockdown, endogenous-locus tagging, or protein overexpression, whole cell lysates were prepared. Cells were harvested by centrifugation and washed twice in phosphate buffered saline (PBS; 140 mM NaCl, 10 mM Na_2HPO_4, 3 mM KCl, pH 7.5) supplemented with 20 mM glucose (PSG). Cells were resuspended in an appropriate volume of Laemmli buffer modified to pH 7.2 (2% w/v SDS, 0.4 M 2-mercaptoethanol, 10% glycerol, 50 mM Tris-HCl), to give a final concentration of $2.5x10^5$ cells/µl, and heated

at 98°C for 5 min. Multipass transmembrane (TM) proteins were typically heated at 70°C for 10 min to reduce protein aggregation.

Whole cell lysates were separated by SDS-polyacrylamide gel electrophoresis. $2.5x10^6$ cell equivalents were resolved on pre-cast 4-20% polyacrylamide Tris-glycine gels in buffer containing 25 mM Tris, 250 mM glycine and 0.1% w/v SDS. Proteins were then transferred to nitrocellulose membrane (0.45 µm pore size) under immersion transfer conditions (Towbin et al.1979) in 25 mM Tris, 192 mM glycine, 0.02% w/v SDS and 10% methanol, for 14 hours at 40 mA. Following transfer, nitrocellulose membranes were stained with Ponceau-S (0.1% w/v in 5% acetic acid) to visualise the whole cell proteome in each lane, providing a loading control. Membranes were blocked for 30 min in 5% w/v milk in TBS (20 mM Tris-HCl pH 7.5, 150 mM NaCl) supplemented with 0.1% Tween-20 (TBS-T).

For the detection of GFP-tagged proteins, primary antibody (anti-GFP mouse monoclonal antibodies (clones 7.1 and 13.1); 0.8 µg/ml; Roche) was diluted in TBS-T and added to the membrane for 1 hour. Membranes were then washed 4 times for 5 min each in TBS-T, followed by the addition of secondary antibody (polyclonal goat anti-mouse IgG conjugated to horseradish peroxidase (HRP); 1:5000, Sigma) for 1 hour. Following 4 lots of 5 min washes in TBS-T. Membranes were detected by HRP-catalyzed chemiluminescence (Western Lightning® Plus- ECL, PerkinElmer) and exposed to x-ray film.

For the detection of KIN17 (either endogenous or overexpressed), the primary antibody (affinity purified rabbit anti-KIN17 polyclonal antibodies, kind gift from Bill Wickstead) was diluted 1:5000, in 1% w/v milk in TBS-T. Secondary antibody (polyclonal goat anti-rabbit IgG conjugated to horseradish peroxidase, Sigma) was diluted 1:20,000 in 1% w/v milk in TBS-T. Both primary and secondary antibodies were incubated for 1 hour. All other steps were performed as described above.

2.5.2. Deglycosylation with Endo-H and PNGase-F

To determine the glycosylation status of GFP-tagged flagellar pocket proteins, cells (typically $3x10^7$) were harvested by centrifugation, washed twice

in PSG and resuspended at a concentration of $2x10^6$ cells/µl in PSG. One volume of 2X NEB Denaturing buffer (1% SDS, 80 mM DTT) was then added and cells heated for 10' at 98°C. Reaction was then split into three to produce the untreated, Endo-H-treated and PNGase-F-treated samples (each at $1x10^6$ cells/µl). For Endo-H treatment, 2000U of Endo-H (cloned from *Streptomyces picatus* and overexpressed in *E. coli*, NEB) and Glycobuffer 3 (50 mM sodium acetate, pH 6.0) were added to reactions; while for PNGase-F treatment, 1000U of PNGase-F (purified from *Flavobacterium meningosepticum,* NEB) and Glycobuffer 2 (50 mM sodium phosphate, pH 7.5) were added in addition to 0.1% v/v Nonidet P40; for untreated samples, double distilled H_2O was added in place of the glycosidases. All reactions were incubated at 37°C for 1 hour and heated for 5 min at 98°C in Laemmli buffer to give $2.5x10^5$ cells/µl.

2.5.3. Cytoskeleton preparation

To determine to amount of overexpressed KIN17 and kin17-rigor protein associated to the cytoskeleton, cells were harvested, washed twice in PSG and resuspended in PBS supplemented with protease inhibitors (5 µM E64-d, 2 mM 1,10-phenanthroline, 0.5 mM PMSF, 50 µM leupeptin and 7.5 µM pepstatin A). Cells were lysed for 5 min on ice, in PBS containing 1% v/v Nonidet P40, 200 µg/ml DNase I, 1 mM EDTA, 1 mM DTT and the aforementioned protease inhibitors. After lysis, half the sample was removed to generate the whole cell lysate. Remaining sample was then centrifuged at 4°C to separate the soluble and insoluble fractions. All samples were precipitated overnight at -20°C in 10 volumes of acetone. After two acetone washes, samples were heated for 5 min in Laemmli buffer to $2.5x10^5$ cell equivalents/µl for whole cell lysate fraction and $5x10^5$ cell equivalents/µl for soluble and insoluble fractions.

2.6. Microscopy

2.6.1. Epi-fluorescence

For fluorescence microscopy, ~$5x10^5$ cells were harvested and washed 3 times with PSG. Cells were settled for 2' on derivatised slides. Derivatisation

of slides was performed prior, by coating sialinised slides with 5% v/v glutaraldehyde in 0.1 M $NaHCO_3$. Cells were then fixed in 2.5% v/v formaldehyde for 10 min and neutralised in PBS containing 0.25% w/v glycine to block unreacted aldehyde groups. Slides were mounted in DAPI (4',6-diamidino-2-phenylindole)-containing mounting medium (200 ng ml^{-1} DAPI, 1% w/v 1,4-diazabicyclo(2.2.2)octane, 90% v/v glycerol and 50 mM sodium phosphate (pH 8.0) and sealed with nail varnish.

To counterstain the surface of trypanosomes, after blocking the unreacted aldehyde groups (see above), samples were incubated with 5 µg/ml ConcanavalinA (ConA) conjugated to tetramethylrhodamine isothiocyanate (TRITC) in PBS. To label the flagellar pocket, cells were stained with tomato lectin (TL) (Sigma) conjugated to fluorescein isothiocyanate (FITC) or Alexa Fluor® 594 (Invitrogen) in PBS, at 10 µg/ml and 25 µg/ml respectively. All incubations were performed for 20 min at room temperature. Slides were mounted as described above.

For the preparation of detergent-extracted whole-mount cytoskeletons, cells were settled on slides as above and then treated for 5 min with 0.1% v/v Nonidet P40 in PMEG buffer (40 mM PIPES pH 6.9, 2 mM $MgSO_4$, 5 mM EGTA, 200 mM glucose). Cells were fixed and mounted as before.

2.6.2. Imaging

Images of cells were all captured using a 100x oil immersion objective (NA 1.35, Olympus) and Photometrics CoolSnap HQ camera (Photometrics) or a Retiga R1™ CCD camera (QImaging) Both cameras had a pixel size of 6.45 µm. Images were processed in ImageJ (National Institute of Health, USA; rsb.info.nih.gov).

2.7. Flow cytometry

To quantify the fluorescence intensity of mSt-KIN17 and mSt-kin17-rigor overexpressing cells, $2x10^6$ cells were washed twice in PSG and fixed in 500 µl of 0.25% v/v formaldehyde in PBS for 10 min. Samples were neutralized with 0.25% glycine and cells analysed on a MoFo Astrios (Beckman Coulter) flow cytometer using a 561nm laser and 614/20 filter. At least 50,000 events were

captured per sample. Data analysis was performed on WEASEL (v3.0.2). Data capture was performed with assistance from the Flow Cytometry Facility (University of Nottingham).

Table 2.1 RNAi targeting fragments for inducible knockdown of FP ESPs. Primers were designed using a perl script (primal.pl) courtesy of Bill Wickstead (University of Nottingham). Parameters were set to select for primers that were between 18 and 25 bases in length, with a Tm between 56°C and 58°C, and to exclude those predicted to form hairpins or primer dimers.

Name	*Gene ID*	*Forward primer (BamHI)*	*Reverse primer (HindIII)*	*Fragment size (bp)*	*Resultant plasmid*
ESP1	Tb927.2.5280	caggatccGAATCGGACTACATGGGC	ccaagcttGCCATCTACGGGAACAC	498	p2T7-177-ESP1
ESP6	Tb927.10.990	caggatccCCTCAAGAATGCGAGTCG	ccaagcttGATCATGTTCAGCCTTCACC	479	p2T7-177-ESP6
ESP10	Tb927.2.1700	caggatccGTTCTGAGACGTGTACGTG	ccaagcttGCGCAACCAATACGTGTA	503	p2T7-177-ESP10
ESP11	Tb927.4.3040	caggatccCTCTAGTAATGCATGCCAATGG	ccaagcttCATCAACCACTGGTCGAG	504	p2T7-177-ESP11
ESP12	Tb927.7.4230	caggatccCTGGTAGGTGTGCTGATTG	ccaagcttTGCTGCAATGAGAATCATGG	509	p2T7-177-ESP12
ESP13	Tb927.7.4260	caggatccGCAATGCTGTTGCTGATC	ccaagcttGTTCTTGACGCTCAGGAG	465	p2T7-177-ESP13
ESP14	Tb927.7.470	caggatccCAATTCGATGCAGACGAATTCA	ccaagcttCTGTACGCCAGTTCAGAG	497	p2T7-177-ESP14
ESP21	Tb927.10.13930	caggatccAATGCGTGAGCGTTACTC	ccaagcttCTTAGGATGATACGCCACAC	516	p2T7-177-ESP21
ESP22	Tb927.10.530	caggatccGCCATCAACTGTGCTGTT	ccaagcttGTCATGTCTGTCCACTGC	520	p2T7-177-ESP22
ESP27	Tb927.3.5530	caggatccTGCACAAGGTTGGTTATGC	ccaagcttGAAGTACCTCCAAAGCTGC	498	p2T7-177-ESP27
ESP29	Tb927.9.12000	caggatccAGAACCACCGGCGATA	ccaagcttCCGCGTACCAACCATT	492	p2T7-177-ESP29
ESP30	Tb927.8.2380	caggatccCCAGCAACAATAACGATGCA	ccaagcttCAAGGAAGAGGATACGCG	498	p2T7-177-ESP30
ESP31	Tb927.8.6720	caggatccCTTTGCACTACGATCGGAG	ccaagcttCGAACATTCAGTGGCATTCTT	518	p2T7-177-ESP31
TbPT0	Tb927.3.4070	caggatccCAGTGCTCATGATGGCAT	ccaagcttAAGGATCAGCGCGTTAG	524	p2T7-177-TbPT0
CLH	Tb927.10.6050	caggatccCTGAAGCATTCCCATCCG	ccaagcttCATAACACGGGCTCTCAC	529	p2T7-177-CLH

Table 2.2. Primers for the generation of pSiS-HhsfG-ESP tagging constructs

Name	*Gene ID*	*Primers for CDS fragment (NotI/XbaI)*	*Primers for UTR fragment (NotI/XbaI/BamHI/HindIII)*	*Resultant plasmid*
ESP26	Tb927.7.6490	catctagaAGGCTCTATAGGATAACCAGG tagcggccgcGTCCTCATTAATGCTCTCCG	tagcggccgcCCCCAACTAATGATGACCC caggatccTAACGACTTCCAGTTCTGAAGA	pSiS-HhsfG-ESP26-Nt
ESP27	Tb927.3.5530	tagcggccgcCACACTGCTACGAGCG catctagaTTGACTGCAGGCTACCC	cacaagcttGATAAACCAATGTGGTGCGT tagcggccgcGGGAGGGTGAACACTAC	pSiS-HhsfG-ESP27-Ct
ESP28	Tb927.8.650	tagcggccgcTGCTGTTAATTACAGGGGC catctagaATCATACTCCGTCAGAAGTTTCA	cacaagcttGGCATTTGTTTGGCAGG tagcggccgcTGCGTTAGGACGTCTTTTC	pSiS-HhsfG-ESP28-Ct
ESP29	Tb927.9.12000	tagcggccgcCCAAAACTACAACACAAAGCC catctagaTTTTGTTAGCAATCGCTCCA	cacaagcttTCGGTACATTAAGGCACCT tagcggccgcGTGGGAAGAGAAGTTTACCC	pSiS-HhsfG-ESP29-Ct
ESP30	Tb927.8.2380	tagcggccgcGGCAGGATTGTACCTTCG catctagaACGTGCGACAGTAGTGA	cacaagcttAGGTAGTTAGTTGAGGGAGG tagcggccgcCACGATGCTCAACAGAGATC	pSiS-HhsfG-ESP30-Ct
ESP31	Tb927.8.6720	tagcggccgcACGATGATGCTTGCTGTTG catctagaCTGTTCTTCTTTCTTCCCATACC	cacaagcttACGTGTTTGTTTTATATGGGACAC tagcggccgcACAGGGAGCAATTATTTTATACCG	pSiS-HhsfG-ESP31-Ct

Table 2.3 Summary of all cell lines generated for experimentation
Background cell line, the plasmid and the resultant cell line are given for each. Information on the drug(s) and working concentration(s) used for the selection of stable transformants are also provided: hyg = Hygromycin, phleo = Phleomycin, blast = Blasticidin, G418 = Geneticin. It should be noted that p2T7-177-ESP12 and p2T7-177-ESP13 plasmids could target *ESP12, ESP13* and *Tb927.7.4280* (another related gene that has not been GFP-tagged in this study). *ESP22* is also part of a multigene family, but p2T7-177-ESP22 will only target *ESP22* and not the other 5 divergent family members.

Plasmid	Background cell line	Resultant cell line	Drug selection (μg ml^{-1}/drug)
p2T7-177-ESP1	S16 +*sfG::ESP1*	S16 + *sfG::ESP1* + *ESP1* RNAi	5/hyg, 2.5/phleo
p2T7-177-ESP6	S16 +*sfG::ESP6*	S16 + *sfG::ESP6* + *ESP6* RNAi	5/hyg, 2.5/phleo
p2T7-177-ESP10	S16 + *ESP10::sfG*	S16 + *ESP10::sfG* + *ESP10* RNAi	5/hyg, 2.5/phleo
p2T7-177-ESP11	S16 + *ESP11::sfG*	S16 + *ESP11::sfG* + *ESP11* RNAi	5/hyg, 2.5/phleo
p2T7-177-ESP12	S16 + *ESP12::sfG*	S16 + *ESP12::sfG* + *ESP12* RNAi	5/hyg, 2.5/phleo
p2T7-177-ESP13	S16 + *ESP13::sfG*	S16 + *ESP13::sfG* + *ESP13* RNAi	5/hyg, 2.5/phleo
p2T7-177-ESP14	S16 + *ESP14::sfG*	S16 + *ESP14::sfG* + *ESP14* RNAi	5/hyg, 2.5/phleo
p2T7-177-ESP21	S16 + *ESP21::sfG*	S16 + *ESP21::sfG* + *ESP21* RNAi	5/hyg, 2.5/phleo
p2T7-177-ESP22	S16 + *ESP22::sfG*	S16 + *ESP22::sfG* + *ESP22* RNAi	5/hyg, 2.5/phleo
p2T7-177-TbPT0	S16 + *TbPT0::sfG*	S16 + *TbPT0::sfG* + *TbPT0* RNAi	5/hyg, 2.5/phleo
p2T7-177-CLH	S16	S16 + *CLH* RNAi	2.5/phleo
pSiS-HhsfG-ESP26	S16	S16 + *sfG::ESP26*	5/hyg
pSiS-HhsfG-ESP27	S16	S16 + *ESP27::sfG*	5/hyg

pSiS-HhsfG-ESP28	S16	S16 + *ESP28::sfG*	5/hyg
pSiS-HhsfG-ESP29	S16	S16 + *ESP29::sfG*	5/hyg
pSiS-HhsfG-ESP30	S16	S16 + *ESP30::sfG*	5/hyg
pSiS-HhsfG-ESP31	S16	S16 + *ESP31::sfG*	5/hyg
p2T7-177-ESP27	S16 + *ESP27::sfG*	S16 + *ESP27::sfG* + *ESP* RNAi	5/hyg, 2.5/phleo
p2T7-177-ESP29	S16 + *ESP29::sfG*	S16 + *ESP29::sfG*+ *ESP* RNAi	5/hyg, 2.5/phleo
p2T7-177-ESP30	S16 + *ESP30-sfG*	S16 + *ESP30::sfG* + *ESP* RNAi	5/hyg, 2.5/phleo
p2T7-177-ESP31	S16 + *ESP31::sfG*	S16 + *ESP31::sfG* + *ESP* RNAi	5/hyg, 2.5/phleo
pEnNsfG-KIN17	SmOxB427	SmOxB427 + *sfG::KIN17*	5/hyg
pEnNsfG-KIN17-B	SmOxB427 + *sfG::KIN17*	SmOxB427 + *sfG-KIN17/sfG::KIN17*	5/hyg, 5/blast
pEnG05	SmOxB427	SmOxB427 + *KIN17::GFP*	5/hyg
pEnNsfG-DYNC1H1	SmOxB427	SmOxB427 + *sfG::DYNC1H1*	5/hyg
KIN17-BLAST KO	SmOxB427	SmOxB427 + *Δkin17*	5/blast
KIN17-NEO KO	SmOxB427 + *Δkin17*	SmOxB427 + *Δkin17/ Δkin17*	5/blast, 2/G418
pDex577-sfG-KIN17	SmOxB427	SmOxB427 + *sfG::KIN17* OE	2.5/phleo
pDex577-sfG-kin17-rigor	SmOxB427	SmOxB427 + *sfG::kin17-rigor* OE	2.5/phleo
pDex577-sfG-KIN17	SmOxB427 + *Δkin17/ Δkin17*	SmOxB427 + *Δkin17/ Δkin17* + *sfG::KIN17* OE	2.5/phleo, 5/blast, 2/G418,

pDex577-sfG-kin17-rigor	SmOxB427 + *Δkin17/Δkin17*	SmOxB427 + *Δkin17/Δkin17* + *sfG::kin17-rigor* OE	2.5/phleo, 5/blast, 2/G418
pDex577-mSt-KIN17	SmOxB427 + *Δkin17/Δkin17*	SmOxB427 + *Δkin17/Δkin17* + *mSt::KIN17* OE	2.5/phleo, 5/blast, 2/G418
pDex577-mSt-kin17-rigor	SmOxB427 + *Δkin17/Δkin17*	SmOxB427 + *Δkin17/Δkin17* + *mSt::kin17-rigor* OE	2.5/phleo, 5/blast, 2/G418
pDex577-mSt-KIN17	SmOxB427 + *sfG-KIN17/sfG::KIN17*	SmOxB427 + *sfG-KIN17/sfG::KIN17* + *mSt::KIN17* OE	2.5/phleo, 5/hyg, 5/blast
pDex577-mSt-kin17-rigor	SmOxB427 + *sfG-KIN17/sfG::KIN17*	SmOxB427 + *sfG-KIN17/sfG::KIN17* + *mSt::kin17-rigor* OE	2.5/phleo, 5/hyg, 5/blast
pDex577-mSt-KIN17	SmOxB427 + *sfG::DYNC1H1*	SmOxB427 + *sfG::DYNC1H1* + *mSt::KIN17* OE	2.5/phleo, 5/hyg,
pDex577-mSt-kin17-rigor	SmOxB427 + *sfG::DYNC1H1*	SmOxB427 + *sfG::DYNC1H1* + *mSt::kin17-rigor* OE	2.5/phleo, 5/hyg,
pV4ΔDex-mSt-KIN17	SmOxB427 + *sfG-KIN17/sfG::KIN17*	SmOxB427 + *sfG-KIN17/sfG::KIN17* + *mSt::KIN17* OE $_{V4}$	2.5/phleo, 5/hyg, 5/blast
pV4ΔDex-mSt-kin17-rigor	SmOxB427 + *sfG-KIN17/sfG::KIN17*	SmOxB427 + *sfG-KIN17/sfG::KIN17* + *mSt::kin17-rigor* OE $_{V4}$	2.5/phleo, 5/hyg, 5/blast

Chapter 3. Investigating the role of flagellar pocket proteins in *Trypanosoma brucei*

3.1. Introduction

3.1.1. Flagellar pocket proteins of *Trypanosoma brucei*

The FP of *T. brucei* is the site of many important cellular functions, such as the uptake of nutrients essential for growth, sensing the extracellular environment and, in bloodstream form (BSF) parasites, clearance of surface-bound antibodies to aid in evasion of the adaptive immune response (Field and Carrington 2009). Disruption of FP function, either by knockdown of clathrin heavy chain (CLH) to inhibit endocytosis (Allen et al. 2003), or by affecting FP biogenesis (Bonhivers et al. 2008), is lethal to the cell, further emphasising the importance of this organelle.

Until relatively recently, only a handful of receptors and transporters had been localised to this region in BSFs. These include the transferrin receptor (TfR) (Salmon et al. 1994), haptoglobin-haemoglobin (HpHbR), aquaglyceroporin 2 (AQP2) (Baker et al. 2012) and a protein associated with the differentiation (PAD2) (Dean et al. 2009), which have been discussed previously in Chapter 1. Importantly, the few FP proteins characterised to date have all been shown to play roles in either the uptake of nutrients, adaption to different host environments, drug resistance, or parasite differentiation, and thus the overall survival and persistence of *T. brucei*.

The number of known flagellar pocket-localised proteins have significantly increased following a recent surface proteomic study (Gadelha et al. 2015). Novel surface components were identified by chemically labelling the surface membrane of live cells with fluorescein. Cells were then lysed, fluorescein-labelled proteins purified by affinity chromatography, and protein identities determined by tandem mass spectrometry. A high-confidence set of 175 putative surface proteins was defined by selecting only proteins with at least five-fold enrichment in the labelled vs unlabelled samples, and filtering them further to include only those with predictions for a signal peptide, GPI-anchor addition site or transmembrane (TM) domain. Validation of this surface

proteome, or ‘surfeome’, consisted of the endogenous-locus tagging of a subset of 25 candidates. Candidates were selected on the basis that they were “hypothetical” proteins at the time of the study, covered a range of protein topologies and signal enrichment. These were termed ESPs for Enriched in Surface Proteome. Of the 25 proteins, 2 could not be detected by microscopy. Of the remaining 23, 18 localised to the cell surface membrane, of which 9 were found to localise predominately to the flagellar pocket (either exclusively, or in combination with other surface domains, Figure 3.1). Among these 9 novel FP proteins, those predicted to be either GPI-anchored or type I TM proteins were found to be trypanosomatid or kinetoplastid specific, respectively; whilst multipass TM proteins were typically conserved across eukaryotes (Gadelha et al. 2015). This distribution suggests parasite-specific roles for GPI-anchored and type I TM proteins, such as immune evasion and adaptation and survival in the different host environments they incur. For a summary of the respective gene IDs, localisation and protein topology for the FP ESPs, see Table 3.1.

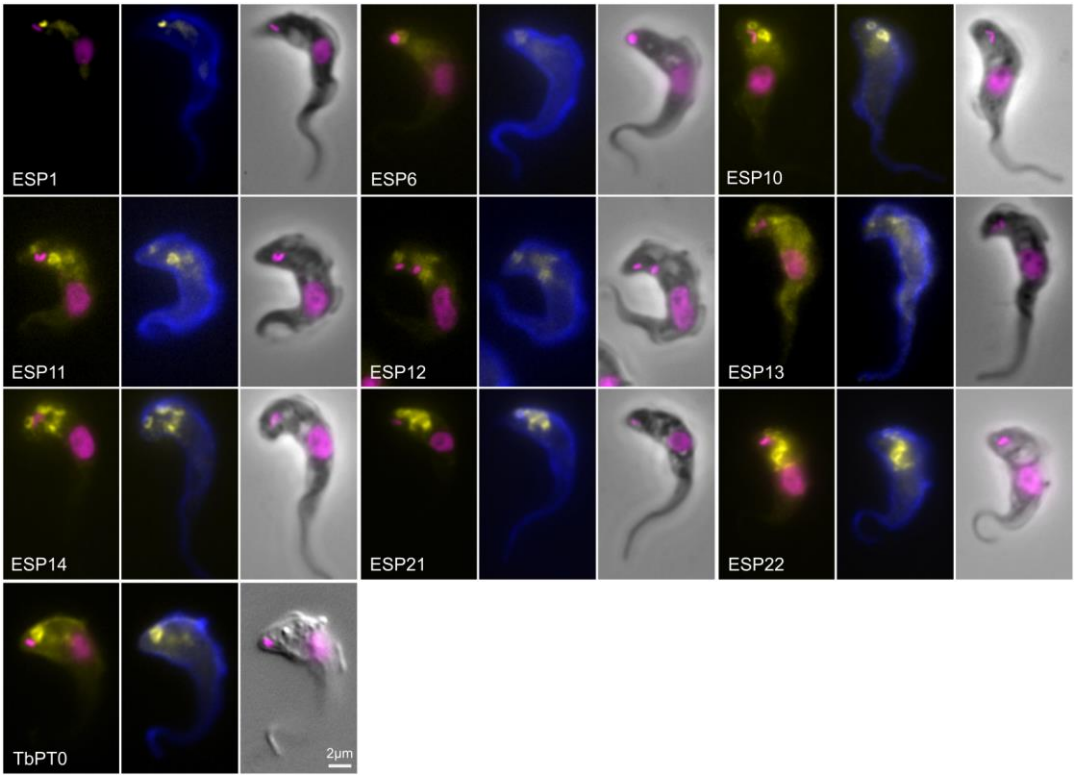


Figure 3.1. Proteomics identify novel FP proteins of BSF *T. brucei.*
Flagellar pocket localisation of ESPs was determined by native fluorescence. GFP signal corresponding to endogenously tagged FP protein is shown in yellow. Surface membrane was counterstained with Concanavalin A (binds to glycan moieties associated with VSG). Cell DNA content (mitochondrial and nuclear) is highlighted in magenta. Native fluorescence images of ESPs from Gadelha *et al*. 2015. TbPT0 (Sanchez 2013) was also localised to FP in our lab and was included as a positive control for downstream experiments.

Table 3.1 Summary of FP-ESPs
Localisation data (as in Gadelha et al. 2015), protein properties and putative annotations summarised for FP ESPs (FP = flagellar pocket; CB = cell body, E = endosomes and FM = flagellar membrane). Transmembrane domains were predicted using TMHMM (Krogh et al. 2001) GPI anchor addition sequences were predicted using PredGPI (Pierleoni et al. 2008).

Name	Gene ID	Cellular Localisation	Protein topology	Gene length (bp)	Mr GFP-fusion (kDa)	Annotation (tritypdb.org)
ESP1	Tb927.2.5280	FP	GPI	2109	101	trans-sialidase, putative
ESP6	Tb927.10.990	FP	GPI	1115	66	hypothetical, conserved
ESP10	Tb927.2.1700	FP + E	Type I TM	2289	114	hypothetical, conserved
ESP11	Tb927.4.3040	FP + E	Type I TM	618	54	hypothetical, conserved
ESP12	Tb927.7.4230	FP + E	Type I TM	696	57	hypothetical, conserved
ESP13	Tb927.7.4260	FP + CB + FM	Type I TM	792	60	hypothetical, conserved
ESP14	Tb927.7.470	FP + E	Type I TM	894	64	hypothetical, conserved
ESP21	Tb927.10.13930	FP + E	Multipass TM	999	68	phosphatidic acid phosphatase, putative
ESP22	Tb927.10.530	FP + E	Multipass TM	2067	108	choline transporter, putative
TbPT0	Tb927.3.4070	FP + CB	Multipass TM	1788	96	pyruvate transporter (Sanchez 2013)

As mentioned, one of the defining criterion for the initial localisation of ESPs by Gadelha and colleagues was that they were annotated as “hypothetical”, thus for which no functional data was available at the start of the study (Gadelha et al. 2015). For the majority, this is indeed still the case. Consequently, the main focus of this chapter is to attempt to determine their function at the flagellar pocket of BSF cells. An exception to this is ESP22, for which knockdown experiments have since been performed in both BSF and PCF cells (Macedo et al. 2013). Based on sequence homology, ESP22 is one of six predicted putative choline transporters in *T. brucei*. Whilst the other five are highly similar in sequence and form a tandem array, *ESP22* has been shown to be phylogenetically distinct (Macedo et al. 2013). RNA interference (RNAi) against either *ESP22* or the other five genes in combination does not affect choline uptake or parasite growth (Macedo et al. 2013). This suggests that either they may not be the major transporters of choline in *T. brucei*, or that choline is not an essential nutrient for BSFs *in vitro*. However, knockdown of *ESP22* as part of a genome-wide RNA interference (RNAi) screen caused a loss of parasite fitness (Alsford et al. 2011). In view of the discrepancy I have included ESP22 in my functional characterisation of the FP-located ESPs.

Some indication of protein function can sometimes be inferred from homology searches or the presence of Pfam domains. Examples of this are ESP1 and ESP21, which have sequence similarity to trans-sialidases and lipid phosphate phosphatases, respectively (Montagna et al. 2006; Alves e Silva et al. 2016), In *T. brucei*, there are two related proteins with annotated phosphatidic acid phosphatase domains, Tb927.10.13400 and Tb927.8.480. Lipid phosphate phosphatases can function in a variety of signal transduction pathways in other systems (Brindley et al. 2009), including roles in life cycle differentiation in *T. cruzi* (Gimenez et al. 2011). It is therefore plausible that this could also be case for ESP21 in *T brucei*. For ESP1, in insect stages at least, this protein does not show either sialidase or trans-sialidase activity (Montagna et al. 2006); so even in instances where putative annotations exist, functional characterisation is still necessary.

In addition to the ESPs, TbPT0 (Tb927.3.4070) has been localised to the flagellar pocket of *T. brucei* (Gadelha et al. 2015) , and is one of five members

of a multigene family that cluster as a tandem array on chromosome 3. Their role in pyruvate export was recently established by yeast complementation experiments (Sanchez, 2013). In addition, knockdown of *TbPT* family in BSFs caused growth arrest and cell death after two weeks of RNAi induction. As TbPT0 is an example of a flagellar-pocket localised protein that also exhibits a growth defect upon knockdown in BSFs, it was included as a positive control for subsequent functional analysis of ESPs.

Overall, the aforementioned surfeome study has produced a validated set of *bona fide* FP proteins with unknown function, as well as a positive control in the form of a lethal FP-localised protein, TbPT0. I can now begin to interrogate the role these proteins may have in parasite survival during the BSF stage of its life cycle.

3.1.2. RNA interference as a tool to interrogate protein function in *T. brucei*

One way to interrogate protein function in cells is by utilising a reverse genetics approach to reduce or remove the protein in question and observe the phenotype that follows. A conventional knockout (KO) strategy can be used to remove all protein from the cell, typically by replacing the gene of interest with a selectable drug marker. However, in a diploid organism such as *T. brucei,* generation of KO lines requires at least two rounds of transfection and screening. This is still suitable for the study of single genes, but when studying a set of 9 proteins, like the FP ESPs, this becomes a very time-consuming process. Furthermore, ~40% of the ESPs are part of multi-gene families; therefore the number of family members that can be ablated in a cell is restricted by the number of drug resistance markers available. Generation of KOs also becomes difficult when trying to interrogate genes that are essential for cell survival.

An alternative for interrogating the function of essential genes in *T. brucei* is a Cre-loxP conditional KO system (Kim et al. 2013). Here, the first allele is deleted and the second allele is replaced with a conditional KO fragment containing an epitope-tagged version of the gene, flanked with loxP sequences, which recombine to delete the second gene copy upon the

induction of a Cre-recombinase. However, similar drawbacks exist as for as conventional KOs.

Although not established in *T. brucei* at the start of this study, the efficiency of gene KO generation as well as the potential to knockdown multiple genes at once, has been vastly improved by the development of a CRISPR-Cas 9 gene editing system (reviewed in Doudna & Charpentier 2014). This technology has since been utilised in kinetoplastids such as *Leishmania spp*. and *T. cruzi* over the last couple of years (Sollelis et al. 2015; Peng et al. 2015). Indeed, in *T. cruzi* CRISPR-Cas 9 was used to knockdown a large family consisting of >50 genes (Peng et al. 2015). More recently, the first use of CRISPR-Cas 9 in *T. brucei* was reported, where they were able to efficiently KO both copies of *GPI-PLC* in a single step process (Beneke et al. 2017).

Whilst the CRISPR-Cas technology is still in the developmental stages, in *T. brucei* at least, RNA interference (RNAi) has predominated when it comes to similarly high-throughput studies at a genome-wide level, as well as more generally, for the study of individual gene function. RNAi relies on the production of dsRNA (Fire et al. 1998), which is then cleaved into ~20bp small interfering RNAs (siRNA) via a protein complex known as Dicer (Bernstein et al. 2001). These siRNAs are subsequently recognised by an RNA-induced silencing complex (RISC) (Hammond et al. 2000, 2001), which separates the two stands of RNA, retaining one as a target strand. This strand is used as a template to identify complementary messenger RNA (mRNA). Upon recognition by RISC, the mRNA is cleaved and degraded by Argonaute (catalytic subunit of RISC) (Liu et al. 2004), thus silencing the expression of the gene.

RNAi has been used extensively in *T. brucei* as a technique to silence individual genes, as well as for functional screens on a genome-wide scale (reviewed in Kolev et al. 2011). At an individual gene level, knockdown is achieved via the use of tetracycline-inducible constructs that produce dsRNA against a chosen target sequence. For genome-wide functional studies that use a forward genetics approach to identify genes involved in a particular cell process, a similar strategy has been adapted to generate a cohort of RNAi plasmids that cover theoretically, the whole genome. Here, rather than an

individual RNAi fragment, *T. brucei* genomic DNA is sonicated and resultant fragments inserted into inducible RNAi constructs. The first of its kind in any organism was generated in Paul Englunds lab, and used as a methodology to screen the *T. brucei* genome for genes involved in expression of the major surface coat protein in PCFs, by screening for genes whose disruption conferred sensitivity to Concanavalin A (Morris et al. 2002). The same library has since been repurposed to investigate mechanisms of anti-trypanosomal drug resistance (Baker et al. 2011; Alsford et al. 2012) and for a loss-of-function screen (Alsford et al. 2011).

Whilst one of the known limitations of RNAi is that is does not always give complete knockdown of the target mRNA, it has many advantages over the alternatives discussed earlier. Firstly, the inducible nature of RNAi, made possible by the generation of cell lines that stably express T7 RNA polymerase in combination with a tetracycline repressor, means this technique can be used in instances where a gene is essential for parasite growth (Wirtz et al. 1999a). Given that the majority of FP-localised proteins characterised to date were found to be essential for parasite survival (e.g. TfR, HpHbR and TbPT0), the same may also be true of the novel FP ESPs. Secondly, the RNAi targeting fragments used to silence the gene(s) of interest can target multiple copies of the same gene family, if they are similar enough at a DNA sequence level. As ~40% of the ESPs are part of multi-gene families, it may be possible to knockdown some or all of these genes in tandem, thus alleviating functional redundancy in this instance. Therefore, in light of the current technologies available to investigate gene function, and the relative benefits and limitations of each, RNAi will be the tool of choice to begin to interrogate the functions of the FP ESPs.

3.2. Results

3.2.1. Testing validated FP components for essentiality *in vitro*

In order to investigate the function of nine novel FP proteins, *ESP* genes were targeted for silencing by inducible RNAi. In addition to the set of *ESP*s, *TbPT0* and *CLH* were included as positive controls, as they both produce growth defects upon knockdown, albeit with different degrees of severity (Allen

et al. 2003; Sanchez 2013). It is unknown whether fragment length or gene target region can influence knockdown efficiency. Thus, a central ~500bp targeting for each gene was chosen.

For each RNAi fragment, Basic Local Alignment Search Tool (BLAST) (blast.ncbi.nlm.nih.gov) searches were performed against the *T. brucei* reference genome to exclude the possibility of off-target effects and to determine which, if any, additional family members would be targeted. For *ESP1* and *ESP22*, of which there are 9 and 5 additional family members respectively (Jackson et al. 2013; Macedo et al. 2013), these genes are sufficiently dissimilar that knockdown can be assumed to be specific to the individual gene. *ESP12* and *ESP13,* on the other hand, are two of four genes in *T. brucei* that were assigned as members of Fam79 (hypothetical transmembrane proteins) as part of a cell surface phylome study (Jackson et al. 2013). The RNAi fragment designed against *ESP12* has ~70% sequence identity to both *ESP13* and *Tb927.7.4280*, therefore it is possible that all three genes could be silenced. Equally, the fragment against *ESP13* has the potential to target *ESP12* and *Tb927.7.4280*, as it also shares ~70% identity to these genes. The fourth member of this gene family, *Tb927.7.4270* is more distantly related (Jackson et al. 2013), and thus it was not possible to design a single RNAi fragment to target all four copies at once. In the case of *TbPT0,* the RNAi targeting fragment used here has >90% sequence identify to all *TbPT* family members, which should simultaneously knockdown all five genes.

In *T. brucei,* inducible vectors such as those used for RNAi typically integrate into transcriptionally silent regions, for example the 177-bp repeat regions of the mini-chromosomes, or upstream of an 18S ribosomal *RNA* gene (*rRNA* spacer) present within a megabase-sized chromosome (Wickstead et al. 2002b; White et al. 1986). However, integration into the *rRNA* spacer has been shown to produce low levels of transcription in the absence of tetracycline induction (Wickstead et al 2002). Consequently, RNAi fragments were introduced into the mini-chromosomal-integrating p2T7-177 plasmid, so that double-stranded RNA (dsRNA) would be produced from two opposing T7 promoters upon the addition of tetracycline. Many functional studies in *T. brucei* involving RNAi, including the aforementioned genome-wide RNAi

screens, have been performed using the head-to-head promoter system, rather than the alternative hairpin RNAi construct.

Once generated, all p2T7-177-ESP RNAi plasmids were transfected into their corresponding GFP-tagged cell lines (from Figure 3.1), which are already RNAi-competent as they express T7 polymerase and tet repressor (Wirtz et al. 1999). By transfecting these constructs into cell lines in which the endogenous protein is GFP-tagged, level of endogenous ESP before and after RNAi induction can be easily monitored for all cell lines by Western blot, using an anti-GFP antibody (negating the need to raise antibodies against each specific ESP). RNAi was induced in transformants by the addition of tetracycline in culture for 24 hours, and knockdown of each ESP was assessed by immunoblotting whole cell lysates with anti-GFP antibodies. For each transfection, 3 independent clones were induced and screened in parallel with their non-induced equivalent and parental (GFP-tagged) cell lines (Supplementary Figure 3-1). The clones showing greatest protein ablation compared to non-induced cells were taken forward for further analysis. In all cases, Western blot results revealed a significant knockdown for all ESPs, with protein reduction below the level of detection of the technique seen for the majority (Figure 3.2A). It should be noted that a reduction in ESP1 and ESP12 cell lines between parental and non-induced cells was also observed, suggestive of 'leaky' expression of RNAi fragments in the absence of induction. For ESP14, 21 and 22, low protein levels could still be detected after 24 hours of induction. However, these ESPs have the highest levels of endogenous protein, so it is possible that the relative proportion of protein ablation is similar across the tested ESPs. Therefore, I was able to generate cell lines exhibiting significant knockdown for the nine ESPs selected for this study (plus TbPT0), allowing me to proceed to their functional analysis.

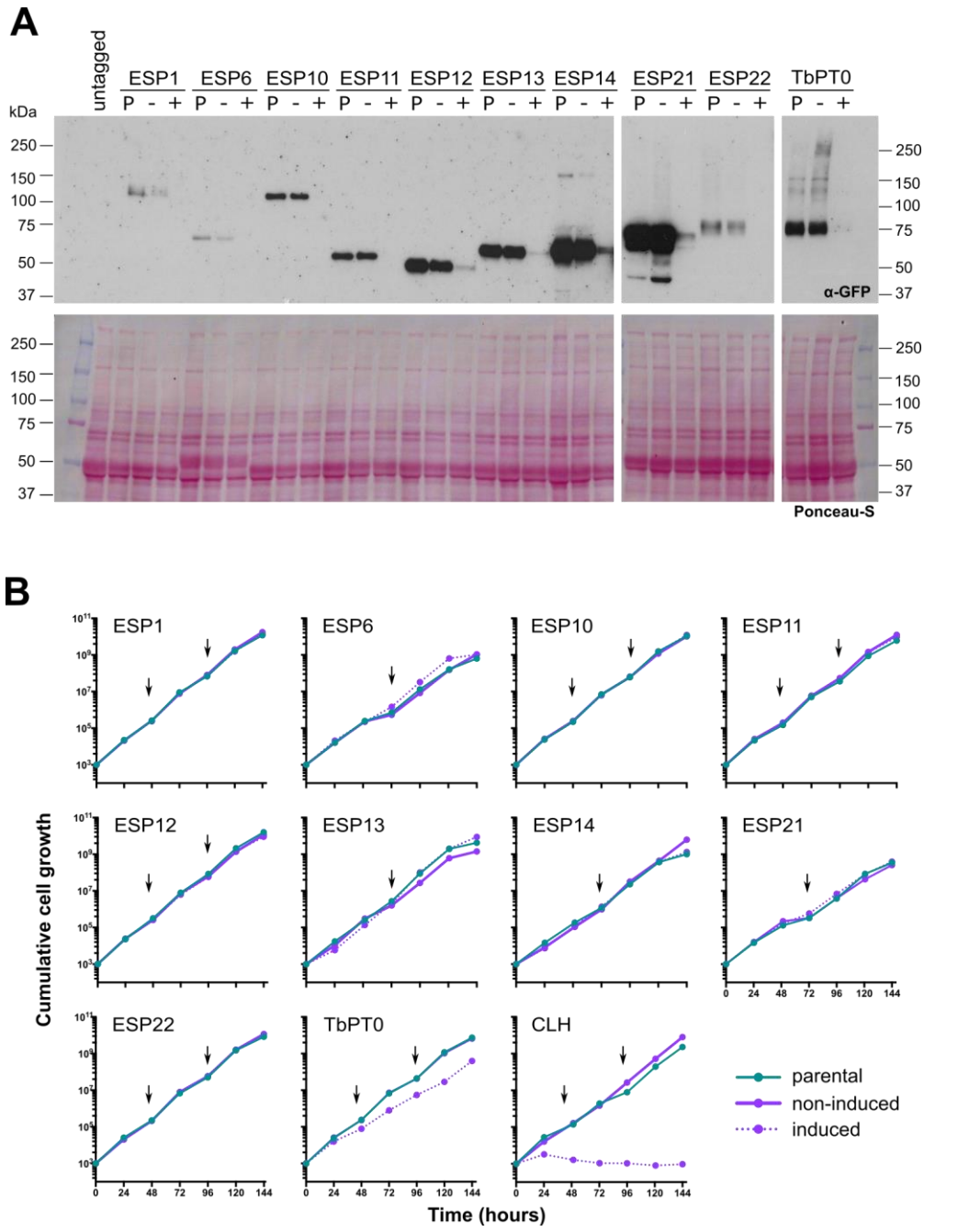


Figure 3.2. Ablation of ESPs does not impair cell growth in culture
A) Immunoblot of ESP-RNAi whole cell lysates probed with an anti-GFP antibody shows a reduction in ESP protein levels after 24 hours of RNAi induction (+) compared to non-induced (-) and parental (P) cell lines. $2.5x10^6$ cells were loaded in each lane. Nitrocellulose membrane stained with Ponceau-S included as a loading control. **B)** Cumulative growth curves of parental, non-induced and induced ESP RNAi lines over 6 days show no growth defect for any of the ESPs. Cell densities were recorded every 24 hours using an ATP-based luciferase assay.TbPT0 and CLH serve as positive controls as they are known to cause growth defects. Arrows indicate time-point at which cells were diluted.

To determine if FP-localised ESPs are required for cell viability *in vitro,* the newly generated RNAi cell lines were grown in the presence or absence of RNAi induction for six days (Figure 3.2). Growth was monitored every 24 hours using an ATP-based luciferase assay. This assay has been shown to be a reproducible and sensitive method for assessing *T. brucei* viability in a high-throughput manner (MacKey et al. 2006; Sykes & Avery 2009). The principle of this assay is that the mono-oxygenation of luciferin to oxyluciferin (catalysed by luciferase) produces a luminescent signal. This reaction only occurs in the presence of ATP, which is supplied by viable cells, making it a good proxy for cell number. To determine whether this would be a useful tool for monitoring growth of ESP-RNAi cell lines, the upper and lower limits of detection of the system were ascertained by titrating cell concentrations from $3.16x10^6$ cells/ml down to $3.16x10^1$ cells/ml on a $\sqrt{10}$ scale, and luminescence values recorded (Supplementary Figure 2). In agreement with previous studies, there was a linear relationship between cell density and luminescence between $1x10^3$ and $1x10^6$ cells/ml, suitable for the monitoring growth of log-phase *T. brucei*. Additionally, the aforementioned assay was chosen over manual counts to facilitate medium-throughput analysis of all nine ESPs plus controls (~35 cell lines total).

Growth of the positive control TbPT0 and CLH-RNAi cell lines was impaired upon RNAi induction as anticipated. For CLH, cell death was apparent as early as 24 hours, reproducing the phenotype observed in a previous study (Allen et al. 2003). Knockdown of *TbPT0* also led to a growth defect but this was less severe than that reported previously (Sanchez 2013), with the major difference between this study and theirs being the use of a hairpin RNAi construct, instead of the head-to-head promoter system used here. It is possible that the stem-loop construct induces a more rapid knockdown and consequently a stronger growth phenotype. While, if knockdown with the head-to-head promoter system is slower, this could give cells more time to respond and adapt to protein loss, similar to compensation effects seen for gene knockouts. Therefore, this could explain why the growth defect observed here is much less severe than that reported for the hairpin RNAi construct. Furthermore, Sanchez reported that it took 2 weeks for complete cell death as result of

TbPT0 knockdown, which could indicate that protein turnover is relatively slow for this transporter, thus it may have been informative to continue the growth analysis for TbPT0 in this study for the full 2 weeks.

Strikingly, no difference in growth was observed between non-induced and induced cells for any of the ESPs tested over the course of the 6-day RNAi induction (Figure 3.2B). This is in spite of significant ESP ablation being achieved (Figure 3.2A). Thus, the majority of FP-localised proteins in this study appear dispensable for the growth of *T. brucei in vitro,* under the conditions tested here. This result is rather surprising given the essentiality of FP receptors characterised to date, including TbPT0 studied here. However, in light of the result for the pyruvate transporter, it is possible that if a hairpin RNAi construct had been used to knockdown these genes, additional growth defects may have been detected that were missed by using the head-to-head promoter approach.

3.2.2. Localisation of putatively essential components to the FP

Based on the results from section 1.2.1, only 1 of 10 FP proteins investigated here was required for survival of *T. brucei in vitro*, and the function of the protein in question (TbPT0) had already been determined (Sanchez 2013). In an attempt to identify additional proteins that were both localised to the flagellar pocket and required for the survival of BSF parasite, an alternative approach was devised. This involved taking the surfeome data set of 175 proteins (Gadelha et al. 2015) and filtering them based on “essentiality” using data from a genome-wide loss-of-fitness screen (Alsford et al. 2011). To do this, raw data from the RNAi library screen were plotted to compare the number of reads for each gene in induced cells (after 6 days RNAi induction) against the number of reads in non-induced cells, covering ~7500 of the ~9200 genes of the *T. brucei* genome (Alsford et al. 2011; Berriman et al. 2005). 83 of the original 175 surfeome components present in this dataset were then highlighted, with 50 of these showing a loss-of-fitness after 6 days of RNAi induction (Figure 3.3A).

A caveat of utilising this approach to identify putatively essential proteins is that 5 out of 9 of FP-localised ESPs (and TbPT0) interrogated in section 1.2.1

were also considered to have a loss-of-fitness according to Alsford and colleagues. As TbPT0 was the only one from this set to show a growth defect upon knockdown by individual RNAi, this was used to apply more stringent threshold, to increase the likelihood of obtaining *bona fide* essential FP proteins (Figure 3.3B). In support of this, applying the same threshold to the original set of ESP proteins excludes 8 out of 9 of these. Applying this threshold to the remainder of the surfeome reduces the number of putatively essential surfeome proteins from 50 to 23. In parallel, in an attempt to increase the probability that these proteins also localise to the cell surface (i.e. the flagellar pocket), anything with a putative annotation suggestive of cytoplasmic localisation (e.g. protein transport protein Sec31) was excluded, as well as anything in which protein function had been characterised previously, e.g. FLA3 (Woods et al. 2013). Utilising these criteria, a new set of six proteins were defined, termed ESP26-31.

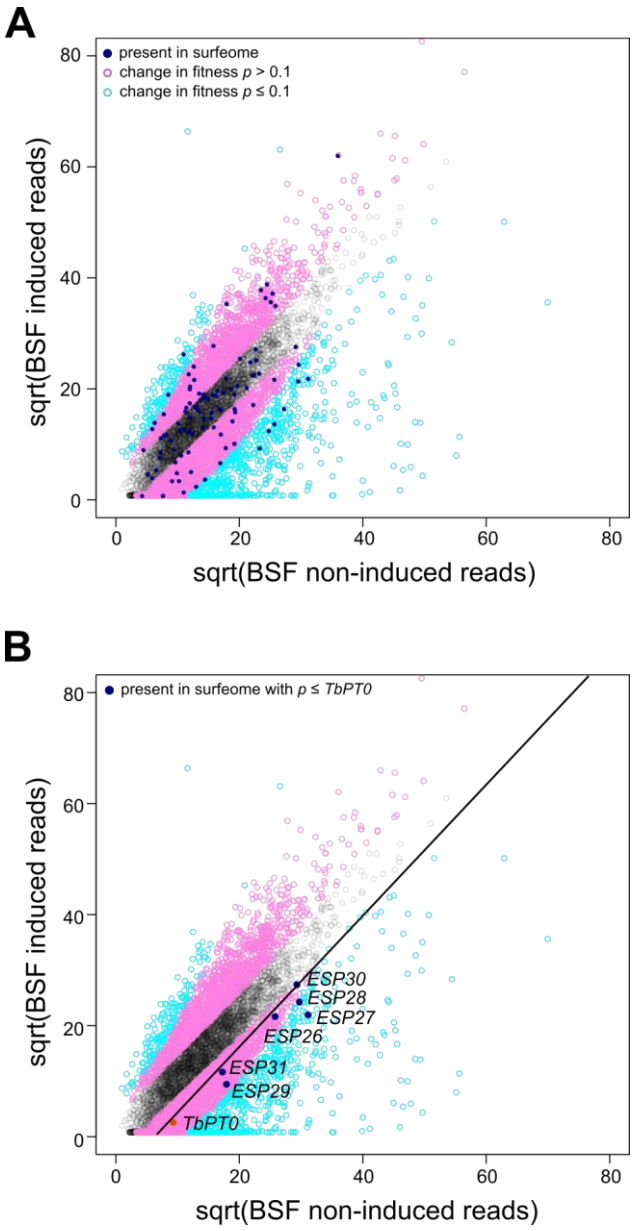


Figure 3.3. Defining a set of novel and essential FP ESPs
A) Comparative analysis of BSF datasets from a genome-wide RNAi screen (Alsford et al. 2011) and a BSF surface proteome (Gadelha et al. 2015). The square root of non-induced RNAi reads were plotted against reads after 6 days of RNAi induction. Each data point represents a single gene, with pink and light blue circles indicating a change in parasite fitness (light blue; p value ≤0.1). Surfeome components are highlighted in navy blue. **B)** A threshold was applied using TbPT0 (orange) to define a new set of ESPs with probability of being essential ≤TbPT0 (right hand side of graph). Image generated with R script courtesy of Bill Wickstead.

Although no work had been done prior to this study to functionally characterise ESP26-31, some information on either their localisation or putative function can already be inferred from the literature:

- ESP27 (or Tb292), for example, has been localised previously to a region between the flagellar pocket and nucleus of *T. brucei* BSFs by immunofluorescence microscopy (Lee et al. 1994). If this likely endosomal localisation is correct, it is possible that ESP27 is also present, at least transiently, in the FP. The protein sequence of ESP27 contains a large octapeptide (EARLRAEE) repeat with similarity to Tb291, a smaller related protein (Lee et al. 1994), and to an S-antigen of *Plasmodium falciparum*, released during schizont rupture in blood stages (Cowman et al. 1985).
- ESP28 and ESP30 have sequence similarity to cation transporting ATPases and ABC transporters respectively, suggestive of roles in transporting molecules across membranes.
- ESP29 is annotated as a putative CDC50 family protein typically interacting with P4-ATPases (phospholipid translocases) and are required for the correct localisation and activity of these transporters (Bryde et al. 2010). In *Leishmania*, LiRos3, the CDC50 subunit of the P4-ATPase MLF (miltefosine) transporter is necessary for both surface membrane localisation of the protein complex as well as the uptake of the anti-leishmanial drug (García-Sánchez et al. 2014).
- Both ESP26 and ESP31 are annotated as hypothetical proteins, predicted to be GPI anchored and multipass TM proteins respectively; no additional information could be found.

To determine the localisation of ESP26-31, the same endogenous-locus tagging strategy was implemented as used previously for ESP1-25 (Gadelha et al. 2015), whereby all proteins were tagged using a vector toolkit designed specifically for the tagging of membrane proteins in BSFs, the pSiS/pSiG series (Figure 3.4). This vector series contains processing signals required for cell surface association, such as an N-terminal signal peptide and GPI-anchor signal sequence (Gadelha et al. 2015). Furthermore, it incorporates superfolder GFP, which has a fast folding capacity and increased resistance

to the change in redox environments encountered in the ER and extracellular space, compared to EGFP (Pédelacq et al. 2006). To form a fluorophore and produce a fluorescent signal, GFP must form a tight beta-barrel structure. EGFP contains two cysteine residues, which flank the internal chromophore. When expressed in oxidising environments, such as the ER lumen, these cysteines are exposed during folding and can potentially bind other GFP molecules forming non-fluorescent oligomers (Aronson et al. 2011). The rapid folding characteristics of superfolder GFP overcome this issue, enabling protein folding to take place before disulphide bonds are able to form, producing fluorescent monomeric protein (Aronson et al. 2011; Pedelacq et al. 2006). ESP26, a predicted GPI-anchored protein, was tagged at the N-terminus, whereas multipass TM proteins ESP27-31 were tagged at the C-terminus. Once generated, tagging constructs were transfected into RNAi-competent cells (Wirtz et al. 1999a), in preparation for downstream functional analysis.

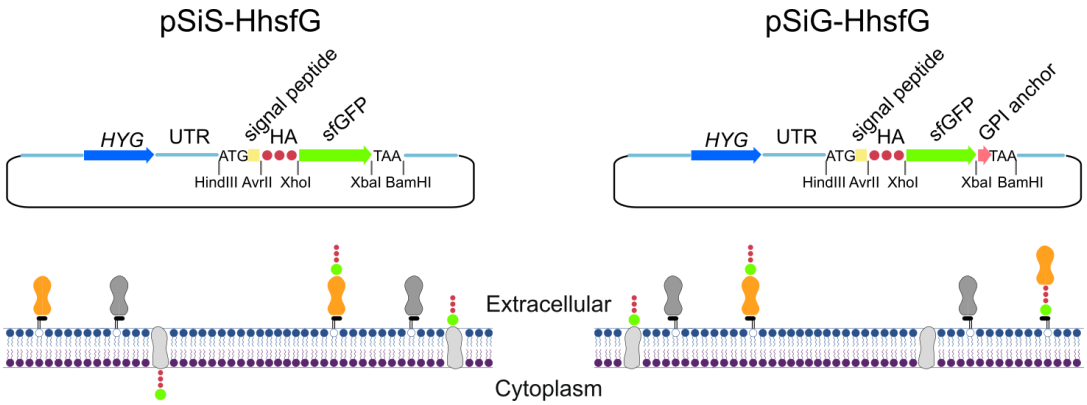


Figure 3.4. A vector toolkit enables the endogenous locus tagging of membrane proteins in BSF *T.brucei*.
Schematic representation of the pSiS/pSiG series of vectors. Both these vectors allow the integration of superfolder GFP (sfGFP) and hemagglutinin (HA) epitope tag at either termini of the gene, under hygromycin (HYG) drug selection. pSiG also contains an additional GPI-anchor addition sequence (derived from VSG221) for tagging GPI-anchored proteins at the C-terminal end, which would typically be used if the protein in question has been experimentally proven to be GPI-anchored. For N-terminal tagging, ORF and 5'UTR fragments are inserted between XbaI and BamHI cloning sites. For C-terminal tagging, 3'UTR and ORF fragments are instead inserted between KpnI and AvrII sites. Adapted from Gadelha et al 2015.

To confirm that correct ESP-sfGFP fusion proteins had been generated for each transfection, 3 independent clones of each cell line were screened by Western blot using anti-GFP monoclonal antibodies (Figure 3.5A). ESP28, 29 and 31 produced chimeric proteins at the predicted molecular weight (160, 75 and 98 kDa respectively). The tagging of ESP27 was most likely correct, yet accurate molecular weight estimation was made difficult due to the ~310 kDa predicted size of the ESP27-sfGFP fusion protein. Correct tagging of ESP27 could thus be confirmed by using a lower percentage polyacrylamide gel, or indeed by diagnostic PCR (see below). ESP30, on the other hand, migrated ~20 kDa lower than its predicted molecular weight of 157 kDa. Whereas chemiluminescence signal on x-ray films corresponding to ESP26 (61 kDa) was not detectable for any of the three clones analysed. I next tested for correct integration of ESP26, ESP27, and ESP30 tagging constructs by diagnostic PCR, designed to discriminate between tagged and untagged copies of each gene (Figure 3.5B). In all instances, PCR products were produced that corresponded to the expected sizes for both the untagged and tagged allele, thus confirming that the tagging constructs had integrated into the genome at the desired locus (Figure 3.5C). This suggests that the altered mobility of ESP30 could be due to post-translational modifications; while the protein level of ESP26 could be below the limit of detection by Western blot. In light of this, ESP26 was excluded from further analysis.

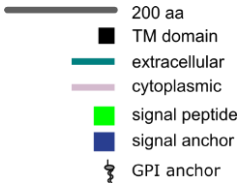
Cellular localisations of ESP27-31 were investigated by native fluorescence microscopy using a surface membrane counterstain (Concanavalin A) to aid in the identification of surface-localised proteins (Figure 3.6). Four out of five fusion proteins localised to the flagellar pocket either in combination with the endosomal system (ESP27, 29 and 30) or the flagellum membrane (ESP31). The localisation of ESP27 to the endosomal region agrees with previous immunofluorescence (Lee et al. 1994), but until now its presence in the FP had not been confirmed. ESP28 appeared to localise exclusively to the ER and consequently was not pursued further.

The number of *bona fide* surface proteins amongst this set (4/5) agrees with the 80% positive hit rate seen for the surfeome (Gadelha et al. 2015), despite the use of different selection criteria. It also highlights the fact that

between this study and that of Gadelha and colleagues, we are unlikely to have exhausted the total cohort of FP proteins present in the surfeome, or indeed the cell. For now, the localisation of ESP27-31 has generated a set of 4 putatively essential FP proteins for functional characterisation, summarised in Table 3.2

Table 3.2 Summary of ESP27-31
Localisation data (determined in this Chapter, Figure 3.6), protein properties and putative annotations summarised for ESP27-31 (FP = flagellar pocket; E = endosomes, FM = flagellar membrane, aa = amino acids). Protein topology determined using TMHMM (Krogh et al. 2001), SignalP 3.0 (Bendtsen et al. 2004 and PredGPI (Pierleoni et al. 2008).

Name	Gene ID	Cellular localisation	Protein topology	Protein length (aa)	Molecular weight (minus GFP/plus GFP)	Annotation (tritypdb.org)
ESP27	Tb927.3.5530	FP+ E		2463	279/310	Tb-292 membrane associated protein
ESP29	Tb927.9.12000	FP+E		388	44/75	CDC50 family, putative
ESP30	Tb927.8.2380	FP + E		1158	126/157	ABC transporter, putative
ESP31	Tb927.8.6720	FP + FM		615	67/98	hypothetical protein, conserved



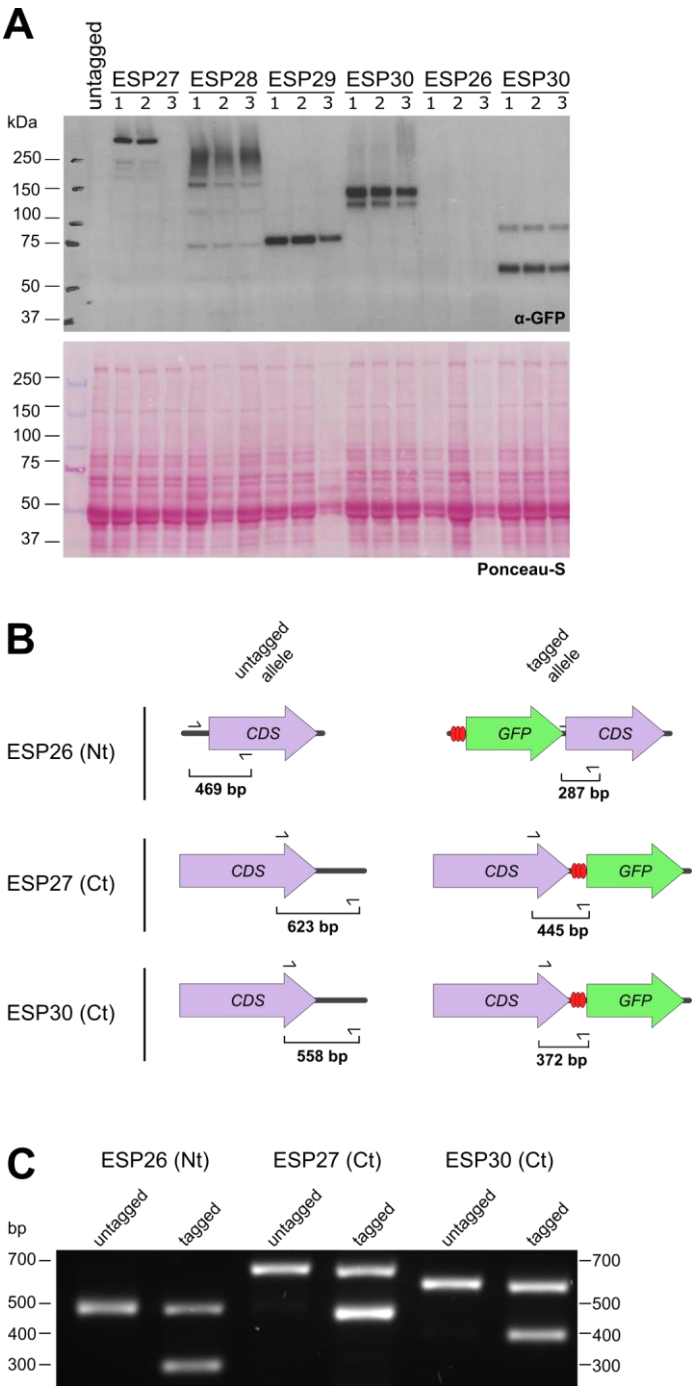


Figure 3.5. Generation of sfGFP fusion proteins for ESP26-31
A) Immunoblot of whole cell lysates for ESP-sfGFP cell lines, detected with monoclonal anti-GFP antibodies, showing chimeric proteins. Predicted molecular weights of the chimeric proteins are as follows: ESP26 = 61 kDa; ESP27 = 310 kDa; ESP28 = 160 kDa; ESP29 = 75 kDa; ESP30 = 157 kDa and ESP31 = 98 kDa. $2.5x10^6$ cells were loaded in each lane. Nitrocellulose membrane stained with Ponceau-S was included as a loading control. **B)** Schematic representation of diagnostic multiplex PCR strategy to check for correct integration of ESP26, 27 and 30. For N-terminal tagging construct (ESP26), a universal reverse primer was designed to anneal within the CDS region, in combination with a forward primer that was specific to either the *GFP* (tagged allele), or 5'UTR (untagged allele). The inverse was the case for C-terminal tags. Primer annealing sites are indicated by arrowheads. Red ovals correspond to HA epitope tag. **C)** Resultant PCR products amplified from either untagged or tagged (ESP-GFP) genomic DNA using the multiplex PCR strategy outlined in B. ESP26, ESP27 and ESP30 tagging constructs have integrated correctly, as PCR products at the expected sizes of ~290, ~450 and ~370bp were produced.

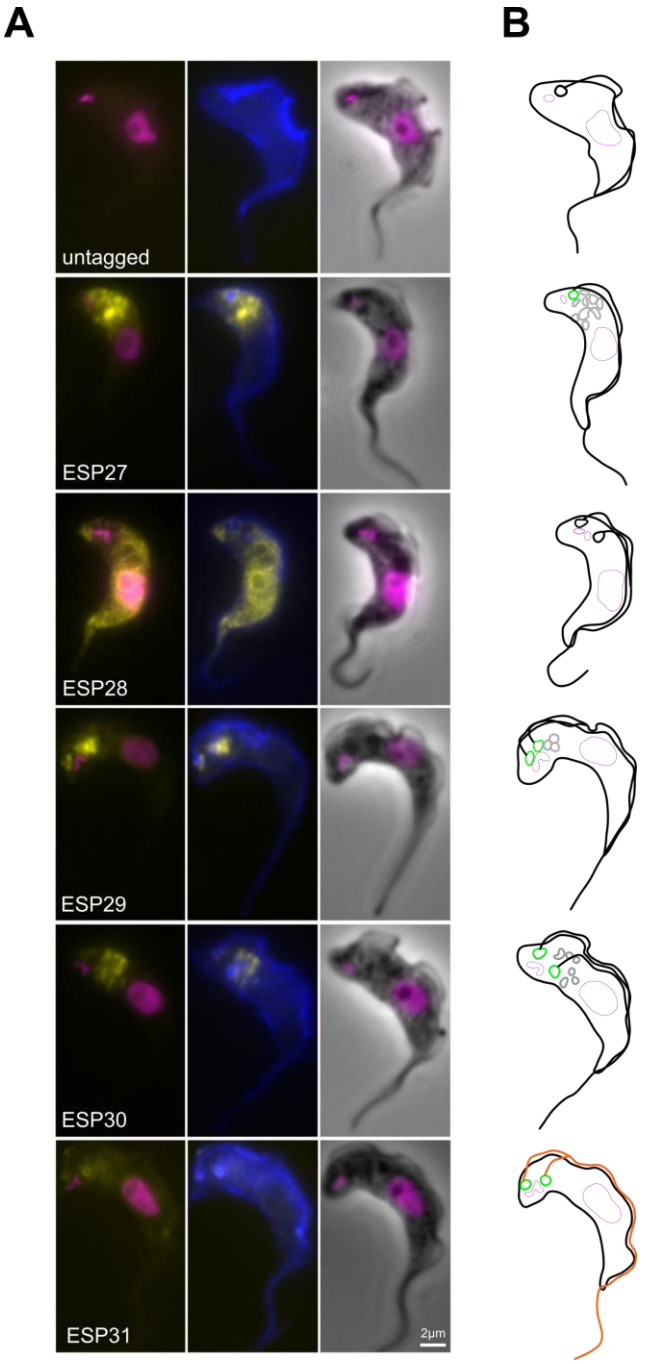


Figure 3.6. Localisation of 4 novel flagellar pocket proteins.
A) Localisation of ESP27-31 as determined by fluorescence microscopy. sfGFP signal (shown in yellow) corresponding to endogenous-locus tagged FP proteins shows ESP27, ESP29 and ESP30 to localise to the FP and endosomes. ESP31 localises to the FP and flagellar membrane; whilst ESP28 localises to the ER. Untagged control was used to determine background levels of fluorescence Surface membrane was counterstained with Concanavalin A (binds to glycan moieties associated with VSG). Cell DNA content is shown in magenta. **B)** Schematic representation of the surface membrane localisations observed for ESP27-31. Overall surface membrane is outlined in black, with flagellar pocket localisations highlighted in green, flagellar membrane signal in orange and endosomal signal in grey. Magenta lines represent DNA content (both mitochondrial and nuclear).

To determine if these FP-localised proteins were required for parasite growth, RNAi cell lines were generated for ESP27-31 as described in section 1.2.1. Briefly, a central, 500bp RNAi targeting fragment for each gene was inserted into a p2T7-177 RNAi vector, and the resultant plasmids transfected into their corresponding GFP-tagged cell line (from Figure 3.6). For each transfection, 3 independent clones were screened by Western blot, using anti-GFP antibodies to monitor the level of tagged protein after 24 hours of RNAi induction (data not shown; for example screen see Supplementary Figure 3-1). For all ESP-RNAi cell lines, clones exhibiting a reduction in protein levels upon RNAi induction were obtained (Figure 3.7A). RNAi against ESP29 appeared to be less effective by comparison to other ESPs, as ESP29 and ESP30 had comparable levels of endogenous protein, yet the amount of protein remaining in ESP29 induced cells was higher than that observed for ESP30. The difference in level of knockdown could be attributed to differences in rate of protein turnover. In addition, there is some evidence to suggest that different RNAi fragments can have different degrees of penetrance for a given gene (Sunter et al. 2015). However, this is likely to be gene dependent, so would require further systematic investigation. In summary, for ESP27-31, RNAi cell lines have been produced in which endogenous protein levels are reduced in response to the addition of tetracycline to the culture medium.

Having obtained RNAi cell lines for ESP27-31, the next step was to determine whether protein ablation was detrimental to cell growth *in vitro*, in accordance with the findings from the genome-wide loss-of-fitness screen (Alsford et al. 2011). To this end, all ESP-RNAi cell lines were induced by the addition of tetracycline, and growth compared to non-induced and parental (tagged) cells over the course of 6-days (Figure 3.7B), monitored as described in section 1.2.1. Despite a visible reduction in protein levels for all ESPs, no growth impairment was observed for any of these cell lines.

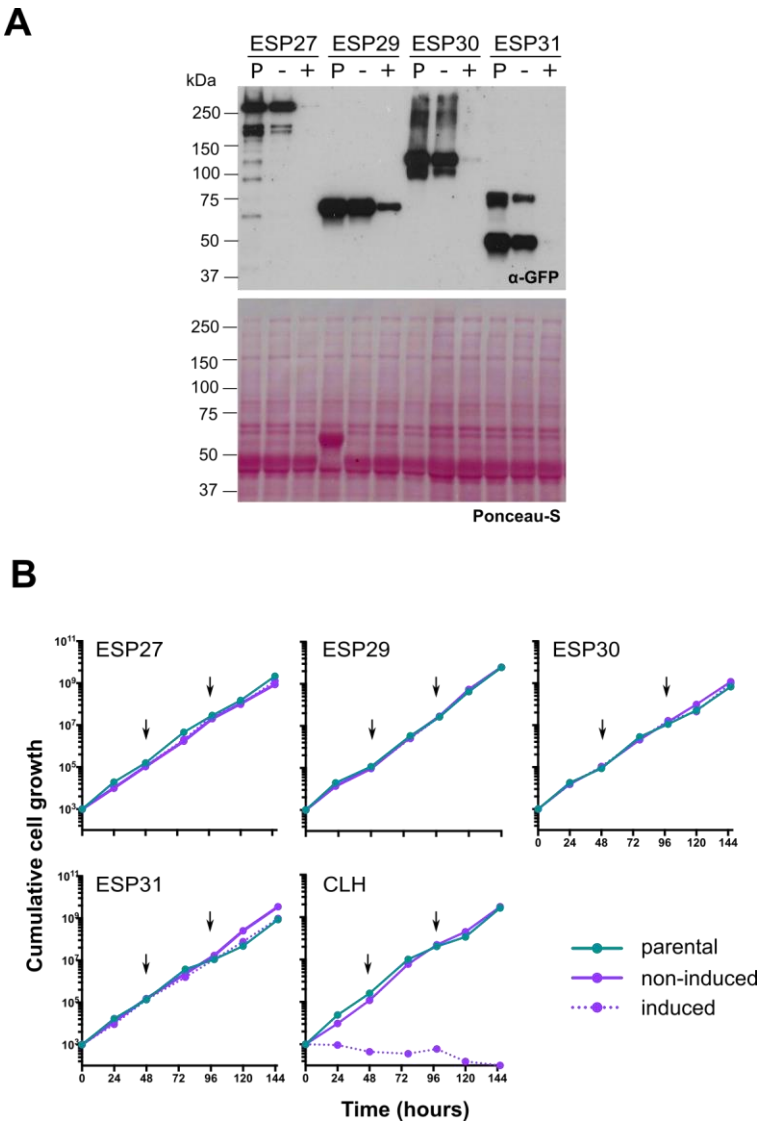


Figure 3.7. Ablation of ESP27-31 does not impair growth in culture
A) Immunoblot of ESP-RNAi whole cell lysates probed with anti-GFP antibodies demonstrating a reduction in protein levels after 24 hours of RNAi induction (+), compared to non-induced (-) and parental (tagged) cell lines. $2.5x10^6$ cells were loaded in each lane. Nitrocellulose membrane stained with Ponceau-S included as a loading control. **B)** Cumulative growth curves of parental, non-induced and induced ESP RNAi lines show no growth defect as a consequence of protein ablation. CLH serves as positive controls as knockdown is known to be lethal. Arrows indicate time-point at which cells were diluted.

A possible reason for the discrepancy between these data and that of the genome-wide RNAi screen, which found that knockdown of ESP27-31 to cause a decrease in parasite fitness, could be due to a difference in experimental design. The experiment performed by Alsford and colleagues is in essence a competition assay, in which any slight growth abnormalities will be emphasised when cells are challenged alongside parasites with normal fitness. As mentioned earlier, there is also some evidence that RNAi penetrance could be fragment specific (Sunter et al 2015). The fragments for the genome-wide study were generated by randomly shearing genomic DNA (i.e. variable in size). Therefore, it is possible the RNAi targeting fragments were both different in length and in targeting region. It is also worth noting that this is not the only example of discrepancies found between this genome-wide RNAi loss-of-fitness screen and individual RNAi: a study in which 101 mitochondrial proteins were individually silenced found 44% of their results to disagree with the RNAi library screen, both in terms of false positives and false negatives (Mbang-Benet et al. 2015).

Given the location of the ESPs at the very interface between the parasite and host, one explanation for the fact they are not essential *in vitro*, could be because the cells are being analysed in culture, without pressure from the host. It is quite possible that our culturing system is not a good proxy for the conditions the parasite is exposed to *in vivo*. One way to address this would be to test their essentiality in a mouse model. Established *in vivo* infection models exist, typically using either monomorphic cells, such as the Lister 427 strain used in this study, grown in outbred mice (e.g. CD1s); or pleomorphic lines such as EATRO1125 (clone Antat1.1) in inbred mice (e.g. C57BL/6Js) (Trindade et al. 2016). These parasite strains result in very different infection profiles. Pleomorphic cells can naturally differentiate into non-replicative, transmissible (stumpy forms) forms in a density-dependent manner. This differentiation limits parasitaemia levels producing a chronic model of infection, with characteristic fluctuations in parasite numbers (Mugnier et al. 2015). Conversely, monomorphic cells induce an acute infection, as the unregulated levels of parasitaemia overwhelm the host after just a few days (Tyler et al. 2001). The roles of the ESPs in the survival of proliferative BSFs could be

addressed via the acute model of the disease, utilising the RNAi cell lines already generated for this study. However, if the ESPs have functions in BSF differentiation or infection dynamics, then the pleomorphic *in vivo* model would be most appropriate. Due to time constraints imposed by the Home Office licence application, was not possible to address these questions during my PhD.

An *in vitro* compromise exists in the form of a minimal medium, for which the standard *T. brucei* culture medium has been modified to contain nutrient levels more akin to those found *in vivo* (Creek et al. 2013). Creeks Minimal Medium (CMM) was developed using a metabolomics approach that compared the metabolite content of fresh vs conditioned media. This revealed a total of 32 nutrients present in excess in standard culture medium, which were either completely removed or adjusted to concentrations that more readily resemble those found in the blood (Creek et al. 2013). A subsequent study used this media when investigating the role of a mitochondrial pyruvate carrier, and indeed found knockdown of this protein to be essential for growth *in vitro* only when cultured in CMM (Štáfková et al. 2016).

To see if challenging cells with CMM affected growth upon ablation of ESP27-31, RNAi was induced as before in cells grown in either HMI-9 or CMM. Initially, growth of wildtype cells was compared in both HMI-9 and CMM and, in concordance with previous findings (Creek et al. 2013), cell growth was unaltered in minimal media (Figure 3.8A). However, this was also the case for ESP27-31 RNAi-induced cells (Figure 3.8B). Therefore, in this instance, growing cells in minimal medium did not uncover any new functions of these proteins, although it may be worth expanding this analysis to the rest of the FP ESPs in future.

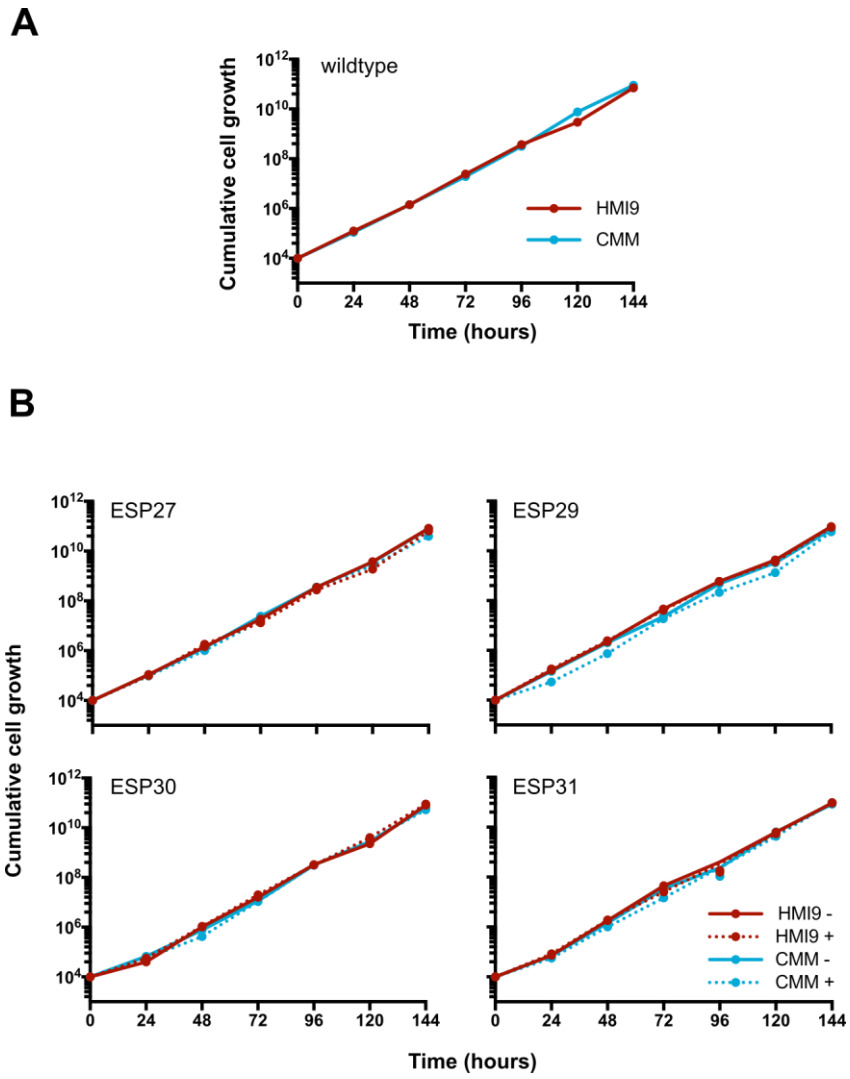


Figure 3.8. ESPs are not essential for growth when challenged in minimal medium. **A)** Cumulative growth curves of wildtype cells growth in HMI-9 (red line) or CMM (blue line) demonstrates cells grow at the same rate in standard medium vs a minimal medium. **B)** No difference in growth rate was observed between ESP-RNAi cell lines in either HMI-9 (red line) or CMM (blue line) in the presence (+) or absence (-) RNAi induction.

3.3. Discussion

Here I show that the majority of novel FP-localised ESPs, identified as part of a surface proteomics study (Gadelha et al. 2015), are dispensable for parasite growth *in vitro*. Combining data-sets from the surfeome and a genome-wide loss-of-fitness screen in an attempt to identify additional "essential" flagellar pocket components led to the discovery of four novel FP-localised proteins. However, like the initial set of FP-ESPs, none of these additional four proteins proved to be required for parasite growth in culture, even when challenged with a minimal medium. This result is perhaps surprising, given their location within such a critical subdomain of the surface membrane. It is possible that this is genuinely the case, and the FP contains many proteins with redundant functions. Alternatively, under the conditions tested here, factors such as incomplete protein ablation, redundancy between gene families or the lack of pressure from the host, may be confounding factors that prevent their functions from being determined.

As mentioned earlier, one of the known disadvantages with using RNAi as a tool to study gene function is that silencing of the mRNA is often incomplete. Indeed, at least for some of the ESPs, low levels of protein were still detectable after 24 hours of RNAi induction. It could be hypothesised that in these cases, the residual protein was sufficient to maintain normal cell growth in culture. This is perhaps best exemplified by the results obtained for TbPT0. In this study, a very mild growth defect was observed, with cells showing signs of recovery by day 6, where growth rates were comparable to non-induced cells. Conversely, when first characterised by Sanchez in 2013, TbPT0 knockdown was reported to result in cell growth impairment as early as ~48 hours, and ultimately cell death after 2 weeks (presumed to be due to the build-up of toxic levels of pyruvate in the cell, Sanchez 2013). This difference in phenotype severity could thus be due to the level of protein ablation achieved in each instance. For example, if TbPT0 is present in the cell at high enough levels, rate of pyruvate export may be sufficient to prevent toxics effects and thus sustain cell survival. The most obvious difference between these two studies is the choice of RNAi construct, which may suggest that the hairpin methodology utilised by Sanchez gives greater RNAi penetrance than the

head-to-head promotor system, at least for this particular gene. For instances like ESP29, where knockdown was seemingly not as efficient as other ESPs, it may be worth readdressing the functionality of this protein using the hairpin RNAi system, or indeed by knocking out the gene completely, as the remaining protein may be masking a growth phenotype.

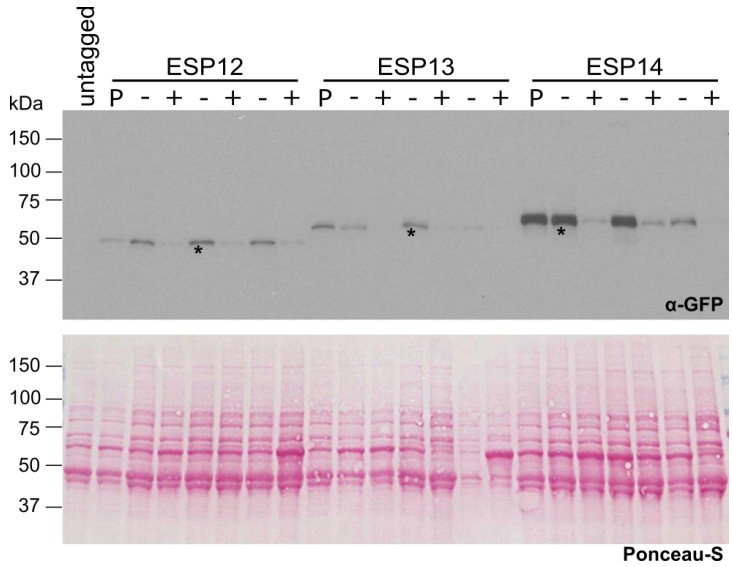
Another possible explanation for the lack of growth defect observed for any of the ESPs could be due to protein redundancy. For another FP localised protein, AQP2, only AQP null mutants lacking all three aquaglyceroporins (*AQP1-3*) have a very slight growth defect in culture, compared to the knockout of *AQP1* alone, or *AQP2* and *AQP3* in tandem (Jeacock et al. 2017). A similar scenario could be anticipated for *ESP12* and *ESP13,* which both belong to a family of four related genes (Jackson et al. 2013). Although the RNAi targeting fragments had the potential to target 3 out of 4 of the genes from Fam79, the degree of knockdown for the other members is unknown. In addition, the fourth remaining Fam79 protein may have been sufficient to compensate for the loss of the other three.

As discussed briefly at the end of section 3.2.2, the function of these proteins may only become apparent when investigated in an *in vivo* setting, with pressure from the host, particularly if they are involved in processes relating to infection dynamics or differentiation into transmissible stumpy forms. An additional aspect to consider is that the blood is not the only environment the parasite is able to survive and replicate in the vertebrate host stages. Recently it has been shown that adipose tissue and skin are both significant parasite reservoirs in mice (Trindade et al. 2016; Capewell et al. 2016). Parasites found in adipose tissue in particular were shown to be metabolically distinct when compared to BSFs, with 2,328 genes differentially expressed (Trindade et al. 2016). This includes some of the FP ESPs, as ESP10 and ESP21 were found to be upregulated 2-3 fold in adipose tissue, whilst 5 other ESPs were downregulated, also by 2-3 fold. With this in mind, it is possible that some transporters or receptors localised to the FP are only crucial for the development of parasite in specific compartments of the host

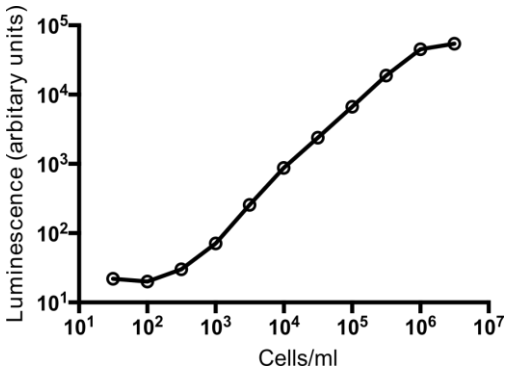
If it is indeed the case that the FP ESP proteins studied here are dispensable for parasite survival both *in vitro* and *in vivo* (the latter is yet to be

determined), this begs the question as to why the parasite maintains these proteins within the FP. One hypothesis it that the flagellar pocket contains the majority of invariant proteins (like the ESPs) to keep the cell surface free of proteins that could potentially elicit an adaptive immune response, thus interfering with antigenic variation. Interestingly, this could well be the case for ESP27 (aka Tb292), as this protein was originally identified as part of a pull-down using IgGs, performed in the non-pathogenic rodent parasite *Trypanosoma lewisi,* with the aim of identifying surface localised proteins in *T. brucei* (Lee et al. 1994). Recognition by IgGs indicates this protein is immunogenic and, coupled with its large mass (310kDa) and long extracellular domains (as predicted by TMHMM, Krogh et al. 2001), it seems plausible that having this protein on the surface may be of detriment to the cell. The precise mechanisms utilised by *T. brucei* to segregate FP proteins between the three biochemically distinct subdomains of the surface plasma membrane remain to be elucidated, and will be the topic of the next chapter.

3.4. Supplemental Figures



Supplementary Figure 3-1. Selection of ESP-RNAi cell lines with greatest ESP protein ablation
Example of a typical screen used to select the ESP RNAi cell line with the greatest level of protein ablation. Immunoblots of ESP-RNAi whole cell lysates were probed with anti-GFP antibodies, showing a decrease protein level after 24 hours of RNAi induction (+), compared to non-induced (-) and parental (tagged) cell lines. Independent clone taken forward for further analysis marked with as asterisk. Approximately $2.5x10^6$ cells were loaded in each lane. Nitrocellulose membrane stained with Ponceau-S was included as a loading control.



Supplementary Figure 3-2. Relationship between cell density and luminescence is linear for log-phase *T. brucei*
Cell were serially diluted from $3.16x10^6$ cells/ml down to $3.16x10^1$ cells/ml on a $\sqrt{10}$ scale and the luminescence values for each, determined using the CellTiter-Glo luminescence assay. A linear relationship between cell density and luminescence was observed between $1x10^3$ and $1x10^6$ cells/ml

Chapter 4. Investigating mechanisms of surface specialisation in *Trypanosoma brucei*

4.1. Introduction

Plasma membrane compartmentalisation into specialised subdomains, each with distinct protein and lipid compositions, is a feature seen across prokaryotes and eukaryotes. In bacteria this typically refers to compartmentalisation during the process of spore formation of *Bacillus subtilis* or stalk formation in *Caulobacter cresentus* (reviewed in Cornejo et al. 2014). In eukaryotes surface compartmentalisation is widely used, with two key examples being the partition of the epithelial plasma membrane into apical and basolateral domains, to the differential accumulation of membrane proteins in the primary cilium (Trimble and Grinstein 2015). *T. brucei* is no exception; the cell surface of the parasite can be segregated into at least three subdomains (**Figure 4.1**A).

Surface-localised proteins in *T. brucei* can occupy one or more of these plasma membrane subdomains indicative of intrinsic sorting mechanisms that direct surface components to a specific region of the cell surface (Gadelha et al. 2015). For example, proteins like ESP11 and ESP12 localises to the FP and endosomes, whilst ESP31 localises to the FP and flagellar membrane (see Chapter 3). Yet, localisation to these domains was found to be independent of protein topology or identifiable sequence motifs (Gadelha et al. 2015).

Restriction of proteins to one or more of these membrane regions implies the presence of diffusion barriers to inhibit the lateral diffusion of molecules across the entire surface. Indeed, by freeze-fracture electron microscopy, rows or plaques of intramembrane particles (IMPs) have been reported at the junction of the FP and neck membranes, and flagellum and FP membranes respectively (Gadelha et al. 2009). Yet, at present the molecular composition of these putative diffusion barriers is unknown. In addition to the organised sets of IMPs, two cytoskeletal structures, the collar and collarette, also delimit the surface membrane boundaries (**Figure 4.1**B).

Surface compartmentalisation is thought to be particularly important for bloodstream form (BSF) *T brucei*. Polarisation of all endocytosis to the FP membrane at the posterior end of the cell facilitates the rapid clearance of surface-bound antibodies and recycling of the variant surface glycoprotein (VSG) coat, promoting survival and persistence in the host bloodstream (Engstler et al. 2004, 2007). As mentioned, antigenic variation relies on the parasite expressing a single VSG, which it periodically switches to an immunologically distinct variant to escape the host's adaptive immune response (reviewed in Morrison et al. 2009). The presence of immunogenic and invariant receptors on the cell surface would interfere with this strategy. Therefore, it is hypothesised that most of these are retained in the FP to avoid immune recognition. Despite the importance of having a specialised surface for parasitism, the mechanisms underlying both protein sorting and retention in *T. brucei* remain to be elucidated.

Currently, two main models have been proposed to try to explain the differential localisation of surface proteins, but both are based on just a handful of proteins. One is that surface localisation is dictated in part by protein abundance, while the other is based on the number of GPI anchors (described in more detail in section 1.4.4) (Schwartz et al. 2005; Mussmann et al. 2004; Engstler et al. 2005).

Another way in which cells can modulate protein sorting to specific membranes is via post-translational modifications such as glycosylation. An example of this is the requirement of N-glycosylation for the correct sorting of proteins to the apical membrane of epithelial cells (Vagin et al. 2009). Therefore, it is possible that glycosylation may also have a role in protein sorting at the host-parasite interface. However, more recent mapping of the N-glycan structures of TfR did not identify any *N*-acetyllactosamine-containing glycans. Instead, they found that TfR is able to bind other glycoproteins, which in turn may bind TL (Mehlert et al. 2012). Therefore the link between N-glycosylation and FP localisation appears more complex than first anticipated.

Moreover, most of the work investigating protein sorting in *T. brucei* thus far, has concentrated almost exclusively on a single protein, TfR. The identification of 14 novel FP-localised components, the ESP (Enriched in

Surface Proteome) proteins to date, described in Chapter 3, has provided the largest set of FP proteins which can be used to investigate protein sorting on a wider scale. In this Chapter, I utilise this cohort of proteins to further investigate the possible link between glycosylation and protein sorting at the host-parasite interface. Additionally, the way in which the cell retains receptors within the FP (i.e. and prevent their free diffusion across the entire surface membrane) also remains largely unknown. Here, I begin to investigate this by removing the very structural boundary between the FP and cell body membranes, the flagellar pocket collar (FPC), to determine the fate of individual FP proteins.

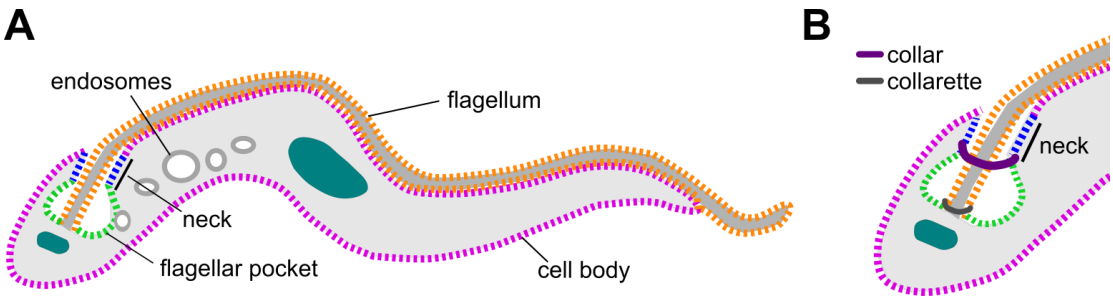


Figure 4.1. Surface architecture of *Trypanosoma brucei.*
A) Schematic representation depicting the distinct domains of the surface membrane of *T. brucei:* the cell body (magenta), flagellum (orange), flagellar pocket (green) and the neck (blue). In teal is the mitochondria and nuclear DNA. **B)** Higher magnification of FP region showing the two cytoskeletal structures located at the boundaries between the FP and neck membranes (collar) and the FP and flagellum membranes (collarette).

4.2. Results

4.2.1. Most ESPs are predicted to be N-glycosylated

In order to investigate whether glycosylation has a role in surface subdomain localisation, my first step was to determine the glycosylation status of the ESPs. In *T brucei,* as in other eukaryotes, protein N-glycosylation occurs post-translationally in the ER lumen and the addition of the oligosaccharide to an asparagine residue is catalysed by oligosaccharyltransferases (OTase). In higher eukaryotes, a single multi-subunit OTase exists. *T. brucei* however, expresses two oligosaccharyltransferases, STT3A and STT3B, with distinct donor specificities (Izquierdo et al. 2009). STT3A is responsible for the transfer of biantennary $Man_5GlcNAc_2$, preferentially to acidic or neutral regions of the target polypeptide. These structures can then be processed further when they reach the Golgi, to either paucimannose ($Man_4GlcNAc_2$ and $Man_3GlcNAc_2$), or elaborated to form complex N-glycans. Conversely, STT3B transfers triantennary $Man_9GlcNAc_2$ (oligomannose) to neutral or basic sequences (Izquierdo et al. 2009). Interestingly, in BSFs *STT3A* is expressed more highly than *STT3B,* and is specifically responsible for the addition of paucimannose (low mannose) and complex N-glycans (Izquierdo et al. 2009). Therefore, enrichment in glycoproteins with these particular N-glycan modifications could be anticipated in BSFs.

N-glycosylation can occur in instances where a protein sequence contains an N-X-S/T motif, where “X” can include any amino acid except proline. The conformational rigidity of proline residues typically preclude N-glycosylation by rendering the asparagine addition site inaccessible to OTases. Although the consensus motif is considered a requirement for N-glycosylation, not all motifs are glycosylated (Varki et al. 2009).

As a first pass, bioinformatics-based prediction tools can be used to determine the number of possible N-glycan addition sites within a given amino acid sequence, as well as the likelihood that sequence is indeed glycosylated *in vivo*. For example, the algorithm used by NetNGlyc (Gupta et al. 2004) scans a protein sequence for the aforementioned N-X-S/T motifs, and the N-glycosylation potential for each is scored using nine neural networks, to predict

which of these are likely to be glycosylated *in vivo*. However, this prediction tool does not consider protein topology, so predictions within transmembrane or cytosolic regions should likely be discounted, as only regions of the protein exposed to the ER lumen can be N-glycosylated (i.e. those that end up being extracellular). It is worth noting that other online prediction tools exist, such as NGlycPred (Chuang et al. 2012), however this particular algorithm requires the structure of the query protein(s) to have been solved.

For all FP-ESPs characterised in Chapter 3, the NetNGlyc prediction tool was used to determine the number and location of putative N-glycan addition sites. The results of this analysis are summarised in Figure 4.2. All ESPs contain N-X-S/T sequons and, for the majority (13 out of 14), at least one of these sites is predicted to be glycosylated (and for 9 out of 14 ESPs, at least one of these predicted N-glycan additions was deemed highly likely). The exception here is ESP22, which has two sites with the required motif, yet neither are predicted to be modified with an N-glycan. Notably, ESP12 and ESP13, despite showing 60% sequence similarity at a protein level, shared no conserved predicted N-glycan addition sites (or consensus sequences). These two proteins have different localisations on the surface domain, so if N-glycosylation does have a role in protein sorting on the surface, then different glycosylation patterns would be anticipated. Overall, most FP-localised ESPs studied here are predicted to be post-translationally modified via N-glycosylation.

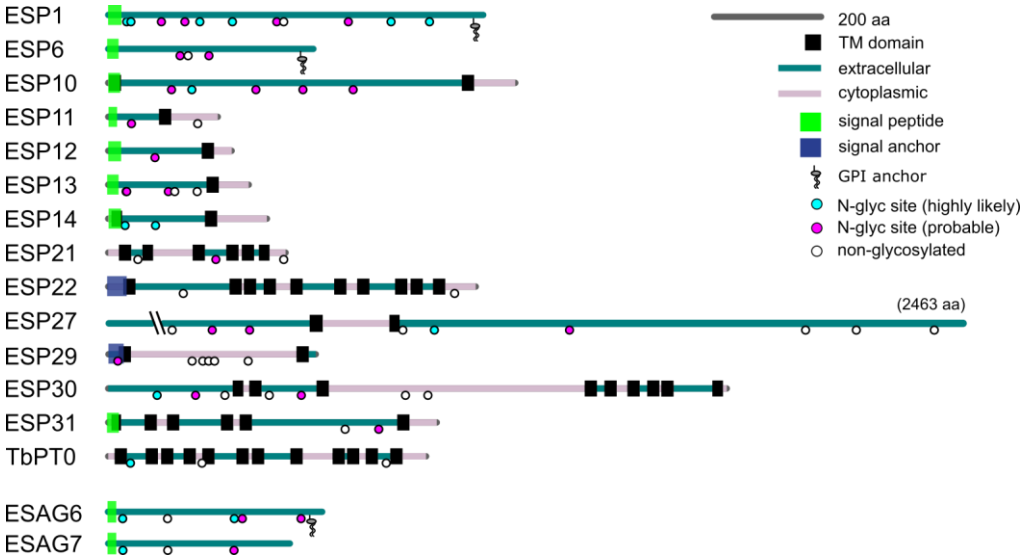


Figure 4.2. Most flagellar pocket-localised ESPs are predicted to be N-glycosylated. Domain architectures for each of the ESPs (as determined by TMHMM (Krogh et al. 2001), SignalP 3.0 (Bendtsen et al. 2004), and PredGPI (Pierleoni et al. 2008) labelled with all possible N-X-S/T motifs at their respective loci (circles) and differentially coloured based to the probability these sites are glycosylated, according to NetNGlyc (Gupta et al. 2004). Magenta circles correspond to probable glycosylation sites with a score >0.5. Light blue circles indicate sites considered highly likely to be glycosylated by NetNGlyc, either with a score >0.7, or >0.5 but with agreement from 9/9 neural networks. All sites deemed not to be glycosylated, either because they have a score <0.5, are present within an intracellular domain, or amino acid X is proline, are shown by white circles.

The NetNGlyc prediction tool was 'trained' using human proteins, so to establish its reliability for *T brucei* proteins specifically, predicted *vs* mapped N-glycan addition sites were compared for the transferrin receptor (TfR) and variant surface glycoprotein (VSG), which encompass two examples of BSF-expressed proteins where the N-glycan site occupancy has been experimentally determined (Zamze et al. 1991; Mehlert et al. 2012).

VSG221 (or MiTaT1.2) has been experimentally shown to be glycosylated at amino acid positions N263 and N428, occupied by a paucimannose/complex and oligomannose N-glycan respectively (Jones et al. 2005; Zamze et al. 1991). NetNGlyc identifies both these residues, but only considers the second of those highly likely to be glycosylated, with residue N263 predicted not to be glycosylated via the default threshold (>0.5).

The transferrin receptor in *T. brucei* is a FP-localised heterodimer composed of two subunits: ESAG6 and ESAG7. ESAG6 has five N-glycan consensus motifs, of which 3 have been shown to be glycosylated *in vivo*. While ESAG7 has three, with one being glycosylated (Mehlert et al. 2012). When comparing these experiments to the *in silico* predictions, the results for ESAG7 were in agreement with one another. However, for ESAG6, 2 out of 3 of the *bona fide* glycosylation sites were deemed to be unoccupied via the NetNGlyc algorithm. In combination with the VSG findings, it seems that this particular prediction tool is not a reliable way to identify glycosylated residues in *T. brucei*.

The comparisons performed here, albeit on only a small subset of proteins, suggest that NetNGlyc is suitable for determining all possible N-glycan addition sites (i.e. scanning the proteins sequence for the N-X-S/T motif). Yet, the probability scores assigned to each residue are perhaps not reflective of true protein glycosylation in *T. brucei,* possibly because the neural networks it uses were developed using human proteins. In addition, this particular kind of analysis cannot be used to infer the type of N-glycan present, which will be important here given the proposed link between a specific type of N-glycan and FP localisation. Thus, to obtain a more accurate estimation of the glycosylation status of the ESPs, with the aim of finding a link between N-glycosylation pattern and surface subdomain localisation, an alternative approach was taken.

4.2.2. Most ESPs are glycosylated *in vivo*

One way of experimentally investigating N-glycosylation status of proteins is to treat whole cell lysates with glycosidases. Two glycosidases are typically used to release the N-glycans attached to asparagine, which enable the distinction between high mannose (oligomannose) and low mannose (paucimannose) or complex N-glycans, due to their different substrate specificities. Peptide N-glycosidase (PNGase-F) can cleave essentially all N-glycans, unless the innermost GlcNAc residue is linked to a fucose. Conversely, Endo-H is less promiscuous, and only releases oligomannnose N-glycans (Figure 4.3A). Cleavage of N-glycan modifications reduces the

apparent molecular weight of a protein, which can be detected by SDS-PAGE and subsequent immunoblotting. As all ESPs to be analysed here are GFP-tagged, glycosylation status of all proteins can be determined by probing the Western blot with an anti-GFP antibody.

To test whether ESPs are indeed glycosylated, whole cell lysates for each tagged cell line (generated in Chapter 3) were treated with Endo-H or PNGase-F, alongside an untreated control to ascertain whether any decreases in molecular weight observed were due to specific activity of the glycosidase or an undesired consequence of proteolysis during the procedure itself. ESAG6 was included as a positive control, as it has been shown previously to contain a mixture of oligomannose and paucimannose N-glycans. Indeed, for ESAG6, a decrease in apparent molecular weight was observed upon treatment with Endo-H compared to the untreated lane, and a greater decrease upon treatment with PNGase-F (Figure 4.3B). Thus, ESAG6 contains both types of N-glycan, confirming previous findings and the validity of the experimental approach taken here.

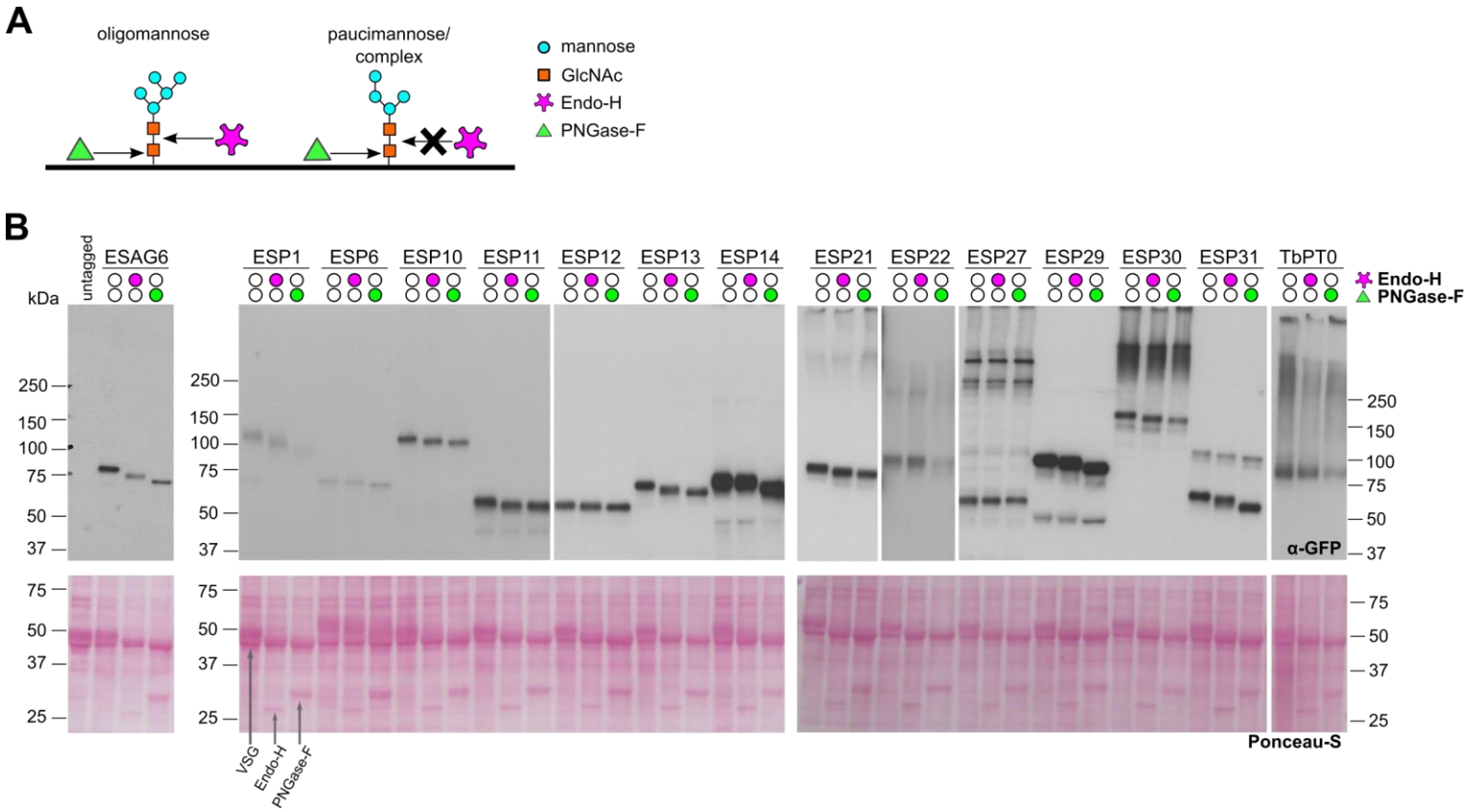


Figure 4.3. Most ESPs are glycosylated *in vivo.*
A) Schematic representation of the different N-glycan specificities of PNGase-F and Endo-H **B)** Immunoblots of ESP whole cell lysates after treatment with PNGase-F (green filled circles) or Endo-H (pink filled circles) with an untreated control (empty circle). Shift in apparent molecular weight in glycosidase-treated samples indicates protein is glycosylated. Western blot was probed with monoclonal anti-GFP antibodies and Ponceau-S stained nitrocellulose membrane serves as a loading control

For the set of FP-localised proteins, which encompasses the ESPs and TbPT0, identical experiments were performed to determine the glycosylation patterns of each. Here, the Ponceau-S stained nitrocellulose membrane, in addition to its usual function as a loading control, provides confirmation that the glycosidases were indeed added to each sample, as PNGase-F and Endo-H create visible protein bands at 36 and 29 kDa respectively. The activity of the enzymes in each treatment is also confirmed by a shift in the band corresponding to VSG (Figure 4.3B).

Of the 14 ESPs investigated, 6 were found to be modified by both classes of N-glycans, as judged by two subsequent shifts in molecular weight upon treatment with Endo-H and PNGase-F when compared to untreated controls. In instances where a decrease in molecular weight was only observed upon treatment with PNGase-F, this suggest that these proteins (ESP6 and ESP14) only contain paucimannose or complex N-glycans, although it is not possible to distinguish which kind. Importantly, there were other proteins (ESP11 and ESP21) that were only modified with oligomannose N-glycans, as a decrease in apparent molecular weight was observed when treated with Endo-H, yet no further decrease upon treatment with PNGase-F. In addition, no clear band shifts were detectable for ESP12, ESP22, ESP27 or TbPT0, suggesting they may not be N-glycosylated.

For ESP27, the lack of detectable N-glycans is perhaps surprising, as this protein had the greatest number of possible N-glycan addition sites. Given the high molecular mass of this protein (~310 kDa), it is possible that any changes in molecular weight were no resolvable with this particular polyacrylamide gel percentage. Equally, as each N-glycan can contribute ~1-5 kDa to the total mass of a protein, dependent on the type and degree of branching, it is possible the single asparagine site available for ESP12 was still glycosylated (perhaps by a small paucimannose N-glycan), which could not be detected in this instance. Therefore, in retrospect, by running these samples on a lower percentage acrylamide gel these potential smaller shifts may have been resolved. Overall, the results from this deglycosylation experiment suggest that the majority of FP-localised proteins are glycosylated; yet differential patterns of glycosylation exist.

4.2.3. Glycosylation pattern alone is not sufficient to dictate surface subdomain localisation.

Having experimentally determined the glycosylation status of FP ESPs by treatment with glycosidases, it was tested whether there was a correlation between the type of N-glycosylation modification present on a given ESP, and its surface subdomain localisation. For example, whether ESPs that localise to the FP in combination with another subdomain (flagellar or cell body membranes) have a different glycosylation pattern to those that reside exclusively in the FP. To do this, results of the deglycosylation experiments (see section above) were compared to both localisation and protein topology data (Figure 4.4). From this analysis, there was no clear association between the type of N-glycan modification and its subdomain localisation. However, this result certainly does not preclude a role for glycosylation in protein sorting at the surface. Indeed, the set of ESPs investigated here is somewhat biased in that all proteins localise to the FP. Hence, to further examine the role of glycosylation in subdomain sorting, proteins that localise exclusively to the flagellar or cell body membranes should be included, such as ESP8 and ESAG4 (Gadelha et al. 2015), as well as proteins that localise elsewhere in the cell.

It is also possible that protein sorting to distinct surface domains of *T. brucei* is influenced by other factors, such as number of N-glycan residues, or the relative positions of these sugars within the protein structure. This could be addressed using mass spectrometry, as performed for VSG and TfR (Mehlert et al. 2012), to map specific N-glycan residues. With this information I could then begin to disentangle the relative contributions each N-glycan makes, if any, to the sorting of FP proteins.

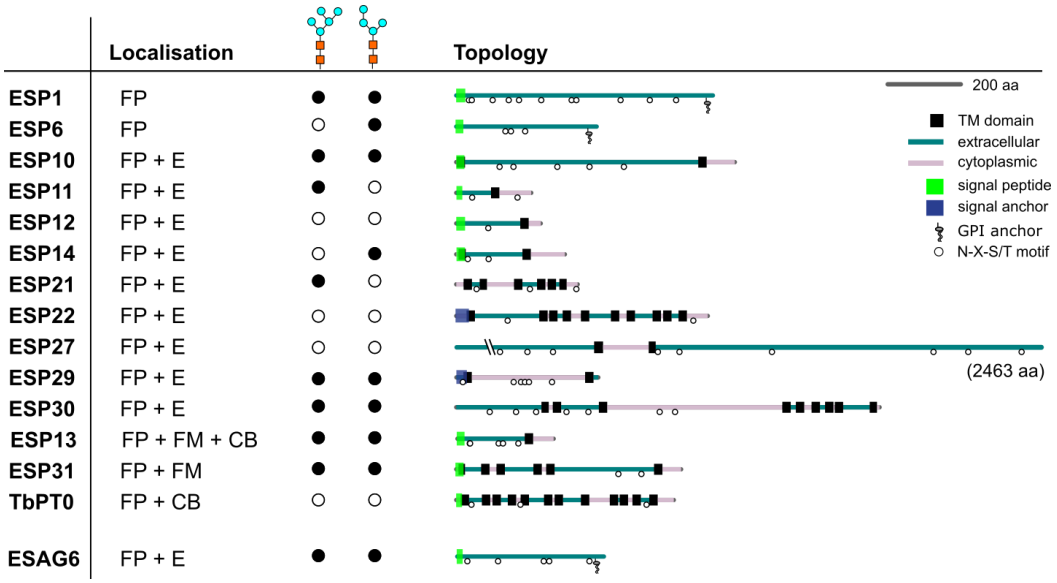


Figure 4.4. Glycosylation pattern alone does not determine ESP localisation.
Comparison of localisation, protein topology and N-glycan type. Protein localisation was determined previously, either in Chapter 3 or by Gadelha and colleagues (2015). Type of N-glycan modification present on each protein as determined in B and presence/absence demonstrated by black/white circles. For topology and definition of N-X-S/T motifs see Figure 4.2.

4.2.4. A component of the FPC has a role in flagellar pocket protein retention

In addition to the signals driving protein sorting to specific surface domains, preservation of a specialised surface architecture, such as that of *T. brucei*, also requires elements that prevent the free diffusion between each of those domains. As mentioned earlier, rows of intramembrane particles have been visualised by freeze-fracture electron microscopy at the junction between the FP and neck domains (Gadelha et al. 2009) Yet, the identities of the proteins contributing to these “diffusion barriers” remain largely unknown. Located at the same membrane junction, but on the cytoplasmic side of the membrane, lies the FPC. Given its localisation at this boundary, it seems plausible that this cytoskeletal structure could function in the retention of FP proteins within the lumen of the pocket. Most likely this would be restricted to proteins that span the lipid bilayer, with cytoplasmic regions that could directly interact with the FPC. Therefore, the remainder of this chapter focus on investigating the role of the FPC in FP protein retention.

The only known component of the FPC published to date is BILBO1 (Bonhivers et al. 2008). In PCFs, knockdown of BILBO1 causes a block in cytokinesis, flagellum detachment and, perhaps most critically, prevents the biogenesis of a new FP (discussed in more detail in Chapter 1). The combination of these factors result in cell death after 48-72 hours of RNAi induction. Knockdown of BILBO1 in BSFs, whilst still causing rapid cell death, appears to have a subtly different phenotype (Bonhivers et al. 2008). After 12 hours of RNAi induction, approximately 50% of cells become round. By 24 hours this percentage had increased to ~100%. Yet, the fate of the BSF FP in the absence of the FPC has not yet been studied.

To gain a greater understanding of the specific effect of BILBO1 knockdown on the FP in BSFs, with the aim of assessing its usefulness as a tool to investigate FP protein retention, an RNAi targeting fragment was designed against BILBO1. As for the knockdown of the ESPs in Chapter 3, the RNAi targeting fragment was inserted into a tetracycline-inducible p2T7-177 RNAi construct (Wickstead et al. 2002), and initially transfected into RNAi-competent wildtype BSF cells (Wirtz et al. 1999). Two independent clones from the transfection were grown in the presence or absence of tetracycline, and

growth rate and percentage of round cells were quantified (Figure 4.5). After 12 and 24 hours of RNAi induction both measurements recapitulated those previously reported by Bonhivers and colleagues, confirming BILBO1 knockdown.

To be able to visualise the specific effect of BILBO1 knockdown on the FP, the BILBO RNAi cell line (from Figure 4.5) was induced with tetracycline, mounted on slides and counterstained with tomato lectin (TL) conjugated to FITC. TL specifically binds poly-N-acetyllactosamine residues present on some FP proteins (Nolan et al. 1999; Atrih et al. 2005); and consequently can be used as a marker for the FP. It was reasoned that, to investigate FP morphology, cells would need to be induced <12 hours, before the majority of cells have rounded up. Furthermore, as the doubling time of a BSF cell is ~8 hours, cells in G1 phase of the cell cycle at the start of the induction would have divided. So, if the phenotype is similar to that seen for PCFs, and FP duplication is affected, this could be visible after 8 hours of RNAi induction.

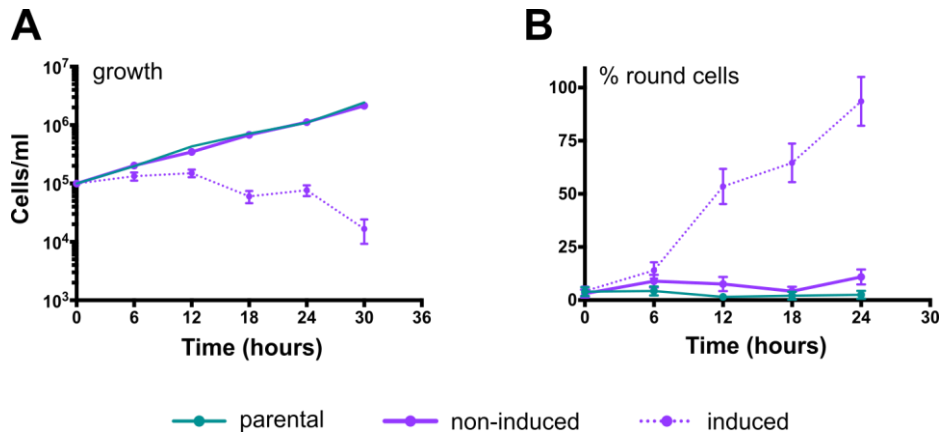


Figure 4.5. Knockdown of BILBO1 causes cell death and formation of round cells.
A) Cell growth after BILBO1 RNAi induction. **B)** Percentage of round cells after BILBO RNAi induction. Both A) and B) recapitulate the phenotype reported by Bonhivers and colleagues (2008). Two clones were analysed for each experiment, but as both clones behaved the same, a representative clone was plotted. Error bars represent SEM

Upon counterstaining with TL, non-induced BSF cells showed a strong signal at the region corresponding to the FP, in addition to much reduced surface staining (Figure 4.6). In contrast, following BILBO1 knockdown, while still detectable, TL-labelled structures resembling FPs appeared significantly smaller and closer to the cell cortex, as if the neck region was absent (Figure 4.6). Notably, FP-like (i.e. TL-enriched) structures were also observed in round cells. Based on these results, it would suggest that BILBO1 knockdown in BSF cells alters normal FP morphology and, as exemplified in dividing cells with two pockets, seems to affect both pockets equally. The presence of TL-enriched FP structures upon BILBO1 ablation suggests that, at least some glycoproteins are retained when the FPC is disrupted. However, it should be noted that without counterstaining these cells with an anti-BILBO1 antibody to label the FPC, the degree of BILBO1 ablation cannot be confirmed. Hence, the fact that FP-like structures still remain upon RNAi induction, could be because a small but sufficient amount of BILBO1 is still present.

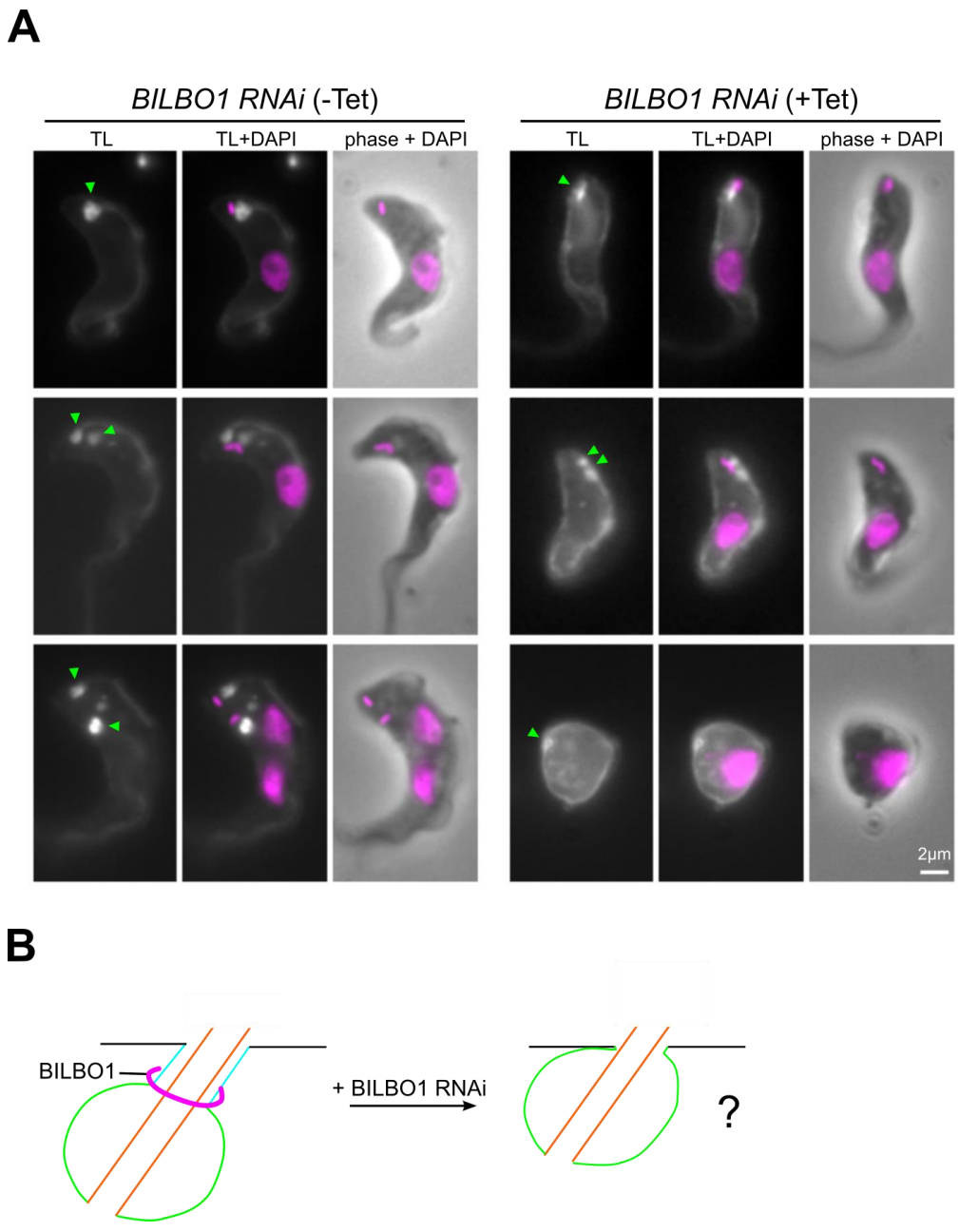


Figure 4.6. Knockdown of BILBO1 alters FP morphology in BSFs.
A) Representative micrographs of cells (n = >32 per condition) counterstained with TL-FITC in *BILBO1* RNAi cell lines, with or without the addition of 1 µg/ml tetracycline over 8 hours. In previously published work on BILBO1 knockdown, the induction was performed for 12 hours (Bonhivers et al. 2008). DAPI was used to counterstain DNA, shown in magenta. Exposure time for each micrograph was set to 1 second (green fluorescence). In all induced cells (both "round" and "normal") evidence of flagellar pocket-like structures exist in the form of TL-enriched foci (green arrowheads). **B)** Possible model to explain the changes in flagellar pocket morphology in the absence of BILBO1. In induced cells, the flagellar pocket (green) appears closer to the cell cortex (black). Therefore it could be hypothesised that the depletion of BILBO1 leads to loss the neck membrane (blue) that connects the pellicular membrane to the flagellar pocket.

TL labels the tri-N-acetyllactosamine moieties of unknown proteins at the flagellar pocket. Thus, monitoring the signal distribution of TL (see Figure 4.6) only provides a general overview of the localisation of FP resident proteins upon BILBO1 ablation. Yet, not all FP-localised proteins directly to TL (Mehlert et al. 2012) and, as discussed earlier, the location of BILBO1 on the cytoplasmic face of the membrane suggests FP protein retention may be topology-specific. So, to investigate this further, the fate of individual FP-localised proteins upon BILBO1 ablation was examined. Here, the BILBO1 RNAi construct, generated and validated previously, was introduced into five different cell lines containing GFP tagged FP proteins: ESP1, ESP10, ESP11, ESP21, and TbPT0; chosen because they had a clear FP signal and covered a range of protein topologies (i.e. GPI, Type I TM and multipass TM). As before, each newly generated cell line was induced with tetracycline for 8 hours, and the localisation of the GFP-tagged protein compared to non-induced cells. In this instance, cells were counterstained with TL conjugated to Alexa Fluor 594 (TL-Alexa594), allowing localisation of both the pool of FP glycoproteins and the GFP-tagged FP ESP simultaneously. As expected, in all instances, induced cells behaved as before, in that smaller and more cortical TL-enriched FP structures were observed (Figure 4.7A).

For ESP10 and ESP11, both type 1 TM proteins, GFP-signal was also absent from the FP, and was not detectable elsewhere in the cell either. Though, for ESP11, this result was only reflective of ~40% of cells; while in ~60% of cells there was either partial or full co-localisation of ESP11-GFP with TL. The interpretation here was that BILBO1 knockdown was not as efficient in these cells, and hence some of ESP11 was retained. To determine whether ESP10 and ESP11 were still expressed, despite the absence of GFP signal by microscopy, whole cell lysates were immunoblotted using monoclonal antibodies against GFP (Figure 4.7B). Western blot analysis showed that GFP-tagged ESP proteins were still produced by these cells upon *BILBO1* RNAi induction (Figure 4.7B). Thus, perhaps like ESP21, ESP10 and ESP11 may have diffused onto the cell body membrane. Indeed, the total cellular protein level for ESP21 is much higher than that of ESP10 and ESP11, which may explain why only ESP21 is detectable on the cell surface. Overall, the data

obtained so far would suggest that these four ESPs are being retained in the FP via the FPC; hence in its absence, these proteins can escape onto the cell body membrane.

The GPI-anchored protein ESP1 behaves differently to the other four ESPs described above, in that its localisation remains unchanged upon *BILBO1* knockdown. Though, it would appear that this protein is an exceptional case, as ESP1 does not co-localise with TL in non-induced cells. ESP1 instead appears to localise to a region distal to the FP (i.e. between the FP and the cell body membrane; a localisation reminiscent of components of the hook complex (e.g. TbMORN1) (Esson et al. 2012a), as well as Kinesin-17 (see Chapter 5), which are both present along the neck region (see Figure 4.1), in close proximity to the FPC. Both TbMORN1 and the FPC are cytoskeletal structures, and so, it was reasoned that this may also be true of ESP1. To test this, the localisation of ESP1-GFP in detergent treated cells was examined, and indeed, ESP1-GFP remains associated to the cytoskeleton after extraction (Figure 4.7C). Therefore, as a cytoskeletal structure itself, it may be impervious to the effects of *BILBO1* knockdown.

On the whole, in the absence of BILBO1, some FP ESPs are lost from the pocket and relocate onto the cell body membrane. These data suggest the major component of the FPC (BILBO1) functions, at least in part, in the maintenance of the distinct subdomains of the parasite surface. This then raises the question as to the mechanisms behind this protein retention, including how the FPC operates as a selective diffusion barrier.

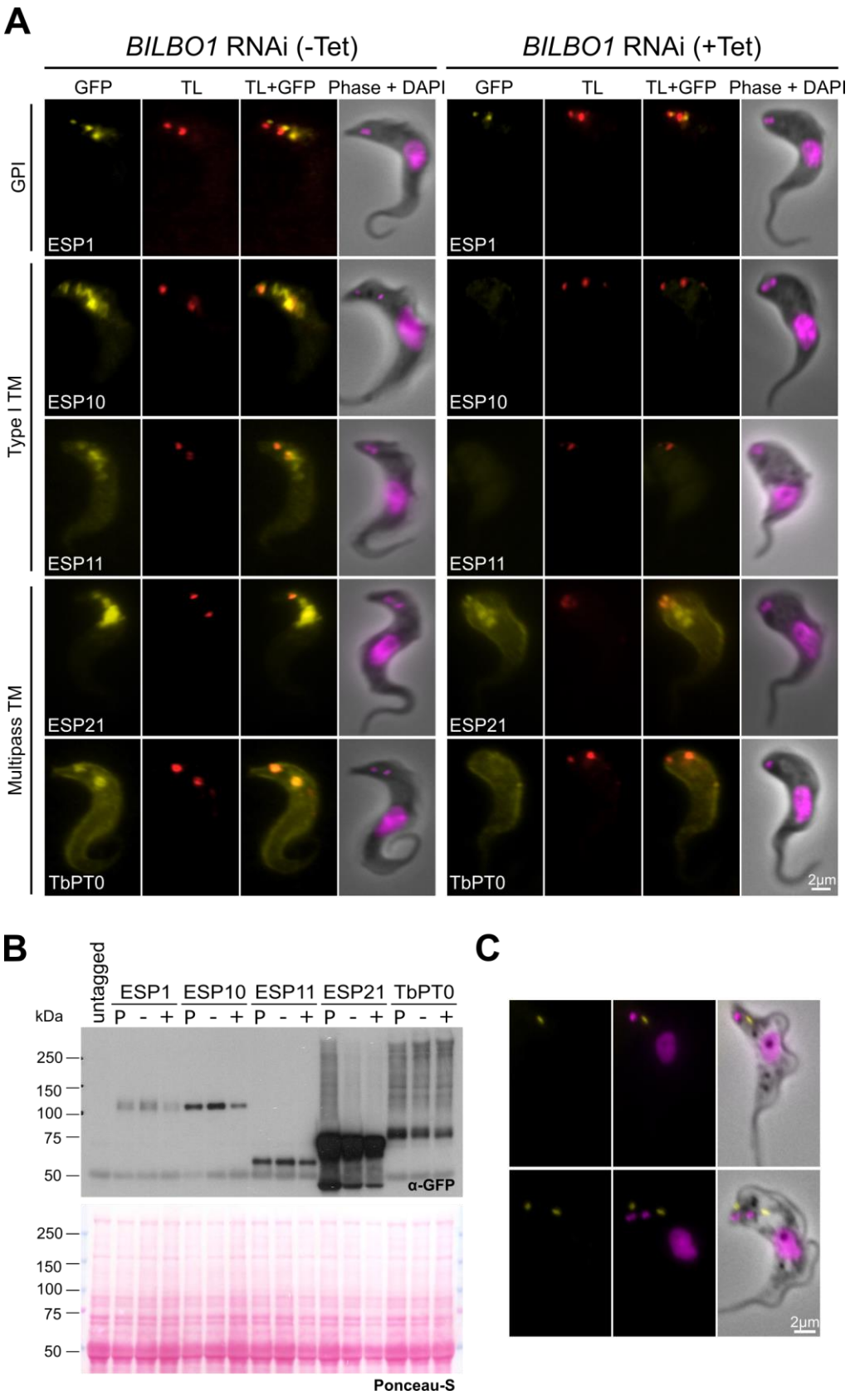

A
BILBO1 RNAi (-Tet)
BILBO1 RNAi (+Tet)
GFP
TL
TL+GFP
Phase + DAPI
GPI
Type I TM
Multipass TM
ESP1
ESP10
ESP11
ESP21
TbPT0
2µm
B
kDa
untagged
ESP1
ESP10
ESP11
ESP21
TbPT0
P - + P - + P - + P - + P - +
250
150
100
75
50
α-GFP
Ponceau-S
C
2µm

Figure 4.7. Knockdown of BILBO1 causes the redistribution of most FP ESPs in BSF cells
A) Representative micrographs of FP-localised ESPs before and after 8 hours of BILBO1 RNAi induction. Only cells that had not yet become “round” were analysed. To mark the FP, cells were stained with TL conjugated to Alexa594. DNA content is shown in magenta Exposure time for each micrograph was set to 2 seconds (green fluorescence) and 1 second (red fluorescence). **B)** Immunoblots of ESP whole cell lysates show amount of ESP protein in the cell remains relatively unchanged upon BILBO1 knockdown, despite loss of GFP signal for ESP10 and ESP11 by microscopy. Western blot was probed with anti-GFP monoclonal antibodies and Ponceau-S stained nitrocellulose membrane is a loading control. **C)** Detergent extraction of cell lines expressing ESP1-GFP show ESP1 is associated with the cytoskeleton.

4.3. Discussion

In this chapter, an insight was provided into the glycosylation status of the largest set of FP-localised proteins to date. It would seem that prediction-based determination of N-glycan addition sites may be an unsuitable way to determine which *T. brucei* sequons are genuinely N-glycosylated *in vivo*. However, an experimental approach using the glycosidase digestion of whole cell lysates with PNGase-F or Endo-H, showed the majority of FP ESPs to be glycosylated with a mixture of oligomannose and paucimannose/complex N-glycans. Although differential patterns of glycosylation were observed, when comparisons between N-glycan type, localisation, and protein topology were made, there was no clear correlation between these three factors. Therefore, if N-glycosylation does play a role in protein sorting, it is likely more complex than previously hypothesised. Indeed, the deglycosylation experiments also revealed that two of the ESPs (ESP11 and ESP21) were only modified by oligomannose N-glycans. This, in combination with the absence of complex N-glycans on TfR (Mehlert et al. 2012) is further evidence to suggest that that the presence of poly-N-acetyllactosamine moieties (found only in complex N-glycans) (Nolan et al. 1999) is not a prerequisite for an FP or endosomal cellular localisation.

The discrepancies between *in silico* predicted N-glycosylated sequons and actual N-glycans present on TfR, VSG and some ESPs could be because N-glycan predictors trained on pattern recognition alone still incur false positives and negatives (Chuang et al. 2012). Predictors based on a combination of sequence patterns and protein structural properties, such as NGlycPred, have been shown to deliver increased accuracy (Chuang et al. 2012), as structural and spatial differences between protein residues surrounding the N-glycan can also influence whether a site is glycosylated or not (Petrescu et al. 2004). Yet, this particular tool could not be used to predict glycosylation of the ESPs as a pre-determined protein structure is required.

Furthermore, prediction tools such as NetNGlyc are typically trained on human proteins. In higher eukaryotes, the OTase responsible for the N-glycan addition to the asparagine residue is a multiprotein complex with an STT3 catalytic domain associated with as many as 7 subunits (Kelleher and Gilmore

2006). These additional subunits have been shown to increase the diversity of glycosylated substrates. On the other hand, *T. brucei* encodes two single-subunit homologues of the *STT3* catalytic domain, with distinct donor and acceptor specificities (Izquierdo et al. 2009, 2012). In doing so, *T. brucei* has achieved a considerably higher N-glycosylation efficiency than other eukaryotes (Izquierdo et al. 2009; Petrescu et al. 2004). Perhaps in combination with the specific upregulation of *STT3A*, this could explain why many of the sites predicted to be non-glycosylated by NetNGlyc were glycosylated *in vivo*. In support of this, the residues NetNGlyc predicted not to be glycosylated for VSG and ESAG6 were found to be occupied by paucimannose N-glycans, suggesting a reduced ability to positively identify residues modified by STT3A specifically. (Zamze et al. 1991; Mehlert et al. 2012).

The importance of N-glycosylation for *T. brucei* survival has been exemplified by experiments involving knockdown of the OTases. Knockdown of both *STT3A* and *STT3B* prevents N-glycosylation and causes a growth arrest *in vitro* (Izquierdo et al. 2009). From this it would seem that glycosylation on the whole is required for cell survival. Yet, cells in which only one OTase was ablated showed normal growth. In these cells, it was found that when one OTase was knocked down, the other compensated for its absence. This was achieved by glycosylating the residues the other OTase would normally modify in addition to its own, albeit with reduced efficiency (Izquierdo et al. 2009). Strikingly, although not required for cell survival *in vitro*, *STT3A* or *STT3B* are both independently essential *in vivo*. (Izquierdo et al. 2009). Therefore, the type of N-glycan present on a glycoprotein is only important when the parasite is exposed to a mammalian host.

The lethality of individual OTase knockdown *in vivo* could be explained by the mislocalisation of immunogenic resident FP proteins onto the cell body membrane, as a consequence of altered protein glycosylation. If this is the case, it would provide evidence that N-glycosylation does affect protein sorting at the host-parasite interface. This could be interrogated *in vitro* using the GFP-tagged FP ESPs to monitor the fate of FP proteins upon OTase knockdown, much like the experiments performed using BILBO1 RNAi lines in this chapter.

If the type of N-glycosylation is critical for FP localisation, you would anticipate redistribution of FP ESPs to different surface subdomains.

In the second part of this Chapter, the role of the FPC in FP protein retention was also investigated. Existing at the boundary between the FP and neck membranes, it seemed plausible that it may function as a cytoskeletal barrier between these two domains. When deciphering the effect of BILBO1 knockdown in BSFs, it was discovered that disruption of the FPC led to an altered FP morphology. Yet, the presence of TL-rich foci in these cells, suggests that despite alterations to FP structure, some glycoproteins are still retained in the FP, upon BILBO1 ablation. When analysing of the fate of individual FP proteins however, it was revealed that loss of BILBO1 prevents the retention of type I TM (ESP10 and ESP11), multipass TM (ESP21 and TbPT0) within the FP. For ESP21 a clear diffusion of GFP signal onto the cell body membrane was observed, suggesting that these proteins escape onto the surface when the FPC is disrupted. To prove whether ESP10 and ESP11 have indeed been redistributed onto the surface membrane, immunofluorescence microscopy could be performed with an anti-GFP (or anti-HA) antibody to amplify any surface signal present. Alternatively, the surface of cells could be labelled with biotin, enabling surface proteins to be isolated from cytoplasmic proteins using streptavidin-agarose (Garcia-Sanchez et al. 2014). Subsequent western blot analysis of the resultant fractions would then inform whether ESP10 or ESP11 were present on the cell surface when BILBO1 is depleted. Overall, at least for the transmembrane proteins studied here, the FPC could be said to have a role in FP protein retention.

At present, it is not clear if the FPC, or indeed the neck, is still present in BILBO1 RNAi cells. To address whether the FPC is present, immunofluorescence using anti-BILBO1 antibodies could be performed to determine the degree of BILBO1 ablation. To investigate the effect BILBO1 depletion has on the neck, electron microscopy could be used to enable the visualisation of the neck membrane (as well as the collar) at an ultrastructural level.

Ablation of the FPC is more likely to affect transmembrane proteins, given its location on the cytoplasmic face of the lipid bilayer. As such, the FPC could only directly interact with the cytoplasmic tails of proteins that span the lipid bilayer. It could be hypothesised that the TL-labelled pool of glycoproteins remaining in the FP are predominately GPI anchored. For these proteins, differential retention mechanisms could be in place. For example, it could be that the GPI valence model of protein sorting (Schwartz et al. 2005), also applies to the retention of GPI-anchored proteins once they reach their target subdomain. Otherwise, the aforementioned rows of intramembrane particles at the junction of FP and neck membranes could facilitate GPI-anchored retention (Gadelha et al. 2009). As these molecules are embedded in the bilayer, they could also directly interact with the lipid moieties of GPI-anchored proteins.

The distinct localisation of ESP1 above the distal boundary of the FP, coupled with its cytoskeleton association, is reminiscent of that seen for components of the hook complex; a cytoskeletal structure present along the neck domain (Esson et al. 2012a). The FP lumen is connected to the extracellular space by channel than runs along the length of the neck membrane, facilitating the uptake and secretion of macromolecules in and out of the FP (Gadelha et al. 2009). TbMORN1, one of the components of the hook complex (Esson et al. 2012a), has a proposed structural role in maintaining channel morphology, and thus enabling entry of macromolecules into the FP lumen (Morriswood 2015; Morriswood and Schmidt 2015). Therefore it is not out of the question that ESP1 interacts with these cytoskeletal structures, and may too have a role at the neck channel.

Chapter 5. Investigating mechanisms of macromolecule transport in and out of the flagellar pocket

5.1. Introduction

The surface membrane invagination that shapes the FP is maintained at least in part by the presence of the FPC, which is thought to hold the flagellum and FP membranes in tight opposition (Figure 5.1A). This forms the FP neck domain; the region connecting the FP and cell body membranes, characterised by a narrowing of the FP at its apical end, until it is little larger in diameter than the flagellum itself. A channel runs along the length of the neck region, connecting the FP lumen to the extracellular space (Gadelha et al. 2009). This channel is closely associated with 4 specialised microtubules (4MT), and at the point where these 4MTs intersect the channel, markers for both receptor mediated-and fluid-phase endocytosis accumulate, suggesting it to be the major means by which macromolecules can gain access to the FP lumen (Gadelha et al 2009).

The smallest dimension of the channel varies from 25 to 150 nm (Gadelha et al. 2009). Such dimensions would be sufficient to allow the passage of both high- and low-density lipoprotein complexes (~8 and 22 nm in diameter respectively), which are scavenged by receptors in the FP (Green et al. 2003). In agreement with this, 20 nm gold particles enter the FP, but 40 nm gold does not (Gadelha et al. 2009), suggesting that selection on the basis of size could operate at the channel.

Alongside the FPC, at least two other cytoskeletal structures exist along the neck region: the hook-shaped TbMORN1, and a centrin arm defined by TbCentrin4 (Esson et al. 2012b; Morriswood 2015) (Figure 5.1B). Ablation of TbMORN1 in BSF causes enlargement of the FP (the “BigEye” phenotype) and obstructs the entry of Concanavalin A (ConA) and bovine serum albumin (BSA) into the FP, but not of dextran. It was estimated that ConA and BSA have a hydrodynamic radius >8 nm of whilst dextran is smaller with a radius of ~2 nm (Morriswood and Schmidt 2015). This suggests that cytoskeletal components may function in maintaining the dimensions of the channel, and

thus, either directly or indirectly, control the movement of macromolecules in and out of the FP.

The proposed involvement of the channel and the abutting 4MTs in trafficking into the FP, suggests a model whereby the channel is an active escalator transporting receptors bound to macromolecules in and out of the FP lumen (Gadelha et al. 2009). This, in turn, would require the participation of molecular motors in the movement of membrane-associated material, in particular the microtubule-binding motor proteins kinesins and dyneins

Kinesins are dimeric proteins consisting of head and tail domains (Figure 5.2A), which bind to microtubules and cargo respectively, and are connected by a stalk region (reviewed in Wang et al. 2015). Defined by a conserved motor domain, kinesins transport bound cargo along a microtubule (MT) track by converting the energy from ATP hydrolysis to mechanical force, which generates their characteristic “stepping” motion (Asbury et al. 2003). Position of the kinesin motor domain, which can be either towards the N-terminus, C-terminus or more centrally, typically dictates direction of transport or function (reviewed in Hirokawa et al. 2009). N-terminal motor domains drive plus end-directed motility, while the motor domain of a minus-end directed kinesin is located in the C-terminal region. Kinesins with a central motor domain function in microtubule depolymerisation rather than translocation.

.

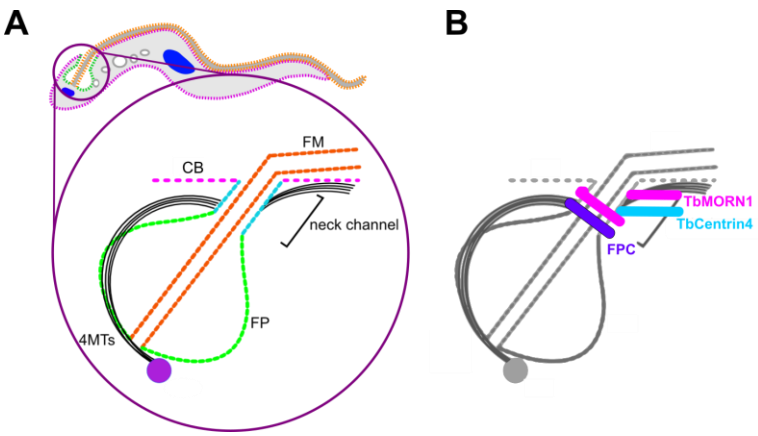


Figure 5.1. Membrane and cytoskeletal architecture of the flagellar pocket.
A) Diagrammatic representation of the distinct surface subdomains: the flagellar pocket (FP) membrane, flagellar membrane (FM) and the plasma membrane (PM). Connecting the FP and PM membrane is a neck membrane (light blue), which is defined by a set of 4 specialised MTs, originating between the basal and probasal bodies (magenta circle), and wrapping around the FP in a left-handed helix. **B)** Summary of the major cytoskeletal components associated with flagellar pocket. These include the flagellar pocket collar (FPC), TbMORN1 (component of the hook complex) and TbCentrin4 (component of the centrin arm).

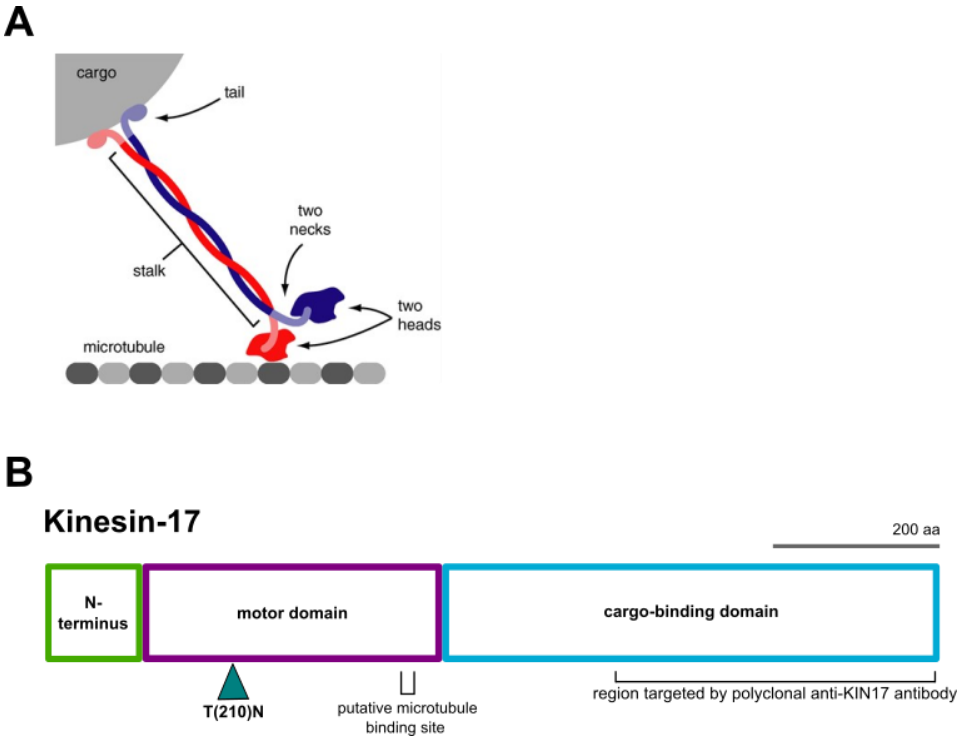


Figure 5.2. Typical structure of a kinesin.
A) Diagram of a typical dimeric kinesin consisting of head and tail domains, which bind to microtubules and cargo respectively. These two domains are connected by a stalk region. Image courtesy of Steven Block, University of Stanford. **B)** Diagrammatic representation of the structure of Kinesin-17. Kinesin-17 has an N-terminal motor domain and so plus-end motility is anticipated. The region of protein used to generate the polyclonal anti-Kin17 antibodies used throughout this Chapter is highlighted (kindly provided by Bill Wickstead, University of Nottingham), in addition to the site of the rigor mutation introduced within the ATP-binding site. In addition, the putative microtubule binding site is shown, which was defined based on sequence alignments with known microtubule binding sites of human Kinesin-3 and Kinesin-13 (Woehlke et al. 1997).

Like kinesins, dyneins also feature a motor domain containing sites for ATP-hydrolysis and MT binding, but it is composed of six tandem AAA (ATPases associated with diverse cellular activities) modules and forms a ring-like structure (Neuwald et al. 1999; Carter 2013). Emerging from the globular head domain are two structures: the stalk and the stem, which associate with the MT and cargo respectively. Dyneins are exclusively minus-end directed molecular motors and can be classified as either cytoplasmic or axonemal. Axonemal dyneins facilitate the bending motion of cilia and flagella, while cytoplasmic dyneins have a much broader range of functions, from chromosome segregation to intracellular transport (Vale 2003; Allan 2011). Often these functions complement that of kinesins. For example, the process of intraflagellar transport (IFT) to assemble new cilia or flagella requires a kinesin for the anterograde transport of IFT complexes to the tip of the flagellum, and a dynein molecule to transport the material back to the cell body (reviewed in Prevo et al. 2017).

The *T. brucei* genome encodes 47 kinesins and 3 dyneins (Berriman et al. 2005; Wickstead and Gull 2007). Two of the dyneins form the heterodimeric cytoplasmic dynein 2 (*DYNC2H1*), which localises to the flagellum and functions in IFT (Blisnick et al. 2014). Localisation and function of the third dynein, cytoplasmic dynein 1 (*DYNC1H1*), remains unknown. Yet, it is interesting to note that this particular protein co-precipitates with clathrin, suggestive of a localisation in the vicinity of the FP (Adung'a et al. 2013) and, thus, potential involvement in FP function.

The kinesin superfamily has been expanded and reclassified over the years as more genomes were sequenced and larger datasets analysed. Currently there are 17 defined families, 14 of which redefined by Wickstead and Gull (2006), and a further 3 identified since (Wickstead et al. 2010). In *T. brucei* GFP-tagged Kinesin-17 (KIN17) has been localised to the neck region in procyclic cells (PCFs) by native fluorescence microscopy (Bill Wickstead, unpublished data) (Figure 5.3A). When investigated at ultrastructural level by immuno-gold labelling of whole mount cytoskeletons, KIN17 localises to the 4MTs specifically along the neck region (Figure 5.3B) (Bill Wickstead and Catarina Gadelha, unpublished data). This localisation highlights KIN17 as a

candidate motor protein of the aforementioned escalator model of macromolecule transport in and out of the FP. If true, based on the polarity of the 4MTs and the presence of the motor domain at the N-terminus, KIN17 would be facilitating plus-end directed transport out of the FP (Figure 5.2B). As such, another motor, here hypothesised to be the DYNC1H1, would be required for macromolecule influx into the FP lumen.

This chapter will focus on the localisation and functional characterisation of both DYNC1H1 and KIN17 in BSF parasites, with the aim of elucidating their potential role in FP function at the host-parasite interface.

5.2. Results

5.2.1. KIN17 localises to the neck region in BSFs

As mentioned earlier, KIN17 localisation has only been investigated in PCF cells. However, to examine the potential role of KIN17 and DYNC1H1 in macromolecule transport at the host-parasite interface, I aimed to determine their localisations in BSF cells. Furthermore, BSFs cells have a higher rate of endocytosis compared to their procyclic counterparts (Morgan et al. 2001) thus, perturbations in nutrient transport are more likely to be of detriment to the cell. Previous studies localising cytoplasmic dynein 2 in *T. brucei* generated GFP-fusion proteins by tagging the N-terminal MT-binding domain (Blisnick et al. 2014). As IFT function was only disrupted upon RNAi-mediated knockdown of cytoplasmic dynein 2, it can be assumed that tagging at this terminus is not detrimental to its function. Therefore, DYNC1H1 here was also tagged at the N-terminus with GFP.

In the case of KIN17, both the N-terminal MT-binding domain and the C-terminal cargo-binding domain were tagged with GFP, in the event that tagging at one end interfered with functionality. For the C-terminal tagging of KIN17, the construct incorporated the endogenous 3' untranslated region (UTR) of KIN17. The 3'-UTR is known to influence mRNA abundance in T. brucei (Berberof et al. 1995), thus by maintaining the KIN17-specific UTR, the resultant protein level should be similar to that of wild-type cells.

For both DYNC1H1 and KIN17, tagging constructs were transfected into BSFs, specifically SmOxB4 cells (Poon et al. 2012), and correct protein fusion was assessed by immunoblotting of whole cell lysates. To detect DYNC1H1, the nitrocellulose membrane was probed with monoclonal antibodies against GFP (Figure 5.4). The presence of a specific band at >250kDa is suggestive that DYNC1H1 has been tagged. However, the high predicted molecular weight of the chimeric protein (623 kDa), made it difficult to precisely resolve this protein by SDS-PAGE. Having assumed that DYNC1H1 was tagged with GFP, the localisation of DYNC1H1 was then determined by native fluorescence microscopy. In the majority of cells, no GFP signal was detectable above background. But in a small number of cells (~20% of the

population), GFP foci were observed at the anterior end of the cell, along part of the flagellum attachment zone (FAZ) (Figure 5.5A).

For KIN17, immunoblotting with anti-KIN17 antibody enabled the direct comparison of N- and C-terminal tagged chimeric proteins *vs* endogenous KIN17 in untagged cells (Figure 5.4). In both instances, GFP-fusions at the predicted molecular weight were produced (146 kDa), which indicates the correct integration of tagging constructs into the genome. In addition, tagging KIN17 at the N-terminus produced a protein level closest to that of the endogenous protein (119 kDa). Conversely, there was considerably less KIN17 detected in C-terminally tagged variant, suggesting the presence of GFP at the cargo binding domain affects protein expression or stability, despite maintaining the endogenous 3'-UTR. Therefore, all subsequent experiments will utilise the N-terminally tagged protein.

For KIN17, an additional cell line was generated in which both alleles were tagged at the N-terminus, to be able to monitor the entire endogenous pool of KIN17, as well as to assess potential deleterious effects of the GFP tag itself. As expected, the double-tagged GFP::KIN17/GFP::KIN17 cell line contained approximately twice as much tagged protein as the respective single-tagged GFP::KIN17 cell line, and correct integration of the second tagging construct was demonstrated by the absence of signal corresponding to the endogenous copy (Figure 5.4). To determine if the tagging of KIN17 was detrimental to the cell survival, growth of GFP::KIN17 and GFP::KIN17/GFP::KIN17 cell lines were monitored. In both instances, no significant growth defect was detected when compared to untagged cells Figure 5.4D), showing that the N-terminal tagging of both alleles of *KIN17* with GFP is not deleterious in BSFs (assuming that a functional KIN17 is required for normal growth).

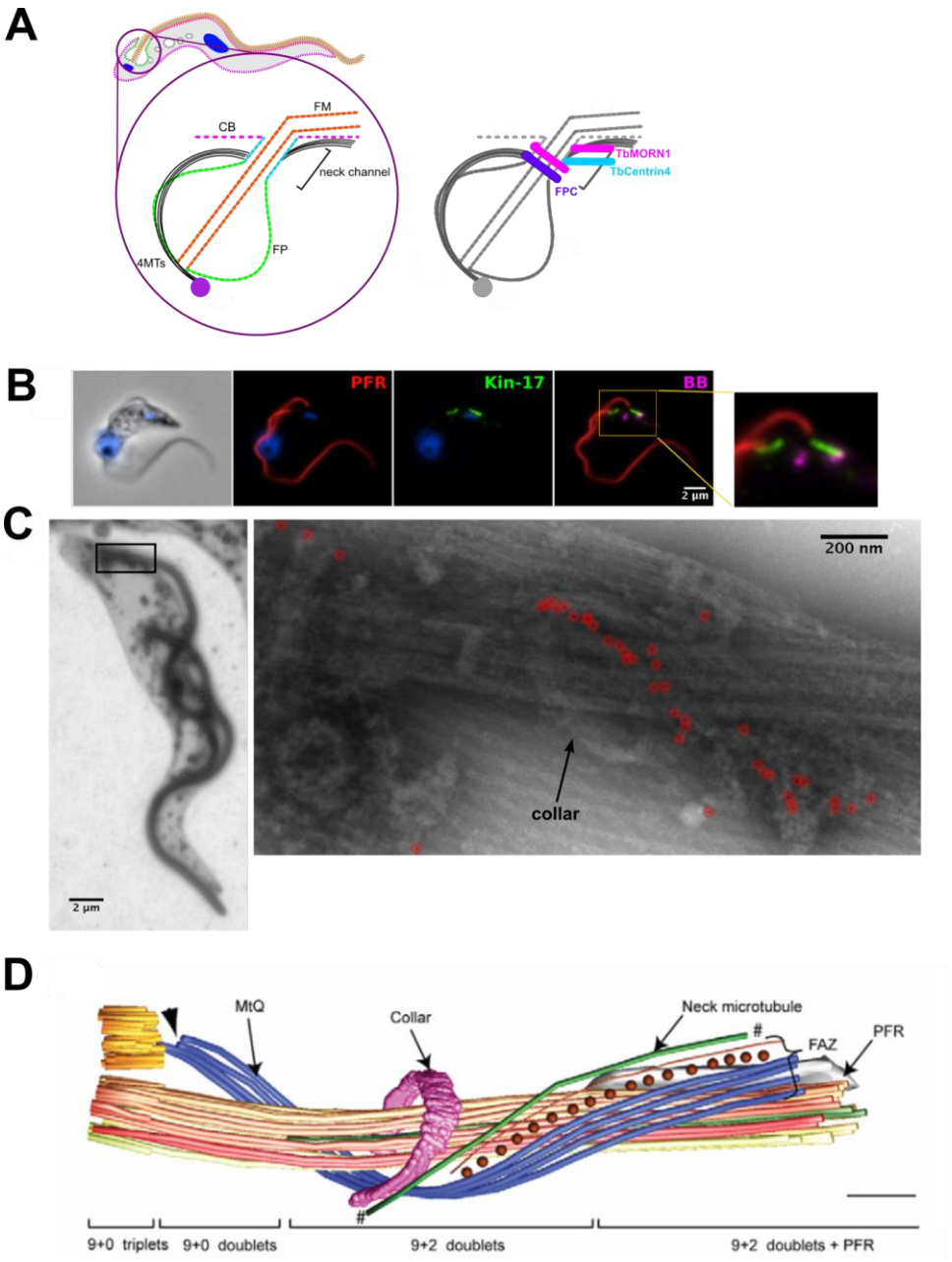


Figure 5.3. Kinesin 17 is partially associated with the 4MTs in procyclic cells.
A) Diagrammatic representation of the distinct surface subdomains: the flagellar pocket (FP) membrane, flagellar membrane (FM) and the plasma membrane (PM). Connecting the FP and PM membrane is a neck membrane (light blue), which is defined by a set of 4 specialised MTs, originating between the basal and probasal bodies (magenta circle), and wrapping around the FP in a left-handed helix. **B)** Micrographs of detergent-extracted procyclic cells in which KIN17 is tagged with GFP. KIN17 (green) localises between the axoneme (PFR, in red) and the basal bodies (BB, in magenta), and thus in proximity to the flagellar pocket. DNA content is shown in blue (Wicktead, unpublished data). **C)** Immuno-gold labelling of negatively-stained whole mount cytoskeletons with antibodies against GFP, demonstrate KIN17-GFP is partially associated to either the 4MTs along the neck region, or the neck microtubule. Red circles were used to emphasise sites of detectable gold particle binding (Wickstead and Gadelha, unpublished data). Localisation may not be identical in BSFs. **D)** Reconstruction of the cytoskeletal elements surrounding the flagellar pocket by 3D electron tomography, to aid in the interpretation of **C**. Abbreviations: MtQ, four microtubules (or 4MTs); FAZ, flagellum attachment zone; PFR, paraflagellar rod.

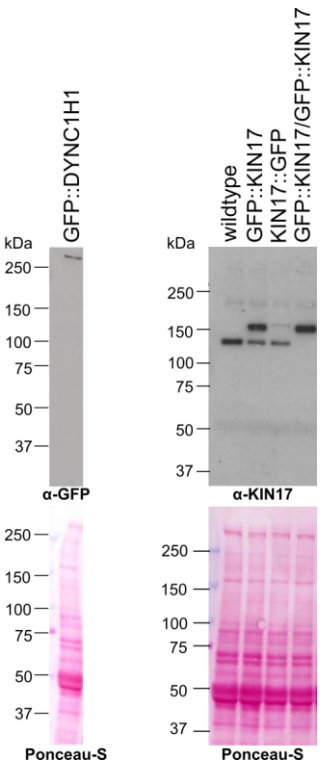


Figure 5.4. Endogenous locus tagging of *DYNC1H1* and *KIN17*.
Immunoblots of whole cell lysates expressing DYNC1H1 or KIN17 GFP-fusion proteins. Monoclonal anti-GFP antibodies were used to detect GFP::DYNC1H1 (623 kDa) and anti-KIN17 polyclonal antibodies were used to detect KIN17-tagged variants. Endogenous KIN17 has a predicted molecular weight of 119 kDa, whist the fusion protein is 146 kDa. Tagging at the N-terminus produced protein levels closest to that of wildtype cells. Ponceau-S stained nitrocellulose membrane provides a loading control. $2.5x10^6$ cells loaded per lane.

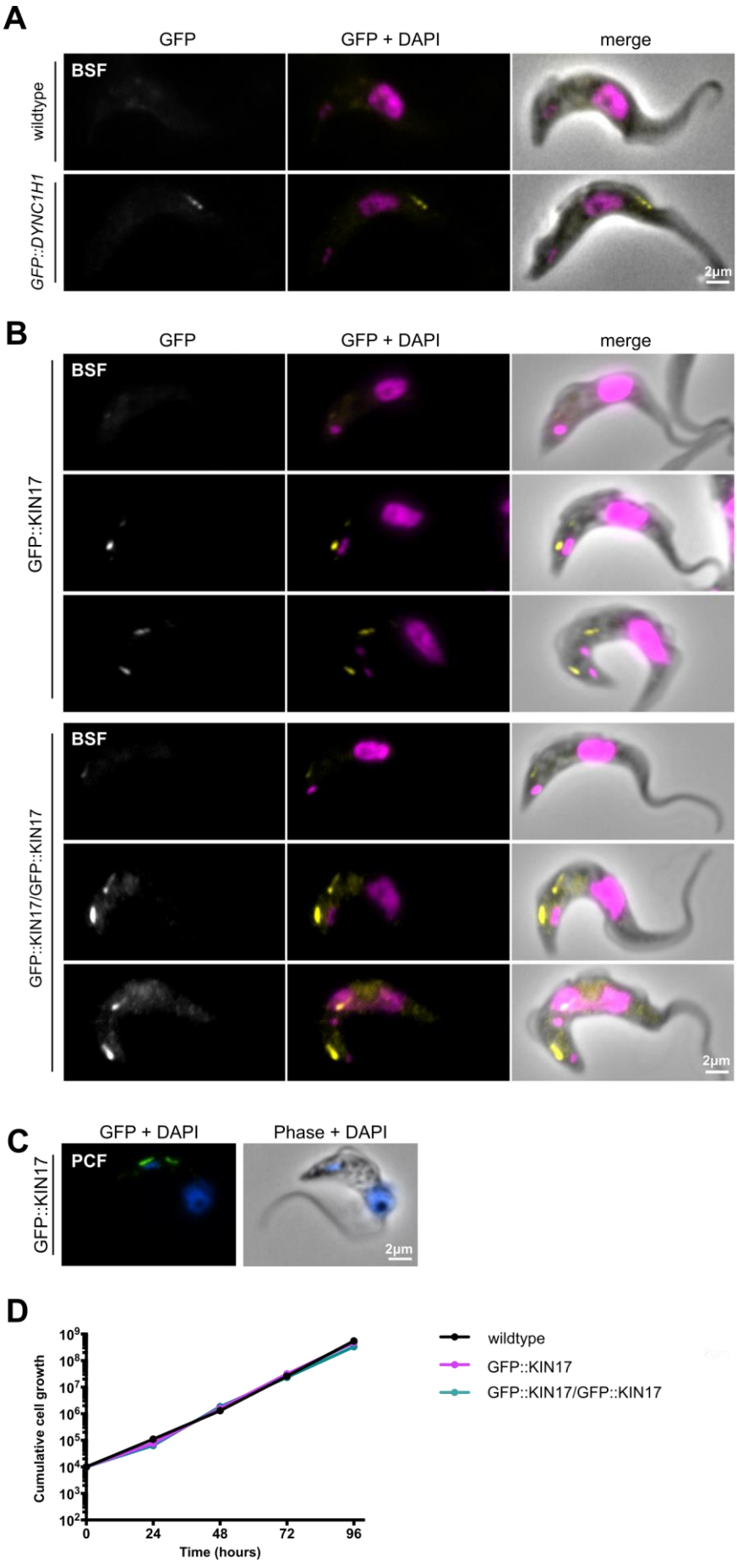

A
GFP
GFP + DAPI
merge
BSF
wildtype
GFP::DYNC1H1
2µm
B
GFP
GFP + DAPI
merge
BSF
GFP::KIN17
BSF
GFP::KIN17/GFP::KIN17
2µm
C
GFP + DAPI
Phase + DAPI
PCF
GFP::KIN17
2µm
D
Cumulative cell growth
Time (hours)
wildtype
GFP::KIN17
GFP::KIN17/GFP::KIN17

Figure 5.5. Localisation of DYNC1H1 and KIN17 in BSFs.
A) Representative micrographs of GFP::DYNC1H1 expressing cells show DYNC1H1 (in yellow) to localise to the FAZ/flagellum region. This is representative of ~20% of the population (n = 31). The remaining ~80% of cells showed no signal above background when processed the same as wildtype cells. DNA content is shown in magenta. **B)** Representative micrographs show KIN17 localises to the posterior end of the cell, in the vicinity of the FP (close to kinetoplasts) in a cell cycle-dependent manner. Both single and double-tagged lines were processed equally; thus the increased signal intensity in GFP::KIN17/GFP::KIN17 cells is reflective of the increased KIN17 protein level in these cells. DNA content is shown in magenta to highlight the kinetoplasts (mitochondrial) and nuclear DNA. **C)** Micrograph of GFP::KIN17 localisation (green) in procyclic (PCF) forms. DNA content is shown in blue**. D)** Growth analysis of GFP::KIN17 and GFP::KIN17/ GFP::KIN17 cell lines demonstrates that the addition of a GFP tag at the N-terminus of protein is not detrimental to normal cell proliferation.

Localisation of the GFP-tagged KIN17 in the newly generated cell lines was determined by native fluorescence microscopy. In all instances, KIN17 localised in close proximity to the FP (Figure 5.5B), reminiscent of the localisation seen in PCFs (Figure 5.5C). The fluorescence signal observed in BSF is here interpreted as compatible with a localisation at the neck region. Notably, the signal intensity increased in a cell-cycle dependent manner: while either weak or absent in G1 cells, the pixel intensity increased by at least 2 fold in cells with elongated or dividing kinetoplasts and, instead of a single focus, two foci were present. This coincides with the division of the FP, which begins during kinetoplast elongation, prior to their division into two discrete structures (Lacomble et al. 2010). Of the two KIN17-GFP foci, it was also evident that signal was more prominent at the most posterior focus prior to kinetoplast division, therefore protein level could be intrinsically linked to the duplication of the FP and/or associated cytoskeletal structures. Overall, given the localisation of KIN17 in close proximity to the FP, it is possible that this motor protein has a role in FP function. That is why the remainder of the chapter primarily focuses on the characterisation of KIN17, rather than DYNC1H1.

5.2.2. KIN17 is not essential for parasite growth *in vitro*

In order to investigate the role of KIN17 in BSFs, a conventional knockout (KO) approach was chosen over RNA interference (RNAi). This strategy was selected because the absence of a loss-of-fitness phenotype for KIN17 in a genome-wide RNAi screen (Alsford et al. 2011) could be attributed to incomplete knockdown. In addition, KO production is eased by the fact that KIN17 is a single copy gene, requiring only two rounds of transfection to achieve complete protein removal.

To remove the two *KIN17* alleles, knockout fragments were generated by fusion PCR (Supplementary Figure 5-1), consisting of a *BLAST* or *NEO* resistance marker flanked by the 5'- and 3'-UTRs of *KIN17*. KO fragments were then transfected into wildtype cells, replacing the *KIN17* ORF by homologous recombination of the 5'- and 3'- UTR regions (Figure 5.6A). The first allele was replaced with *BLAST* resistance marker, enabling the selection of hemi-KO lines with blasticidin. Once the integration of the first KO fragment was

confirmed by diagnostic PCR (Figure 5.6B), the second allele was replaced with a KO fragment containing *NEO,* under G418 selection, to generate a *KIN17* double-KO line (*Δkin17::BLAST/ Δkin17::NEO)* (Figure 5.6B).

Successful generation of the *KIN17* double KO line was confirmed by diagnostic PCR, which showed that one *KIN17* allele was replaced by *BLAST* and the other by *NEO* resistance marker (Figure 5.6B). Immunoblots of *Δkin17::BLAST/Δkin17::NEO* cell lysates using anti-KIN17 antibodies revealed that the amount of KIN17 in the hemi-KO line was reduced compared to endogenous (Figure 5.6C). Whilst in the double-KO line no KIN17 was detectable (Figure 5.6C). This confirmed that no gene duplication events had occurred as a result of drug pressure and thus, *bona fide* KIN17-null cell lines were produced.

As *Δkin17::BLAST/Δkin17::NEO* transformants could be obtained, this indicates that loss of KIN17 is not lethal to parasites in culture. Yet, growth of mutants may still be impaired. In order to address this, cell growth of both hemi- and double-KO lines was monitored over 5 days, alongside wildtype cells as control (Figure 5.6D). Cell proliferation was unaffected by either reduction or complete loss of KIN17. This result is in agreement with the genome-wide RNAi data, as removal of KIN17 from BSF cells is not detrimental to parasite survival, at least *in vitro*.

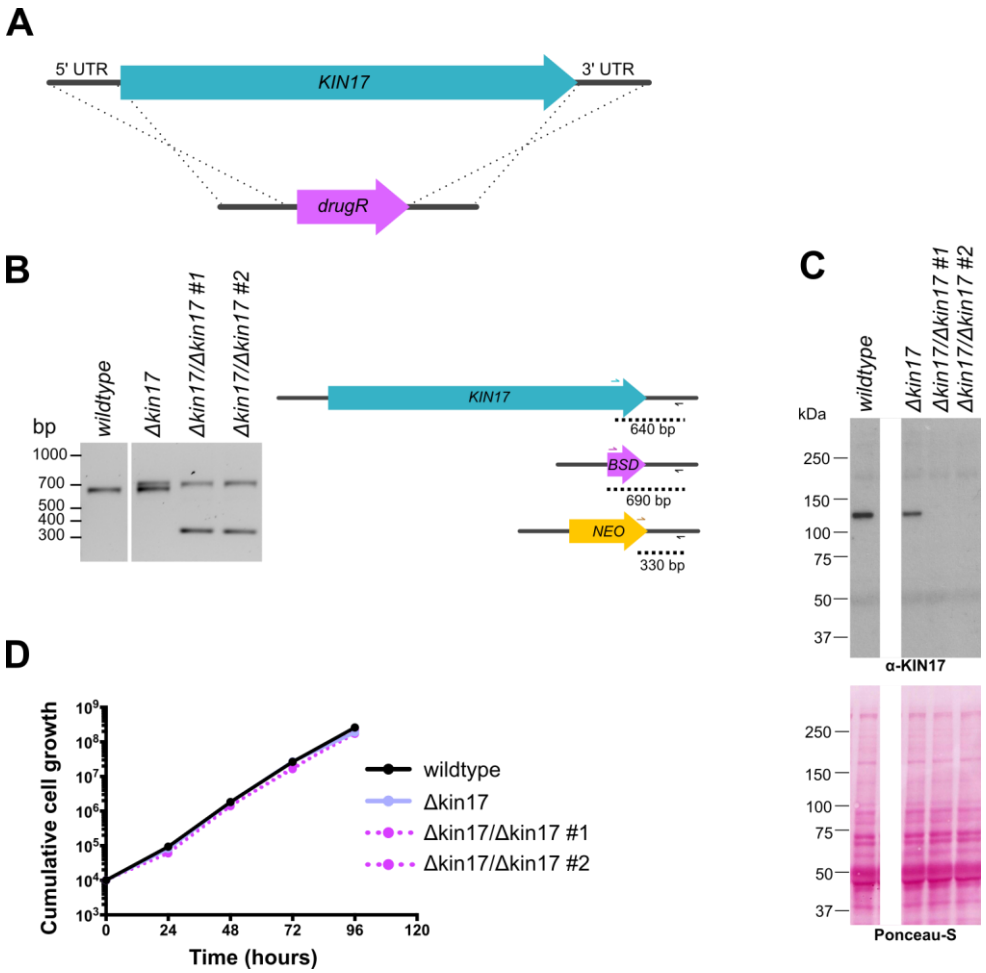


Figure 5.6. KIN17 null mutants are viable *in vitro*.
A) Schematic representation of KO strategy to replace *KIN17* ORF with drug resistance markers (either *NEO* or *BLAST*). **B)** Diagnostic PCR on mutant cell lines shows correct integration of KO fragments in both hemi- and double-KO lines. For *ΔKIN17::BLAST (ΔKIN17)*, a PCR product of 640 bp was produced, demonstrating integration of the BSD-containing fragment. For *ΔKIN17::BLAST/ΔKIN17::NEO (ΔKIN17/ΔKIN17)*, two clones were analysed. In addition to the band at 640 bp, a smaller fragment of 330 bp confirms integration of the *NEO* fragment. The absence of PCR product corresponding to the endogenous copy (690 bp) confirms KO of both alleles. **C)** Immunoblotting of hemi- and double-KIN17 KO lines with polyclonal antibodies against KIN17 shows partial and complete ablation of KIN17, respectively. 2.5x10^6 cell equivalents loaded in each lane. Ponceau-S stained nitrocellulose membrane serves as a loading control. **D)** Growth of cells in culture is unaffected by either partial or full loss of KIN17 from the cell.

5.2.3. Impairment of KIN17 function causes a severe growth defect

When it comes to studying molecular motors, the use of dominant negative mutations to express a non-functional protein is an alternative way to investigate protein function. For kinesins in particular, generation of a dominant negative mutant can be achieved by introducing a point mutation to the ATP binding site of the motor domain, preventing ATP hydrolysis and generating a rigor kinesin that cannot detach from MTs (Nakata and Hirokawa 1995). This concept was first described for the *Saccharomyces cerevisiae* kinesin-like motor KAR3 and the *Drosophila melanogaster* kinesin-like nod protein, where mutations within the GX_4GKT/S ATP binding motif rendered the kinesins irreversibly associated to the MT cytoskeleton (Meluh & Rose 1990; Rasooly et al. 1991) and has since been used in a variety of kinesin functional studies (Nakata and Hirokawa 1995; Straube et al. 2006; Messitt et al. 2008; Dawson et al. 2007).

To apply this approach to KIN17, multiple sequence alignments were performed against both KAR3 and nod protein (see above), to identify the GX_4GKT/S motif within the KIN17 amino acid sequence (Figure 5.7). Then, based on these alignments, full length *KIN17* ORF was amplified and mutated, using a fusion PCR strategy to introduce a Thr to Asn mutation at amino acid position 210 within the aforementioned GX_4GKT/S ATP binding motif; thus generating a rigor mutant. The mutated ORF was inserted downstream of either GFP or mStrawberry (mSt) in a pDex-577 vector (Kelly et al. 2007). This vector enables the tetracycline-inducible, ectopic overexpression (OE) of the full-length, N-terminally-tagged fusion protein, from the transcriptionally silent 177-bp repeats of the mini-chromosomes. Alongside the rigor mutant, a second construct was generated containing full-length wildtype *KIN17* ORF as control, to disentangle whether a phenotype associated with the OE is due to the OE itself, or specifically the rigor aspect of the kinesin.

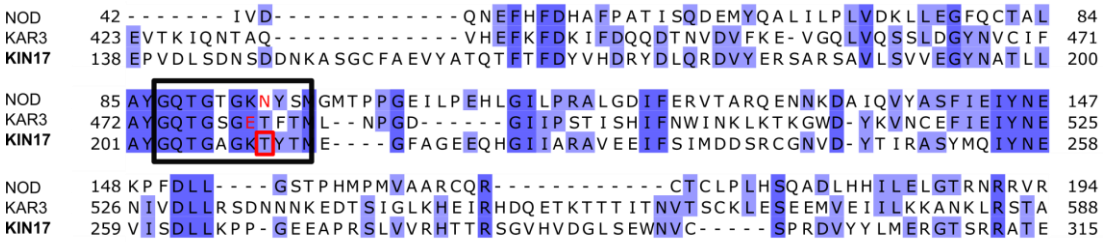


Figure 5.7. Site of KIN17 rigor mutation
Snapshot from a multiple sequence alignment of *KIN17*, *NOD* and *KAR*. The ATP binding motif of the motor domain (see Figure 5.2B) is highlighted by a black box. Red box highlights site of threonine to asparagine rigor mutation introduced to produce kin17-rigor in this study. Red lettering indicates the mutations used to generate rigor mutants in previous studies (Meluh & Rose 1990; Rasooly et al. 1991). Numbers at the side of the alignments provide amino acid position and amino acids are coloured in blue based on percentage identity.

To determine the effect of overexpressing rigor KIN17, the pDex-577-based plasmids were transfected into a selection of cell lines where endogenous KIN17 was either present or absent, summarised in Figure 5.8. This included cell lines generated previously, in which both endogenous copies of KIN17 were tagged with GFP (Figure 5.5B,C), to be able to visualise the displacement of wildtype KIN17 with the over-expressed mutant; or a DYNC1H1 tagged cell line (Figure 5.5A) in the event that OE of a kinesin rigor mutant influenced its localisation. A mixture of both GFP-tagged and mSt-tagged KIN17 and kin17-rigor OE plasmids were generated to control for any fluorescent-protein specific effects.

From each transfection, at least 3 independent clones were screened by immunoblotting with anti-KIN17 antibodies after 48 hours induction with tetracycline (Supplementary Figure 5-3). For each KIN17 and kin17-rigor cell line, the clone demonstrating the highest level of OE was taken forward for further analysis (Figure 5.9). It is worth noting that, on the whole, the kin17-rigor cell lines taken forward demonstrated higher level of overexpression that their non-rigor equivalents. This potentially indicates that the higher protein amount is intrinsic to the rigor mutant. However, it should also be stressed that the occurrence of the “high” kin17-rigor expressers was restricted to 1 in 5 clones screened on average (Supplementary Figure 5-3).

As KIN17 and kin17-rigor overexpression lines were obtained, the next step was to assess the localisation of the exogenously expressed kinesin. To this end, all cell lines were visualised by native fluorescence microscopy after 48 hours of induction (Figure 5.10). In addition to the neck localisation observed for endogenous KIN17 (Figure 5.5B), ectopically-expressed KIN17 was also found in the cytoplasm (Figure 5.10B). In the cell line where endogenous KIN17 was GFP-tagged, it was evident that OE of mSt-tagged KIN17 or kin17-rigor displaced the GFP signal (Figure 5.10A), confirming a dominant-negative effect. The localisation of GFP-DYNC1H1 was not affected by the expression of KIN17 or kin17-rigor (data not shown).

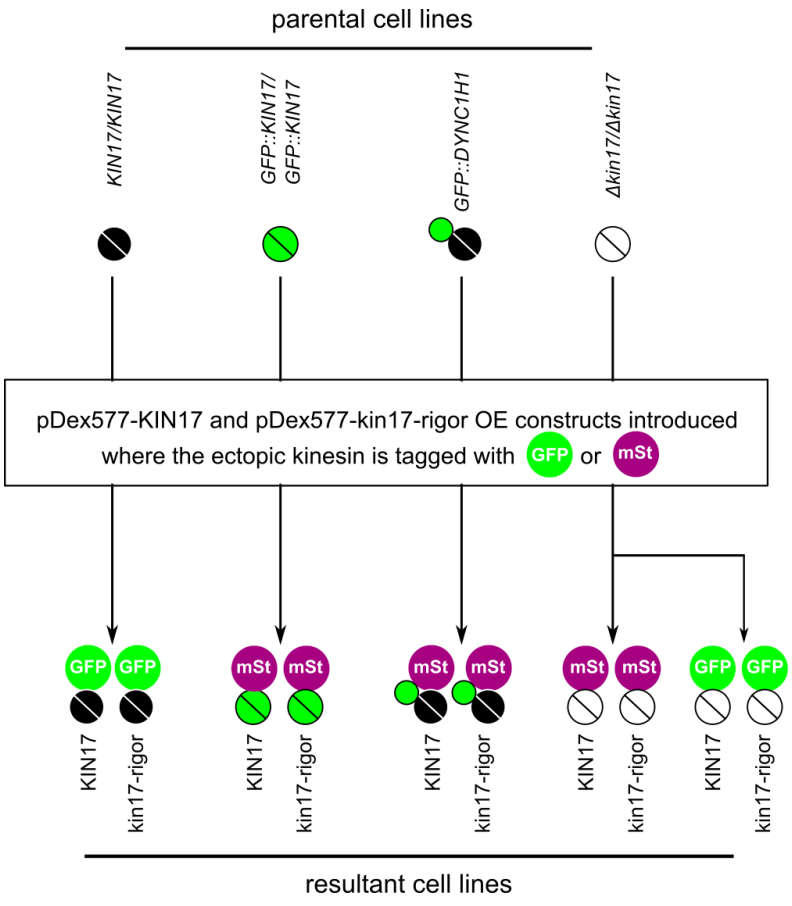


Figure 5.8. Summary of KIN17 overexpression cell lines generated.
Flow diagram to summarise the different KIN17 overexpression cell lines produced. Parental cell lines (small circles) were transfected with pDex-577-KIN17 or pDex-577-kin17-rigor overexpression constructs (large circles), tagged with either GFP or mStrawberry (mSt), to produce the resultant cell lines depicted above. These symbols will be used throughout this chapter to differentiate between these cell lines.

The presence of the cytoplasmic signal made it difficult to interpret whether there were any differences in localisation between KIN17 and kin17-rigor at the neck region. Therefore, the same analysis was performed in detergent-extracted cells to remove the cytoplasmic signal, specifically on cells OE GFP-KIN17 and kin17-rigor, as the GFP fluorescence was much brighter than mSt. Localisation of OE wildtype KIN17 resembled that of endogenous, with extended bar-shaped foci seen in the proximity of neck/FP region (Figure 5.11A). The fact that KIN17 remained present upon detergent extraction provides confirmatory evidence that KIN17 is stably associated to the cytoskeleton in BSFs, like in PCFs. Strikingly, for the rigor mutant, in the majority of cells, rather than the long bar-shape seen KIN17, the GFP signal at the neck region was more punctate, often forming >2 distinct rounded foci (Figure 5.11A,B). This difference could be explained by the rigor properties of the kinesin, in that the multiple foci observed likely represent irreversibly bound kin17-rigor that cannot travel along the MT.

To determine whether the OE of a non-functional KIN17 had an effect on cell viability, all clones previously selected for having the highest level of OE (see Figure 5.9) were induced over the course of 4 days, and growth monitored. Non-induced and parental cell lines were grown alongside for comparison (Figure 5.12A). OE of wildtype KIN17 had a very mild effect on cell growth for one of five cell lines, where KIN17 was overexpressed in a kin17 double-KO background (Figure 5.12A). Whereas OE of kin17-rigor caused a gross growth defect in 3 out of 5 of the cell lines tested, detectable as early as 24 hours post-induction (Figure 5.12A). Coincidently, these were the three cell lines in which endogenous KIN17 was still present. Whilst counting cells for growth analysis, a significant increase in enlarged cells (Figure 5.12B), or cells forming rosettes-like structures with three or more cells joined at the posterior end was noted (Figure 5.12B), suggestive of incomplete cytokinesis.

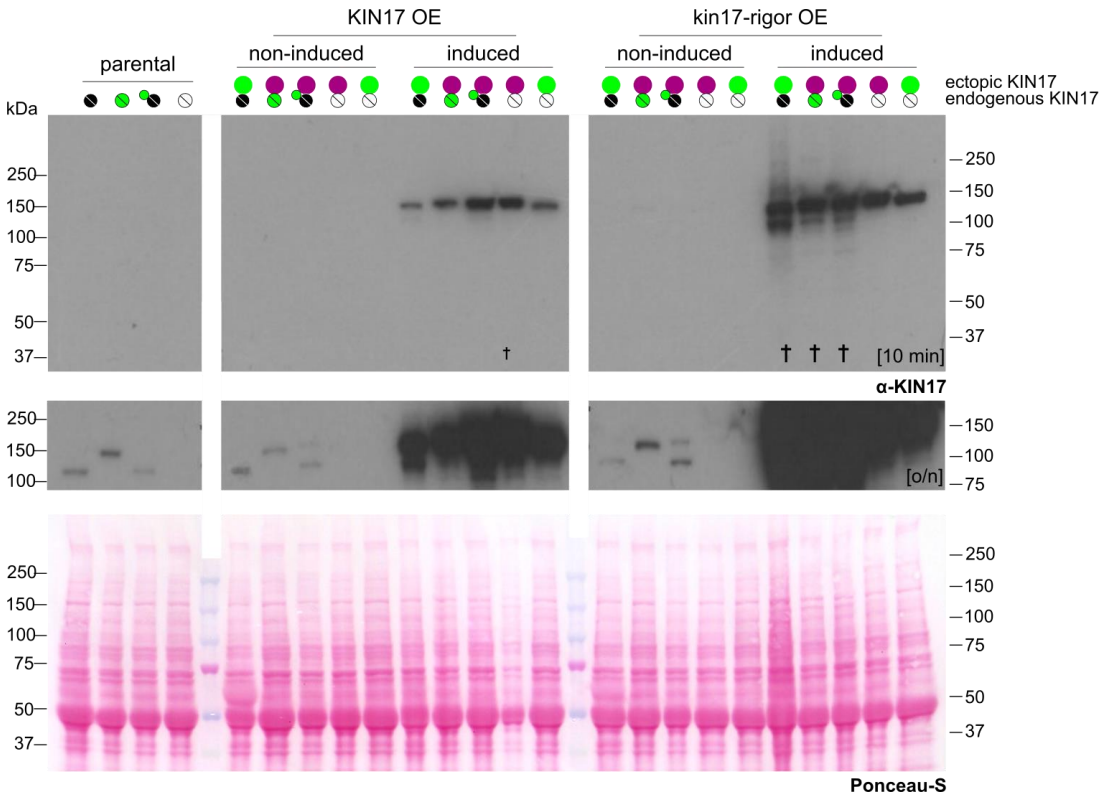


Figure 5.9. Ectopic overexpression of KIN17 and kin17-rigor mutants.
Immunoblotting whole cell lysates of KIN17 OE cell lines, probed with polyclonal antibodies against KIN17, shows overexpression of KIN17 and kin17-rigor mutants relative to non-induced and parental cell lines (see Figure 5.4 for comparison), after 48 hour inductions in the presence of 1 µg/ml tetracycline. Film exposure times are displayed in square brackets. Cell lines are depicted by symbols which show the parental background (endogenous KIN17) and the OE construct it now contains (ectopic KIN17). See Figure 5.8 for a more detailed explanation of the symbols. Ponceau-S stained nitrocellulose membrane serves as a loading control. Cross symbols indicate cell lines with a mild (small cross) or severe (large cross) growth defect (as determined in Figure 5.12)

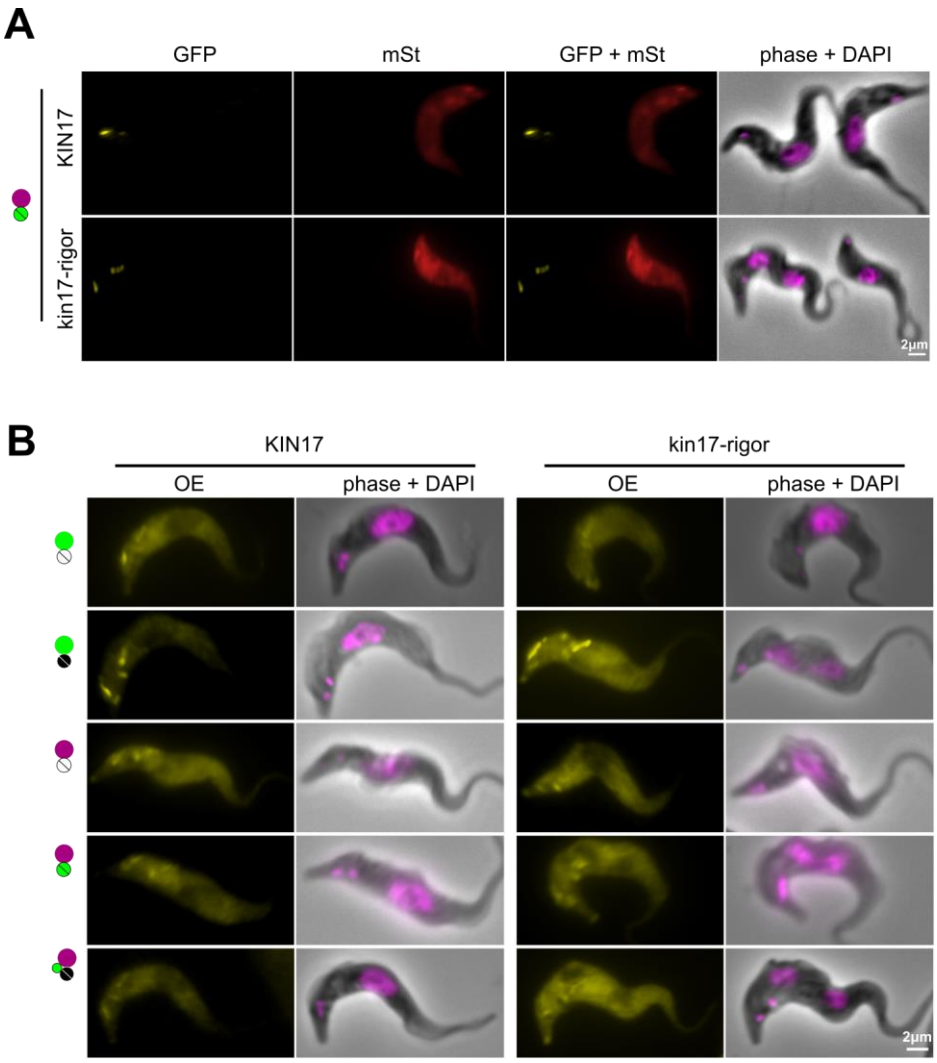


Figure 5.10. KIN17 localises to the neck region and cytoplasm upon overexpression.
A) Representative micrographs shows the displacement of endogenous GFP-tagged KIN17 (shown in yellow) when mSt-tagged KIN17 or kin17-rigor is overexpressed (shown in red). **B)** Representative micrographs of KIN17 and kin17-rigor OE cell lines show the kinesin localises to the neck and cytoplasm in all cell lines, after 48 hours of induction (shown in yellow regardless of fluorescent protein for easier comparison). Cell lines are indicated by the symbol to the left of each micrograph (for explanation of each symbol see Figure 5.8) DNA content is shown in magenta.

The cell lines with impaired growth were those that showed the highest level of KIN17 or kin17-rigor OE by Western blot (Figure 5.9) which suggests that, above a certain threshold, this kinesin is detrimental to the cell. However, at present, it is still unclear as to whether the phenotype is caused by the OE itself, or rigor attributes of the kinesin, as it was not possible to obtain KIN17 OE lines with matching level of overexpression. In addition, for the two kin17-rigor mutants that did not produce a phenotype (Figure 5.12A), endogenous KIN17 was absent from the cell; therefore, it cannot be ruled out that the cell background may influence whether or not OE of kin17-rigor is detrimental.

The variability in overexpression levels between clones and cell lines could be intrinsic to the integration of pDex-577 plasmid into the 177-bp repeats of the mini-chromosomes. It has been shown previously that integration of a tetracycline-inducible *GFP*-expression plasmid into an alternative mini-chromosomal locus, the *VSG-G4* locus, results in increased homogeneity in GFP levels between independent clones, as well as a marginal increase in average cellular GFP content, compared to integration into the 177-bp repeats (Wickstead et al. 2002a). Based on this information, it was reasoned that expression of KIN17 or kin17-rigor from the *VSG-G4* locus could resolve the issue of non-matching protein levels between rigor and non-rigor cell lines, as well as increase the consistency of cell lines that incur a growth defect upon OE. To this end, the 177-bp repeat targeting fragment of the pDex577 plasmid was replaced with one to direct recombination to the *VSG-G4* (V4) site to produce pV4Δ-Dex-mSt series of plasmids (Brusini and Wickstead, unpublished work). KIN17 and kin17-rigor fragments generated previously were inserted into pV4-Dex-mSt to create OE expression plasmids capable of expressing N-terminal mSt-tagged KIN17 or kin17-rigor upon tetracycline induction. Both constructs were then transfected into the GFP::KIN17/ GFP::KIN17 cell line.

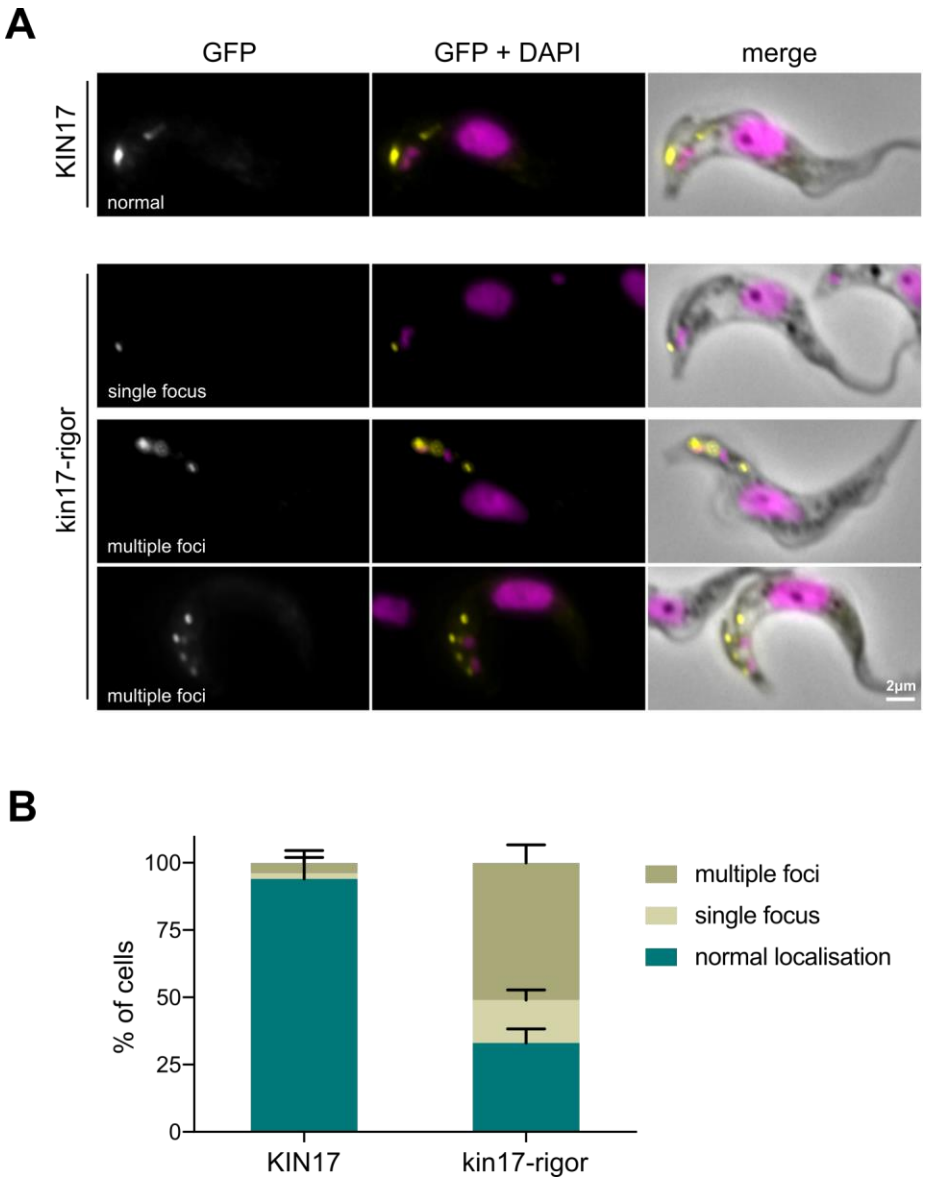


Figure 5.11. Kin17-rigor mutant shows distinct localisation at the neck region.
A) Representative micrographs of detergent extracted cells expressing KIN17 or kin17-rigor (GFP-tagged). OE of wildtype KIN17 (in yellow) shows a typical, elongated KIN17 signal close to each kinetoplast. The majority of cells expressing kin17-rigor have either a single, rounded focus, or multiple foci, greater than the number of kinetoplasts present. DNA content is labelled in magenta. **B)** Quantification of the different localisations seen for kin17-rigor (*P* <0.005 for each outcome; Chi-squared test). n= 87 for KIN17, n = 116 for kin17-rigor.

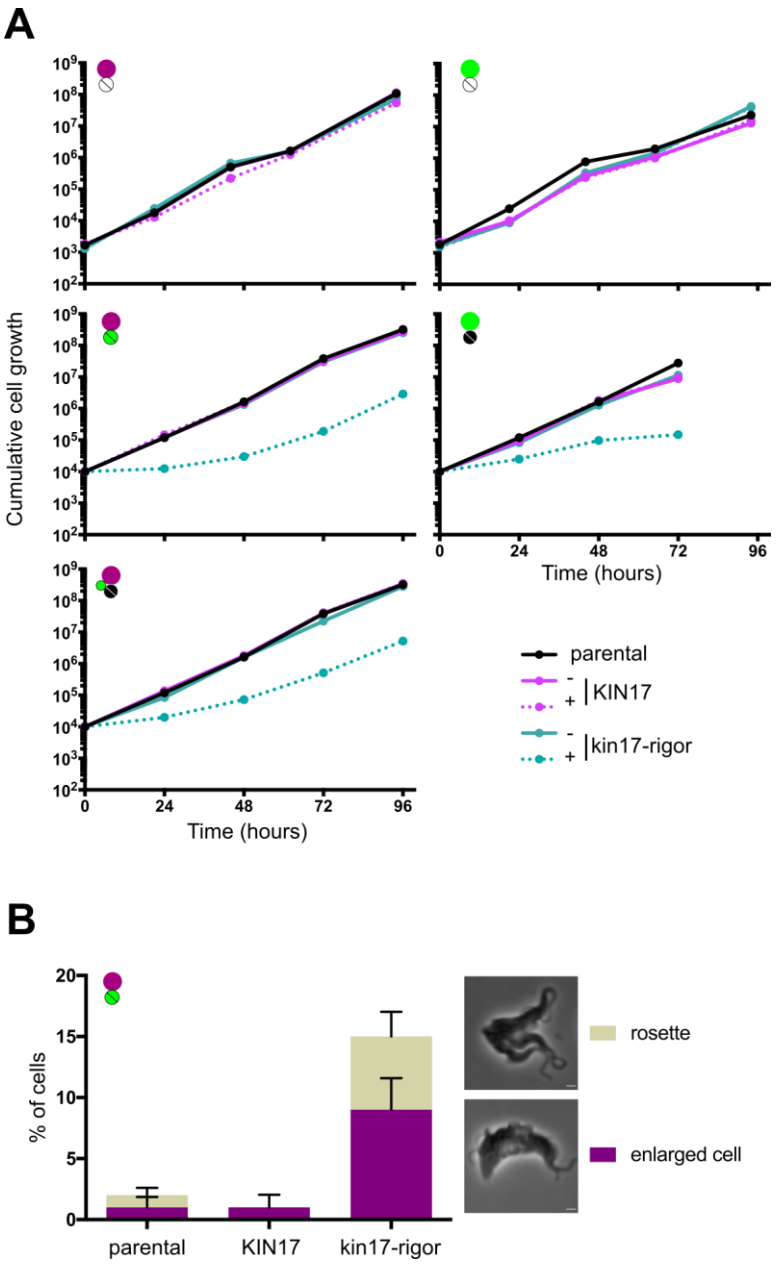


Figure 5.12. OE of kinesin rigor mutant affects normal cell growth and morphology.
A) Cell growth in culture upon induction of OE of KIN17 or kin17-rigor (+). Non-induced (-) and parental cell lines were grown alongside as controls. Cell lines are indicated by the symbol shown in the top left-hand corner of each graph (for explanation of each symbol see Figure 5.6) **B)** Quantification of the different cell morphologies observed for one of the kin17-rigor mutants with a gross growth defect (P <10-5 for each outcome; Chi-squared test). n = 164, 135 and 139, for parental, KIN17 and kin17-rigor cells, respectively. Error bars = SEM.

Previously, 3 independent clones from each transfection were screened by Western blot to select for overexpression-competent cell lines (Supplementary Figure 5-3). This time, one of the rigor mutants that produced a growth phenotype in previous analyses (Figure 5.12B) was used in the screen of pV4-Dex-mSt clones (n=3) as a threshold for the total protein amount required to cause growth defect. Immunoblots probed with anti-KIN17 demonstrated that all clones expressed mSt-KIN17 or mSt-kin17-rigor after 48 hours of induction (Figure 5.13A); and overall, the protein levels were roughly homogenous across clones. Importantly, protein amounts at a population level were comparable between clone 1 of both KIN17 and kin17-rigor lines, as well as to the rigor mutant that had a growth phenotype previously. Microscopy analysis of these new clones also confirmed the same neck and cytoplasmic localisation seen for the other KIN17 OE cells lines (Figure 5.13B).

As before, growth of the VSG-G4-integrated overexpression cell lines were monitored over 4 days, comparing induced, non-induced and parental cells (Figure 5.13C). No growth defect was apparent for the OE of mSt-KIN17. Surprisingly, only a very mild growth defect was observed for the rigor mutant in induced cells, despite protein amount at a population level matching that of the rigor mutant (Figure 5.13A) exhibiting a severe growth defect (Figure 5.12) Based on this result, it was hypothesised that, although these cells lines showed similar amounts of kin17-rigor production at a population level, there may be variability at an individual cell level, or indeed in the amount of protein actually associated to the MTs in these cells.

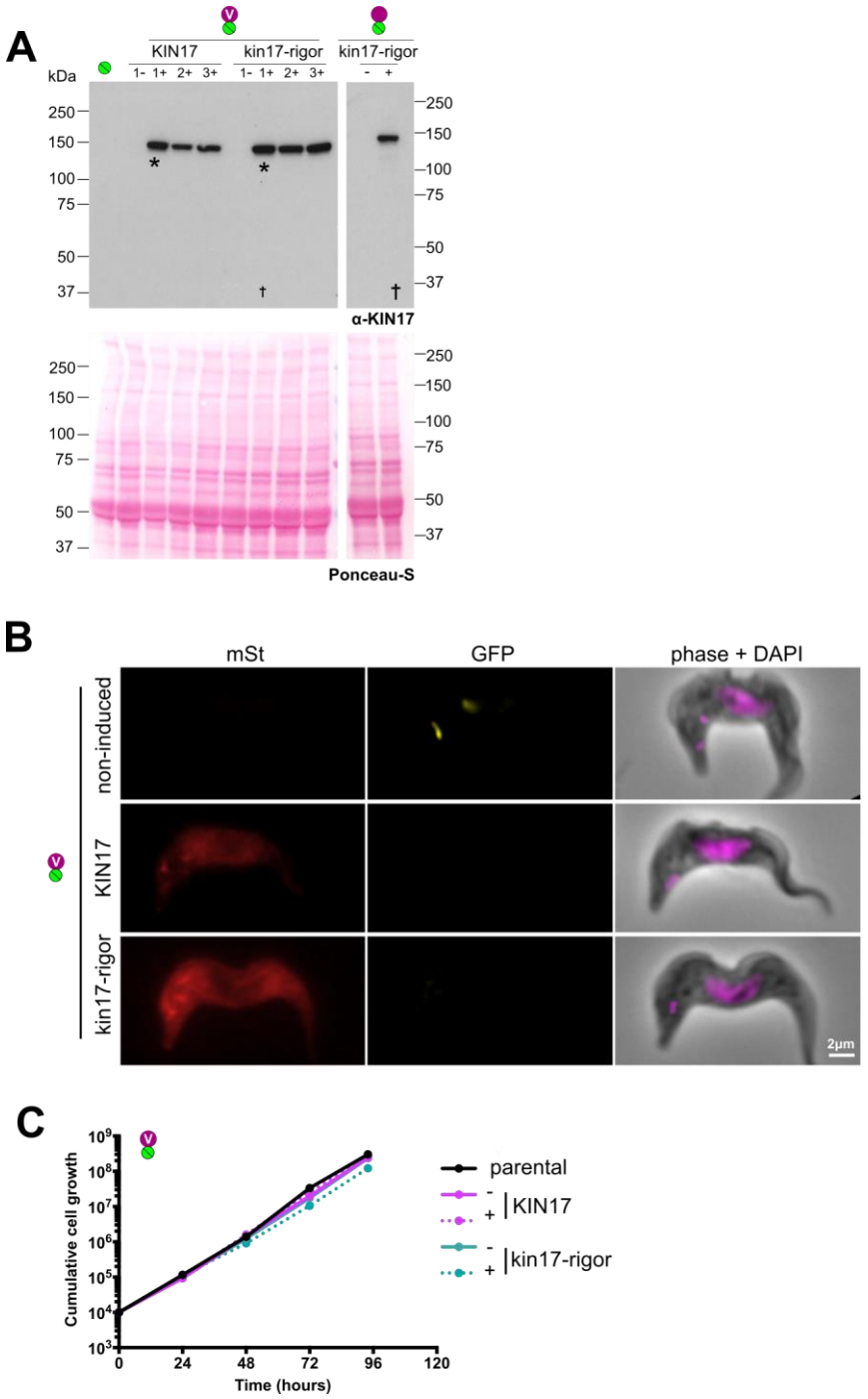


Figure 5.13. OE of KIN17or kin17-rigor from the VSG-G4 locus.
A) Immunoblots probed with anti-KIN17 polyclonal antibodies confirm OE of KIN17 or kin17-rigor upon induction (+). kin17-rigor cell line from earlier experiments was included to show the amount of protein present in cells with a growth defect. Symbols above lane/sets of lanes indicate genotype (see figure 5.6 for symbol description). Here, a 'V' within the larger circle indicates expression from VSG-G4 locus. Asterisks indicate clones taken forward for further analysis. Cross symbols indicate a mild or severe growth defect (as determined in part **C**, and Figure 5.10). Ponceau S- stained nitrocellulose membrane serves as a loading control ($2.5x10^6$ cells/lane). **B)** Micrographs of KIN17/kin17-rigor over-expressed from a VSG-G4 locus show kinesin localised to the neck region and cytoplasm (in red), displacing the endogenous GFP-tagged protein (yellow). Noninduced cell was representative of KIN17 and kin17-rigor. Cells were induced for 48 hours and DNA content is shown in magenta. **C)** Cell growth in culture after OE of KIN17 or kin17-rigor, produces a marginal growth defect for kin17-rigor OE, compared to non-induced and parental cell lines.

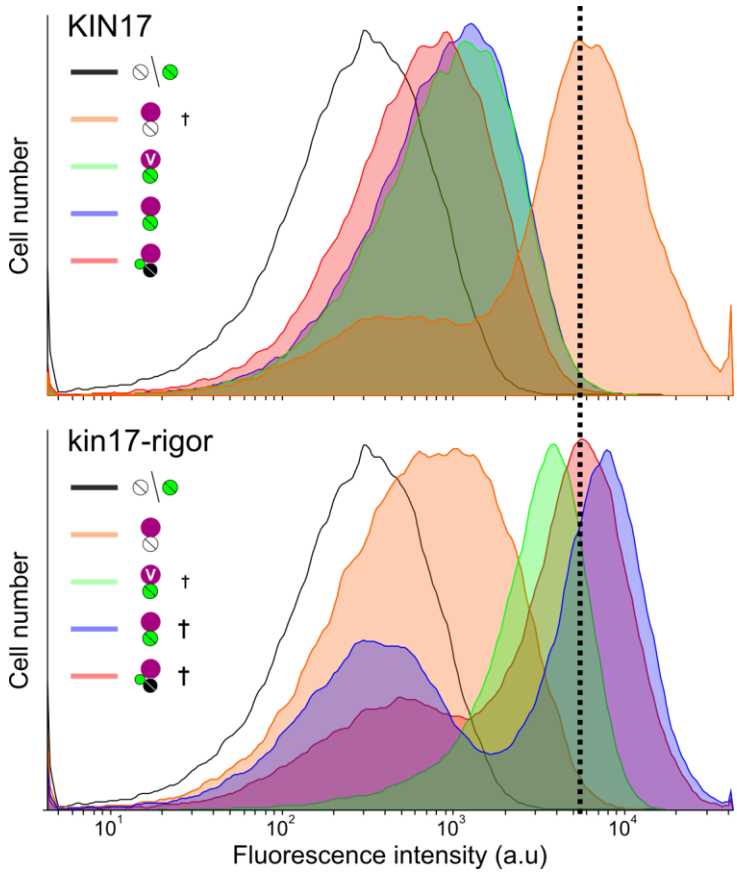


Figure 5.14. Growth defect associated with kin17-rigor OE correlates with greater amount of protein in the cell.
Flow cytometry analysis of cell lines expressing mSt-KIN17 or mSt-kin17-rigor show the relative fluorescence intensity profiles of each cell line. Dotted line indicates lowest mean fluorescence intensity of kin17-rigor mutant with a gross growth defect. Circular symbols represent the genotype of each cell line and their associated fluorescence intensity profiles (see figure 5.6 for symbol description). Cross symbols indicate a mild (small cross) or severe (large cross) growth defect determined in figures 5.10 and 5.11. For associated dot-plots of forward and side scatter values as well as gating, see Supplementary Figure 5-2. At least 50,000 events captured for each cell line.

To determine the extent of the variability in protein amounts at a single cell level, the fluorescence of mSt-KIN17 and mSt-kin17-rigor cell lines was determined by flow cytometry after 48 hours of induction. The cell lines analysed included both OE mutants with and without growth defect, as well as parental cell lines to determine background fluorescence. From the resultant fluorescence intensity profiles for each cell line, it was apparent that rigor mutants with an associated growth defect contained a subset of cells with higher levels of kin17-rigor protein (Figure 5.14). The mean fluorescence intensity of this subset was ~6 times higher than that of the rigor mutants with normal growth rates (Figure 5.12A), and ~2 times higher than the pV4-Dex-

mSt-kin17-rigor cell line, for which only a slight defect was observed (Figure 5.13C).

Collectively, this suggests that the expression of kin17 rigor mutant is detrimental to parasite survival when protein level in the cell builds up above a certain threshold. Furthermore, the wildtype mSt-KIN17 cell line that showed a very marginal defect had a fluorescence profile similar to that of the phenotypic mSt-kin17-rigor cells (Figure 5.14). Therefore, the cell death observed in mSt-kin17-rigor cells can be assigned to the rigor properties of the kinesin rather than the presence of excess kinesin in the cell. Altered forward and side-scatter profiles for phenotypic mSt-kin17-rigor cell lines is also further evidence for altered cell morphologies in lines exhibiting growth defect (Supplementary Figure 5-2).

Given that cell death seems to be related to high amount of rigor kinesin in the cell, this could be a consequence of the build-up of excess kin17-rigor on MTs. However, there is currently no evidence to suggest that more kinesin is associated with the MTs in these cells. To address this, the same cell lines analysed by flow cytometry were induced for 48 hours, subjected to detergent lysis, and then fractionated into insoluble (MT-bound) and soluble fractions. The GFP::KIN17/GFP::KIN17 cell line was included as a control, to demonstrate the relative amount of KIN17 associated to the MTs in what is essentially a wildtype cell. The resultant cell lysates and fractions were immunoblotted with anti-KIN17 antibodies to determine the relative abundance of KIN17 in each fraction (Figure 5.15). Here, it was discovered that a greater proportion KIN17 was present in the insoluble, MT-associated fraction, in cell lines in where OE of mSt-kin17-rigor was lethal. These data, in combination with the microscopy on detergent-extracted cells suggest that, at least at a population level, the mutants with a growth defect have a greater amount of kinesin bound to MTs at the neck region.

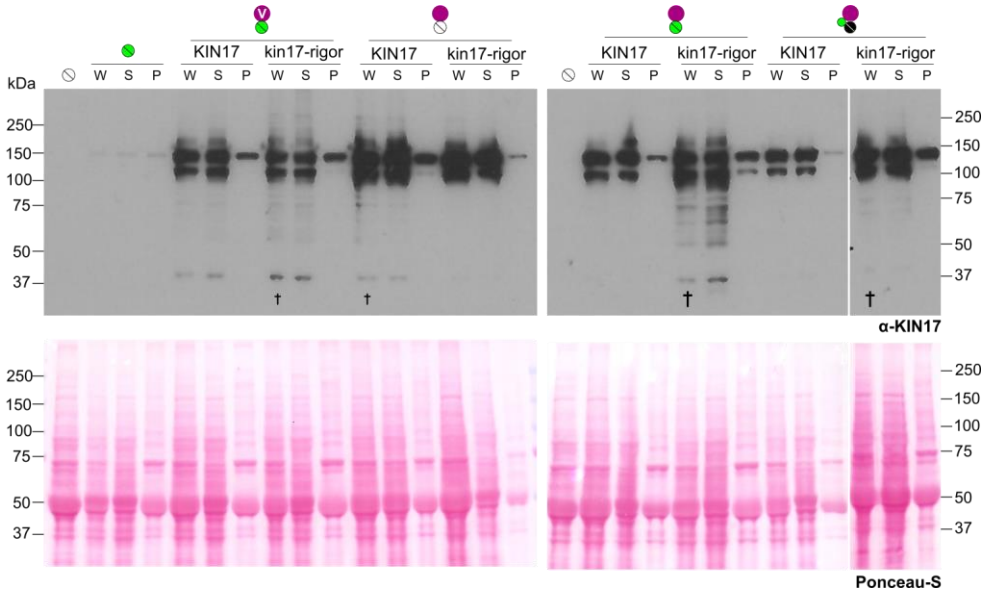


Figure 5.15. Greater amount of kin17-rigor is associated to the cytoskeleton in cells with a growth defect.
Immunoblotting of KIN17 OE cell lines probed with anti-KIN17 antibodies. Whole cell lysates (W) were separated into soluble (S) and pellet (P) fractions after 48 hours of induction. Protein in the pellet fraction constitutes cytoskeleton-associated material. Cross symbols indicate cell lines with a mild (small cross) or severe (large cross) growth defect (as determined in Figure 5.10). Cell lines are depicted by symbols corresponding to genotype (See figure 5.6 for detailed explanation of the symbols). Ponceau-S stained nitrocellulose membrane serves as a loading control.

5.3. Discussion

Data presented in this chapter relates to the characterisation of two motor proteins in *T. brucei*, focusing specifically on their potential roles at the flagellar pocket. Localisation data showed KIN17 to localise to the vicinity of the FP/neck and, by drawing similarities to the localisation seen in PCFs (Wickstead and Gadelha, unpublished data), it is likely that KIN17 also localises to the 4MTs along the neck channel. In accordance with this, KIN17 in BSFs is associated to the cytoskeleton at the neck region in detergent-extracted cells, which implies its binding to MT. DYNC1H1 showed a more anterior localisation, interpreted here as the flagellum attachment zone. Given that the 4MTs extend from the FP along the FAZ to the anterior end of the cell, it is plausible that this motor protein is also associated with the 4MTs, but at their opposite end. It is tempting to suggest that DYNC1H1 could be transporting cargo towards the FP, with its minus-end directionality, whilst KIN17 transports material out. This would fit with the escalator model of transport of macromolecules previously proposed (Gadelha et al. 2009). Although it would also raise the question as to why DYNC1H1 would maintain the bulk of the protein at the anterior end of the cell, if its primary function were in cargo transport into the FP lumen.

When investigating the function of KIN17 at the FP neck region, complete removal of KIN17 from the cell had no effect on cell viability *in vitro*. This is not entirely surprising, as kinesins often work co-operatively to transport cargo, often with assistance from other family members (reviewed in Mallik et al. 2013). This co-operation extends to members of different families, such as kinesins 5 and 7, which exhibit functional redundancy during mitosis (reviewed in Cross & McAinsh 2014). If this is also true for KIN17, being the sole *T. brucei* representative of its family, KIN17 would need to function alongside kinesins from different families. Possible partner candidates might include *T. brucei* kinesins that, like KIN17, are restricted to organisms that possess cilia/flagella, such as kinesins 9 and 16 (Wickstead and Gull 2006).

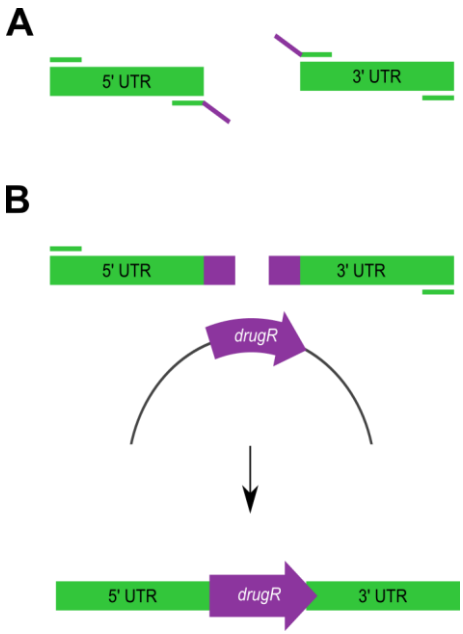
It was only upon the over-expression of a rigor kinesin that the parasite encountered difficulties. In cells producing sufficiently high levels of kin17-rigor protein, as determined by Western blot and flow cytometry analyses, a severe

growth defect coupled with aberrant cell morphologies was observed. There was also a correlation between cells with impaired growth and a greater amount of kin17-rigor associated to the cytoskeleton, which is perhaps expected given that a rigor mutant becomes irreversibly bound to MTs. Collectively, the data obtained here suggest that the build-up on kin17-rigor on the MTs is detrimental to cell survival. Therefore, it could be speculated that the accumulation of kin17-rigor on the 4MTs could interfere with the function of other motors associated with the 4MTs, or indeed the 4MTs themselves.

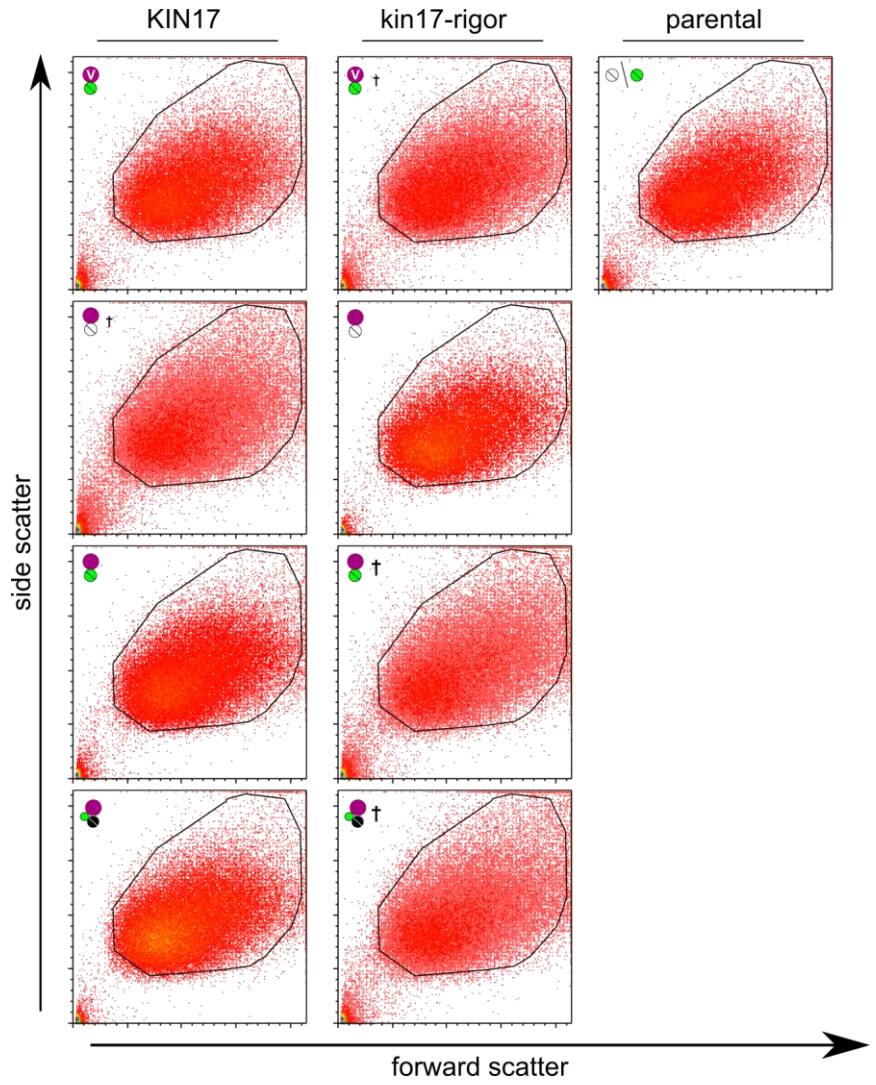
The abnormal morphologies observed in rigor mutant cells included a significant increase in “rosette” structures. These rosettes consisted of 3 or more cells that remained associated by their posterior ends, suggestive of incomplete cytokinesis. In *T. brucei*, cytokinesis is uni-directional and occurs via a cleavage furrow that originates at the tip of the daughter FAZ filament, and follows the line of the FAZ from the anterior to posterior end of the cell (Vaughan and Gull 2008; Wheeler et al. 2013). As the 4MTs are closely associated with the FAZ, it follows that interfering with 4MT function could potentially affect cell division.

It remains to be seen as to whether KIN17, or indeed DYNC1H1, have roles in the movement of macromolecules in or out of the FP lumen. For KIN17 in particular, if this is the case, as KIN17 is dispensable for cell survival, it suggests this motor protein is not working alone.

Supplemental Figures

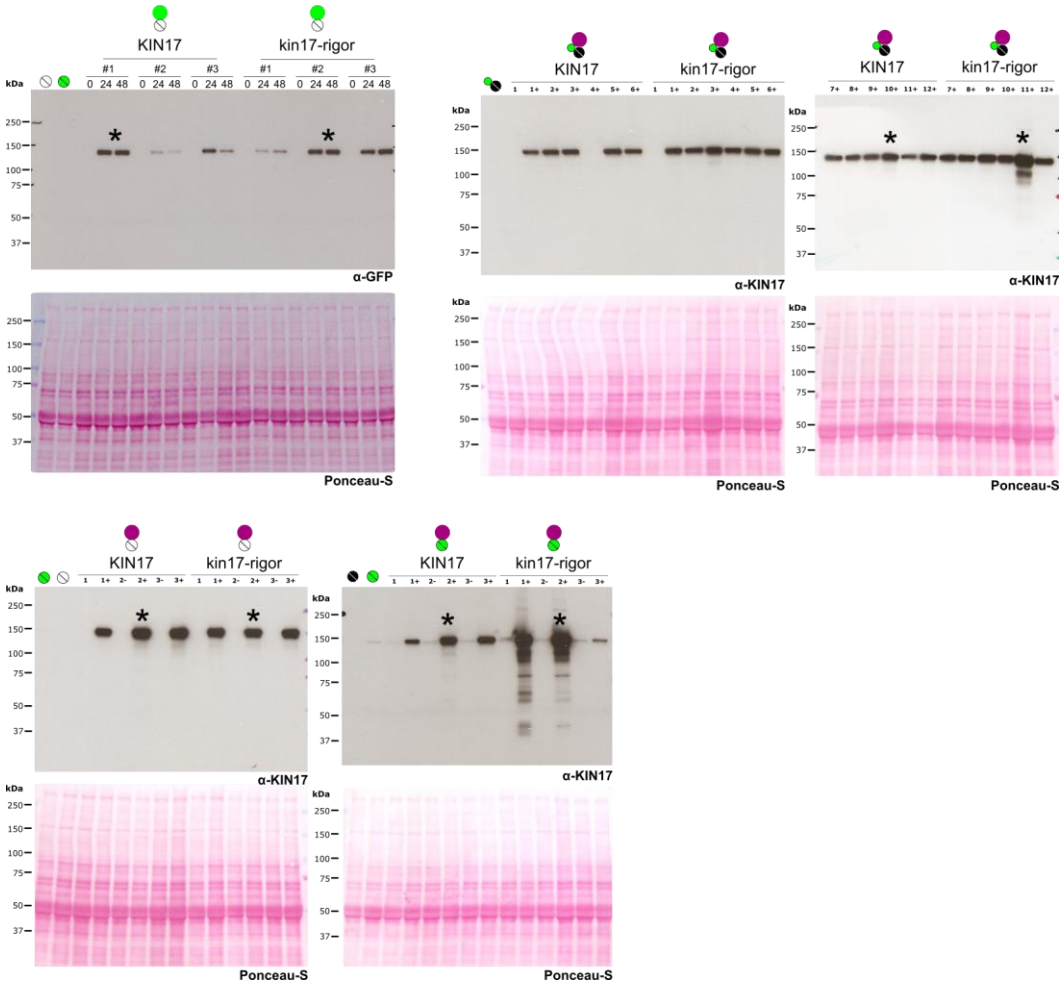


Supplementary Figure 5-1 Fusion PCR strategy to generate KIN17 KO fragments
Schematic representation of a typical fusion PCR reaction. **A)** Initial PCR to amplify 5' and 3' UTR fragments for *KIN17*, using primers with complementary overhangs to either the *NEO* or *BLAST* drug resistance marker (purple). **B)** Fusion PCR reaction to combine 5' and 3' UTR fragments with the drug resistance gene. Here, the complimentary overhangs (purple) produced from the first PCR (**A**) act as primers to amplify the drug resistance gene, and the outermost primers in the 5' and 3' UTRs (green) then amplify the full length fragment.



Supplementary Figure 5-2 Altered forward and side scatter profiles for mutants showing growth defect

Dot plots of forward vs side scatter for KIN17 and kin17-rigor OE lines analysed by flow cytometry. Area marked with a black line shows gating applied for Figure 1.12. Cell lines are depicted by circular symbols which correspond to their respective genotype (See figure 1.6 for detailed explanation). Cross symbols indicate a mild (small cross) or severe (big cross) growth defect determined in figures 1.10 and 1.11.



Supplementary Figure 5-3 Screening KIN17 and kin17-rigor OE clones for inducible overexpression
Immunoblotting of whole cell lysates from KIN17 OE lines, probed with antibodies against either KIN17 or GFP. Clones showing the greatest overexpression after 48 hours of induction are indicated with an asterisk. See figure 1.6 for a detailed explanation of cell genotype symbols. Ponceau-S stained nitrocellulose membrane serves as a loading control.

Chapter 6. Discussion

6.1. Flagellar pocket proteins: essential or redundant?

The flagellar pocket as an organelle is central to the survival and persistence of *T. brucei*. Yet, out of the 9 FP ESPs identified during the validation of *T. brucei* surfeome (Gadelha et al. 2015), and 4 novel FP proteins localised as part of this thesis, none exhibited a growth defect upon individual knockdown by RNAi, suggesting that the majority of FP-localised proteins to date are not essential for BSF parasite growth *in vitro*. This lack of growth phenotype is in striking contrast to the parasite's reliance for survival on the two best characterised FP receptors –TfR and HpHbR (Vanhollebeke et al. 2008; Tiengwe et al. 2016). Given the multitude of functions performed by the FP, the ESPs may have a role in processes not addressed here, such as host adaptation, cell differentiation or immune evasion (Field and Carrington 2009). This was indeed the case for other FP-localised proteins such as PAD2 and ESAG4, which are involved in bloodstream-to-procyclic differentiation and the modulation of the host immune system, respectively (Dean et al. 2009; Salmon et al. 2012a). Functions in line with the latter could be hypothesised for ESP13 and ESP31, as like ESAG4 these ESPs localise to the flagellar membrane in addition to the FP (Gadelha et al. 2015).

Interrogation of ESP function related to infection dynamics should thus be investigated *in vivo*. This could be achieved by pooling the set of FP ESP-RNAi cell lines described in this thesis, and inoculating mice with the resultant cell population. By design, this experimental set-up is in essence a competition assay; as such, it also has the potential to highlight genes whose knockdown only causes a marginal growth defect. The abundance of each cell line could be monitored over the course of infection via quantitative PCR, and abundance compared between induced and non-induced cells. Though, as the current cell lines are monomorphic (deficient in stumpy-form parasite generation), to address roles related to cell differentiation and infection control, pleomorphic equivalents would need to be produced (see section 3.2.2). It is also likely that the phenotype *in vitro* could differ between monomorphic and pleomorphic strains.

It is also possible that receptors are retained in the FP not only for performing critical functions, but because their presence on the cell body membrane is detrimental to parasite survival. ISGs for example, have a cell body localisation, and are immunogenic during a mouse infection (Ziegelbauer and Overath 1993). Yet, their low copy number, partial shielding by the variant surface glycoprotein (VSG) coat, and clearance of ISG-antibody complexes by hydrodynamic flow, are all factors proposed to contribute towards preventing the antibody titre from reaching critical levels (Schwede et al. 2015). If the majority of invariant proteins were also localised to the cell body membrane rather than sequestered in the FP, this would likely counteract these preventative measures.

The HpHbR is an example of a BSF-specific, FP-restricted protein, modelled to protrude beyond the VSG coat, with its extended conformation necessary for ligand binding (Higgins et al. 2013). Interestingly, in the related African trypanosome, *T. congolense,* HpHbR is expressed primarily during the late developmental stages in the fly, rather than in the host bloodstream, and here the receptor localises across the whole cell surface (Lane-Serff et al. 2016). It has been suggested that the shift to BSF expression in *T. brucei* coupled with reduced receptor density (1000-fold less), increased affinity for Hp-Hb, and restriction to the FP, is a consequence of immune pressure (Higgins et al. 2017). Therefore, it is possible that this is also the case for other FP-localised proteins, such as the ESPs. In particular ESP27: it is reasonable that its presence on the cell body could be disadvantageous to the parasite, as ESP27 has been predicted to be highly immunogenic and to have two large extracellular arms that could protrude above the VSG coat (Chapter 3, Lee et al. 1994). In this instance it could be insightful to increase ESP27 expression level (and indeed that of other ESPs) with the aim of promoting a cell body localisation, as was done for TbMBAP (Engstler et al. 2005). If surface localisation was achieved, antibody recognition could be assessed *in vitro* using anti-GFP antibodies (as the C-terminal GFP-tag on ESP27 is predicted to be extracellular), similar to experiments performed previously on live cells using antibodies against ISGs or VSG (Chung et al. 2004). Though here, the bulky nature of GFP would limit is use as a direct read-out for protein-

recognition *in vivo*. Thus, overexpression of an untagged variant on the parasite surface during a mouse infection would be required for *in vivo* validation, or the use of smaller epitope tags such as HA may also be suitable. Though the former would not only inform whether specific antibodies are raised against the surface-localised ESP, but whether the antibody titre is sufficient for parasite clearance. Ultimately this could begin to answer whether the FP really does provide a protective environment for invariant surface proteins; while the protein overexpression itself provides another way to interrogate ESP function.

6.2. The collar as a flagellar pocket barrier

It is not yet understood how the parasite maintains its specialised surface domain architecture. Yet, at the boundary between the FP and neck membranes lie the flagellar pocket collar (FPC), with a ring-shaped structure resembling that of septin diffusion barriers in other eukaryotes (Caudron and Barral 2009; Saarikangas and Barral 2011; Palander et al. 2017). In procyclic forms (PCFs), knockdown of the only published FPC component, *BILBO1*, produces elongated cells lacking a new daughter FP, ultimately resulting in cell death (Bonhivers et al. 2008). In BSFs, *BILBO1* knockdown is also lethal, yet round cells rather than elongated ones are produced (Bonhivers et al. 2008).

Here, I utilised *BILBO1* knockdown as a tool to investigate the fate of FP-localised proteins in BSF cells, in the absence of the major FPC component. Strikingly, the effect of BILBO1 on the FP as a whole was somewhat different to that observed for procyclics (Bonhivers et al. 2008). When counterstaining the FP of dividing cells with tomato lectin (TL), structures corresponding to both the old and new FPs were present, upon BILBO1 ablation. However, both FPs appeared smaller and more cortical in location. The reduced invagination of the FP could indicate that the region connecting the FP to the cell body, the neck, is reduced or absent. Given the location of the collar at the point of FP membrane constriction, which forms the neck domain (Lacomble et al. 2009), it follows that disruption to the FPC may alter the membrane organisation of this region. Investigation of FP morphology at an ultrastructural level by electron microscopy would be needed to shed further light on this.

Furthermore, it would be useful to assess the degree of BILBO1 ablation at each FP with an anti-BILBO1 antibody to aid with the interpretation of this phenotype. It should also be noted that micrographs demonstrating the absence of a daughter FP in PCFs were obtained after 48 hours of RNAi induction (Bonhivers et al. 2008), rather than the shorter 8 hour inductions performed here on BSF parasites. So, it could be argued that after the same induction period, biogenesis of the new FP could also be inhibited in BSF cells, yet the rounded cells and more severe growth defect made this difficult to assess.

Alternatively, the difference in the resultant *BILBO1* knockdown phenotype in BSFs *vs* PCFs could be explained by a difference in FPC biogenesis. As BILBO1 ablation in insect forms primarily affects the new FPC (and FP), this would suggest that the collar is assembled *de novo* (Bonhivers et al. 2008). In BSFs, the seemingly equal impact of BILBO1 ablation on both pre-existing and new pockets could imply that the old FPC is used to form the new FPC. This was shown to be the case for another cytoskeletal protein located in the vicinity of the FP, TbMORN1, where both old and new hook-shaped structures are affected following RNAi knockdown in BSFs (Morriswood and Schmidt 2015). This could suggest a general difference in the duplication of cytoskeletal components between the two life cycle stages. Indeed, BSFs undergo a more bilateral, symmetrical cytokinesis than PCFs, which could be linked to this apparent symmetrical division of cytoskeletal structures (Wheeler et al. 2013). Furthermore, there are a number of cytoskeletal proteins associated to the subpellicular microtubule array that are differentially expressed between life cycle stages (Portman and Gull 2012, 2014). As knockdown of these genes leads to cytokinesis defects, it suggests further differences in cytoskeleton organisation between BSFs and PCFs.

TL is known to bind the sugar moieties of glycoproteins enriched in the FP (Nolan et al. 1999; Mehlert et al. 2012). The presence of TL-labelled FP structures in BILBO1 RNAi cells indicated that some resident FP proteins were retained despite FPC disruption. This initially prompted the conclusion that the FPC may have a role in maintaining FP morphology, but not necessarily function as a membrane protein barrier. Yet, when the fate of five individual FP

ESPs were assessed in BILBO1 ablated cells, four out of five showed reduced GFP signal in FP. For ESP21 in particular, this signal visibly diffused onto the cell body membrane, which could imply that BILBO1 (or the collar as a whole) may ordinarily aid in restricting this protein to the FP membrane. Though, at present, this interpretation only takes into account the effect on a small-subset of FP proteins and only considers proteins containing transmembrane domains. The fifth protein (ESP1), was initially included to provide a representative for GPI-anchored proteins, though subsequent work established ESP1 to be stably associated to the cytoskeleton, so this is not a typical GPI-anchored FP protein. Thus, extension of this analysis to include other GPI-anchored proteins (and a larger cohort of transmembrane proteins) is required in order to draw more robust conclusions on the influence of protein topology on FP retention.

Considering its location on the cytoplasmic side of the plasma membrane, the FPC could interact with the cytoplasmic tails of transmembrane domain proteins, regulating their movement between the FP and cell body membranes. However, it is also tempting to speculate that the FPC associates with the row of intramembrane particles that span the bilayer at the same membrane boundary (Gadelha et al. 2009). This would be reminiscent of the scenario observed in neuron specialisation. Between the axon and the somatodentritic membranes, a diffusion barrier is formed by creating “pickets” of transmembrane proteins, which are held in place via the underlying cortical cytoskeleton (Nakada et al. 2003; Caudron and Barral 2009). To investigate this in *T. brucei*, freeze fracture electron microscopy could be performed on BILBO1 RNAi cells, to see if the rows of IMPs remain intact in the absence of the FPC. If the IMPs are absent, this could imply that BILBO1 is required to anchor them at along this membrane region. This would then raise questions as to whether BILBO1 itself was directly involved in FP protein retention, or indirectly via maintaining the rows of IMPs.

To fully appreciate the role of the FPC in FP protein retention, the phenotype in BSF cells requires further characterisation. For example, the endocytic activity of the old and new FPs in BILBO RNAi cells has not been interrogated, though the reported accumulation of VSG-containing vesicles in

the cytoplasm would imply defective trafficking (Perdomo et al. 2016). If exocytosis is perturbed in these cells, it follows that FP proteins may not be efficiently delivered to the pocket in the first instance. Equally, if protein turnover is affected, protein could build up in the FP, and if the saturable hypothesis is correct, they have the potential to be redistributed onto the cell body membrane as a consequence of protein abundance rather than a defective FPC barrier *per se*. It would also be insightful to investigate the fate of FP proteins in PCF cells where the FP (and FPC) is completely absent upon *BILBO1* RNAi. This could provide further insight into whether additional membrane barriers are in place to maintain the biochemically distinct sub-domains of the surface plasma membrane.

6.3. Glycosylation as a potential flagellar pocket protein sorting factor

Links between protein N-glycosylation and FP localisation in *T. brucei* had been proposed previously (Nolan et al. 1999; Atrih et al. 2005; Mehlert et al. 2012). Initially, an association between components of the endocytic pathway (i.e. those localised to the FP or endosomes) and proteins modified with linear poly-N-acetyllactosamine-containing sugars was noted. (Nolan et al. 1999). Later, mapping of the TfR N-glycans revealed that this particular N-glycan moiety was not always present on FP-localised proteins (Mehlert et al. 2012). The large cohort of FP ESP provided a platform on which to further investigate the role of N-glycosylation in FP localisation. Here, glycosidase treatment showed that the majority of FP ESPs were glycosylated. It is thus conceivable that this post-translational modification could influence FP targeting, as has been shown for apical membrane sorting in epithelia (Vagin et al. 2009; Stoops and Caplan 2014). However, a limitation of this work is that it only focused on proteins with an FP localisation. Therefore, a systematic comparison would need to be drawn against non-FP localised proteins, to clarify whether this is an FP protein-specific targeting signal. A site-directed mutagenesis approach could also be taken to investigate the relative contribution (if any) that each N-glycan residue makes towards a protein's localisation to the FP. Interpretation of these results, however, could potentially be complicated by protein mis-localisation as a consequence of mis-folding, rather than the N-glycans absence directly (Xu and Ng 2015).

Treatment of whole cell lysates with either PNGase-F or Endo-H enabled the distinction between oligomannose or paucimannose/complex N-glycan modifications on ESPs. It was hypothesised that N-glycosylation pattern may influence whether a protein localises predominately to the FP, or the FP in combination with the flagellum or cell body membrane domains (Gadelha et al. 2015). For example, the FP is enriched in glycans containing long linear N-glycan chains (Nolan et al. 1999), so perhaps their existence facilitates an FP localisation. Comparative analysis between N-glycan type (i.e oligomannose or paucimannose/complex) and ESP sub-domain localisation did not reveal an obvious correlation between these two factors, or indeed protein topology. Furthermore, the absence of complex N-glycans noted for ESP11 and ESP21, in addition to the same findings for TfR (Mehlert et al. 2012), demonstrate that the presence of poly-N-acetyllactosamine-containing sugars alone is not required to produce an endosomal or pocket-localised glycoprotein, although it may still be sufficient. Mapping of the N-glycan addition sites by mass spectrometry could be the next step towards deciphering whether there is a more complex pattern between N-glycan protein decoration and surface sub-domain localisation. This would, in turn, aid in a possible site directed-mutagenesis approach, as described above.

Glycosylation is certainly not the only possible determinant of protein localisation. In *T. brucei* PCFs for example, the FP-localised CRAM protein contains signals within its cytoplasmic tail that are necessary for its transport from the endoplasmic reticulum to the FP, as well as FP retention (Yang et al. 2000; Qiao et al. 2006). Truncations of more than 19 of the 41 amino acids encompassed in its cytoplasmic C-terminus are sufficient to cause CRAM to redistribute across the cell body membrane (Qiao et al. 2006). Although purely speculative, by comparison with the redistribution of some FP proteins onto the cell body membrane upon *BILBO1* knockdown, it could be feasible that the truncated C-terminus prevents CRAM from interacting with FPC and therefore its restriction to the FP is lifted. However, CRAM also mis-localises onto the flagellar membrane (Qiao et al. 2006), which could suggest that protein truncations enable CRAM to surpass diffusion barriers at the base of the flagellum too.

Although not explored specifically in this thesis, comments can be made with regards to one of the models proposed to explain the lateral movement of proteins on the surface membrane, which is based on protein abundance. Increasing protein expression caused two endosomal and FP-localised proteins to be redistributed onto the cell body membrane (Engstler et al. 2005; Mussmann et al. 2003). Interestingly, of the 13 ESPs plus TbPT0 tested here, those that localised to the cell body in addition to the FP (i.e. ESP13 and TbPT0) did not exhibit the highest cellular protein level as detected by immunoblotting. While ESP14 and ESP21 demonstrated significantly higher protein levels, yet were confined to the FP and endosomes. This suggests that if a saturable mechanism of FP retention indeed exists, the system may be protein-dependent. Such a mechanism could be addressed quite simply, and systematically, by the over-expression of FP-specific ESPs and monitoring of their resultant (if any) redistribution across the cell surface membrane. Whether such artificial protein overexpression informs modes of parasite-controlled surface sub-domain specialisation is unclear. Though, as exemplified by the up-regulation and subsequent cell body re-location of a previously FP-restricted transmembrane protein (PAD2) upon parasite ingestion by the fly (Dean et al. 2009), this phenomenon does seem to occur *in vivo.*

6.4. Overexpression of a kinesin rigor mutant is detrimental to parasite survival

The localisation of a motor protein, KIN17, to the neck region supports the suggestion that molecular motors may be involved in macromolecule transport between the FP lumen and extracellular space. This was first proposed based on the accumulation of endocytic markers within the neck channel, along a region of membrane demarcated by a set of 4MTs, when endocytosis is blocked (Gadelha et al. 2009). This observation was unexpected given that the neck membrane is not thought to be competent for endocytosis.

In PCF, KIN17 localises specifically to the 4MTs along the length of the neck (Wickstead & Gadelha, unpublished data). In this study, I have shown that the same cellular location is true in BSF cells, as seen by native

fluorescence microscopy. When investigating KIN17 function, kin17-null mutants were viable in culture, implying that if KIN17 is involved in transport of membrane-associated material across the neck channel, it is unlikely to be facilitating this alone. Cooperation is not uncommon between kinesins (Mallik et al. 2013). Thus, KIN17 could be aided by other motor proteins that have yet to be localised to the FP channel. To explore this further, immunoprecipitation experiments could be performed with KIN17, which have the potential to isolate additional motor proteins, as well as the receptors that must be binding the aforementioned endocytic markers along this region. This has been done successfully for an orphan kinesin in *T. brucei*, TbKIN-D, which associates with the subpellicular microtubules and is required to maintain correct cell morphology (Hu et al. 2012a). Immunoprecipitation experiments revealed its major protein interactor to be TbKIN-C, a kinetoplastid-specific kinesin (Hu et al. 2012b). Interestingly knockdown of each of these kinesins independently produced a similar phenotype, and from this it was suggested that they may perform similar functions, potentially as a heterodimer (Hu et al. 2012a, 2012b).

Alternatively, the lack of growth defect could be attributed to the gene knockout approach chosen. One of the potential drawbacks associated with the production of gene knockouts to interrogate protein function is that there is a risk of obtaining cells that have adapted or compensated for the loss of that gene (Rossi et al. 2015). For example, other kinesins may have been upregulated in response to the loss of KIN17, potentially masking a phenotype. This possibility could be explored further using an inducible knockout system, such as the Cre-LoxP conditional knockout system (Kim et al. 2013).

When overexpressed to a sufficiently high level in the cell, a kin17-rigor mutant caused a severe growth defect accompanied by morphological abnormalities indicative of a cytokinesis block. Though, this cytokinesis block would need to be confirmed by determining the DNA content in these mutant cells. As rigor mutants cannot hydrolyse ATP and thus bind to MTs irreversibly (Meluh and Rose 1990; Nakata and Hirokawa 1995; Dawson et al. 2007), the detriment to parasite survival may have been a consequence of the accumulation of kin17-rigor on the 4MTs abutting the neck, disrupting trafficking along these cytoskeletal tracks. RNAi ablation of Spef1, another

4MT-associated protein, inhibited the assembly of a new set of 4MTs prior to cell division, leading to defects in cytokinesis (Gheiratmand et al. 2013). The similarity between Spef1 knockdown and kin17-rigor overexpression phenotypes could support defective 4MT function in rigor mutant cell lines. However, it should be noted that cytokinesis defects are a common occurrence when disrupting the cell cytoskeleton in general (Bonhivers et al. 2008; Hu et al. 2012b, 2012a; Portman and Gull 2014), so further evidence for a definitive link between kin17-rigor overexpression and the perturbation of 4MT function is required.

For KIN17, it would also be important to show that it localises specifically to the 4MTs in bloodstream form cells, by repeating the analysis performed on procyclic form whole mount cytoskeletons expressing KIN17-GFP (see Figure 5.3). Co-localisation of KIN17-GFP with an anti-Spef1 antibody could also give an indication of KIN17's association to the 4MTs. Furthermore, the rigor properties of the mutant kinesin could be assessed in more detail by incubating purified kin17-rigor protein with immobilised microtubules and comparing its ability to traverse the microtubule lattice, with that of non-rigor KIN17 (Patel et al. 2016).

Overall, the work presented in this thesis has shed some light on FP function by characterising novel FP components and investigating mechanisms of surface membrane specialisation, while the role of KIN17 in macromolecule transport along neck channel remains an enigma.

References

Absalon S, Blisnick T, Bonhivers M, Kohl L, Cayet N, Toutirais G, Buisson J, Robinson D, Bastin P. 2008. Flagellum elongation is required for correct structure, orientation and function of the flagellar pocket in *Trypanosoma brucei*. *J Cell Sci* **121**: 3704–16.

Acosta-Serrano A, Vassella E, Liniger M, Kunz Renggli C, Brun R, Roditi I, Englund PT. 2001. The surface coat of procyclic *Trypanosoma brucei:* programmed expression and proteolytic cleavage of procyclin in the tsetse fly. *Proc Natl Acad Sci U S A* **98**: 1513–8.

Adung'a VO, Gadelha C, Field MC. 2013. Proteomic analysis of clathrin interactions in trypanosomes reveals dynamic evolution of endocytosis. *Traffic* **14**: 440–57.

Ahearn IM, Haigis K, Bar-Sagi D, Philips MR. 2011. Regulating the regulator: post-translational modification of RAS. *Nat Rev Mol Cell Biol* **13**: 39–51.

Aitcheson N, Talbot S, Shapiro J, Hughes K, Adkin C, Butt T, Sheader K, Rudenko G. 2005. VSG switching in *Trypanosoma brucei* : antigenic variation analysed using RNAi in the absence of immune selection. *Mol Micro* **57**: 1608–22.

Alcantara CL, Vidal JC, de Souza W, Cunha-e-Silva NL. 2014. The three-dimensional structure of the cytostome-cytopharynx complex of *Trypanosoma cruzi* epimastigotes. *J Cell Sci* **127**: 2227–37.

Allan VJ. 2011. Cytoplasmic dynein. *Biochem Soc Trans* **39**: 1169–78.

Allen CL, Goulding D, Field MC. 2003. Clathrin-mediated endocytosis is essential in *Trypanosoma brucei*. *EMBO J* **22**: 4991–5002.

Alsford S, Eckert S, Baker N, Glover L, Sanchez-Flores A, Leung KF, Turner DJ, Field MC, Berriman M, Horn D. 2012. High-throughput decoding of antitrypanosomal drug efficacy and resistance. *Nature* **482**: 232–6.

Alsford S, Turner DJ, Obado SO, Sanchez-Flores A, Glover L, Berriman M, Hertz-Fowler C, Horn D. 2011. High-throughput phenotyping using parallel sequencing of RNA interference targets in the African trypanosome. *Genome Res* **21**: 915–24.

Alves e Silva TL, Savage AF, Aksoy S. 2016. Transcript abundance of putative lipid phosphate phosphatases during development of *Trypanosoma* brucei in the tsetse fly. *Am J Trop Med Hyg* **94**: 890–3.

Angelopoulos E. 1970. Pellicular Microtubules in the Family Trypanosomatidae. *J Protozool* **17**: 39–51.

Aronson DE, Costantini LM, Snapp EL. 2011. Superfolder GFP is fluorescent in oxidizing environments when targeted via the sec translocon. *Traffic* **12**: 543-8.

Asbury CL, Fehr AN, Block SM. 2003. Kinesin moves by an asymmetric hand-over-hand mechanism. *Science* **302**: 2130–4.

Atrih A, Richardson JM, Prescott AR, Ferguson MAJ. 2005. *Trypanosoma brucei* glycoproteins contain novel giant poly-N-acetyllactosamine carbohydrate chains. *J Biol Chem* **280**: 865–71.

Baker N, Glover L, Munday JC, Aguinaga Andrés D, Barrett MP, de Koning HP, Horn D. 2012. Aquaglyceroporin 2 controls susceptibility to melarsoprol and pentamidine in African trypanosomes. *Proc Natl Acad Sci* **109**: 10996–1001.

Bakker BM, Michels PAM, Opperdoes FR, Westerhoff H V. 1997. Glycolysis in bloodstream form *Trypanosoma brucei* can be understood in terms of the kinetics of the glycolytic enzymes. *J Biol Chem* **272**: 3207–15.

Bananis E. 2004. Microtubule-dependent movement of late endocytic vesicles *in vitro*: requirements for dynein and kinesin. *Mol Biol Cell* **15**: 3688–97.

Baron DM, Ralston KS, Kabututu ZP, Hill KL. 2007. Functional genomics in *Trypanosoma brucei* identifies evolutionarily conserved components of motile flagella. *J Cell Sci* **120**: 478–91.

Bart JM, Cordon-Obras C, Vidal I, Reed J, Perez-Pastrana E, Cuevas L, Field MC, Carrington M, Navarro M. 2015. Localization of serum resistance-associated protein in *Trypanosoma brucei rhodesiense* and transgenic *Trypanosoma brucei brucei. Cell Microbiol* **17**: 1523–35.

Bartholomeu DC, de Paiva RMC, Mendes TAO, DaRocha WD, Teixeira SMR. 2014. Unveiling the intracellular survival gene kit of trypanosomatid parasites. *PLoS Pathog* **10**: e1004399.

Bashkirov P V., Akimov SA, Evseev AI, Schmid SL, Zimmerberg J, Frolov VA. 2008. GTPase cycle of dynamin is coupled to membrane squeeze and release, leading to spontaneous fission. *Cell* **135**: 1276–86.

Bassarak B, Uzcátegui NL, Schönfeld C, Duszenko M. 2011. Functional characterization of three aquaglyceroporins from Trypanosoma brucei in osmoregulation and glycerol transport. *Cell Physiol Biochem* **27**: 411–20.

Bendtsen JD, Nielsen H, Heijne G Von, Brunak S. 2004. Improved prediction of signal peptides: SignalP 3.0. *J Mol Biol* **340**: 783–95.

Beneke T, Madden R, Makin L, Valli J, Sunter J, Gluenz E. 2017. A CRISPR Cas9 high-throughput genome editing toolkit for kinetoplastids. *R Soc Open Sci* **4**: 170095.

Benz C, Stribrna E, Hashimi H, Lukes J. 2017. Dynamin-like proteins in *Trypanosoma brucei*: A division of labour between two paralogs? *PLoS One* **12**: e0177200

Berberof M, Vanhamme L, Tebabi P, Pays A, Jefferies D, Welburn S, Pays E. 1995. The 3'-terminal region of the mRNAs for VSG and procyclin can confer stage specificity to gene expression in *Trypanosoma brucei*. *EMBO J* **14**: 2925–34.

Bernstein E, Caudy AA, Hammond SM, Hannon GJ. 2001. Role for a bidentate ribonuclease in the initiation step of RNA interference. *Nature* **409**: 363–6.

Berriman M, Ghedin E, Hertz-Fowler C, Blandin G, Renauld H, Bartholomeu DC, Lennard NJ, Caler E, Hamlin NE, Haas B, et al. 2005. The genome of the African trypanosome *Trypanosoma brucei*. *Science* **309**: 416–22.

Bigay J, Antonny B. 2012. Curvature, lipid packing, and electrostatics of membrane organelles: defining cellular territories in determining specificity. *Dev Cell* **23**: 886–95.

Blisnick T, Buisson J, Absalon S, Marie A, Cayet N, Bastin P. 2014. The intraflagellar transport dynein complex of trypanosomes is made of a heterodimer of dynein heavy chains and of light and intermediate chains of distinct functions. *Mol Biol Cell* **25**: 2620–33.

Bonhivers M, Nowacki S, Landrein N, Robinson DR. 2008. Biogenesis of the trypanosome endo-exocytotic organelle is cytoskeleton mediated. *PLoS Biol* **6**: e105

Bonifacino JS, Glick BS. 2004. The mechanisms of vesicle budding and fusion. *Cell* **116**: 153–66.

Bridges AA, Jentzsch MS, Oakes PW, Occhipinti P, Gladfelter AS. 2016. Micron-scale plasma membrane curvature is recognized by the septin cytoskeleton. *J Cell Biol* **213**: 23–32.

Brindley DN, Pilquil C, Sariahmetoglu M, Reue K. 2009. Phosphatidate degradation: Phosphatidate phosphatases (lipins) and lipid phosphate phosphatases. *Biochim Biophys Acta* **1791**: 956–61.

Brock SC, Heck JM, Mcgraw PA, Crowe JE. 2005. The transmembrane domain of the respiratory syncytial virus F protein is an orientation-independent apical plasma membrane sorting sequence. *J Virol* **79**: 12528–35.

Bryde S, Hennrich H, Verhulst PM, Devaux PF, Lenoir G, Holthuis JCM. 2010. CDC50 proteins are critical components of the human class-1 P 4-ATPase transport machinery. *J Biol Chem* **285**: 40562–72.

Busija AR, Patel HH, Insel PA. 2017. Caveolins and cavins in the trafficking, maturation, and degradation of caveolae: implications for cell physiology. *Am J Physiol Cell Physiol* **312**: 459–77.

Capewell P, Cren-Travaillé C, Marchesi F, Johnston P, Clucas C, Benson RA, Gorman TA, Calvo-Alvarez E, Crouzols A, Jouvion G, et al. 2016. The skin is a significant but overlooked anatomical reservoir for vector-borne African trypanosomes. *Elife* **5**: e17716.

Carter AP. 2013. Crystal clear insights into how the dynein motor moves. *J Cell Sci* **126**: 705-13.

Castorino JJ, Deborde S, Deora A, Schreiner R, Gallagher-Colombo SM, Rodriguez-Boulan E, Philp NJ. 2011. Basolateral sorting signals regulating tissue-specific polarity of heteromeric monocarboxylate transporters in epithelia. *Traffic* **12**: 483–98.

Caudron F, Barral Y. 2009. Septins and the lateral compartmentalization of eukaryotic membranes. *Dev Cell* **16**: 493–506.

Chanez A-L, Hehl AB, Engstler M, Schneider A. 2006. Ablation of the single dynamin of *Trypanosoma brucei* blocks mitochondrial fission and endocytosis and leads to a precise cytokinesis arrest. *J Cell Sci* **119**: 2968–74.

Cheng J, Grassart A, Drubin DG. 2012. Myosin 1E coordinates actin assembly and cargo trafficking during clathrin-mediated endocytosis. *Mol Biol Cell* **23**: 2891–904.

Cheng Y, Boll W, Kirchhausen T, Harrison SC, Walz T. 2007. Cryo-electron tomography of clathrin-coated vesicles: structural implications for coat assembly. *J Mol Biol* **365**: 892–99.

Chia PZC, Gleeson PA. 2014. Membrane tethering. *F1000Prime Rep* **6**: 74

Chuang GY, Boyington JC, Gordon Joyce M, Zhu J, Nabel GJ, Kwong PD, Georgiev I. 2012. Computational prediction of N-linked glycosylation incorporating structural properties and patterns. *Bioinformatics* **28**: 2249–55.

Chung WL, Carrington M, Field MC. 2004. Cytoplasmic targeting signals in transmembrane invariant surface glycoproteins of trypanosomes. *J Biol Chem* **279**: 54887–95.

Cocucci E, Aguet F, Boulant S, Kirchhausen T. 2012. The first five seconds in the life of a clathrin-coated pit. *Cell* **150**: 495–507.

Cornejo E, Abreu N, Komeili A. 2014. Compartmentalization and organelle formation in bacteria. *Curr Opin Cell Biol* **26**: 132–8.

Cowman AF, Saint RB, Coppel RL, Brown G V, Anders RF, Kemp DJ. 1985. Conserved sequences flank variable tandem repeats in two s-antigen genes of *Plasmodium falciparum*. **40**: 775–83.

Creek DJ, Nijagal B, Kim DH, Rojas F, Matthews KR, Barrett MP. 2013. Metabolomics guides rational development of a simplified cell culture medium for drug screening against *Trypanosoma brucei*. *Antimicrob Agents Chemother* **57**: 2768–79.

Cross GA. 1975. Identification, purification and properties of clone-specific glycoprotein antigens constituting the surface coat of *Trypanosoma brucei*. *Parasitology* **71**: 393–417.

Cross GAM, Kim HS, Wickstead B. 2014. Capturing the variant surface glycoprotein repertoire (the VSGnome) of *Trypanosoma brucei* Lister 427. *Mol Biochem Parasitol* **195**: 59–73.

Cross RA., McAinsh A. 2014. Prime movers: the mechanochemistry of mitotic kinesins. *Nat Rev Mol Cell Biol* **15**: 257–71.

D'Archivio S, Wickstead B. 2017. Trypanosome outer kinetochore proteins suggest conservation of chromosome segregation machinery across eukaryotes. *J Cell Biol* **216**: 379–91.

Daniels J, Gull K, Wickstead B. 2010. Cell biology of the trypanosome genome. *MMBR* **74**: 552–69.

Dawson SC, Sagolla MS, Mancuso JJ, Woessner DJ, House SA, Fritz-Laylin L, Cande WZ. 2007. Kinesin-13 regulates flagellar, interphase, and mitotic microtubule dynamics in *Giardia intestinalis*. *Eukaryot Cell* **6**: 2354–64.

de Morais CGV, Castro Lima AK, Terra R, dos Santos RF, Da-Silva SAG, Dutra PML. 2015. The dialogue of the host-parasite relationship: *Leishmania* spp. and *Trypanosoma cruzi* infection. *Biomed Res Int* **2015**: 1–19.

Dean S, Marchetti R, Kirk K, Matthews K. 2009. A surface transporter family conveys the trypanosome differentiation signal. *Nature* **459**: 213–17.

De Pablos LM, Osuna A. 2012. Multigene families in *Trypanosoma cruzi* and their role in infectivity. *Infect Immun* **80**: 2258–64.

De Souza W, Martfnez-Palomof A, Gonzalez-Roblesf A. 1978. The cell surface of *Trypanosoma cruzi*: cytochemistry and freeze-fracture. *J Cell Sci* **33**: 285–99.

Demmel L, Schmidt K, Lucast L, Havlicek K, Zankel A, Koestler T, Reithofer V, de Camilli P, Warren G. 2014. The endocytic activity of the flagellar pocket in *Trypanosoma brucei* is regulated by an adjacent phosphatidylinositol phosphate kinase. *J Cell Sci* **127**: 2351–64.

Doudna JA, Charpentier E. 2014. The new frontier of genome engineering with CRISPR-Cas9. *Science* **346**: 1258096

Dragsten PR, Blumenthal R, Handler JS. 1981. Membrane asymmetry in epithelia: is the tight junction a barrier to diffusion in the plasma membrane? *Nature* **294**: 718–22.

Dunbar LA, Aronson P, Caplan MJ. 2000. A transmembrane segment determines the steady-state localization of ion-transporting adenosine triphosphatase. *J Cell Biol* **148**: 769–78.

Edeling MA, Mishra SK, Keyel PA, Steinhauser AL, Collins BM, Roth R, Heuser JE, Owen DJ, Traub LM. 2006. Molecular switches involving the AP-2 β2 appendage regulate endocytic cargo selection and clathrin coat assembly. *Dev Cell* **10**: 329–42.

Eisenthal R, Panes A. 1985. The aerobic/anaerobic transition of glucose metabolism in Trypanosoma brucei. *FEBS Lett* **181**: 23–7.

Elkin SR, Lakoduk AM, Schmid SL. 2016. Endocytic pathways and endosomal trafficking: a primer. *Wien Med Wochensch* **166**: 196–204.

Emmer BT, Daniels MD, Taylor JM, Epting CL, Engman DM. 2010. Calflagin inhibition prolongs host survival and suppresses parasitemia in *Trypanosoma brucei* infection. *Eukaryot Cell* **9**: 934–42.

Engstler M, Boshart M. 2004. Cold shock and regulation of surface protein trafficking convey sensitization to inducers of stage differentiation in *Trypanosoma brucei*. *Genes Dev* **18**: 2798–811.

Engstler M, Pfohl T, Herminghaus S, Boshart M, Wiegertjes G, Heddergott N, Overath P. 2007. Hydrodynamic flow-mediated protein sorting on the cell surface of trypanosomes. *Cell* **131**: 505–15.

Engstler M, Thilo L, Weise F, Grünfelder CG, Schwarz H, Boshart M, Overath P. 2004. Kinetics of endocytosis and recycling of the GPI-anchored variant surface glycoprotein in *Trypanosoma brucei*. *J Cell Sci* **117**: 1105–15.

Engstler M, Weise F, Bopp K, Grünfelder CG, Günzel M, Heddergott N, Overath P. 2005. The membrane-bound histidine acid phosphatase TbMBAP1 is essential for endocytosis and membrane recycling in *Trypanosoma brucei*. *J Cell Sci* **118**: 2105–18.

Esson HJ, Morriswood B, Yavuz S, Vidilaseris K, Dong G, Warren G. 2012. Morphology of the trypanosome bilobe, a novel cytoskeletal structure. *Eukaryot Cell* **11**: 761–72.

Ferguson S, Raimondi A, Paradise S, Shen H, Mesaki K, Ferguson A, Destaing O, Ko G, Takasaki J, Cremona O, et al. 2009. Coordinated actions of actin and BAR proteins upstream of dynamin at endocytic clathrin-coated pits. *Dev Cell* **17**: 811–22.

Field MC, Carrington M. 2009. The trypanosome flagellar pocket. *Nat Rev Microbiol* **7**: 775–86.

Field MC, Natesan SK, Gabernet-Castello C, Koumandou VL. 2007. Intracellular trafficking in the trypanosomatids. *Traffic* **8**: 629–39.

Fire A, Xu S, Montgomery MK, Kostas SA, Driver SE, Mello CC. 1998. Potent and specific genetic interference by double-stranded RNA in *Caenorhabditis elegans*. *Nature* **391**: 806–11.

Flesch FM, Gadella BM. 2000. Dynamics of the mammalian sperm plasma membrane in the process of fertilization. *Biochim Biophys Acta* **1469**: 197–235.

Florimond C, Sahin A, Vidilaseris K, Dong G, Landrein N, Dacheux D, Albisetti A, Byard EH, Bonhivers M, Robinson DR. 2015. BILBO1 is a scaffold protein of the flagellar pocket collar in the pathogen *Trypanosoma brucei. PLoS Pathog* **11**: e1004654.

Ford MGJ. 2001. Simultaneous binding of PtdIns(4,5)P2 and clathrin by ap180 in the nucleation of clathrin lattices on membranes. *Science* **291**: 1051–5.

Ford MGJ, Mills IG, Peter BJ, Vallis Y, Praefcke GJK, Evans PR, McMahon HT. 2002. Curvature of clathrin-coated pits driven by epsin. *Nature* **419**: 361–6.

Fujiwara T, Ritchie K, Murakoshi H, Jacobson K, Kusumi A. 2002. Phospholipids undergo hop diffusion in compartmentalized cell membrane. *J Cell Biol* **157**: 1071–1081.

Furuse M. 2010. Molecular basis of the core structure of tight junctions. *Cold Spring Harb Perspect Biol* **2**: 14.

Furuse M, Fujita K, Hiiragi T, Fujimoto K, Tsukita S. 1998. Claudin-1 and-Novel integral membrane proteins localizing at tight junctions with no sequence similarity to occluding. *J Cell Biol* **141**: 1539–50.

Furuse M, Hirase T, Itoh M, Nagafuchi A, Yonemura S, Tsukita S, Tsukita S. 1993. Occludin: A novel integral membrane protein localizing at tight junctions. *J Cell Biol* **123**: 1777–88.

Gabernet-Castello C, Dacks JB, Field MC. 2009. The single ENTH-domain protein of trypanosomes; endocytic functions and evolutionary relationship with epsin. *Traffic* **10**: 894–911.

Gadelha C, Holden JM, Allison HC, Field MC. 2011. Specializations in a successful parasite: what makes the bloodstream-form African trypanosome so deadly? *Mol Biochem Parasitol* **179**: 51–8.

Gadelha C, Rothery S, Morphew M, McIntosh JR, Severs NJ, Gull K. 2009. Membrane domains and flagellar pocket boundaries are influenced by the cytoskeleton in African trypanosomes. *Proc Natl Acad Sci U S A* **106**: 17425–30.

Gadelha C, Zhang W, Chamberlain JW, Chait BT, Wickstead B, Field MC. 2015. Architecture of a host–parasite interface: complex targeting mechanisms revealed through proteomics. *Mol Cell Proteomics* **14**: 1911–26.

García-Sánchez S, Sánchez-Cañete MP, Gamarro F, Castanys S. 2014. Functional role of evolutionarily highly conserved residues, N-glycosylation level and domains of the Leishmania miltefosine transporter-Cdc50 subunit. *Biochem J* **459**: 83–94.

Gerrits H, Mussmann R, Bitter W, Kieft R, Borst P. 2002. The physiological significance of transferrin receptor variations in *Trypanosoma brucei*. *Mol Biochem Parasitol* **119**: 237–47.

Gheiratmand L, Brasseur A, Zhou Q, He CY. 2013. Biochemical characterization of the bi-lobe reveals a continuous structural network linking the bi-lobe to other single-copied organelles in *Trypanosoma brucei*. *J Biol Chem* **288**: 3489–99.

Gimenez AM, Santander VS, Villasuso AL, Pasquaré SJ, Giusto NM, MacHado EE. 2011. Regulation of phosphatidic acid levels in *Trypanosoma cruzi*. *Lipids* **46**: 969–79.

Gladfelter AS, Pringle JR, Lew DJ. 2001. The septin cortex at the yeast mother-bud neck. *Curr Opin Microbiol* **4**: 681–89.

Goldston AM, Sharma AI, Paul KS, Engman DM. 2014 Acylation in trypanosomatids: an essential process and potential drug target. *Trends Parasitol* **30**: 350-360.

Graham S V, Barry JD. 1995. Transcriptional regulation of metacyclic variant surface glycoprotein gene expression during the life cycle of *Trypanosoma brucei*. *Mol Cell Biol* **15**: 5945–56.

Grandgenett PM, Otsu K, Wilson HR, Wilson ME, Donelson JE. 2007. A function for a specific zinc metalloprotease of African trypanosomes. *PLoS Pathog* **3**: 1432–45.

Granger E, McNee G, Allan V, Woodman P. 2014. The role of the cytoskeleton and molecular motors in endosomal dynamics. *Semin Cell Dev Biol* 1–10.

Green HP, Del Pilar Molina Portela M, St. Jean EN, Lugli EB, Raper J. 2003. Evidence for a *Trypanosoma brucei* lipoprotein scavenger receptor. *J Biol Chem* **278**: 422–7.

Haanstra JR, van Tuijl A, Kessler P, Reijnders W, Michels PAM, Westerhoff H V, Parsons M, Bakker BM. 2008. Compartmentation prevents a lethal turbo-explosion of glycolysis in trypanosomes. *Proc Natl Acad Sci U S A* **105**: 17718–23.

Hammond SM, Bernstein E, Beach D, Hannon GJ. 2000. An RNA-directed nuclease mediates post-transcriptional gene silencing in *Drosophila* cells. *Nature* **404**: 293–6.

Hammond SM, Boettcher S, Caudy AA, Kobayashi R, Hannon GJ. 2001. Argonaute2, a link between genetic and biochemical analyses of RNAi. *Science* **293**: 1146–50.

Hansen CG, Nichols BJ. 2009. Molecular mechanisms of clathrin-independent endocytosis. *J Cell Sci* **122**: 1713–21.

Harris KP, Littleton JT. 2011. Vesicle trafficking: A Rab family profile. *Curr Biol* **21**: 841–3.

Hartsock A, Nelson WJ. 2008. Adherens and tight junctions: Structure, function and connections to the actin cytoskeleton. *Biochim Biophys Acta* **1778**: 660–9.

Henley GL, Lee CM, Takeuchi A. 1978. Electron microscopy observations on *Trypanosoma brucei*: Freeze-cleaving and thin-sectioning study of the apical part of the flagellar pocket. **187**: 181–7.

Hertz-Fowler C1, Ersfeld K, Gull K. 2001. CAP5.5, a life-cycle-regulated, cytoskeleton-associated protein is a member of a novel family of calpain-related proteins in *Trypanosoma brucei*. *Mol Biochem Parasitol* **116**: 25-34.

Hertz-Fowler C, Figueiredo L, Quail M, Becker M, Jackson A, Bason N, Brooks K, Churcher C, Fahkro S, Goodhead I, et al. 2008. Telomeric expression sites are highly conserved in *Trypanosoma brucei*. *PLoS One* **3**: e3527.

Higgins MK, Lane-Serff H, MacGregor P, Carrington M. 2017. A receptor's tale: an eon in the life of a trypanosome receptor. *PLoS Pathog* **13**: e1006055.

Higgins MK, Tkachenko O, Brown A, Reed J, Raper J, Carrington M. 2013. Structure of the trypanosome haptoglobin-hemoglobin receptor and implications for nutrient uptake and innate immunity. *Proc Natl Acad Sci U S A* **110**: 1905–10.

Hinshaw JE, Schmid SL. 1995. Dynamin self-assembles into rings suggesting a mechanism for coated vesicle budding. *Nature* **374**: 190–2.

Hirokawa N, Noda Y, Tanaka Y, Niwa S. 2009. Kinesin superfamily motor proteins and intracellular transport. *Nat Rev Mol Cell Biol* **10**: 682–96.

Hirumi H, Hirumi K. 1989. Continuous cultivation of *Trypanosoma brucei* blood stream forms in a medium containing a low concentration of serum protein without feeder cell layers. *J Parasitol* **75**: 985–9.

Höning S, Ricotta D, Krauss M, Späte K, Spolaore B, Motley A, Robinson M, Robinson C, Haucke V, Owen DJ. 2005. Phosphatidylinositol-(4,5)-bisphosphate regulates sorting signal recognition by the clathrin-associated adaptor complex AP2. *Mol Cell* **18**: 519–31.

Horn D. 2014. Antigenic variation in African trypanosomes. *Mol Biochem Parasitol* **195**: 123–9.

Hovel-Miner G, Mugnier MR, Goldwater B, Cross GAM, Papavasiliou FN. 2016. A conserved DNA repeat promotes selection of a diverse repertoire of *Trypanosoma brucei* surface antigens from the genomic archive. *PLoS Genet* **12**: e1005994.

Hu H, Hu L, Yu Z, Chasse AE, Chu F, Li Z. 2012a. An orphan kinesin in trypanosomes cooperates with a kinetoplastid-specific kinesin to maintain cell morphology by regulating subpellicular microtubules. *J Cell Sci* **125**: 4126–36.

Hu L, Hu H, Li Z. 2012b. A kinetoplastid-specific kinesin is required for cytokinesis and for maintenance of cell morphology in *Trypanosoma brucei*. *Mol Microbiol* **83**: 565–78.

Hu Q, Milenkovic L, Jin H, Scott MP, Nachury M V, Spiliotis ET, Nelson WJ. 2010. A septin diffusion barrier at the base of the primary cilium maintains ciliary membrane protein distribution. *Science* **329**: 436–9.

Hung CH, Qiao X, Lee PT, Lee MGS. 2004. Clathrin-dependent targeting of receptors to the flagellar pocket of procyclic-form *Trypanosoma brucei*. *Eukaryot Cell* **3**: 1004–14.

Ihara M, Kinoshita A, Yamada S, Tanaka H, Tanigaki A, Kitano A, Goto M, Okubo K, Nishiyama H, Ogawa O, et al. 2005. Cortical organization by the septin cytoskeleton is essential for structural and mechanical integrity of mammalian spermatozoa. *Dev Cell* **8**: 343–352.

Izquierdo L, Mehlert A, Ferguson MAJ. 2012. The lipid-linked oligosaccharide donor specificities of *Trypanosoma brucei* oligosaccharyltransferases. *Glycobiology* **22**: 696–703.

Izquierdo L, Schulz BL, Rodrigues JA, Güther MLS, Procter JB, Barton GJ, Aebi M, Ferguson MAJ. 2009. Distinct donor and acceptor specificities of *Trypanosoma brucei* oligosaccharyltransferases. *EMBO J* **28**: 2650–61.

Jackson AP, Allison HC, Barry JD, Field MC, Hertz-Fowler C, Berriman M. 2013. A cell-surface phylome for African trypanosomes. *PLoS Negl Trop Dis* **7**: e2121.

Jarsch IK, Daste F, Gallop JL. 2016. Membrane curvature in cell biology: An integration of molecular mechanisms. *J Cell Biol* **214**: 375–87.

Jeacock L, Baker N, Wiedemar N, Mäser P, Horn D. 2017. Aquaglyceroporin-null trypanosomes display glycerol transport defects and respiratory-inhibitor sensitivity. *PLoS Pathog* **13**: e1006307.

Jones DC, Mehlert A, Güther MLS, Ferguson MAJ. 2005. Deletion of the glucosidase II gene in *Trypanosoma brucei* reveals novel N-glycosylation mechanisms in the biosynthesis of variant surface glycoprotein. *J Biol Chem* **280**: 35929–42.

Kassem A, Pays E, Vanhamme L. 2014. Transcription is initiated on silent variant surface glycoprotein expression sites despite monoallelic expression in *Trypanosoma brucei*. *Proc Natl Acad Sci U S A* **111**: 8943–8948.

Kelleher DJ, Gilmore R. 2006. An evolving view of the eukaryotic oligosaccharyltransferase. *Glycobiology* **16**: 47–62.

Kelly S, Reed J, Kramer S, Ellis L, Webb H, Sunter J, Salje J, Marinsek N, Gull K, Wickstead B, et al. 2007. Functional genomics in *Trypanosoma brucei:* A collection of vectors for the expression of tagged proteins from endogenous and ectopic gene loci. *Mol Biochem Parasitol* **154**: 103–109.

Kieft R, Capewell P, Turner CMR, Veitch NJ, MacLeod A, Hajduk S. 2010. Mechanism of *Trypanosoma brucei gambiense* (group 1) resistance to human trypanosome lytic factor. *Proc Natl Acad Sci U S A* **107**: 16137–41.

Kim HS, Li Z, Boothroyd C, Cross GAM. 2013. Strategies to construct null and conditional null *Trypanosoma brucei* mutants using Cre-recombinase and loxP. *Mol Biochem Parasitol* **191**: 16–19.

Kim S, Dynlacht BD. 2013. Assembling a primary cilium. *Curr Opin Cell Biol* **25**: 506–11.

Kolev NG, Tschudi C, Ullu E. 2011. RNA interference in protozoan parasites: achievements and challenges. *Eukaryot Cell* **10**: 1156–63.

Krogh A, Larsson B, von Heijne G, Sonnhammer EL. 2001. Predicting transmembrane protein topology with a hidden markov model: application to complete genomes. *J Mol Biol* **305**: 567–80.

Kuo S-M, Wang L-Y, Yu S, Campbell CE, Valiyaparambil SA, Rance M, Blumenthal KM. 2013. The N-terminal basolateral targeting signal unlikely acts alone in the differential trafficking of membrane transporters in MDCK cells. *Biochemistry* **52**: 5103–16.

Kusumi A, Shirai YM, Koyama-Honda I, Suzuki KGN, Fujiwara TK. 2010. Hierarchical organization of the plasma membrane: Investigations by single-molecule tracking vs. fluorescence correlation spectroscopy. *FEBS Lett* **584**: 1814–1823.

Lacomble S, Vaughan S, Gadelha C, Morphew MK, Shaw MK, McIntosh JR, Gull K. 2010. Basal body movements orchestrate membrane organelle division and cell morphogenesis in *Trypanosoma brucei*. *J Cell Sci* **123**: 2884–91.

Lacomble S, Vaughan S, Gadelha C, Morphew MK, Shaw MK, McIntosh JR, Gull K. 2009. Three-dimensional cellular architecture of the flagellar pocket and associated cytoskeleton in trypanosomes revealed by electron microscope tomography. *J Cell Sci* **122**: 1081–90.

Lane-Serff H, Macgregor P, Peacock L, Macleod OJS, Kay C, Gibson W, Higgins MK, Carrington M. 2016. Evolutionary diversification of the trypanosome haptoglobin-haemoglobin receptor from an ancestral haemoglobin receptor. *Elife* **5**: 1–20.

Langousis G, Hill KL. 2014. Motility and more: the flagellum of *Trypanosoma brucei*. *Nat Rev Microbiol* **12**: 505–18.

Lee MG, Russell DG, D'Alesandro PA, Van Der Ploeg LHT. 1994. Identification of membrane-associated proteins in *Trypanosoma brucei* encoding an internal, EARLRAEE amino acid repeat. *J Biol Chem* **269**: 8408–15.

Lemmon MA. 2008. Membrane recognition by phospholipid-binding domains. *Nat Rev Mol Cell Biol* **9**: 99–111.

Letort G, Ennomani H, Gressin L, Théry M, Blanchoin L. 2015. Dynamic reorganization of the actin cytoskeleton. *F1000Research* **4**: 1–11.

Li X, Kumar Y, Zempel H, Mandelkow E-M, Biernat J, Mandelkow E. 2011. Novel diffusion barrier for axonal retention of Tau in neurons and its failure in neurodegeneration. *EMBO J* **30**: 4825–37.

Liu J, Carmell MA, Rivas F V, Marsden CG, Thomson JM, Song J-J, Hammond SM, Joshua-Tor L, Hannon GJ. 2004. Argonaute2 Is the catalytic engine of mammalian RNAi. *Science* **305**:1437-41

Longtine MS, Bi E. 2003. Regulation of septin organization and function in yeast. *Trends Cell Biol* **13**: 403–409.

Macedo JP, Schmidt RS, Mäser P, Rentsch D, Vial HJ, Sigel E, Bütikofer P. 2013. Characterization of choline uptake in *Trypanosoma brucei* procyclic and bloodstream forms. *Mol Biochem Parasitol* **190**: 16–22.

MacGregor P, Szöőr B, Savill NJ, Matthews KR. 2012. Trypanosomal immune evasion, chronicity and transmission: an elegant balancing act. *Nat Rev Microbiol* **10**: 431-8.

Magalhaes MAO, Glogauer M. 2010. Pivotal Advance: Phospholipids determine net membrane surface charge resulting in differential localization of active Rac1 and Rac2. *J Leukoc Biol* **87**: 545–55.

Mallik R, Rai AK, Barak P, Rai A, Kunwar A. 2013. Teamwork in microtubule motors. *Trends Cell Biol* **23**: 575–82.

Manna PT, Gadelha C, Puttick AE, Field MC. 2015. ENTH and ANTH domain proteins participate in AP2-independent clathrin-mediated endocytosis. *J Cell Sci* **128**: 2130–42.

Manna PT, Kelly S, Field MC. 2013. Adaptin evolution in kinetoplastids and emergence of the variant surface glycoprotein coat in African trypanosomatids. *Mol Phylogenet Evol* **67**: 123–8.

Martin-Belmonte F, Mostov K. 2008. Regulation of cell polarity during epithelial morphogenesis. *Curr Opin Cell Biol* **20**: 227–34.

Mayor S, Pagano RE. 2007. Pathways of clathrin-independent endocytosis. *Nat Rev Mol Cell Biol* **8**: 603–12.

Mayor S, Parton RG, Donaldson JG. 2017. Clathrin-independent pathways of endocytosis. *Cold Spring Harb Perspect Biol* **6**: a016758

Mbang-Benet D-E, Sterkers Y, Crobu L, Sarrazin A, Bastien P, Pagès M. 2015. RNA interference screen reveals a high proportion of mitochondrial proteins essential for correct cell cycle progress in *Trypanosoma brucei. BMC Genomics* **16**: 297

McCulloch R, Rudenko G, Borst P. 1997. Gene conversions mediating antigenic variation in *Trypanosoma brucei* can occur in variant surface glycoprotein expression sites lacking 70-base-pair repeat sequences. *Mol Cell Biol* **17**: 833–43.

McMahon HT, Boucrot E. 2011. Molecular mechanism and physiological functions of clathrin-mediated endocytosis. *Nat Rev Mol Cell Biol* **12**: 517–33.

Mehlert A, Wormald MR, Ferguson MAJ. 2012. Modeling of the N-glycosylated transferrin receptor suggests how transferrin binding can occur within the surface coat of *Trypanosoma brucei*. *PLoS Pathog* **8**: e1002618.

Meluh PB, Rose MD. 1990. KAR3, a kinesin-related gene required for yeast nuclear fusion *Cell* **60**: 1029–41.

Messitt TJ, Gagnon JA, Kreiling JA, Pratt CA, Yoon YJ, Mowry KL. 2008. Multiple kinesin motors coordinate cytoplasmic RNA transport on a subpopulation of microtubules in *Xenopus* oocytes. *Dev Cell* **15**: 426–36.

Michels PA, Van der Ploeg LH, Liu AY, Borst P. 1984. The inactivation and reactivation of an expression-linked gene copy for a variant surface glycoprotein in *Trypanosoma brucei*. *EMBO J* **3**: 1345–51.

Milder R, Deane MP. 1969. The cytostome of *Trypanosoma cruzi* and *T. conorhini. J Protozool* **16**: 730–7.

Molla-Herman A, Ghossoub R, Blisnick T, Meunier A, Serres C, Silbermann F, Emmerson C, Romeo K, Bourdoncle P, Schmitt A, et al. 2010. The ciliary pocket: an endocytic membrane domain at the base of primary and motile cilia. *J Cell Sci* **123**: 1785–95.

Montagna GN, Donelson JE, Frasch AC. 2006. Procyclic *Trypanosoma brucei* expresses separate sialidase and trans-sialidase enzymes on its surface membrane. *J Biol Chem* **281**: 33949–58.

Mony BM, MacGregor P, Ivens A, Rojas F, Cowton A, Young J, Horn D, Matthews K. 2014. Genome-wide dissection of the quorum sensing signalling pathway in *Trypanosoma brucei*. *Nature* **505**: 681–5.

Morgan GW, Allen CL, Jeffries TR, Hollinshead M, Field MC. 2001. Developmental and morphological regulation of clathrin-mediated endocytosis in *Trypanosoma brucei*. *J Cell Sci* **114**: 2605–15.

Morgan GW, Goulding D, Field MC. 2004. The single dynamin-like protein of *Trypanosoma brucei* regulates mitochondrial division and is not required for endocytosis. *J Biol Chem* **279**: 10692–701.

Morrison LJ, Marcello L, McCulloch R. 2009. Antigenic variation in the African trypanosome: molecular mechanisms and phenotypic complexity. *Cell Microbiol* **11**: 1724–34.

Morriswood B. 2015. Form, Fabric, and Function of a Flagellum-Associated Cytoskeletal Structure. *Cells* **4**: 726–47.

Morriswood B, Havlicek K, Demmel L, Yavuz S, Sealey-Cardona M, Vidilaseris K, Anrather D, Kostan J, Djinović-Carugo K, Roux KJ, et al. 2013. Novel bilobe components in *Trypanosoma brucei* identified using proximity-dependent biotinylation. *Eukaryot Cell* **12**: 356–67.

Morriswood B, Schmidt K. 2015. A MORN repeat protein facilitates protein entry into the flagellar pocket of *Trypanosoma brucei. Eukaryot Cell* **14**: 1081–93.

Morita YS, Acosta-Serrano A, Buxbaum LU, Englund PT. 2000. Glycosyl phosphatidylinositol myristoylation in African trypanosomes. New intermediates in the pathway for fatty acid remodeling. *J Biol Chem* **275**: 14147-54.

Mowatt MR, Wisdom GS, Clayton CE. 1989. Variation of tandem repeats in the developmentally regulated procyclic acidic repetitive proteins of *Trypanosoma brucei. Mol Cell Biol* **9**: 1332–5.

Mugnier MR, Cross GA, Papavasiliou FN. 2015. The *in vivo* dynamics of antigenic variation in *Trypanosoma brucei*. *Science* **347**: 1470–3.

Mussmann R, Engstler M, Gerrits H, Kieft R, Toaldo CB, Onderwater J, Koerten H, van Luenen HG, Borst P. 2004. Factors affecting the level and localization of the transferrin receptor in *Trypanosoma brucei*. *J Biol Chem* **279**: 40690–8.

Mussmann R, Janssen H, Calafat J, Engstler M, Ansorge I, Clayton C, Borst P. 2003. The expression level determines the surface distribution of the transferrin receptor in *Trypanosoma brucei*. *Mol Microbiol* **47**: 23–35.

Nakada C, Ritchie K, Oba Y, Nakamura M, Hotta Y, Iino R, Kasai RS, Yamaguchi K, Fujiwara T, Kusumi A. 2003. Accumulation of anchored proteins forms membrane diffusion barriers during neuronal polarization. *Nat Cell Biol* **5**: 626–32.

Nakata T, Hirokawa N. 1995. Point mutation of adenosine triphosphate-binding motif generated rigor kinesin that selectively blocks anterograde lysosome membrane transport. *J Cell Biol* **131**: 1039–53.

Navarro M, Gull K. 2001. A pol I transcriptional body associated with VSG mono-allelic expression in *Trypanosoma brucei*. *Nature* **414**: 759–63.

Neuwald AF, Aravind L, Spouge JL, Koonin EV. 1999. AAA+: A class of chaperone-like ATPases associated with the assembly, operation, and disassembly of protein complexes. *Genome Res* **9**: 27–43.

Nolan DP, Geuskens M, Pays E. 1999. N-linked glycans containing linear poly-N-acetyllactosamine as sorting signals in endocytosis in *Trypanosoma* brucei. *Curr Biol* **9**: 1169–72.

Numrich J, Ungermann C. 2014. Endocytic Rabs in membrane trafficking and signaling. *Biol Chem* **395**: 327–333.

Oberholzer M, Langousis G, Nguyen HT, Saada EA, Shimogawa MM, Jonsson ZO, Nguyen SM, Wohlschlegel JA, Hill KL. 2011. Independent analysis of the flagellum surface and matrix proteomes provides insight into flagellum signaling in mammalian-infectious *Trypanosoma brucei*. *Mol Cell Proteomics* **10**: M111.010538.

Oli M, Cotlin L, Shiflett A, Hajduk S. 2006. Serum resistance-associated protein blocks lysosomal targeting of trypanosome lytic factor in *Trypanosoma brucei*. *Eukaryot Cell* **5**: 132–9.

Overath P, Engstler M. 2004. Endocytosis, membrane recycling and sorting of GPI-anchored proteins: *Trypanosoma brucei* as a model system. *Mol Microbiol* **53**: 735–44.

Paindavoine P, Rolin S, van Assel S, Geuskens M, Jauniaux J-C, Dinsart C, Huet G, Pays E. 1992. A gene from the variant surface glycoprotein expression site encodes one of several transmembrane adenylate cyclases located on the flagellum of *Trypanosoma brucei*. *Mol Cell Biol* **12**: 1218–25.

Paladino S, Lebreton S, Tivodar S, Campana V, Tempre R, Zurzolo C. 2008. Different GPI-attachment signals affect the oligomerisation of GPI-anchored proteins and their apical sorting. *J Cell Sci* **121**: 4001–4007.

Palander O, El-Zeiry M, Trimble WS. 2017. Uncovering the roles of septins in cilia. *Front Cell Dev Biol* **5**: 36.

Parton RG, Collins BM. 2016. Unraveling the architecture of caveolae. *Proc Natl Acad Sci U S A* **113**: 14170–2.

Patel JT. Belsham HR, Rathbone AJ. Wickstead B, Gell C, and Friel CT. 2016. The family-specific α4-helix of the kinesin-13, MCAK, is critical to microtubule end recognition. *Open Biology* **6** 160223.

Pawson T. 2004. Specificity in signal transduction: from phosphotyrosine-sh2 domain interactions to complex cellular systems. *Cell* **116**: 191–203.

Pédelacq J-D, Cabantous S, Tran T, Terwilliger TC, Waldo GS. 2006. Engineering and characterization of a superfolder green fluorescent protein. *Nat Biotechnol* **24**: 79–88.

Peng D, Kurup SP, Yao PY, Minning TA, Tarleton R. 2015. CRISPR-Cas9-mediated single-gene and gene family disruption in *Trypanosoma cruzi*. **6**: e02097-14

Perdomo D, Bonhivers M, Robinson DR. 2016. The trypanosome flagellar pocket collar and its ring forming protein-TbBILBO1. *Cells* **5**: 9.

Pérez-Morga D, Vanhollebeke B, Paturiaux-Hanocq F, Nolan DP, Lins L, Homblé F, Vanhamme L, Tebabi P, Pays A, Poelvoorde P, et al. 2005. Apolipoprotein L-I promotes trypanosome lysis by forming pores in lysosomal membranes. *Science* **309**: 469–72.

Peterson LW, Artis D. 2014. Intestinal epithelial cells: regulators of barrier function and immune homeostasis. *Nat Rev Immunol* **14**: 141–53.

Petrescu AJ, Milac AL, Petrescu SM, Dwek RA, Wormald MR. 2004. Statistical analysis of the protein environment of N-glycosylation sites: Implications for occupancy, structure, and folding. *Glycobiology* **14**: 103–14.

Pierleoni A, Martelli P, Casadio R. 2008. PredGPI: a GPI-anchor predictor. *BMC Bioinformatics* **9**: 392.

Poon SK, Peacock L, Gibson W, Gull K, Kelly S. 2012. A modular and optimized single marker system for generating *Trypanosoma brucei* cell lines expressing T7 RNA polymerase and the tetracycline repressor. *Open Biol* **2**: 110037.

Portman N, Gull K. 2014. Identification of paralogous life-cycle stage specific cytoskeletal proteins in the parasite *Trypanosoma brucei*. *PLoS One* **9**. e106777.

Portman N, Gull K. 2012. Proteomics and the *Trypanosoma brucei* cytoskeleton: advances and opportunities. *Parasitology* **139**: 1168–77.

Porto-Carreiro I, Attias M, Miranda K, De Souza W, Cunha-e-Silva N. 2000. *Trypanosoma cruzi* epimastigote endocytic pathway: cargo enters the cytostome and passes through an early endosomal network before storage in reservosomes. *Eur J Cell Biol* **79**: 858–869.

Prevo B, Scholey JM, Peterman EJG. 2017. Intraflagellar transport: Mechanisms of motor action, cooperation, and cargo delivery. *FEBS J* **18**: 2905-31

Qiao X, Chuang BF, Jin Y, Muranjan M, Hung CH, Lee PT, Lee MG. 2006. Sorting signals required for trafficking of the cysteine-rich acidic repetitive transmembrane protein in *Trypanosoma brucei*. *Eukaryot Cell* **5**: 1229–42.

Ramey-Butler K, Ullu E, Kolev NG, Tschudi C. 2015. Synchronous expression of individual metacyclic variant surface glycoprotein genes in *Trypanosoma brucei*. *Mol Biochem Parasitol* **200**: 1–4.

Rasooly RS, New CM, Zhang P, Hawley RS, Baker BS. 1991. The lethal(1)TW-6cs mutation of *Drosophila* melanogaster is a dominant antimorphic allele of nod and is associated with a single base change in the putative ATP-binding domain. *Genetics* **129**: 409–22.

Reiter JF, Leroux MR. 2017. Genes and molecular pathways underpinning ciliopathies. *Nat Rev Mol Cell Biol* **18**: 533–547.

Robinson DR, Beattie P, Sherwin T, Gull K. 1991. Microtubules, tubulin, and microtubule-associated proteins of trypanosomes. *Cell*, **105**: 285–99.

Robinson DR, Sherwin T, Ploubidou A, Byard EH, Gull K. 1995. Microtubule polarity and dynamics in the control of organelle positioning, segregation, and cytokinesis in the trypanosome cell cycle. *J Cell Biol* **128**: 1163–72.

Roditi I, Schwarz H, Pearson TW, Beecroft RP, Liu MK, Richardson JP, Buhring H-J, Pleiss J, Bulow R, Williams RO, et al. 1989. Procyclin gene expression and loss of the variant surface glycoprotein during differentiation of *Trypanosoma brucei*. *J Cell Biol* **108**: 737–46.

Roignot J, Peng X, Mostov K, Stephenson RO, Rossant J, Tam PL. 2013. Polarity in Mammalian Epithelial Morphogenesis Polarity in Mammalian Epithelial Morphogenesis. 1–16.

Ross R, Thomson D. 1910. A case of sleeping sickness studied by precise enumerative methods: regular periodical increase of the parasites disclosed. *Proc R Soc B Biol Sci* **82**: 411–5.

Rossi A, Kontarakis Z, Gerri C, Nolte H, Hölper S, Krüger M, Stainier DYR. 2015. Genetic compensation induced by deleterious mutations but not gene knockdowns. *Nature* **577**: 230–3.

Saarikangas J, Barral Y. 2011. The emerging functions of septins in metazoans. *EMBO Rep* **12**: 1118–1126.

Salmon D, Geuskens M, Hanocq F, Hanocq-Quertier J, Nolan D, Ruben L, Pays E. 1994. A novel heterodimeric transferrin receptor encoded by a pair of VSG expression site-associated genes in *Trypanosoma brucei*. *Cell* **78**: 75–86.

Salmon D, Hanocq-Quertier J, Paturiaux-Hanocq F, Pays A, Tebabi P, Nolan DP, Michel A, Pays E. 1997. Characterization of the ligand-binding site of the transferrin receptor in *Trypanosoma brucei* demonstrates a structural relationship with the N-terminal domain of the variant surface glycoprotein. *EMBO J* **16**: 7272–8.

Salmon D, Vanwalleghem G, Morias Y, Denoeud J, Krumbholz C, Lhomme F, Bachmaier S, Kador M, Gossmann J, Dias FB, et al. 2012. Adenylate cyclases of *Trypanosoma brucei* inhibit the innate immune response of the host. *Science* **337**: 463–6.

Sanchez MA. 2013. Molecular identification and characterization of an essential pyruvate transporter from Trypanosoma brucei. *J Biol Chem* **288**: 14428–37.

Satoh D, Sato D, Tsuyama T, Saito M, Ohkura H, Rolls MM, Ishikawa F, Uemura T. 2008. Spatial control of branching within dendritic arbors by dynein-dependent transport of Rab5-endosomes. *Nat Cell Biol* **10**: 1164–71.

Schell D, Borowy NK, Overath P. 1991. Transferrin is a growth factor for the bloodstream form of *Trypanosoma brucei*. *Parasitol Res* **30**: 9–10.

Schlossman DM, Schmid SL, Braell WA, Rothman JE. 1984. An enzyme that removes clathrin coats: Purification of an uncoating ATPase. *J Cell Biol* **99**: 723–33.

Schumann Burkard G, Jutzi P, Roditi I. 2011. Genome-wide RNAi screens in bloodstream form trypanosomes identify drug transporters. *Mol Biochem Parasitol* **175**: 91–94.

Schwartz KJ, Peck RF, Tazeh NN, Bangs JD. 2005. GPI valence and the fate of secretory membrane proteins in African trypanosomes. *J Cell Sci* **118**: 5499–511.

Schwede A, Jones N, Engstler M, Carrington M. 2011. The VSG C-terminal domain is inaccessible to antibodies on live trypanosomes. *Mol Biochem Parasitol* **175**: 201–4.

Schwede A, Macleod OJS, MacGregor P, Carrington M. 2015. How does the vsg coat of bloodstream form african trypanosomes interact with external proteins? *PLoS Pathog* **11**: e1005259.

Serricchio M, Schmid AW, Steinmann ME, Sigel E, Rauch M, Julkowska D, Bonnefoy S, Fort C, Bastin P, Butikofer P. 2015. Flagellar membranes are rich in raft-forming phospholipids. *Biol Open* **4**: 1143–53.

Sharma AI, Olson CL, Engman DM. 2017. The lipid raft proteome of african trypanosomes contains many flagellar proteins. *Pathog,* **6**: 39.

Sharpe HJ, Stevens TJ, Munro S. 2010. A comprehensive comparison of transmembrane domains reveals organelle-specific properties. *Cell* **142**: 158–169.

Shimogawa MM, Saada EA, Vashisht AA, Barshop WD, Wohlschlegel JA, Hill KL. 2015. Cell surface proteomics provides insight into stage-specific remodeling of the host-parasite interface in *Trypanosoma brucei. MCP* **14**: 1977-88.

Silvester E, McWilliam KR, Matthews KR. 2017. The cytological events and molecular control of life cycle development of *Trypanosoma brucei* in the mammalian bloodstream. *Pathogens* **6**: 29.

Simpson L. 1986. Kinetoplast DNA in trypanosomid flagellates. *Int Rev Cytol* **99**: 119–79.

Sollelis L, Ghorbal M, Macpherson CR, Martins RM, Kuk N, Crobu L, Bastien P, Scherf A, Lopez-Rubio JJ, Sterkers Y. 2015. First efficient CRISPR-Cas9-mediated genome editing in *Leishmania* parasites. *Cell Microbiol* **17**: 1405–12.

Štáfková J, Mach J, Biran M, Verner Z, Bringaud F, Tachezy J. 2016. Mitochondrial pyruvate carrier in *Trypanosoma brucei*. *Mol Microbiol* **3**: 442-56.

Steverding D. 2000. The transferrin receptor of *Trypanosoma brucei*. *Parasitol Int* **48**: 191–8.

Steverding D, Sexton DW, Chrysochoidi N, Cao F. 2012. *Trypanosoma brucei* transferrin receptor can bind C-lobe and N-lobe fragments of transferrin. *Mol Biochem Parasitol* **185**: 99–105.

Steverding D, Stierhof YD, Fuchs H, Tauber R, Overath P. 1995. Transferrin-binding protein complex is the receptor for transferrin uptake in *Trypanosoma brucei*. *J Cell Biol* **131**: 1173–82.

Stoops EH, Caplan MJ. 2014. Trafficking to the apical and basolateral membranes in polarized epithelial cells. *J Am Soc Nephrol* **25**: 1375–86.

Straube A, Hause G, Fink G, Steinberg G. 2006. Conventional kinesin mediates microtubule-microtubule interactions *in vivo*. *Mol Biol Cell* **17**: 907–16.

Subota I, Julkowska D, Vincensini L, Reeg N, Buisson J, Blisnick T, Huet D, Perrot S, Santi-Rocca J, Duchateau M, et al. 2014. Proteomic analysis of intact flagella of procyclic *Trypanosoma brucei* cells identifies novel flagellar proteins with unique sub-localization and dynamics. *Mol Cell Proteomics* **13**: 1769–86.

Sullivan L, Wall SJ, Carrington M, Ferguson MAJ. 2013. Proteomic selection of immunodiagnostic antigens for Human African Trypanosomiasis and generation of a prototype lateral flow immunodiagnostic device. *PLoS Negl Trop Dis* **7**: e2087

Sunter J, Webb H, Carrington M. 2013. Determinants of GPI-PLC localisation to the flagellum and access to GPI-anchored substrates in trypanosomes. *PLoS Pathog* **9**.

Sunter JD, Benz C, Andre J, Whipple S, McKean PG, Gull K, Ginger ML, Lukeš J. 2015. Flagellum attachment zone protein modulation and regulation of cell shape in *Trypanosoma brucei* life cycle transitions. *J Cell Sci* 3117–30.

Sweitzer SM, Hinshaw JE. 1998. Dynamin undergoes a GTP-dependent conformational change causing vesiculation. *Cell* **93**: 1021–9.

Szempruch AJ, Sykes SE, Kieft R, Dennison L, Becker AC, Gartrell A, Martin WJ, Nakayasu ES, Almeida IC, Hajduk SL, et al. 2016. Extracellular vesicles from *Trypanosoma brucei* mediate virulence factor transfer and cause host anemia. *Cell* **164**: 246–57.

Takizawa P a, DeRisi JL, Wilhelm JE, Vale RD. 2000. Plasma membrane compartmentalization in yeast by messenger RNA transport and a septin diffusion barrier. *Science* **290**: 341–4.

Tang VW, Goodenough DA. 2003. Paracellular ion channel at the tight junction. *Biophys J* **84**: 1660–73.

Tiengwe C, Bush PJ, Bangs JD. 2017. Controlling transferrin receptor trafficking with GPI-valence in bloodstream stage African trypanosomes. *PLoS Pathog* **13**: e1006366.

Tiengwe C, Muratore KA, Bangs JD. 2016. Surface proteins, ERAD and antigenic variation in *Trypanosoma brucei*. *Cell Microbiol* **18**: 1673–88.

Trimble WS, Grinstein S. 2015. Barriers to the free diffusion of proteins and lipids in the plasma membrane. *J Cell Biol* **208**: 259–271.

Trindade S, Rijo-Ferreira F, Carvalho T, Pinto-Neves D, Guegan F, Aresta-Branco F, Bento F, Young SA, Pinto A, Van Den Abbeele J, et al. 2016. *Trypanosoma brucei* parasites occupy and functionally adapt to the adipose tissue in mice. *Cell Host Microbe* **19**: 837–848.

Turner CM. 1997. The rate of antigenic variation in fly-transmitted and syringe-passaged infections of *Trypanosoma brucei*. *FEMS Microbiol Lett* **153**: 227–31.

Tyler KM, Fridberg A, Toriello KM, Olson CL, Cieslak JA, Hazlett TL, Engman DM. 2009. Flagellar membrane localization via association with lipid rafts. *J Cell Sci* **122**: 859–66.

Tyler KM, Higgs PG, Matthews KR, Gull K. 2001. Limitation of *Trypanosoma brucei* parasitaemia results from density-dependent parasite differentiation and parasite killing by the host immune response. *Proc Biol Sci* **268**: 2235–43.

Urwyler S, Studer E, Renggli CK, Roditi I. 2007. A family of stage-specific alanine-rich proteins on the surface of epimastigote forms of *Trypanosoma brucei*. *Mol Microbiol* **63**: 218–228.

Uzcategui NL, Szallies A, Pavlovic-Djuranovic S, Palmada M, Figarella K, Boehmer C, Lang F, Beitz E, Duszenko M. 2004. Cloning, heterologous expression, and characterization of three aquaglyceroporins from *Trypanosoma brucei. J Biol Chem* **279**: 42669–76.

Uzureau P, Uzureau S, Lecordier L, Fontaine F, Tebabi P, Homblé F, Grélard A, Zhendre V, Nolan DP, Lins L, et al. 2013. Mechanism of *Trypanosoma brucei gambiense* resistance to human serum. *Nature* **501**: 430-4

Vagin O, Kraut JA, Sachs G. 2009. Role of N-glycosylation in trafficking of apical membrane proteins in epithelia. *Am J Physiol Ren Physiol* **296**: 459-69.

Vale RD. 2003. The molecular motor toolbox for intracellular transport. *Cell* **112**: 467–80.

van Luenen HG, Kieft R, Mussmann R, Engstler M, ter Riet B, Borst P. 2005. Trypanosomes change their transferrin receptor expression to allow effective uptake of host transferrin. *Mol Microbiol* **58**: 151–65.

Van Xong H, Vanhamme L, Chamekh M, Chimfwembe CE, Van Den Abbeele J, Pays A, Van Melrvenne N, Hamers R, De Baetselier P, Pays E. 1998. A VSG expression site-associated gene confers resistance to human serum in *Trypanosoma rhodesiense*. *Cell* **95**: 839–46.

Vanhamme L, Paturiaux-Hanocq F, Poelvoorde P, Nolan DP, Lins L, Van Den Abbeele J, Pays A, Tebabi P, Van Xong H, Jacquet A et al. 2003. Apolipoprotein L-I is the trypanosome lytic factor of human serum. *Nature* **422**: 83–7.

Vanhollebeke B, De Muylder G, Nielsen MJ, Pays A, Tebabi P, Dieu M, Raes M, Moestrup SK, Pays E. 2008. A haptoglobin-hemoglobin receptor conveys innate immunity to *Trypanosoma brucei* in humans. *Science* **320**: 677–81.

Vassella E, Reuner B, Yutzy B, Boshart M. 1997. Differentiation of African trypanosomes is controlled by a density sensing mechanism which signals cell cycle arrest via the cAMP pathway. *J Cell Sci* **110**: 2661–71.

Vassella E, Van Den Abbeele J, Bütikofer P, Renggli CK, Furger A, Brun R, Roditi I. 2000. A major surface glycoprotein of *Trypanosoma brucei* is expressed transiently during development and can be regulated post-transcriptionally by glycerol or hypoxia. *Genes Dev* **14**: 615–26.

Vatarunakamura C, Ueda-Nakamura T, Souza W De. 2005. Visualization of the cytostome in *Trypanosoma cruzi* by high resolution field emission scanning electron microscopy using secondary and backscattered electron imaging. *FEMS Microbiol Lett* **242**: 227–30.

Vaughan S, Gull K. 2008. The structural mechanics of cell division in *Trypanosoma brucei*. *Biochem Soc Trans* **36**: 421–4.

Vidal JC, Alcantara C de L, de Souza W, Cunha-E-Silva NL. 2016. Loss of the cytostome-cytopharynx and endocytic ability are late events in *Trypanosoma cruzi* metacyclogenesis. *J Struct Biol* **196**: 319–28.

Vidilaseris K, Lesigang J, Morriswood B, Dong G. 2015. Assembly mechanism of *Trypanosoma brucei* BILBO1 at the flagellar pocket collar. *Commun Integr Biol* **8**: e992739.

Vidilaseris K, Morriswood B, Kontaxis G, Dong G. 2014. Structure of the TbBILBO1 protein N-terminal domain from *Trypanosoma brucei* reveals an essential requirement for a conserved surface patch. *J Biol Chem* **289**: 3724–35.

Vieira OV, Gaus K, Verkade P, Fullekrug J, Vaz WL, Simons K. 2006. FAPP2, cilium formation, and compartmentalization of the apical membrane in polarized Madin-Darby canine kidney (MDCK) cells. *Proc Natl Acad Sci U S A* **103**: 18556–61.

Wahl S, Katiyar R, Schmitz F. 2013. A local, periactive zone endocytic machinery at photoreceptor synapses in close vicinity to synaptic ribbons. *J Neurosci* **33**: 10278–300.

Wang W, Cao L, Wang C, Gigant B, Knossow M. 2015. Kinesin, 30 years later: Recent insights from structural studies. *Protein Sci* **24**: 1047–56.

Waters CM, Bassler BL. 2005. Quorum sensing: cell-to-cell communication in bacteria. *Annu Rev Cell Dev Biol* **21**: 319–46.

Webb H, Carnall N, Vanhamme L, Rolin S, Van Den Abbeele J, Welburn S, Pays E, Carrington M. 1997. The GPI-phospholipase C of *Trypanosoma brucei* is non essential but influences parasitemia in mice. *J Cell Biol* **139**: 103–14.

Webster P, Russell DG. 1993. The flagellar pocket of trypanosomatids. *Parasitol Today* **9**: 201–6.

Wheeler RJ, Scheumann N, Wickstead B, Gull K, Vaughan S. 2013. Cytokinesis in *Trypanosoma brucei* differs between bloodstream and tsetse trypomastigote. *Mol Microbiol* **90**: 1339-55

Wheeler RJ, Sunter JD, Gull K. 2016. Flagellar pocket restructuring through the *Leishmania* life cycle involves a discrete flagellum attachment zone. *J Cell Sci* **129**: 854-67

White TC, Rudenko G, Borst P. 1986. Three small RNAs within the 10 KB trypanosome rRNA transcription unit are analogous to domain VII of other eukaryotic 28S rRNAs. *Nucleic Acids Res* **14**: 9471–89.

Wickstead B, Carrington JT, Gluenz E, Gull K. 2010. The expanded Kinesin-13 repertoire of trypanosomes contains only one mitotic Kinesin indicating multiple extra-nuclear roles. *PLoS One* **5**: e15020.

Wickstead B, Ersfeld K, Gull K. 2002. Targeting of a tetracycline-inducible expression system to the transcriptionally silent minichromosomes of *Trypanosoma brucei*. *Mol Biochem Parasitol* **125**: 211–6.

Wickstead B, Gull K. 2006. A 'holistic' kinesin phylogeny reveals new kinesin families and predicts protein functions. *Mol Biol Cell* **17**: 1734–43.

Wickstead B, Gull K. 2007. Dyneins across eukaryotes: A comparative genomic analysis. *Traffic* **8**: 1708–21.

Winckler B, Forscher P, Mellman I. 1999. A diffusion barrier maintains distribution of membrane proteins in polarized neurons. *Nature* **397**: 698–701.

Wirtz E, Leal S, Ochatt C, Cross GA. 1999. A tightly regulated inducible expression system for conditional gene knock-outs and dominant-negative genetics in *Trypanosoma brucei*. *Mol Biochem Parasitol* **99**: 89–101.

Woehlke G, Ruby AK, Hart CL, Ly B, Hom-Booher N, Vale RD. 1997. Microtubule interaction site of the kinesin motor. *Cell* **90**: 207-216.

Woods K, Nic a'Bhaird N, Dooley C, Perez-Morga D, Nolan DP. 2013. Identification and characterization of a stage specific membrane protein involved in flagellar attachment in *Trypanosoma brucei*. *PLoS One* **8**: e52846.

Xu C, Ng DT. 2015. Glycosylation-directed quality control of protein folding. *Nat Rev Mol Cell Biol* **16**: 742–52.

Yang H, Russell DG, Zheng B, Eiki M, Lee MG. 2000. Sequence requirements for trafficking of the CRAM transmembrane protein to the flagellar pocket of African trypanosomes. *Mol Cell Biol* **20**: 5149–63.

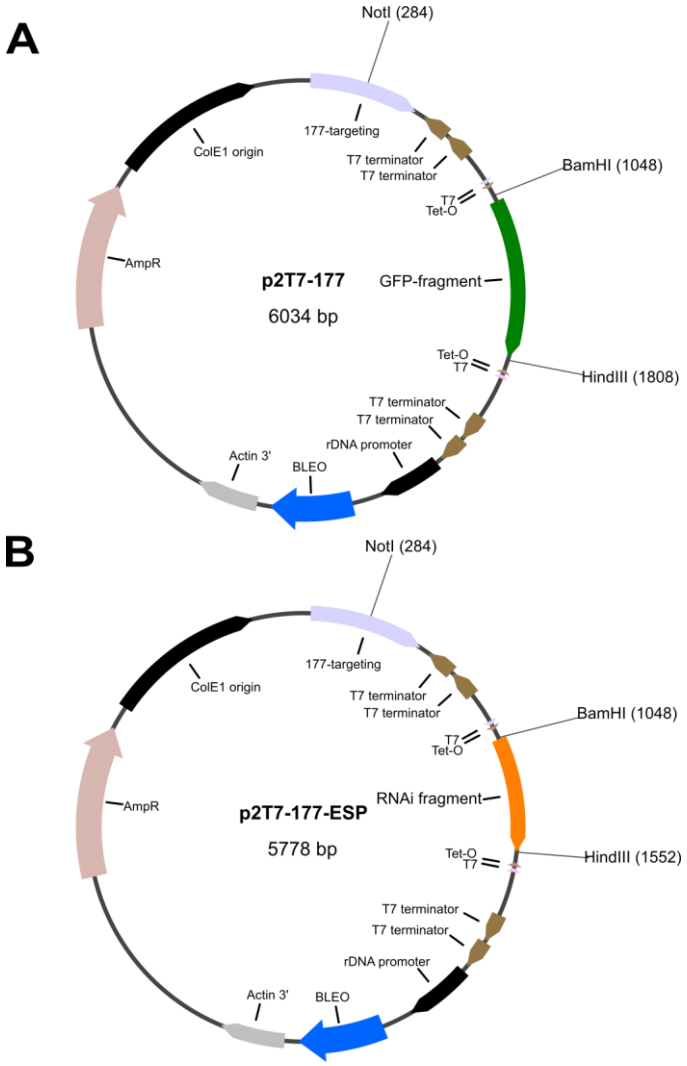
Zajac AL, Goldman YE, Holzbaur ELF, Ostap EM. 2013. Local cytoskeletal and organelle interactions impact molecular-motor-driven early endosomal trafficking. *Curr Biol* **23**: 1173–1180.

Zamze SE, Ashford DA, Wooten EW, Rademacher TW, Dwek RA. 1991. Structural characterization of the asparagine-linked oligosaccharides from *Trypanosoma brucei* type II and type III variant surface glycoproteins. *J Biol Chem* **266**: 20244–61.

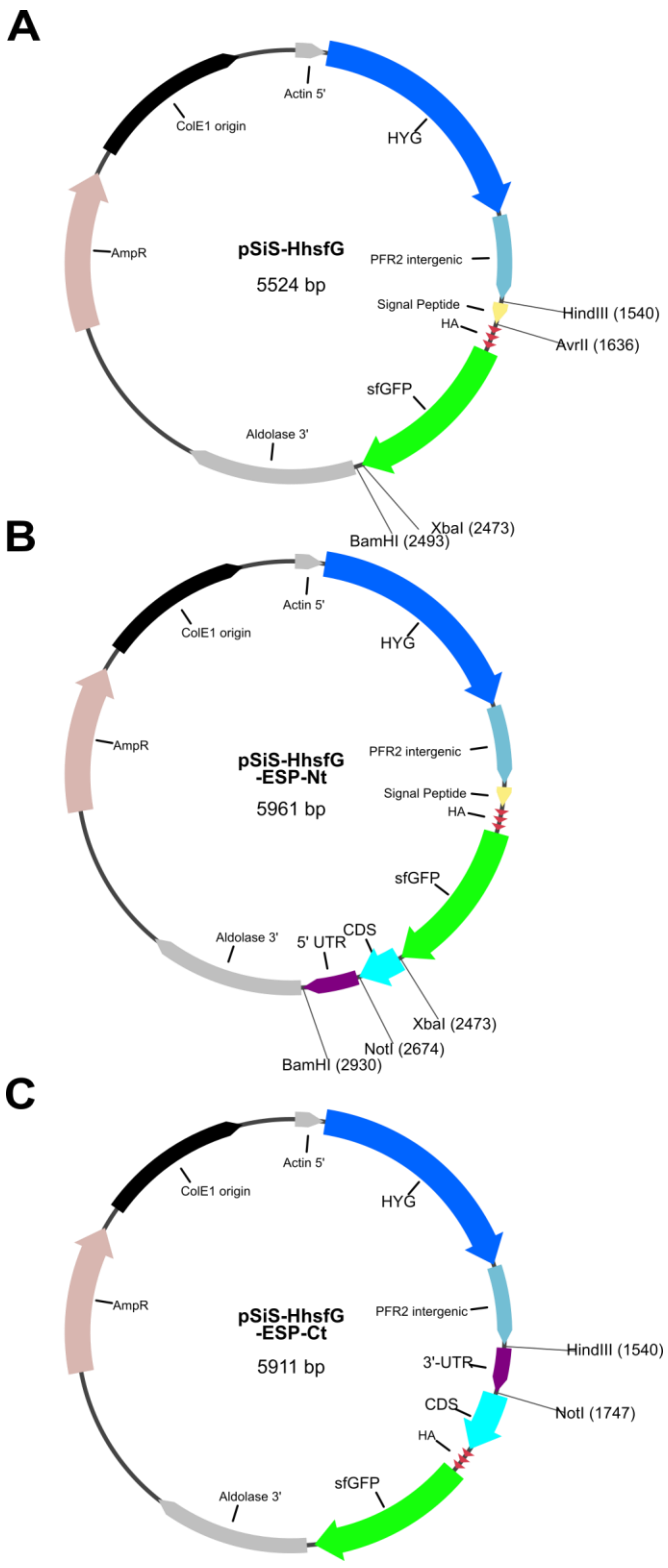
Ziegelbauer K, Overath P. 1992. Identification of invariant surface glycoproteins in the bloodstream stage of *Trypanosoma brucei. J Biol Chem* **267**: 10791–6.

Ziegelbauer K, Overath P. 1993. Organization of two invariant surface glycoproteins in the surface coat of *Trypanosoma brucei*. *Infect Immun* **61**: 4540–5

Appendix

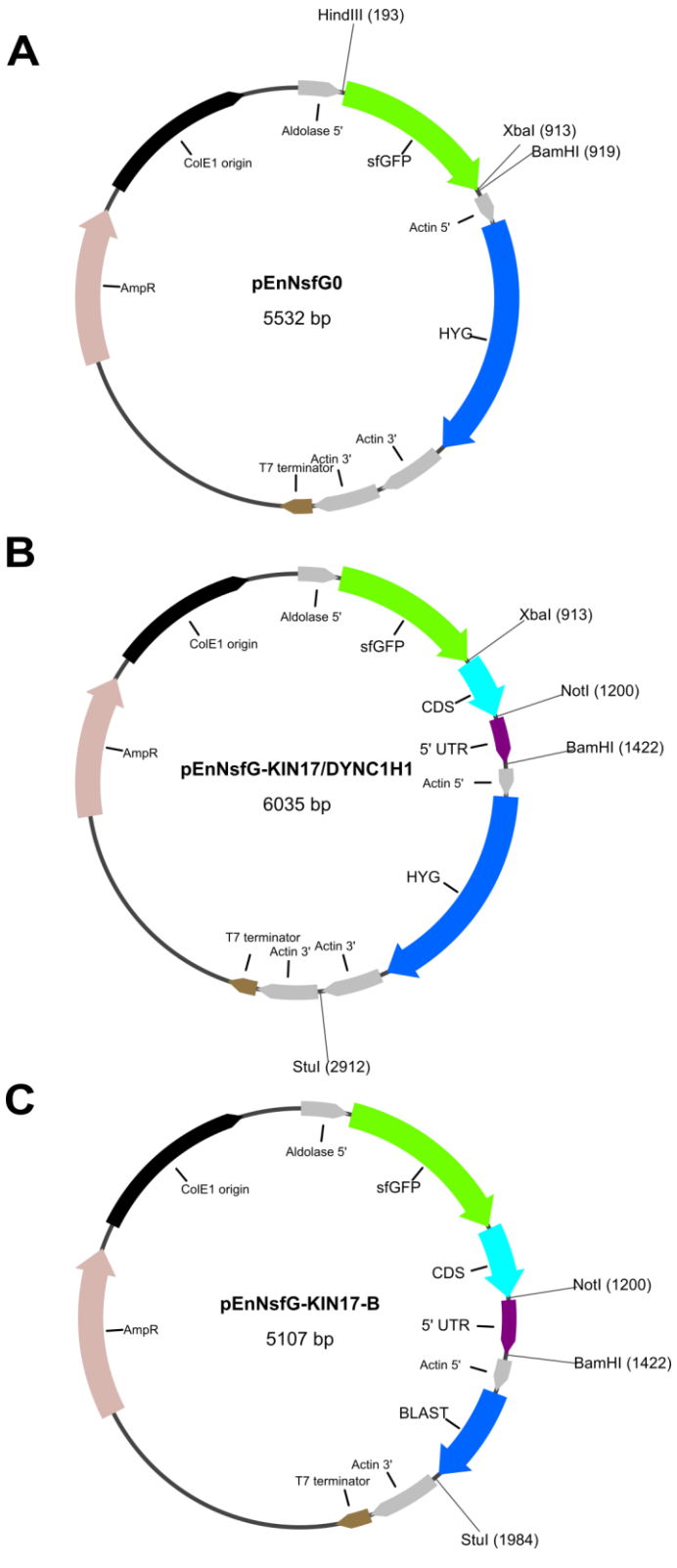


Appendix 1. Plasmid maps for the generation of ESP RNAi constructs
A) Parental plasmid. **B**) Resultant plasmid containing ESP RNAi targeting fragment. Restriction sites used for cloning and linearisation are labelled.

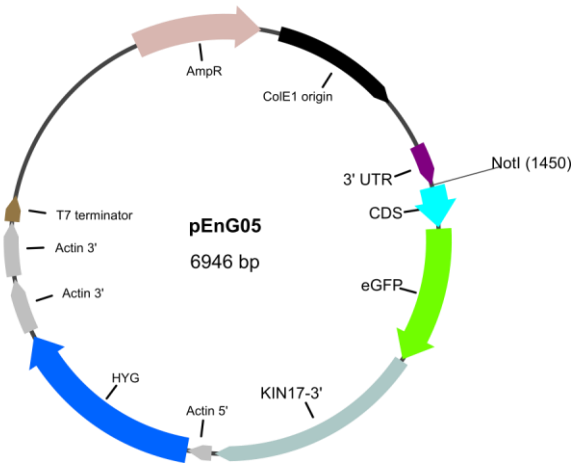


Appendix 2. Plasmid maps for the generation of ESP endogenous locus tagging constructs

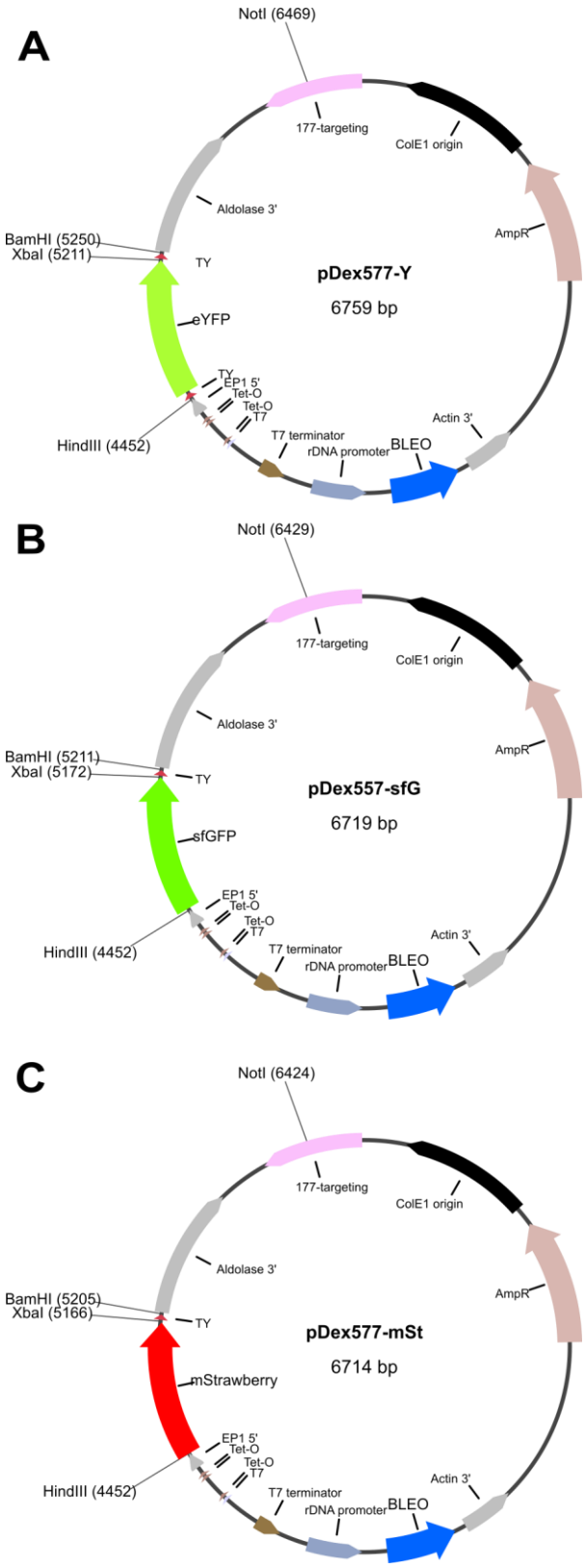
A) Parental plasmid. **B**) Resultant plasmid for N-terminal ESP tagging construct. **C**) Resultant plasmid for C-terminal ESP tagging construct. Restriction sites used for cloning and linearisation are labelled.


A
HindIII (193)
Aldolase 5'
ColE1 origin
sfGFP
XbaI (913)
BamHI (919)
Actin 5'
AmpR
pEnNsfG0
5532 bp
HYG
Actin 3'
T7 terminator
Actin 3'
B
Aldolase 5'
ColE1 origin
sfGFP
XbaI (913)
CDS
NotI (1200)
5' UTR
BamHI (1422)
AmpR
pEnNsfG-KIN17/DYNC1H1
6035 bp
Actin 5'
HYG
T7 terminator
Actin 3'
Actin 3'
StuI (2912)
C
Aldolase 5'
ColE1 origin
sfGFP
CDS
NotI (1200)
pEnNsfG-KIN17-B
5107 bp
5' UTR
AmpR
Actin 5'
BamHI (1422)
BLAST
Actin 3'
T7 terminator
StuI (1984)

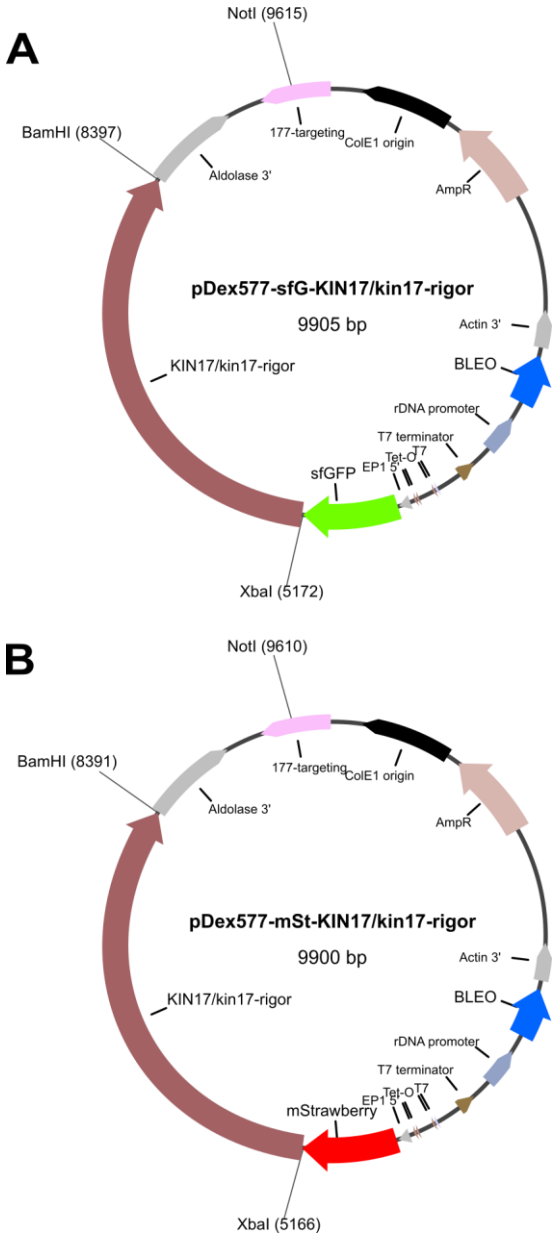
D



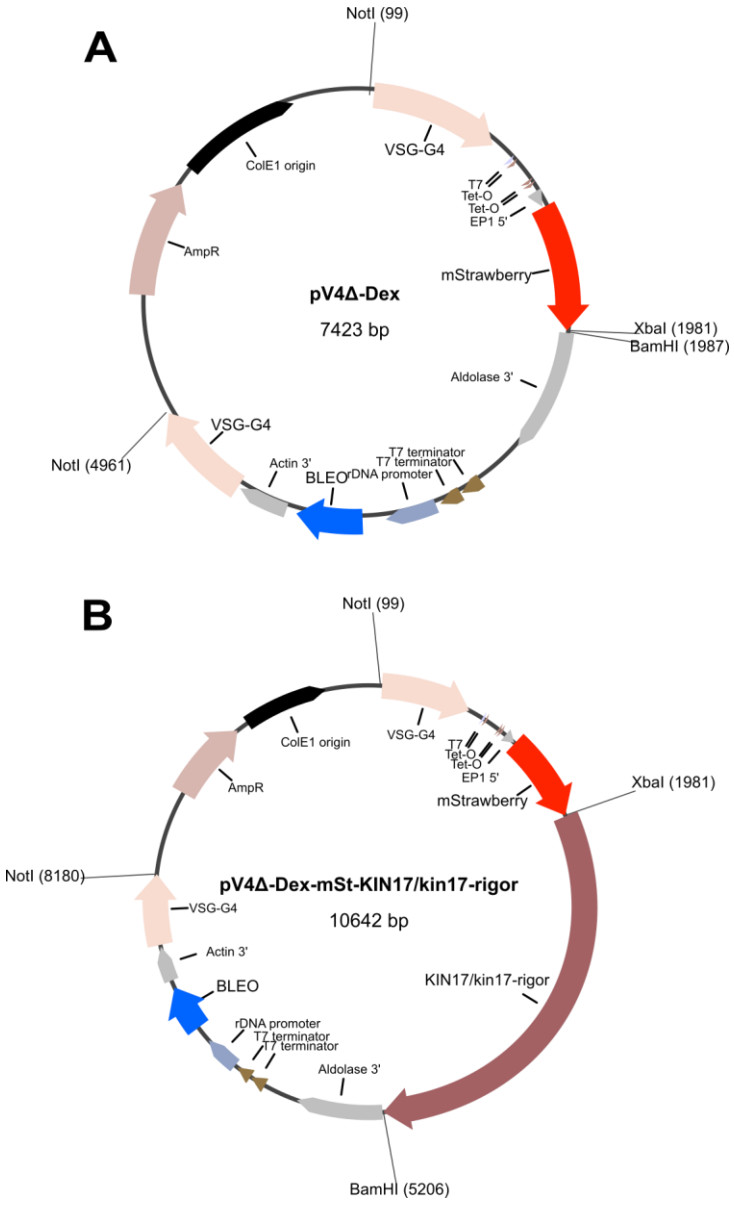
Appendix 3. Plasmid maps for the generation of KIN17 and DYNC1H1 endogenous locus tagging constructs.
A) Parental plasmid. **B**) Resultant plasmid for N-terminal KIN17/DYNC1H1 tagging constructs. **C**) Plasmid for tagging the second allele of KIN17 where *HYG* resistance has been switched for *BLAST*, derived from B. **D**) Plasmid for C-terminal tagging of KIN17 (kindly provided by Bill Wickstead). Restriction sites used for cloning and linearisation are labelled.



Appendix 4. Plasmid maps for inducible overexpression
A) Parental plasmid. **B** and **C**) Superfolder GFP and mStrawberry derivatives of A, respectively. Restriction sites used for cloning and linearisation are labelled.



Appendix 5. Plasmid maps for the inducible overexpression of KIN17/kin17-rigor
Resultant plasmids for the overexpression of KIN17/kin17-rigor, with either an N-terminal sfGFP tag (**A**), or an N-terminal mStrawberry tag (**B**). These were derived from vectors in Appendix 4. Restriction sites used for cloning and linearisation are labelled.



Appendix 6. Plasmid maps for the inducible overexpression of KIN17/kin17-rigor from a VSG-V4 locus

A) Parental plasmid. **B)** Resultant plasmid for the overexpression of KIN17/kin17-rigor with an N-terminal mStrawberry tag, which integrates into the VSG-G4 locus rather than 177-bp repeats (as is the case for plasmids in Appendix 5).